Acta Biomed. - Vol. 90 - Suppl. 5 - April 2019 | ISSN 0392 - 4203

ACTA BIOMEDICA SUPPLEMENT

ATENEI PARMENSIS | FOUNDED 1887

Official Journal of the Society of Medicine and Natural Sciences of Parma and Centre on health systems' organization, quality and sustainability, Parma, Italy

The Acta Biomedica is indexed by Index Medicus / Medline Excerpta Medica (EMBASE), the Elsevier BioBASE, Scopus (Elsevier) and Bibliovigilance

Advances in diagnostic and interventional radiology

Guest Editors: Massimo De Filippo, Luca Brunese, Alfonso Reginelli

Free on-line www.actabiomedica.it

Mattioli 1885

Pubblicazione trimestrale - Poste Italiane s.p.a. - Sped. in A.P. - D.L. 353/2003 (conv. in L. 27/02/2004 n. 46) art. 1, comma 1, DCB Parma - Finito di stampare April 2019

Acta Bio Medica

Atenei parmensis

founded 1887

Official Journal of the Society of Medicine and Natural Sciences of Parma and Centre on Health System's Organization, Quality and Sustainability, Parma, Italy

free on-line: www.actabiomedica.it

EDITORIAL OFFICE MANAGER
Valeria Ceci
Mattioli 1885 srl - Casa Editrice
Strada di Lodesana 649/sx, Loc. Vaio
43036 Fidenza (PR), Italy
Tel. ++39 0524 530383
Fax ++39 0524 82537
contact@actabiomedica.it

Francesco Covino
Società di Medicina e Scienze Naturali
Azienda Ospedaliero-Universitaria
di Parma - Cattani Building, 2nd floor
Via Gramsci, 14 - Parma, Italy
Tel./Fax ++39 0521 033730
francesco.covino@unipr.it

PUBLISHER
Mattioli 1885 srl Casa Editrice
Strada di Lodesana, 649/sx, Loc. Vaio
43036 Fidenza (PR), Italy
Tel. ++39 0524 530383
Fax ++39 0524 82537
E-mail: edit@mattioli1885.com

Acta BioMedica is the official Journal of the Society of Medicine and Natural Sciences of Parma. The Journal publishes Original Articles, Commentaries, Review Articles, Case Reports of experimental and general medicine. The manuscript must be submitted using the journal web site: **http://www.actabiomedica.it**
The Editorial Office will forward the text to the Editor-in-Chief, Prof. Maurizio Vanelli (University of Parma).
For any information please refer to:
Acta BioMedica – Editorial Office
Dr. Anna Scotti
Mattioli 1885 srl
Strada di Lodesana 649/sx, Loc. Vaio - 43036 Fidenza (PR) - Italy
E-mail: contact@actabiomedica.it - Fax: 0039-(0)524-82537
The Journal does not hold itself responsible for statements made by contributors or for loss or damage of mailed manuscripts. They should be ac-companied by an undertaking that they are submitted to this Journal only. Papers must be submitted in English. Papers are accepted on the understanding that they may be subject to editorial revision.
All Original Articles are subject to review and authors are urged to be brief. Long papers with many tables and figures may require shortening if they are to be accepted for publication. All manuscripts should include a total text word count and an abstract word count on the cover page. Total text word count does not include title page, figure legends, references, or tables. Only under exceptional circumstances will Original Articles longer than 5500 words be considered, and under no circumstances will abstracts greater than 250 words be published. Editorials and Reviews are normally invited contributions but suitable papers may be submitted to the Editor for consideration for this purpose. The presentation of Case Reports should be as short as possible. Reports of co-existence of two diseases or conditions without proof of causal relationship are discouraged. Letters to the Editor should not exceed 600 words of text, one figure or table and up to six references. Because space limitation, publication of submitted Letters will depend on priority rating.

TITLE PAGE must contain:
- a concise informative title
- author(s) names
- department or institution where work was done
- name and address of author to whom correspondence about the manuscript and request for reprints should be referred, as well as fax, E-mail and telephone number
- a running title of no more than 40 characters.

Be certain to list the FAX number and E-mail of the corresponding author on the title page. **All correspondence will be by E-mail and web site only.**

MANUSCRIPT should be typed in 12-point type and double spacing should be used throughout. It should carry an abstract of not more than 250 words including 4 paragraphs labeled: Background and aim of the work, Methods, Results, and Conclusions. Below the abstract provide 3-10 key words that will assist indexers in cross-indexing the article. Paragraphs to be set in a smaller type should be marked with an "s" (small) in the left hand margin. Avoid footnotes; when essential they are numbered consecutively and typed at the foot of the appropriate page.

ILLUSTRATIONS. It is the authors' responsibility to obtain permission (from the author and copyright holder) to reproduce illustrations, tables, etc. from other publications. Photographs and graphics should be sent as high resolution files: not less than 300 d.p.i. and with a base of the same size as a column of the Journal (8 cm). A letter of permission must accompany all photographs when there is a possibility of identification. Authors will pay for colour illustrations. Present rate for a full page colour illustration is about $ 600-1200. Final quotation will be given by the publisher. Legends should be typed on a separate "word" document.

TABLES should be numbered consecutively with Arabic numerals. Type each table on a separate document, together with a brief caption. We do not welcome large tables of unanalysed data.

REFERENCES should be numbered consecutively in the order in which they appear in the text. References cited only in tables or in legends to figures should be numbered in accordance with the sequence established by the first identification in the text. The list of references should be typed in numerical order and indicate: authors' names (all authors when six or less; when seven or more list only the first three and add "et al."); article title, name of the Journal (abbreviated as in Index Medicus), publication year, volume and first and last page numbers. Example:
Rizzato G, Marazzini L. Thoracoabdominal mechanics in elderly men. J Appl Physiol 1970; 28: 457-60.
If the reference is concerning a book, give authors' names, full title, name and address of publisher and publication year. Personal communications should not be included in the references, but may be cited in the text in parentheses.

COPYRIGHT. Please include a signed release of copyright to Acta Bio Medica Society of Medicine and Natural Sciences of Parma with your text. Include the title of the article being submitted, as well as the date. Include the signature of coauthors.
The corresponding author must certify that the submitted manuscript is an original article and that he is able to prove this originality if required from the Referees. Without this declaration the manuscript will not be considered.

GALLEY PROOF. Unless indicated otherwise, galley proofs are sent to the first author and should be returned without delay. Alterations to galley proofs, other than those due to printer's error, are charged to the author. Accepted and rejected manuscripts are retained for six months after publication or rejection, then destroyed.

REPRINTS. Reprints are available at cost if they are ordered when the proof is returned. Order form and a price list are sent with the galley proofs; payment must be made with the order.

NOTICE TO SUBSCRIBERS

Acta Bio Medica Society of Medicine and Natural Sciences of Parma is published quarterly. Individual annual subscription for 2019 is 35,00 Euro in Italy, 45,00 Euro outside Italy. Institutional subscription is 45,00 Euro in Italy, 45,00 Euro outside Italy. The publisher accepts no responsibility for replacing Journal issues unless notified of non-receipt within 5 months of issue date. Payment should be made to the publisher: Mattioli 1885 srl, Strada di Lodesana 649/sx, Loc. Vaio, 43036 Fidenza (PR), Italy, Tel. 0039-(0)524-530383, Fax 0039-(0)524-82537, E-mail: subscribe@mattioli1885.com

COPYRIGHT

Editor-in-Chief: M. Vanelli
Printed in: April 2019
Registrazione del Tribunale di Parma n° 253 del 21/7/1955

Mattioli 1885
srl- Strada di Lodesana 649/sx
43036 Fidenza (Parma)
tel 0524/530383
fax 0524/82537
www.mattioli1885.com

Index

Volume 90 / Suppl. 5 April 2019

Acta Biomed 2019; Vol. 90, Supplement 5: 5-8 DOI: 10.23750/abm.v90i5-S.8327

Editorial

Advances in diagnostic and interventional radiology

Massimo De Filippo[1], *Luca Brunese*[2], *Alfonso Reginelli*[3]

[1] Department of Medicine and Surgery, Unit of Radiologic Science, University of Parma, Maggiore Hospital, Parma, Italy; [2] Department of Medicine and Health Sciences "V. Tiberio", University Of Molise, Campobasso, Italy; [3] Department of Precision Medicine, University of Campania "L. Vanvitelli", Naples, Italy

This Special Issue includes a series of contributions whose central theme are the recent advances in the field of diagnostic and interventional radiology. In recent years, in fact, technological innovations, together with clinical research, have led to the development of new imaging applications in clinical practice (1-8). These innovations have involved the purely diagnostic aspect of imaging, thanks to the implementation of new protocols and advanced sequences, but also have given a significant boost to the ever-increasing use of interventional radiology procedures for the treatment of various diseases in different fields (9-18). The articles published in this volume are intended to give an overview of some of these new applications, focusing on, or reviewing, the state of the art in specific diagnostic and interventional settings (19-27).

The first article entitled "Internal hernias: a difficult diagnostic challenge. Review of CT signs and clinical findings", by Lanzetta et al., is a review article focused on a rather rare but of fundamental clinical and diagnostic importance pathological picture that general, emergency and abdominal radiologists have to confront with. The authors carefully summarize the most important clinical and imaging aspects of this pathology, often of difficult assessment.

Still on the subject of diagnostic radiology, Bruno et al., in the second article "Application of Diffusion Tensor Imaging (DTI) and MR-tractography in the evaluation of peripheral nerve tumours: state of the art and review of the literature", present the role of a particular novel advanced MRI technique in the preoperative study of peripheral nerves, whose results are very promising, with important clinical implications.

The importance of imaging in clinical management (28-30) is also underlined by Danti et al., the authors of the article "Relationship between diagnostic imaging features and prognostic outcomes in gastrointestinal stromal tumors (GIST)", focused on the CT classification systems in the diagnostic imaging of GIST, and their role in risk stratification (31-35).

Starting from the description of a case (36, 37), Mariniello et al., in their article "Radiation-induced brain cavernomas in elderly: review of the literature and a rare case report", review the literature of radiation-induced cavernomas with their pathological features and imaging findings.

Interventional radiology nowadays gained application for the treatment of degenerative, traumatic, and tumor diseases in several fields (38-46). A very effective procedure used in the musculoskeletal field is the percutaneous lavage of rotator cuff calcifications, described in terms of technique and results by Pagnini et al. in their article "Ultrasound-guided percutaneous irrigation of calcific tendinopathy: technical developments".

Another clinically relevant interventional radiology technique is the execution of biopsies in almost all body districts (47-53). In the article "Percutaneous needle biopsy of retroperitoneal lesions: technical developments" by Bevilacqua et al., the authors describe the difficult but fundamental role of the imaging guidance in the biopsy of retroperitoneal lesions, underlining the primary role of the interventional radiologist in the choice of the imaging modality, the approaches and the techniques to be used.

A multimodal imaging approach is often useful for an accurate diagnosis of certain diseases. In their

article "Magnetic Resonance Enterography (MRE) and Ultrasonography (US) in the study of the small bowel in Crohn's disease: state of the art and review of the literature", Manetta et al. describe the state of the art of diagnostic imaging in the study of this condition, comparing the advantages and limitations of the two techniques.

Beyond diagnostic purposes, imaging plays a determinant role in the monitoring of therapeutic regimens in particular settings where novel or advanced therapies are administered. The contribution by Reginelli et al. "Diagnostic value/performance of radiological liver imaging during chemotherapy for gastrointestinal malignancy: a critical review" is a diagnostic focus on the imaging of liver alterations during systemic therapy in cancer patients, with particular reference to the chemotherapic agents and the diagnostic challenges that can be encountered in these cases.

The last article by Zappia et al., entitled "Imaging of long head biceps. A multimodality pictorial essay" is an all-round review of the diagnostic imaging modalities in the evaluation of the LHBT of the shoulder.

We are sure that the contributions of this volume can represent an opportunity for updating both for the radiologists and for the clinicians of various specialties, and we thank the authors for the intense commitment and the excellent scientific value of their work.

References

1. Valeri G, Mazza FA, Maggi S, et al. Open source software in a practical approach for post processing of radiologic images. Radiol Med 2015; 120: 309-23.
2. Grassi R, Cavaliere C, Cozzolino S, et al. Small animal imaging facility: New perspectives for the radiologist. Radiol Med 2009; 114: 152-67.
3. Di Cesare E, Gennarelli A, Di Sibio A, et al. Image quality and radiation dose of single heartbeat 640-slice coronary CT angiography: A comparison between patients with chronic Atrial Fibrillation and subjects in normal sinus rhythm by propensity analysis. Eur J Radiol 2015; 84: 631-36.
4. De Cecco CN, Buffa V, Fedeli S, et al. Preliminary experience with abdominal dual-energy CT (DECT): True versus virtual nonenhanced images of the liver. Radiol Med 2010; 115: 1258-66.
5. Buffa V, Solazzo A, D'Auria V, et al. Dual-source dual-energy CT: dose reduction after endovascular abdominal aortic aneurysm repair. Radiol Med 2014; 119: 934-41.
6. Iacobellis F, Segreto T, Berritto D, et al. A rat model of acute kidney injury through systemic hypoperfusion evaluated by micro-US, color and PW-Doppler. Radiol Med 2018;
7. Cappabianca S, Iaselli F, Reginelli A, et al. Value of diffusion-weighted magnetic resonance imaging in the characterization of complex adnexal masses. Tumori 2013; 99: 210-17.
8. Barile A, La Marra A, Arrigoni F, et al. Anaesthetics, steroids and platelet-rich plasma (PRP) in ultrasound-guided musculoskeletal procedures. Br J Radiol 2016; 89: 20150355.
9. Masciocchi C, Arrigoni F, Ferrari F, et al. Uterine fibroid therapy using interventional radiology mini-invasive treatments: current perspective. Med Oncol 2017; 34: 52.
10. Cappabianca S, Porto A, Petrillo M, et al. Preliminary study on the correlation between grading and histology of solitary pulmonary nodules and contrast enhancement and [18F] fluorodeoxyglucose standardised uptake value after evaluation by dynamic multiphase CT and PET/CT. J Clin Pathol 2011; 64: 114-19.
11. Cantisani V, Grazhdani H, Drakonaki E, et al. Strain US Elastography for the Characterization of Thyroid Nodules: Advantages and Limitation. Int J Endocrinol 2015; 2015: 908575.
12. Muccio CF, Di Blasi A, Esposito G, Brunese L, D'Arco F, Caranci F. Perfusion and spectroscopy magnetic resonance imaging in a case of lymphocytic vasculitis mimicking brain tumor. Pol J Radiol 2013; 78: 66-69.
13. Cirillo M, Caranci F, Tortora F, et al. Structural neuroimaging in dementia. J Alzheimers Dis 2012; 29: 16-19.
14. Zappia M, Capasso R, Berritto D, et al. Anterior cruciate ligament reconstruction: MR imaging findings. Musculoskelet Surg 2017; 101: 23-35.
15. Barile A, Arrigoni F, Bruno F, et al. Computed Tomography and MR Imaging in Rheumatoid Arthritis. Radiol Clin North Am 2017; 55: 997-1007.
16. Valentini V, Buquicchio GL, Galluzzo M, et al. Intussusception in Adults: The Role of MDCT in the Identification of the Site and Cause of Obstruction. Gastroenterol Res Pract 2016; 2016: 5623718-18.
17. Di Cesare E, Patriarca L, Panebianco L, et al. Coronary computed tomography angiography in the evaluation of intermediate risk asymptomatic individuals. Radiol Med 2018; 123: 686-94.
18. Lo Re G, Cappello M, Tudisca C, et al. CT enterography as a powerful tool for the evaluation of inflammatory activity in Crohn's disease: Relationship of CT findings with CDAI and acute-phase reactants. Radiol Med 2014; 119: 658-66.
19. Barile A, Bruno F, Mariani S, et al. What can be seen after rotator cuff repair: a brief review of diagnostic imaging findings. Musculoskelet Surg 2017; 101: 3-14.
20. Splendiani A, Perri M, Marsecano C, et al. Effects of serial macrocyclic-based contrast materials gadoterate meglumine and gadobutrol administrations on gadolinium-related dentate nuclei signal increases in unenhanced T1-weighted brain: a retrospective study in 158 multiple sclerosis (MS) patients. Radiol Med 2018; 123: 125-34.
21. Scialpi M, Cappabianca S, Rotondo A, et al. Pulmonary

congenital cystic disease in adults. Spiral computed tomography findings with pathologic correlation and management. Radiol Med 2010; 115: 539-50.
22. Tedeschi E, Caranci F, Giordano F, Angelini V, Cocozza S, Brunetti A. Gadolinium retention in the body: what we know and what we can do. Radiol Med 2017; 122: 589-600.
23. Vivarelli M, Vincenzi P, Montalti R, et al. ALPPS Procedure for Extended Liver Resections: A Single Centre Experience and a Systematic Review. PLoS One 2015; 10: e0144019.
24. Di Cesare E, Cademartiri F, Carbone I, et al. Clinical indications for the use of cardiac MRI. by the SIRM Study Group on Cardiac Imaging. Radiol Med 2013; 118: 752-98.
25. Zappia M, Castagna A, Barile A, Chianca V, Brunese L, Pouliart N. Imaging of the coracoglenoid ligament: a third ligament in the rotator interval of the shoulder. Skeletal Radiol 2017; 46: 1101-11.
26. Di Pietto F, Chianca V, de Ritis R, et al. Postoperative imaging in arthroscopic hip surgery. Musculoskelet Surg 2017; 101: 43-49.
27. Barile A, Bruno F, Arrigoni F, et al. Emergency and Trauma of the Ankle. Semi Musc Rad 2017; 21: 282-89.
28. Salvolini L, Urbinati C, Valeri G, Ferrara C, Giovagnoni A. Contrast-enhanced MR cholangiography (MRCP) with GD-EOB-DTPA in evaluating biliary complications after surgery. Radiol Med 2012; 117: 354-68.
29. Francone M, Di Cesare E, Cademartiri F, et al. Italian registry of cardiac magnetic resonance. Eur J Radiol 2014; 83: e15-e22.
30. Perrotta FM, Astorri D, Zappia M, Reginelli A, Brunese L, Lubrano E. An ultrasonographic study of enthesis in early psoriatic arthritis patients naive to traditional and biologic DMARDs treatment. Rheumatol Int 2016; 36: 1579-83.
31. Lai Q, Nicolini D, Inostroza M, et al. A novel prognostic index in patients with hepatocellular cancer waiting for liver transplantation Time-Radiological-response-Alpha-feto-protein-INflammation (TRAIN) score. Ann Surg 2016; 264: 787-96.
32. Mocchegiani F, Vincenzi P, Coletta M, et al. Prevalence and clinical outcome of hepatic haemangioma with specific reference to the risk of rupture: A large retrospective cross-sectional study. Dig Liver Dis 2016; 48: 309-14.
33. Cortellini A, Verna L, Porzio G, et al. Predictive value of skeletal muscle mass for immunotherapy with nivolumab in non-small cell lung cancer patients: A "hypothesis-generator" preliminary report. Thorac Cancer 2019; 10: 347-51.
34. Cortellini A, Palumbo P, Porzio G, et al. Single-institution study of correlations between skeletal muscle mass, its density, and clinical outcomes in non-small cell lung cancer patients treated with first-line chemotherapy. Thorac Cancer 2018; 9: 1623-30.
35. Maurizi N, Passantino S, Spaziani G, et al. Long-term Outcomes of Pediatric-Onset Hypertrophic Cardiomyopathy and Age-Specific Risk Factors for Lethal Arrhythmic Events. JAMA Cardiol 2018; 3: 520-25.
36. Caranci F, Napoli M, Cirillo M, Briganti G, Brunese L, Briganti F. Basilar artery hypoplasia. Neuroradiol J 2012; 25: 739-43.
37. Battipaglia G, Avilia S, Morelli E, Caranci F, Perna F, Camera A. Posterior reversible encephalopathy syndrome (PRES) during induction chemotherapy for acute myeloblastic leukemia (AML). Ann Hematol 2012; 91: 1327-28.
38. Arrigoni F, Gregori LM, Zugaro L, Barile A, Masciocchi C. MRgFUS in the treatment of MSK lesions: A review based on the experience of the university of L'aquila, Italy. Transl Cancer Res 2014; 3: 442-48.
39. Barile A, Arrigoni F, Zugaro L, et al. Minimally invasive treatments of painful bone lesions: state of the art. Med Oncol 2017; 34: 53.
40. Ferrari F, Arrigoni F, Miccoli A, et al. Effectiveness of Magnetic Resonance-guided Focused Ultrasound Surgery (MRgFUS) in the uterine adenomyosis treatment: technical approach and MRI evaluation. Radiol Med 2016; 121: 153-61.
41. Barile A, Arrigoni F, Bruno F, et al. Present role and future perspectives of interventional radiology in the treatment of painful bone lesions. Future Oncol 2018; 14: 2945-55.
42. Arrigoni F, Bruno F, Zugaro L, et al. Developments in the management of bone metastases with interventional radiology. Acta Biomed 2018; 89: 166-74.
43. Briganti F, Leone G, Marseglia M, Cicala D, Caranci F, Maiuri F. P64 Flow Modulation Device in the treatment of intracranial aneurysms: Initial experience and technical aspects. J Neurointerv Surg 2016; 8: 173-80.
44. Arrigoni F, Barile A, Zugaro L, et al. Intra-articular benign bone lesions treated with Magnetic Resonance-guided Focused Ultrasound (MRgFUS): imaging follow-up and clinical results. Med Oncol 2017; 34: 55.
45. Macchi M, Belfiore MP, Floridi C, et al. Radiofrequency versus microwave ablation for treatment of the lung tumours: LUMIRA (lung microwave radiofrequency) randomized trial. Med Oncol 2017; 34: 96.
46. Dialetto G, Reginelli A, Cerrato M, et al. Endovascular stent-graft treatment of thoracic aortic syndromes: A 7-year experience. Eur J Radiol 2007; 64: 65-72.
47. Gatta G, Parlato V, Di Grezia G, et al. Ultrasound-guided aspiration and ethanol sclerotherapy for treating endometrial cysts. Radiol Med 2010; 115: 1330-39.
48. Bertolini L, Vaglio A, Bignardi L, et al (2011). Subclinical interstitial lung abnormalities in stable renal allograft recipients in the era of modern immunosuppression. Transplantation Proceedings, vol. 43, p. 2617-2623, ISSN: 0041-1345, doi: 10.1016/j.transproceed.2011.06.033.
49. Palma BD, Guasco D, Pedrazzoni M, et al. Osteolytic lesions, cytogenetic features and bone marrow levels of cytokines and chemokines in multiple myeloma patients: Role of chemokine (C-C motif) ligand20. Leukemia. 2016 Feb;30(2):409-16. doi: 10.1038/leu.2015.259. Epub 2015 Sep 30.
50. Bozzetti C, Nizzoli R, Tiseo M, et al. ALK and ROS1 rearrangements tested by fluorescence in situ hybridization in cytological smears from advanced non-small cell lung can-

cer patients. Diagnostic Cytopathology, vol. 43, p. 941-946, ISSN: 8755-1039, doi: 10.1002/dc.23318.
51. De Filippo M, Gira F, Corradi D, Sverzellati N, Zompatori M, Rossi C. (2011). Benefits of 3D technique in guiding percutaneous retroperitoneal biopsies. RAD. MED, vol. 116(3), p. 407-416, ISSN: 0033-8362, doi: 10.1007/s11547-010-0604-2
52. De Filippo M, Onniboni M, Rusca M, et al. (2008). Advantages of multidetector row CT with multiplanar reformation in guiding percutaneous lung biopsies. RAD. MED, vol. 113, p. 945-953, ISSN: 0033-8362, doi: 10.1007/s11547-008-0325-y
53. Carrafiello G, Fontana F, Mangini M, et al. Initial experience with percutaneous biopsies of bone lesions using XperGuide cone-beam CT (CBCT): Technical note. Radiol Med 2012; 117: 1386-97.

Acta Biomed 2019; Vol. 90, Supplement 5: 9-19 DOI: 10.23750/abm.v90i5-S.8343

Review

Relationship between diagnostic imaging features and prognostic outcomes in gastrointestinal stromal tumors (GIST)

Ginevra Danti[1], Gloria Addeo[1], Diletta Cozzi[1], Nicola Maggialetti[2], Monica Marina Lanzetta[1], Gianluca Frezzetti[1], Antonella Masserelli[1], Silvia Pradella[1], Andrea Giovagnoni[3], Vittorio Miele[1]

[1] Department of Radiology, Careggi University Hospital, Florence, Italy; [2] Department of Medicine and Health Sciences "V. Tiberio", University of Molise, Campobasso, Italy; [3] Department of Radiology, Università Politecnica delle Marche, Ancona, Italy

Summary. Gastrointestinal stromal tumors (GISTs), the most frequent mesenchymal neoplasms of the gastrointestinal tract, are a relatively recently described entity. GISTs can occur across any age but are more common in patients older than 50 years. GISTs most commonly are in the stomach (60-70%), followed by the small intestine (20%-30%); they also rarely occur in the abdominal cavity, such as in the mesentery, the omentum and the retroperitoneum. Contrast-enhanced multi-detector computed tomography (MDCT) is the most largely used imaging modality for the localization, characterization and staging of GISTs. All patterns of enhancement on contrast-enhanced MDCT can be seen with GISTs, including hypoenhancing, isoenhancing, and hyperenhancing neoplasms. A lot of prognostication systems have been proposed for the risk stratification of GISTs. This review outlines the relationship between different diagnostic imaging features and prognostic outcomes in GISTs. (www.actabiomedica.it)

Key words: gastrointestinal stromal tumors, imaging features, computed tomography, prognostication system, outcome

Introduction

Gastrointestinal stromal tumors (GISTs) are the most frequent mesenchymal tumors of the gastrointestinal tract, they are thought to arise from the interstitial cells of Cajal, which are intestinal pacemaker cells that allow peristalsis and segmentation of the smooth muscle (1-3).

Rubin et al. in their study said that GISTs have no predilection for either sex, and although they occur over a wide age distribution, in fact about 75% are diagnosed in patients older than 50 years (4). These tumors can arise everywhere in the gastrointestinal tract, but their most common locations are the stomach (60-70%) and the small bowel (20-30%) (5-7). About 5% of GISTs are in the colon and rectum, another 5% in the esophagus (4, 8-11). A small part of these tumors also develops within the mesentery, omentum, retroperitoneum, and pelvis (E-GIST) (12, 13).

Usually patients have non-specific symptoms including early satiety, bloating, gastrointestinal bleeding, fatigue from anemia, or obstruction (14). Bleeding can take the form of slow, intraluminal gastrointestinal bleeding or massive intraperitoneal bleeding following the rupture and can be seen regardless of the enhancement pattern (15). Aggressive GISTs have a defined pattern of metastasis to the liver or throughout the abdomen (usually as multiple serosal-based nodules), or

both (5). Contrasting GISTs in elderly patients, lymphatic metastases represent a common route of initial spread in young patients (< or = 40 years) (16). Extra-abdominal diffusion is mainly to the lungs and bone but isn't usual (17). Gold et al. showed that a lot of patients have localized disease (79.4%), but approximately 11.4% have regional-distant metastatic disease at the time of presentation; recurrences have been reported up to 30 years after initial diagnosis and resection (18).

GISTs have the classic tendency of exophytic growth, especially since they arise from the outer muscular layer. There is frequently some growth towards the lumen however, as up to 50% of GISTs will exhibit mucosal ulceration on the luminal surface. Among other macroscopic characteristics, there can be focal areas of hemorrhage, necrosis, calcifications, intralesional cavitation or cystic degeneration (19).

Histologically, GISTs can be classified into three main subtypes: spindle cell type (most common, 70%), epithelioid type (20%), and mixed (10%). The cellularity is also highly variable, passing from hypocellular to highly cellular with high mitotic rates (20, 21).

Kindblom et al. in their study described that GISTs can have many histological patterns and can be positive for c-KIT (95%), CD34 (60-70%), ACAT2 (smooth muscle actin; 30-40%), S100 (5%), DES (desmin; 1-2%), and keratin (1-2%) (22-25).

Zao et al. showed how C-KIT is the most specific and sensitive marker in differentiating GISTs from other entities (20). Mol et al. described how C-KIT positive tumors benefit from system therapy with imatinib mesylate, defined as a target therapy (26-28). However, a subset of the 5% of tumors that are c-KIT-negative might benefit from c-KIT-targeted therapy (29).

The wide range of clinical presentations along with non-specific symptoms can pose a challenge in differential diagnosis of GISTs. To date contrast-enhanced multi-detector computed tomography (MDCT) is the most largely used imaging modality for the localization, characterization and staging of GISTs (30).

In fact radiologists have a leading role in timely and accurate diagnosis for the frequent tumor's variability in relation to location, pattern of enhancement, and other imaging features such as necrosis or cavitation.

Prediction of prognosis of primary tumors has been studied intensively. In their study Fletcher et al. proposed tumor size and mitotic activity as the two main factors for the risk stratification system (23).

We considered the correlation between AFIP criteria and MDCT features of GISTs; evaluating mitotic count and tumor size, this system incorporated tumor location as an additional variable and stratified prognosis of GISTs into 5 classes (none, very low, low, moderate, high) (31).

In this review of recent literature, we evaluated how some CT features such as location, size, margins, contrast enhancement are closely related to the malignancy risk and therefore to the outcome.

Imaging features

Cross-sectional imaging techniques are largely used for a variety of conditions and diseases both for diagnostic and interventional purposes (32-49). Ultrasonography is a radiation-free and well-tolerated imaging examination (50-53), but has a limited role in gastrointestinal pathology (54-61). MR has an excellent soft tissue contrast (62-65), but contrast-enhanced MDCT is the preferred technique for the diagnosis, staging and follow-up (66-73). The aspect of GISTs on imaging is highly variable with regards to location, relation to stomach-bowel wall, size, margins, pattern of enhancement and other imaging features that modify homogeneity of the lesion at non contrast-enhanced MDCT (hemorrhage, necrosis, calcifications, intralesional cavitation and cystic degeneration) (74, 75).

At the time of diagnosis with imaging GISTs could have variable dimensions range, measuring less than 1 cm to very large lesions measuring upwards of 35 cm (median 5 cm) (15). The tumors generally present as single nodules but they can consist also of multiple nodules. They are usually solid but can have central cystic degeneration. Calcification is an unusual feature of GISTs; it may occur in a smudged pattern or be present extensively throughout the tumor (Fig. 1) (22-24). Sharp et al. in their cases showed that central areas of low attenuation coincide with hemorrhage, necrosis, or cyst formation (76). Scatarige et al. said that lesions with extensive hemorrhage or necro-

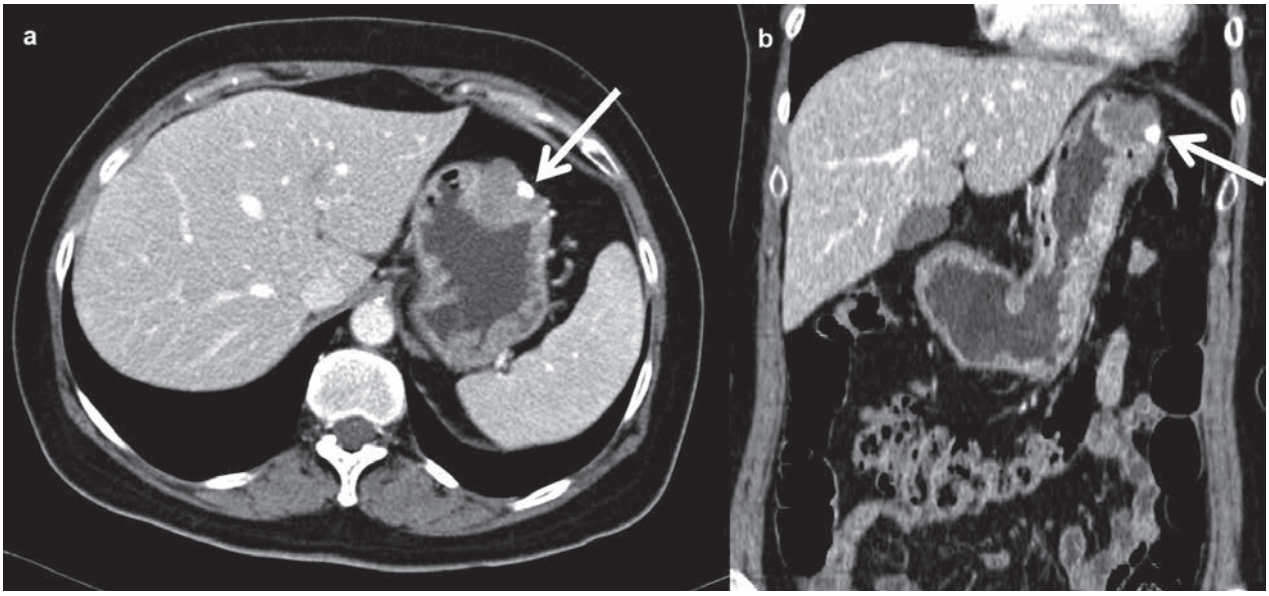

Figure 1. Axial (a) and coronal (b) contrast enhanced MDCT images in the portal venous phase show an intraluminal mass of gastric corpus (white arrows). This GIST presents heterogeneous contrast enhancement, irregular margins and size < 5 cm with centimetric intralesional calcification

sis may form large cystic spaces or cavities which may communicate with the gastro-intestinal lumen (77).

Through evaluation with contrast-enhancement MDCT, these tumors may show smooth and regular margins or irregular and jagged borders (78, 79) (Fig. 2, Fig. 3).

All patterns of enhancement on contrast-enhanced MDCT can be seen with GISTs, including hypoenhancing, isoenhancing, and hyperenhancing neoplasms (Fig. 4).

A peripheral enhancement pattern is present in the majority (92%) of cases on contrast-enhanced MDCT images. Homogeneous enhancement is present in a small part (8%) of cases (80). Contrast-enhanced MDCT may also demonstrate evidence of adjacent organ invasion, ascites, omental and peritoneal diffusion of tumor, or liver metastases (81-83) (Fig. 5, Fig. 6).

Prognostic system

Numerous prognostic systems have been proposed for the assessment of disease progression risk of GISTs, defined as the appearance of metastasis or tumor-related death. The most widely used systems today are the AFIP, the NIH, Joensuu modified NIH, and the Memorial Sloan Kettering Cancer Center nomogram.

The AFIP criteria were developed by Miettinen et al. in 2006 and based on previous AFIP studies reporting on 1055 gastric, 156 duodenal, 906 jejunal/ileal and 144 colorectal GISTs with no statistical validation.

Nevertheless, it remains uncertain which system is the most accurate. More validation and comparison studies are required to determine the optimal prognostic system for GISTs (23, 30, 84).

Imaging vs Prognosis

In the assessment of risk stratification, the AFIP criteria allow to subdivide these neoplasms in relation to the site of origin, GISTs located in the stomach turn out to be the least aggressive, followed by the duodenum or rectum and jejunum or ileum, characterized by greater risk of progression (85, 86).

One of the three main prognostic factors in Miettinen classification is tumor size: tumors smaller than 5 cm have a favorable prognosis, intermediate

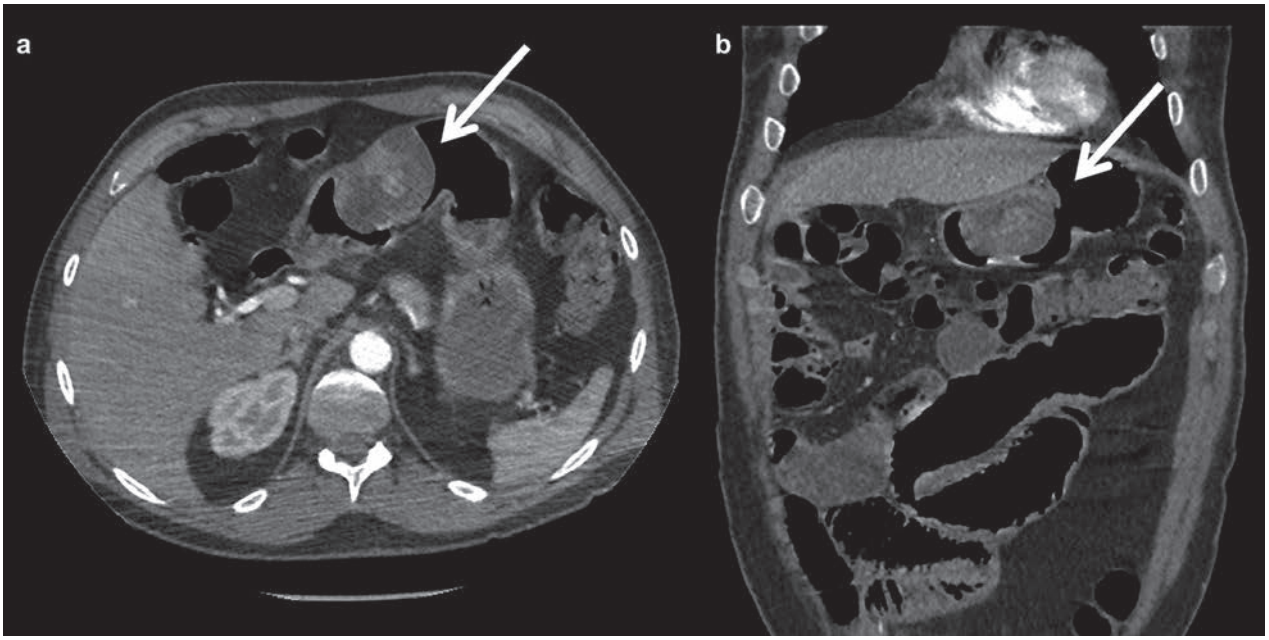

Figure 2. Axial (a) and coronal (b) contrast enhanced MDCT images in the arterial phase demonstrate a voluminous GIST on the anterior wall of gastric corpus (white arrows). The lesion shows heterogeneous contrast enhancement, regular margins and size > 5 ≤ 10 cm

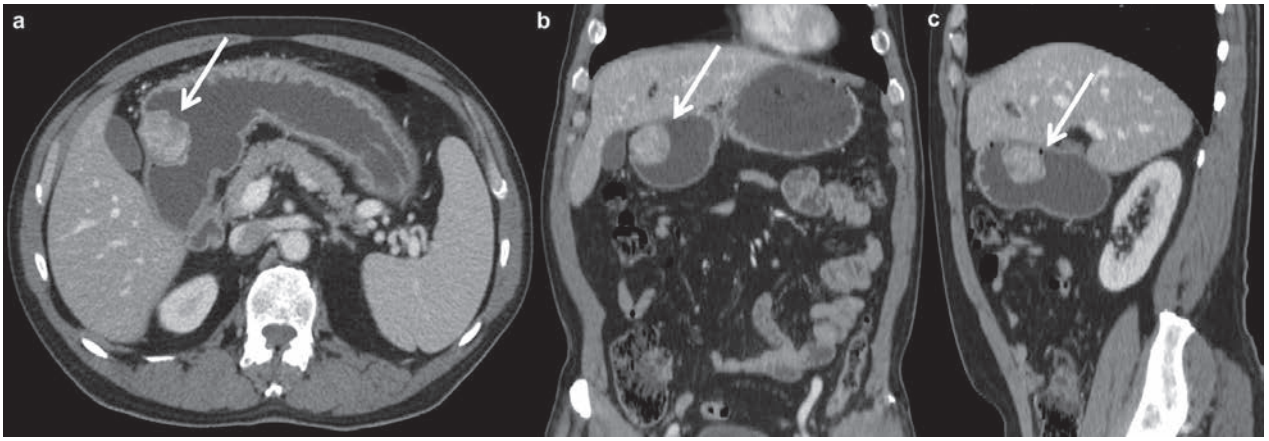

Figure 3. Axial (a), coronal (b) and sagittal (c) contrast enhanced MDCT images in the portal venous phase demonstrate an intraluminal mass of gastric corpus (white arrows). The lesion presents heterogeneous contrast enhancement, irregular margins and size < 5 cm.

between 5 and 10 cm and unfavorable greater than 10 cm (31).

Another important aspect to stress is the significant associations of several MDCT features with the size of the tumor. Some MDCT features could be observed more frequently with increasing tumor size. In fact neoplasm size seems to be statistically significantly associated with the pattern of contrast enhancement, necrosis, the shape of margins and adjacent organ invasion (76).

Zhou et al. in their study demonstrated that the analysis of the distribution of all these parameters among the different classes of size showed that heterogeneous contrast enhancement, irregular margins, and the other previously mentioned features (hemorrhage, necrosis, intralesional cavitation, cystic degeneration)

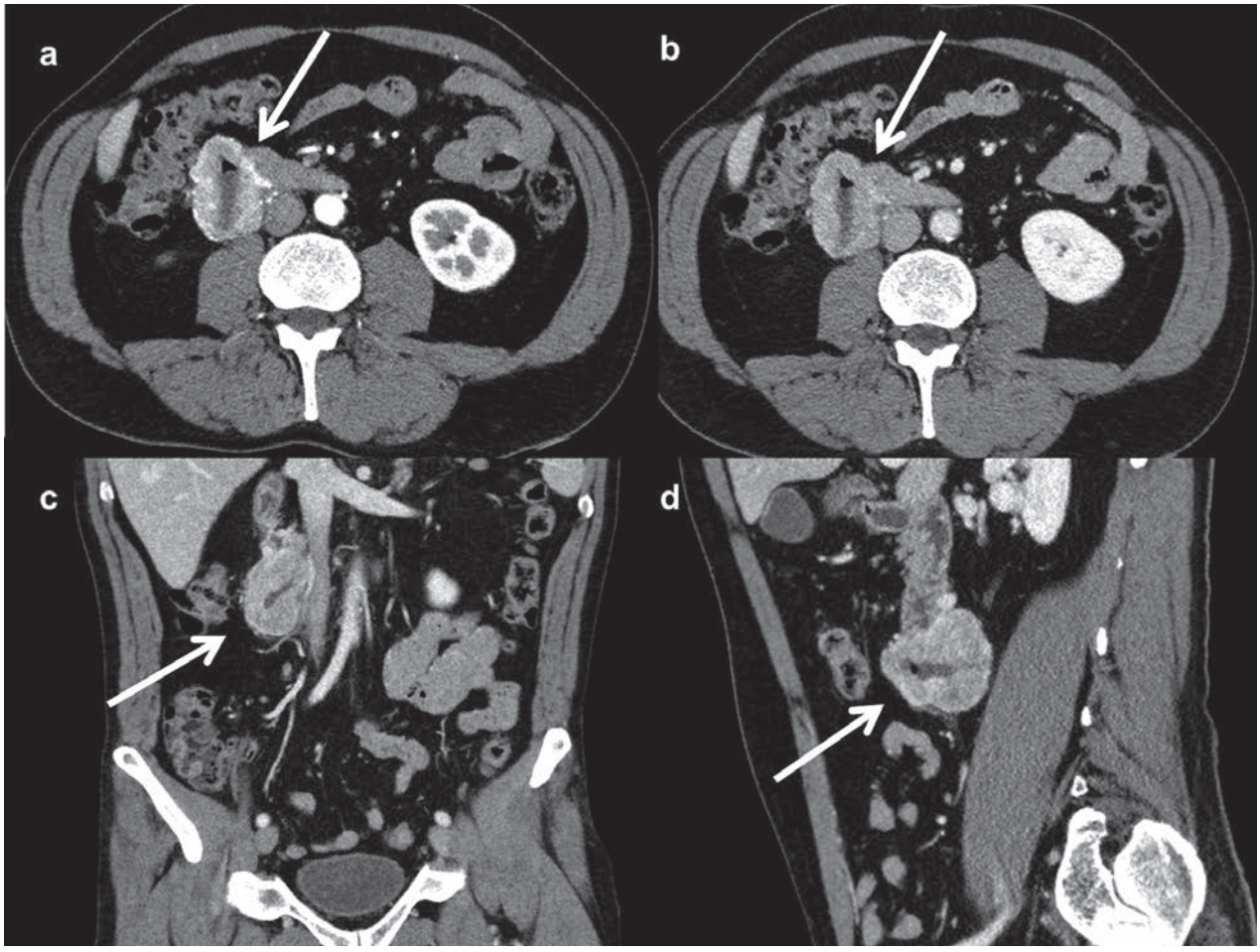

Figure 4. Axial (a,b), coronal (c) and sagittal (d) contrast enhanced MDCT images in the arterial (a) and the portal venous phase (b,c,d) show an exophytic mass of the duodenum (white arrows), strictly adjacent to the inferior vena cava. This GIST presents heterogeneous contrast enhancement, irregular margins, size > 5 ≤ 10 cm and a central area with necrosis and cavitation

trend to grow up with the increase of the size of tumor, being mostly detected in tumors sized 5 to 10 and greater than 10 cm (87-90).

The presence of single or multiple nodules is not correlated with an increased risk of disease progression. The finding of intralesional calcifications seems to be an aspecific parameter and not related to the prognosis. On the other hand, hemorrhage, necrosis, intralesional cavitation and cystic degeneration are associated with an increased risk of malignancy and therefore of disease progression (91).

Moreover, a significant association has been observed between shape of lesion margins and mitotic index (closely related to the outcome): most of lesions with a number of mitoses less than or equal to 5/50 HPFs showed regular margins, suggesting that solid lesions with smooth and not crispy borders could be less aggressive than the ones with jagged borders (75, 80). The presence of irregular margins showed a linear correlation with the risk classes, as it was absent in the none, very low, and low classes, whereas it could be observed in the moderate class and in high class (75, 80). In fact the mean number of mitoses was higher among the lesions with irregular margins compared with the mean value of mitoses detected in neoplasms showing regular margins (80, 92-95).

Many studies demonstrate that the presence of heterogeneous pattern of contrast enhancement is mainly observed in GISTs belonging to the moderate and high classes of risk. On the other hand, tumors

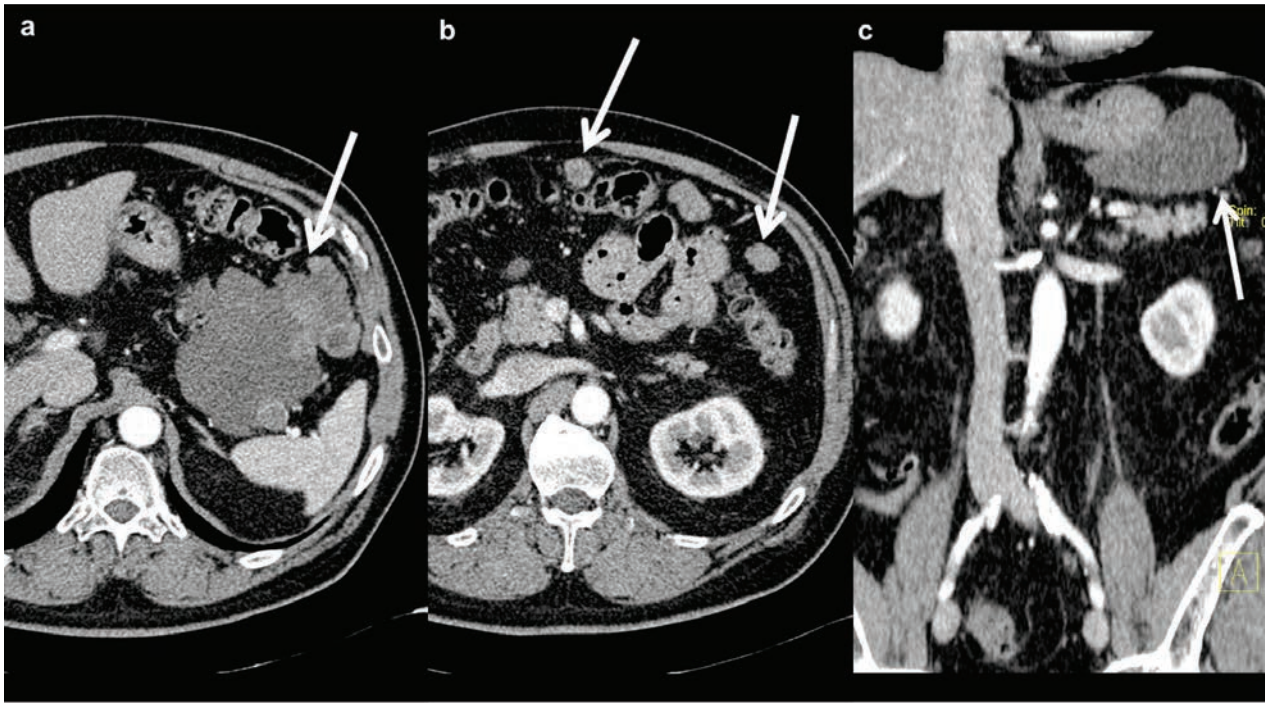

Figure 5. Axial (a) and coronal (c) contrast enhanced MDCT images in the arterial phase demonstrate an extraluminal mass of gastric fundus (white arrows). The lesion shows heterogeneous contrast enhancement, irregular margins and size > 10 cm. Axial (b) contrast-enhanced MDCT image in the arterial phase shows some over-centimetric serosal-based nodules located in mesenteric adipose tissue (white arrows)

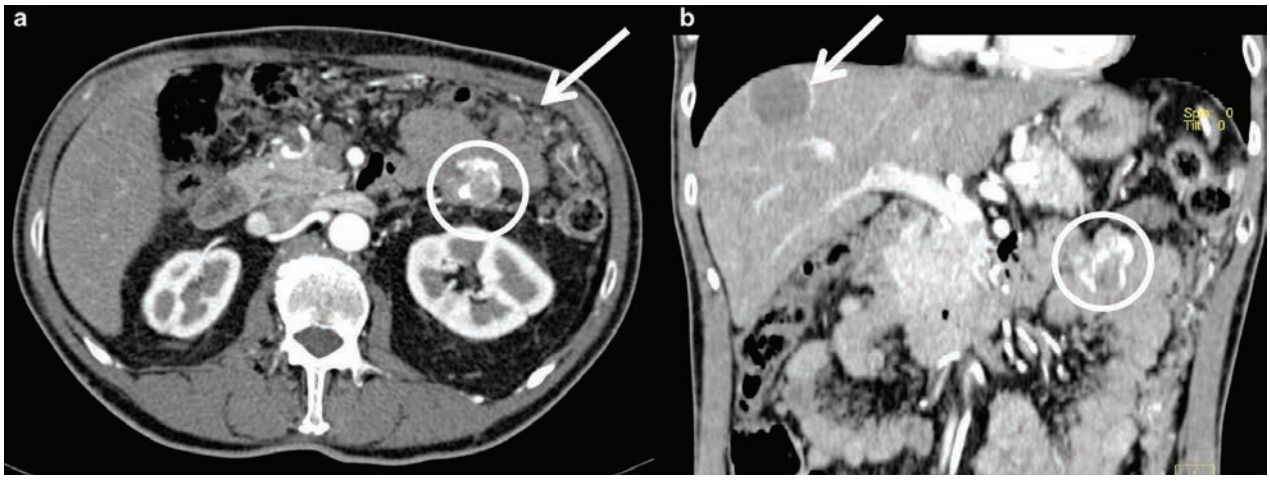

Figure 6. Axial (a) and coronal (b) contrast enhanced MDCT images in the arterial phase demonstrate a nodular mass of the jejunum (white circles). This GIST presents heterogeneous contrast enhancement, irregular margins and size < 5 cm. Just above, there is a diffuse reticular thickening of mesenteric adipose tissue (a, white arrow), suggestive for multiple serosal-based nodules. Furthermore coronal (b) contrast-enhanced MDCT image shows a hypovascular liver metastasis (white arrow)

belonging to the none and very low risk classes appear in most cases as lesions with a homogenous pattern of contrast enhancement (94, 96-104) (Table 1).

Even Levy et al. in their study notice that the degree of contrast enhancement, if high, was considered as a remarkable characteristic of tumor biological activity (74) (Table 2).

Table 1. Relationship between different diagnostic imaging features on MDCT and prognostic outcomes in GISTs

CT characteristics	Favorable prognosis	Intermediate prognosis	Unfavorable prognosis	Author, Year
Site	Stomach	Duodenum or rectum	Jejunum or ileum	Al-Thani et al., 2014
Size	<5 cm	>5 cm <10 cm	>10 cm	Miettenen et al., 2006
Single or multiple	Not related	Not related	Not related	Maldonado et al., 2018
Margins	Regular	/	Irregular	Iannicelli et al., 2009
Enhancement	Homogenous	/	Heterogeneous	Levy et al., 2003

Table 2. GISTs MDCT features that modify the homogeneity: hemorrhage, necrosis, calcifications, intralesional cavitation and cystic degeneration

Tumor characteristics	Characteristics	Prognosis	Author, Year
Hemorrhage	Area of hyper/iso/hypodensity	Unfavorable	Zhou et al., 2016
Necrosis	Area of hypodensity	Unfavorable	Lee et al., 2004
Calcifications	Focal or smudged hyperdensity	Not related	Maldonado et al., 2018
Intra-lesional cavitation	Intralesional hypodensity (air density)	Unfavorable	Kim et al., 2004
Cystic degeneration	Central area of hypodensity	Unfavorable	Maldonado et al., 2018

Discussion

To the best of our knowledge, only few studies had investigated the correlation of GISTs MDCT findings with pathology (74, 90-93). The study of Iannicelli et al. could be considered the first article where many features related to GISTs prognosis and behavior are compared with CT findings to assess whether any MDCT findings could be predictive or specific of the Miettinen classes of risk (80).

In this review we want to underline how unfavorable prognostic aspects are represented by the jejunal-ileal localization, tumor size greater than 10 cm, irregular margins, heterogeneous enhancement and other imaging features that modify homogeneity of lesion at non contrast-enhanced MDCT (hemorrhage, necrosis, intralesional cavitation and cystic degeneration) (87-91). Intermediate prognostic features are duodenal or rectal localization and lesion dimensions between 5 and 10 cm (31, 85). Favorable prognostic elements consist of gastric localization, tumor size below 5 cm, smooth margins, lesion with homogeneous density and homogeneous enhancement (74, 75, 91). The presence of single or multiple lesions and the intralesional calcifications (focal or smudged) do not seem to be correlated with the prognosis (91).

In conclusion MDCT imaging features are crucial in GISTs detection and contribute to the risk stratification evaluating localization and size of the tumor; moreover, MDCT morphological features could be correlated with pathological parameters like the mitotic rate which is the expression of the tumor biology. Therefore, MDCT parameters could give a first step orientation, before the pathological examination, of the biological behavior and the prognostic outcome of GISTs.

Ethical approval: This article does not contain any studies with human participants performed by any of the authors.

Conflict of interest: None to declare

References

1. Scola D, Bahoura L, Copelan A, Shirkhoda A, Sokhandon F. Getting the GIST: a pictorial review of the various patterns of presentation of gastrointestinal stromal tumors on imaging. Abdom Radiol (NY) 2017; 42: 1350-64.
2. Koumarianou A, Economopoulou P, Katsaounis P, et al. Gastrointestinal Stromal Tumors (GIST): A Prospective Analysis and an Update on Biomarkers and Current Treatment Concepts. Biomark Cancer 2015; 7: 1-7.
3. Sanders KM, Koh SD, Ward SM. Interstitial cells of cajal as pacemakers in the gastrointestinal tract. Annu Rev Physiol 2006; 68: 307-43.
4. Rubin BP, Heinrich MC, Corless CL. Gastrointestinal stromal tumour. Lancet 2007; 369: 1731-41.

5. DeMatteo RP, Lewis JJ, Leung D, Mudan SS, Woodruff JM, Brennan MF. Two hundred gastrointestinal stromal tumors: recurrence patterns and prognostic factors for survival. Ann Surg 2000; 231: 51-8.
6. Miettinen M, Sobin LH, Lasota J. Gastrointestinal stromal tumors of the stomach: a clinicopathologic, immunohistochemical, and molecular genetic study of 1765 cases with long-term follow-up. Am J Surg Pathol 2005; 29: 52-68.
7. Tworek JA, Appelman HD, Singleton TP, Greenson JK. Stromal tumors of the jejunum and ileum. Mod Pathol 1997; 10: 200-9.
8. Miettinen M, Sarlomo-Rikala M, Sobin LH, Lasota J. Gastrointestinal stromal tumors and leiomyosarcomas in the colon: a clinicopathologic, immunohistochemical, and molecular genetic study of 44 cases. Am J Surg Pathol 2000; 24: 1339-52.
9. Tworek JA, Goldblum JR, Weiss SW, Greenson JK, Appelman HD. Stromal tumors of the anorectum: a clinicopathologic study of 22 cases. Am J Surg Pathol 1999; 23: 946-54.
10. Tworek JA, Goldblum JR, Weiss SW, Greenson JK, Appelman HD. Stromal tumors of the abdominal colon: a clinicopathologic study of 20 cases. Am J Surg Pathol 1999; 23: 937-45.
11. Miettinen M, Sarlomo-Rikala M, Sobin LH, Lasota J. Esophageal stromal tumors: a clinicopathologic, immunohistochemical, and molecular genetic study of 17 cases and comparison with esophageal leiomyomas and leiomyosarcomas. Am J Surg Pathol 2000; 24: 211-22.
12. Reith JD, Goldblum JR, Lyles RH, Weiss SW. Extragastrointestinal (soft tissue) stromal tumors: an analysis of 48 cases with emphasis on histologic predictors of outcome. Mod Pathol 2000; 13: 577-85.
13. Miettinen M, Monihan JM, Sarlomo-Rikala M, et al. Gastrointestinal stromal tumors/smooth muscle tumors (GISTs) primary in the omentum and mesentery: clinicopathologic and immunohistochemical study of 26 cases. Am J Surg Pathol 1999; 23: 1109-18.
14. Romano L, Pinto A, Imaging of Alimentary Tract Perforation, Springer International Publishing, Springer International Publishing Switzerland, 2015.
15. Demetri GD, Benjamin R, Blanke CD, et al. NCCN Task Force report: optimal management of patients with gastrointestinal stromal tumor (GIST)--expansion and update of NCCN clinical practice guidelines. J Natl Compr Canc Netw 2004; 2 Suppl 1: S-1-26.
16. Agaimy A, Wunsch PH. Lymph node metastasis in gastrointestinal stromal tumours (GIST) occurs preferentially in young patients < or = 40 years: an overview based on our case material and the literature. Langenbecks Arch Surg 2009; 394: 375-81.
17. Miettinen M, Furlong M, Sarlomo-Rikala M, Burke A, Sobin LH, Lasota J. Gastrointestinal stromal tumors, intramural leiomyomas, and leiomyosarcomas in the rectum and anus: a clinicopathologic, immunohistochemical, and molecular genetic study of 144 cases. Am J Surg Pathol 2001; 25: 1121-33.
18. Gold JS, Gonen M, Gutierrez A, et al. Development and validation of a prognostic nomogram for recurrence-free survival after complete surgical resection of localised primary gastrointestinal stromal tumour: a retrospective analysis. Lancet Oncol 2009; 10: 1045-52.
19. Zhao X, Yue C. Gastrointestinal stromal tumor. J Gastrointest Oncol 2012; 3: 189-208.
20. Foo WC, Liegl-Atzwanger B, Lazar AJ. Pathology of gastrointestinal stromal tumors. Clin Med Insights Pathol 2012; 5: 23-33.
21. Miettinen M, Lasota J. Gastrointestinal stromal tumors--definition, clinical, histological, immunohistochemical, and molecular genetic features and differential diagnosis. Virchows Arch 2001; 438: 1-12.
22. Kindblom LG, Remotti HE, Aldenborg F, Meis-Kindblom JM. Gastrointestinal pacemaker cell tumor (GIPACT): gastrointestinal stromal tumors show phenotypic characteristics of the interstitial cells of Cajal. Am J Pathol 1998; 152: 1259-69.
23. Fletcher CD, Berman JJ, Corless C, et al. Diagnosis of gastrointestinal stromal tumors: A consensus approach. Hum Pathol 2002; 33: 459-65.
24. Sarlomo-Rikala M, Kovatich AJ, Barusevicius A, Miettinen M. CD117: a sensitive marker for gastrointestinal stromal tumors that is more specific than CD34. Mod Pathol 1998; 11: 728-34.
25. Palma BD, Guasco D, Pedrazzoni M, et al. Osteolytic lesions, cytogenetic features and bone marrow levels of cytokines and chemokines in multiple myeloma patients: Role of chemokine (C-C motif) ligand 20. Leukemia 2016; 30: 409-16.
26. Mol CD, Dougan DR, Schneider TR, et al. Structural basis for the autoinhibition and STI-571 inhibition of c-Kit tyrosine kinase. J Biol Chem 2004; 279: 31655-63.
27. Canu L, Pradella S, Rapizzi E, et al. Sunitinib in the therapy of malignant paragangliomas: report on the efficacy in a SDHB mutation carrier and review of the literature. Arch Endocrinol Metab 2017; 61: 90-97.
28. Kitayama H, Kanakura Y, Furitsu T, et al. Constitutively activating mutations of c-kit receptor tyrosine kinase confer factor-independent growth and tumorigenicity of factor-dependent hematopoietic cell lines. Blood 1995; 85: 790-8.
29. Nilsson B, Bumming P, Meis-Kindblom JM, et al. Gastrointestinal stromal tumors: the incidence, prevalence, clinical course, and prognostication in the preimatinib mesylate era--a population-based study in western Sweden. Cancer 2005; 103: 821-9.
30. Kang HC, Menias CO, Gaballah AH, et al. Beyond the GIST: mesenchymal tumors of the stomach. Radiographics 2013; 33: 1673-90.
31. Miettinen M, Lasota J. Gastrointestinal stromal tumors: pathology and prognosis at different sites. Semin Diagn Pathol 2006; 23: 70-83.
32. Masciocchi C, Arrigoni F, Ferrari F, et al. Uterine fibroid therapy using interventional radiology mini-invasive treatments: current perspective. Med Oncol 2017; 34: 52.

33. Ferrari F, Arrigoni F, Miccoli A, et al. Effectiveness of Magnetic Resonance-guided Focused Ultrasound Surgery (MRgFUS) in the uterine adenomyosis treatment: technical approach and MRI evaluation. Radiol Med 2016; 121: 153-61.
34. Gatta G, Parlato V, Di Grezia G, et al. Ultrasound-guided aspiration and ethanol sclerotherapy for treating endometrial cysts. Radiol Med 2010; 115: 1330-39.
35. Scialpi M, Cappabianca S, Rotondo A, et al. Pulmonary congenital cystic disease in adults. Spiral computed tomography findings with pathologic correlation and management. Radiol Med 2010; 115: 539-50.
36. Battipaglia G, Avilia S, Morelli E, Caranci F, Perna F, Camera A. Posterior reversible encephalopathy syndrome (PRES) during induction chemotherapy for acute myeloblastic leukemia (AML). Ann Hematol 2012; 91: 1327-28.
37. Briganti F, Leone G, Marseglia M, Cicala D, Caranci F, Maiuri F. P64 Flow Modulation Device in the treatment of intracranial aneurysms: Initial experience and technical aspects. J Neurointerv Surg 2016; 8: 173-80.
38. Arrigoni F, Barile A, Zugaro L, et al. Intra-articular benign bone lesions treated with Magnetic Resonance-guided Focused Ultrasound (MRgFUS): imaging follow-up and clinical results. Med Oncol 2017; 34: 55.
39. Cirillo M, Caranci F, Tortora F, et al. Structural neuroimaging in dementia. J Alzheimers Dis 2012; 29: 16-19.
40. Lagana D, Carrafiello G, Mangini M, et al. Radiofrequency ablation of primary and metastatic lung tumors: preliminary experience with a single center device. Surg Endosc 2006; 20: 1262-7.
41. Bertolini L, Vaglio A, Bignardi L, et al. Subclinical interstitial lung abnormalities in stable renal allograft recipients in the era of modern immunosuppression. Transplant Proc 2011; 43: 2617-23.
42. Sverzellati N, Calabrò E, Chetta A, et al. Visual score and quantitative CT indices in pulmonary fibrosis: Relationship with physiologic impairment. Radiol Med 2007; 112: 1160-72.
43. Carrafiello G, Dionigi G, Ierardi AM, et al. Efficacy, safety and effectiveness of image-guided percutaneous microwave ablation in cystic renal lesions Bosniak III or IV after 24 months follow up. Int J Surg 2013; 11 Suppl 1: S30-5.
44. Macchi M, Belfiore MP, Floridi C, et al. Radiofrequency versus microwave ablation for treatment of the lung tumours: LUMIRA (lung microwave radiofrequency) randomized trial. Med Oncol 2017; 34: 96.
45. Tarantini G, Favaretto E, Napodano M, et al. Design and methodologies of the postconditioning during coronary angioplasty in acute myocardial infarction (POST-AMI) trial. Cardiology 2010; 116: 110-16.
46. Regine G, Stasolla A, Miele V. Multidetector computed tomography of the renal arteries in vascular emergencies. Eur J Radiol 2007; 64: 83-91.
47. De Cecco CN, Buffa V, Fedeli S, et al. Preliminary experience with abdominal dual-energy CT (DECT): True versus virtual nonenhanced images of the liver. Radiol Med 2010; 115: 1258-66.
48. Buffa V, Solazzo A, D'Auria V, et al. Dual-source dual-energy CT: dose reduction after endovascular abdominal aortic aneurysm repair. Radiol Med 2014; 119: 934-41.
49. Cappabianca S, Iaselli F, Reginelli A, et al. Value of diffusion-weighted magnetic resonance imaging in the characterization of complex adnexal masses. Tumori 2013; 99: 210-17.
50. Brunese L, Romeo A, Iorio S, et al. Thyroid B-flow twinkling sign: a new feature of papillary cancer. Eur J Endocrinol 2008; 159: 447-51.
51. Mocchegiani F, Vincenzi P, Coletta M, et al. Prevalence and clinical outcome of hepatic haemangioma with specific reference to the risk of rupture: A large retrospective cross-sectional study. Dig Liver Dis 2016; 48: 309-14.
52. di Giacomo V, Trinci M, van der Byl G, Catania VD, Calisti A, Miele V. Ultrasound in newborns and children suffering from non-traumatic acute abdominal pain: imaging with clinical and surgical correlation. J Ultrasound 2015; 18: 385-93.
53. Iacobellis F, Segreto T, Berritto D, et al. A rat model of acute kidney injury through systemic hypoperfusion evaluated by micro-US, color and PW-Doppler. Radiol Med 2018;
54. Dionigi G, Dionigi R, Rovera F, et al. Treatment of high output entero-cutaneous fistulae associated with large abdominal wall defects: single center experience. Int J Surg 2008; 6: 51-6.
55. Ierardi AM, Lucchina N, Petrillo M, et al. Systematic review of minimally invasive ablation treatment for locally advanced pancreatic cancer. Radiol Med 2014; 119: 483-98.
56. Lo Re G, Cappello M, Tudisca C, et al. CT enterography as a powerful tool for the evaluation of inflammatory activity in Crohn's disease: Relationship of CT findings with CDAI and acute-phase reactants. Radiol Med 2014; 119: 658-66.
57. Salvolini L, Urbinati C, Valeri G, Ferrara C, Giovagnoni A. Contrast-enhanced MR cholangiography (MRCP) with GD-EOB-DTPA in evaluating biliary complications after surgery. Radiol Med 2012; 117: 354-68.
58. Cappabianca S, Reginelli A, Monaco L, Del Vecchio L, Di Martino N, Grassi R. Combined videofluoroscopy and manometry in the diagnosis of oropharyngeal dysphagia: Examination technique and preliminary experience. Radiol Med 2008; 113: 923-40.
59. Maggialetti N, Capasso R, Pinto D, et al. Diagnostic value of computed tomography colonography (CTC) after incomplete optical colonoscopy. Int J Surg 2016; 33 Suppl 1: S36-44.
60. Mandato Y, Reginelli A, Galasso R, Iacobellis F, Berritto D, Cappabianca S. Errors in the Radiological Evaluation of the Alimentary Tract: Part I. Semin Ultrasound CT MR 2012; 33: 300-07.
61. Reginelli A, Mandato Y, Solazzo A, Berritto D, Iacobellis F, Grassi R. Errors in the Radiological Evaluation of the Alimentary Tract: Part II. Semin Ultrasound CT MR 2012; 33: 308-17.
62. Schicchi N, Valeri G, Moroncini G, et al. Myocardial perfusion defects in scleroderma detected by contrast-enhanced

cardiovascular magnetic resonance. Radiol Med 2014; 119: 885-94.
63. Maggialetti N, Ferrari C, Minoia C, et al. Role of WB-MR/DWIBS compared to 18F-FDG PET/CT in the therapy response assessment of lymphoma. Radiol Med 2016; 121: 132-43.
64. Cortellini A, Verna L, Porzio G, et al. Predictive value of skeletal muscle mass for immunotherapy with nivolumab in non-small cell lung cancer patients: A "hypothesis-generator" preliminary report. Thorac Cancer 2019; 10: 347-51.
65. Cortellini A, Palumbo P, Porzio G, et al. Single-institution study of correlations between skeletal muscle mass, its density, and clinical outcomes in non-small cell lung cancer patients treated with first-line chemotherapy. Thorac Cancer 2018; 9: 1623-30.
66. Splendiani A, Perri M, Marsecano C, et al. Effects of serial macrocyclic-based contrast materials gadoterate meglumine and gadobutrol administrations on gadolinium-related dentate nuclei signal increases in unenhanced T1-weighted brain: a retrospective study in 158 multiple sclerosis (MS) patients. Radiol Med 2018; 123: 125-34.
67. Grassi R, Rambaldi PF, Di Grezia G, et al. Inflammatory bowel disease: Value in diagnosis and management of MDCT-enteroclysis and 99mTc-HMPAO labeled leukocyte scintigraphy. Abdom Imaging 2011; 36: 372-81.
68. Tedeschi E, Caranci F, Giordano F, Angelini V, Cocozza S, Brunetti A. Gadolinium retention in the body: what we know and what we can do. Radiol Med 2017; 122: 589-600.
69. Cappabianca S, Porto A, Petrillo M, et al. Preliminary study on the correlation between grading and histology of solitary pulmonary nodules and contrast enhancement and [18F] fluorodeoxyglucose standardised uptake value after evaluation by dynamic multiphase CT and PET/CT. J Clin Pathol 2011; 64: 114-19.
70. Valentini V, Buquicchio GL, Galluzzo M, et al. Intussusception in Adults: The Role of MDCT in the Identification of the Site and Cause of Obstruction. Gastroenterol Res Pract 2016; 2016: 5623718-18.
71. Pradella S, Lucarini S, Colagrande S. Liver lesion characterization: the wrong choice of contrast agent can mislead the diagnosis of hemangioma. AJR Am J Roentgenol 2012; 199: W662.
72. Sforza V, Martinelli E, Ciardiello F, et al. Mechanisms of resistance to anti-epidermal growth factor receptor inhibitors in metastatic colorectal cancer. World J Gastroenterol 2016; 22: 6345-61.
73. Valeri G, Mazza FA, Maggi S, et al. Open source software in a practical approach for post processing of radiologic images. Radiol Med 2015; 120: 309-23.
74. Levy AD, Remotti HE, Thompson WM, Sobin LH, Miettinen M. Gastrointestinal stromal tumors: radiologic features with pathologic correlation. Radiographics 2003; 23: 283-304, 456; quiz 532.
75. Iannicelli E, Scavone G, Speranza A, Sessa B, David V. [MDCT in GIST evaluation.]. Clin Ter 2009; 160: 201-6.
76. Sharp RM, Ansel HJ, Keel SB. Best cases from the AFIP: gastrointestinal stromal tumor. Armed Forces Institute of Pathology. Radiographics 2001; 21: 1557-60.
77. Scatarige JC, Fishman EK, Jones B, Cameron JL, Sanders RC, Siegelman SS. Gastric leiomyosarcoma: CT observations. J Comput Assist Tomogr 1985; 9: 320-7.
78. Sandrasegaran K, Rajesh A, Rushing DA, Rydberg J, Akisik FM, Henley JD. Gastrointestinal stromal tumors: CT and MRI findings. Eur Radiol 2005; 15: 1407-14.
79. Ghanem N, Altehoefer C, Furtwangler A, et al. Computed tomography in gastrointestinal stromal tumors. Eur Radiol 2003; 13: 1669-78.
80. Iannicelli E, Carbonetti F, Federici GF, et al. Evaluation of the Relationships Between Computed Tomography Features, Pathological Findings, and Prognostic Risk Assessment in Gastrointestinal Stromal Tumors. J Comput Assist Tomogr 2017; 41: 271-78.
81. Hong X, Choi H, Loyer EM, Benjamin RS, Trent JC, Charnsangavej C. Gastrointestinal stromal tumor: role of CT in diagnosis and in response evaluation and surveillance after treatment with imatinib. Radiographics 2006; 26: 481-95.
82. Burkill GJ, Badran M, Al-Muderis O, et al. Malignant gastrointestinal stromal tumor: distribution, imaging features, and pattern of metastatic spread. Radiology 2003; 226: 527-32.
83. Faggian A, Fracella MR, D'Alesio G, et al. Small-Bowel Neoplasms: Role of MRI Enteroclysis. Gastroenterol Res Pract 2016; 2016: 9686815.
84. Khoo CY, Chai X, Quek R, Teo MCC, Goh BKP. Systematic review of current prognostication systems for primary gastrointestinal stromal tumors. Eur J Surg Oncol 2018; 44: 388-94.
85. Al-Thani H, El-Menyar A, Rasul KI, et al. Clinical presentation, management and outcomes of gastrointestinal stromal tumors. Int J Surg 2014; 12: 1127-33.
86. Min KW, Leabu M. Interstitial cells of Cajal (ICC) and gastrointestinal stromal tumor (GIST): facts, speculations, and myths. J Cell Mol Med 2006; 10: 995-1013.
87. Zhou C, Duan X, Zhang X, Hu H, Wang D, Shen J. Predictive features of CT for risk stratifications in patients with primary gastrointestinal stromal tumour. Eur Radiol 2016; 26: 3086-93.
88. Lee CM, Chen HC, Leung TK, Chen YY. Gastrointestinal stromal tumor: Computed tomographic features. World J Gastroenterol 2004; 10: 2417-8.
89. Tang L, Li J, Li ZY, et al. MRI in predicting the response of gastrointestinal stromal tumor to targeted therapy: a patient-based multi-parameter study. BMC Cancer 2018; 18: 811.
90. Kim HC, Lee JM, Choi SH, et al. Imaging of gastrointestinal stromal tumors. J Comput Assist Tomogr 2004; 28: 596-604.
91. Maldonado FJ, Sheedy SP, Iyer VR, et al. Reproducible imaging features of biologically aggressive gastrointestinal stromal tumors of the small bowel. Abdom Radiol (NY) 2018; 43: 1567-74.

92. Pinaikul S, Woodtichartpreecha P, Kanngurn S, Leelakiatpaiboon S. 1189 Gastrointestinal stromal tumor (GIST): computed tomographic features and correlation of CT findings with histologic grade. J Med Assoc Thai 2014; 97: 1189-98.
93. Baheti AD, Shinagare AB, O'Neill AC, et al. MDCT and clinicopathological features of small bowel gastrointestinal stromal tumours in 102 patients: a single institute experience. Br J Radiol 2015; 88: 20150085.
94. Tateishi U, Hasegawa T, Satake M, Moriyama N. Gastrointestinal stromal tumor. Correlation of computed tomography findings with tumor grade and mortality. J Comput Assist Tomogr 2003; 27: 792-8.
95. Rossi S, Miceli R, Messerini L, et al. Natural history of imatinib-naive GISTs: a retrospective analysis of 929 cases with long-term follow-up and development of a survival nomogram based on mitotic index and size as continuous variables. Am J Surg Pathol 2011; 35: 1646-56.
96. Horton KM, Juluru K, Montogomery E, Fishman EK. Computed tomography imaging of gastrointestinal stromal tumors with pathology correlation. J Comput Assist Tomogr 2004; 28: 811-7.
97. Da Ronch T, Modesto A, Bazzocchi M. Gastrointestinal stromal tumour: spiral computed tomography features and pathologic correlation. Radiol Med 2006; 111: 661-73.
98. Kim HC, Lee JM, Kim KW, et al. Gastrointestinal stromal tumors of the stomach: CT findings and prediction of malignancy. AJR Am J Roentgenol 2004; 183: 893-8.
99. Bozzetti C, Nizzoli R, Tiseo M, et al. ALK and ROS1 rearrangements tested by fluorescence in situ hybridization in cytological smears from advanced non-small cell lung cancer patients. Diagnostic Cytopathology, vol. 43, p. 941-946, ISSN: 8755-1039, doi: 10.1002/dc.23318
100. De Filippo M, Onniboni M, Rusca M, et al. (2008). Advantages of multidetector row CT with multiplanar reformation in guiding percutaneous lung biopsies. RAD. MED, vol. 113, p. 945-953, ISSN: 0033-8362, doi: 10.1007/s11547-008-0325-y
101. Gafà G, Sverzellati N, Bonati E, et al (2012). Follow-up in pulmonary sarcoidosis: comparison between HRCT and pulmonary function tests. RAD. MED, vol. 117, p. 968-978, ISSN: 0033-8362, doi: 10.1007/s11547-012-0827-5
102. Barile A, Bruno F, Mariani S, et al. What can be seen after rotator cuff repair: a brief review of diagnostic imaging findings. Musculoskelet Surg. 2017 Mar;101(Suppl 1):3-14. doi: 10.1007/s12306-017-0455-2. Epub 2017 Feb 13. Review.
103. De Filippo M, Gira F, Corradi D, Sverzellati N, Zompatori M, Rossi C. (2011). Benefits of 3D technique in guiding percutaneous retroperitoneal biopsies. RAD. MED, vol. 116(3), p. 407-416, ISSN: 0033-8362, doi: 10.1007/s11547-010-0604-2
104. Ulusan S, Koc Z, Kayaselcuk F. Gastrointestinal stromal tumours: CT findings. Br J Radiol 2008; 81: 618-23.

Received: 26 March 2019
Accepted: 4 April 2019
Correspondence:
Silvia Pradella, MD
Department of Radiology - Careggi University Hospital
L.go G.A. Brambilla, 3 - 50134 Florence, Italy
E-mail: pradella3@yahoo.it

Acta Biomed 2019; Vol. 90, Supplement 5: 20-37 DOI: 10.23750/abm.v90i5-S.8344

Review

Internal hernias: a difficult diagnostic challenge. Review of CT signs and clinical findings

Monica Marina Lanzetta[1], Antonella Masserelli[1], Gloria Addeo[1], Diletta Cozzi[1], Nicola Maggialetti[2], Ginevra Danti[1], Lina Bartolini[1], Silvia Pradella[1], Andrea Giovagnoni[3], Vittorio Miele[1]

[1]Department of Radiology, Careggi University Hospital, Florence, Italy; [2]Department of Medicine and Health Sciences "V. Tiberio", University of Molise, Campobasso, Italy; [3] Department of Radiology, Università Politecnica delle Marche, Ancona, Italy

Summary. Although internal hernias are uncommon, they must be beared in mind in the differential diagnosis in cases of intestinal obstruction, especially in patients with no history of previous surgery or trauma. Because of the high possibility of strangulation and ischemia of the affected loops, internal hernias represent a potentially life-threatening condition and surgical emergency that needs to be quickly recognized and managed promptly. Imaging plays a leading role in the diagnosis and in particular multidetector computed tomography (MDCT), with its thin-section and high-resolution multiplanar reformatted (MPR) images, represents the first line image technique in these patients. The purpose of the present paper is to illustrate the characteristic anatomic location, the clinical findings and the CT appearance associated with main types of internal hernia, including paraduodenal, foramen of Winslow, pericecal, sigmoid-mesocolon- and trans-mesenteric- related, transomental, supravesical and pelvic hernias. (www.actabiomedica.it)

Key words: internal hernias, computed tomography, peritoneal cavity, small bowel obstruction, strangulation, mesentery, Roux -en-Y anastomosis

Introduction

An internal hernia (IH) is defined as the protrusion of abdominal viscera, most commonly small bowel loops, through a peritoneal or mesenteric aperture into a compartment in the abdominal and pelvic cavity (1-3). Cross-sectional imaging (MRI, CT and US) (4-7) techniques, gained large application in gastrointestinal radiology in the emergency department; they are is indicated as first line techniques in the diagnosis, staging and follow-up (8-23).

Hernial orifices can be congenital, including both normal foramina or recesses and unusual apertures resulting from anomalies of peritoneal attachment and internal rotation, or acquired if caused by inflammation, trauma and previous surgery, like gastric by-pass for bariatric treatment and liver transplantation. Due to the growing popularity of these surgical procedures, the overall incidence of internal hernias has been recently increasing (24). Although relatively uncommon, they represent a potentially life-threatening condition and a surgical emergency since the bowel entrapment in one of the defects can lead to acute intestinal obstruction with rapid evolution, if left untreated, into strangulation and ischemia. According to various investigators, internal hernias cause up to 5,8% of all small bowel obstruction (SBO) (3, 24-27), with a high overall mortality rate that can exceed 50% (26).

The most common manifestation of an internal hernia is strangulating SBO, that occurs after a closed-

loop obstruction (2, 11, 28, 29). However, the clinical manifestations range from mild digestive symptoms to acute abdomen, as symptom severity relates to duration and reducibility of the hernia and the presence or absence of strangulation and incarceration (24, 25, 30, 31). IHs may remain clinically silent if easily reducible, but the larger ones often cause mild discomfort ranging from constant vague epigastric pain to intermittent periumbilical pain as they occasionally show spontaneous reduction, abdominal distention, nausea and vomiting. Physical examination may reveal a palpable mass of herniated loops with localized tenderness (2, 32, 33).

This non-specific clinical presentation often leads to a delay in diagnosis, in most cases made at the time of laparotomy (3, 26), and consequently in proper treatment, carrying risk of serious complications; therefore, when the possibility of internal hernia is considered, a rapid imaging evaluation is necessary to aid an early diagnosis and a prompt intervention. Multidetector Computed Tomography (MDCT), with its wide availability, has become the first line imaging technique in these patients and play an important role in the preoperative diagnosis and planning of surgical intervention (33-37).

Classification

According to the traditional classification devised by Welch, eight main types of internal hernia can be identified on the basis of the topographic distribution of bowel loops related to the anatomic location of the orifice (38) (Fig. 1).

Despite classically paraduodenal hernia has been described as the most common type of IH, recently transmesenteric hernias have reached a higher incidence, in relation to the increasing frequency of surgical procedures in which a Roux-en-Y loop is constructed (39, 40)

Doishita et al. proposed a categorization of the various types of internal hernia in three main groups according to the type of hernia orifice, depending on whether the herniation occurs through a normal foramen, an unusual peritoneal fossa or recess into the retroperitoneum, or an abnormal opening in a mesentery or peritoneal ligament (33).

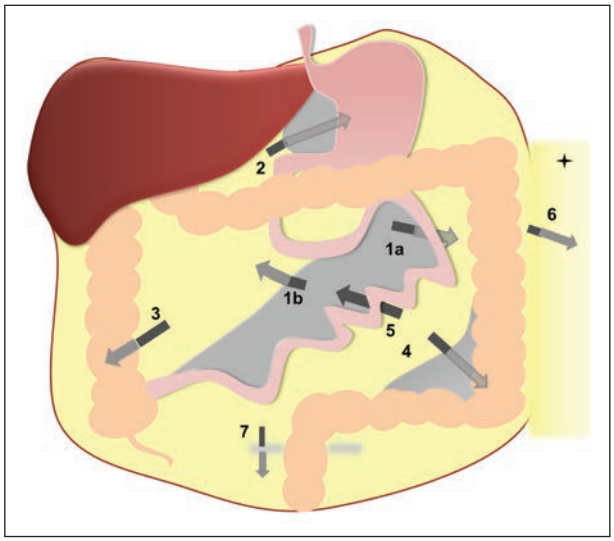

Figure 1. Drawing shows the anatomic sites of internal hernias: 1a: left paraduodenal hernia, 1b: right paraduodenal hernia, 2: foramen of Winslow hernia; 3: pericecal hernia; 4: sigmoid-mesocolon- related hernia; 5:transmesenteric hernia; 6: transomental hernia; 7:supravesical and pelvic hernia. Asterisk: greater omentum open and reflected laterally

Role of computed tomography

Since the interval between intestinal obstruction and ischemia may be short, a time-consuming diagnostic workup before surgery may be dangerous for an acutely ill patient (25, 41). CT, with its speed of execution, is the imaging modality of choice for the investigation of acute abdominal conditions (3, 42-45) and in particular is recommended for the evaluation of patients with acute SBO, particularly when clinical and initial plain film radiography indicates a higher grade obstruction or remains indeterminate e/o strangulation is suspected (46). Several studies have demonstrated the accuracy of CT in the detection of small bowel obstruction, with a sensitivity and specificity of 94-100% and 90-95% respectively (47-50). CT plays a more active role compared to conventional imaging methods in the identification of the site, level, cause of obstruction and the presence of ischemic changes at the involved bowel. Currently, with the possibility of using high quality three dimensional reformation techniques such as multiplanar reformation (MPR), maximum intensity projection (MIP) and volume rendering (VR), CT provides important advantages in

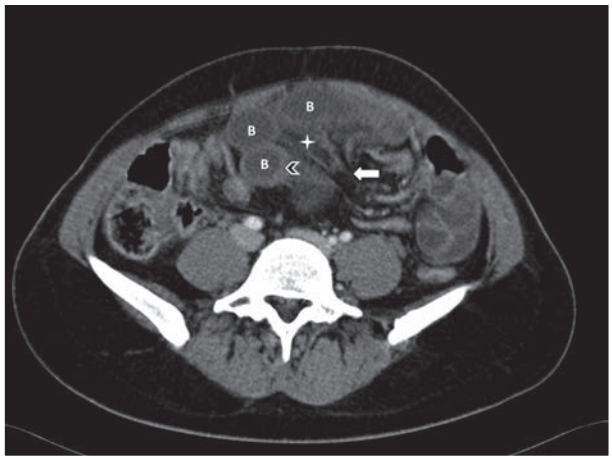

Figure 2. Closed loop small bowel obstruction. Contrast enhanced axial CT scan shows a radial array of distended small bowel loops (B) with stretched and thickened mesenteric vessels converging to a central point (white arrow). Bowel wall thickening (arrowhead) and mesenteric edema (asterisk) can also be observed.

evaluation of small bowel and surrounding structure, increasing the diagnostic confidence in the localization of the transition zone (32, 46). Small bowel obstruction of an internal hernia is usually a closed-loop obstruction, in which a segment of the bowel is occluded at two adjacent points along its course. Direct signs of a closed-loop at CT are a U- or C- shaped, fluid filled, distended intestinal loop or a radial array of distended loops with stretched and thickened mesenteric vessels converging to a central point (33, 47, 48) (Fig. 2). In this setting, a cluster of dilated loops or a 'sac-like appearance' of crowded small bowel loops owing to encapsulation within the hernia sac at an abnormal anatomic location is highly suggestive for IH (26, 33, 51). CT scans show the convergence of bowel, mesenteric fat and vessels of the closed loop in correspondence of the hernia orifice and abnormal displacement of surrounding structure and key vessels around the hernia sac (33) (Tab. 1). If intestinal strangulation is present, engorgement, twisting and dislocation of mesenteric vessels in correspondence of the hernia orifice can also be observed (46),with the detection of reduced bowel wall enhancement in cases of ischemia and pneumoperitoneum, focal discontinuity of the bowel wall and abscess or peritoneal fluid if intestinal perforation occurs (52, 53). Specific CT findings of each internal hernia are reported in table 2.

In the suspicion of IHs the use of intravenous contrast material is crucial for depicting mesenteric vessels, allowing an easier detection of hernias, and for the assessment of bowel wall vascularity. A non-enhanced scan should be obtain to detect an increased unenhanced bowel wall attenuation reflecting haemorrhagic congestion in cases of strangulation(33). A suitable CT protocol is shown in table 3.

Paraduodenal hernias (PDHs)

Background

In the classic literature paraduodenal hernias account for approximately 53% of all cases of internal hernias (3, 32). They are found more frequently in men than in women, with a ratio of 3:1, having a sex predilection unlike most types of internal hernias. There are two main subtypes: left-sided, which account for 75% of all PDHs, and right-sided, which account for the remaining 25% (32, 54, 55). Paraduodenal hernias occur when small bowel loops enter into a congenital, unusual peritoneal fossa in the vicinity of the duode-

Table 1. CT key points of internal hernias

Bowel configuration	• a saclike mass or cluster of dilated small bowel loops within an abnormal anatomic location in the setting of small bowel obstruction
Mesenteric abnormalities	• convergence of vessels and mesenteric fat at the hernia orifice • displacement of key mesenteric vessels • engorgement, crowding, twisting, stretching of mesenteric vessels if strangulation is present
Position of surrounding viscera	• displacement of surrounding structures around the hernia sac

Table 2 CT findings of internal hernia

	Bowel configuration	Mesenteric abnormalities / Anatomic landmark vessels	Effect on surrounding structures
LEFT PARADUODENAL HERNIA	encapsulated agglomerated small bowel loops with a sac-like appearance in the LUQ, lateral to the ascending duodenum, between the stomach and the pancreas, or behind the pancreatic tail, or between the transverse colon and the left adrenal gland	convergence of engorged vessels grouped together at the entrance of the hernia orifice enlargement, stretching and displacement of IMV anteriorly and leftward. IMV and left colic artery at the anterior and medial border of the hernia orifice	displacement of the posterior stomach wall anteriorly and the duodenal flessure and the transverse colon inferiorly
RIGHT PARADUODENAL HERNIA	encapsulated agglomerated small bowel loops with a sac-like appearance in the RUQ, lateral and inferior to the descending duodenum frequent association with small bowel non-rotation	convergence of engorged vessels grouped together at the entrance of the hernia orifice displacement of the SMA, right colic vein and ileocolic artery anteriorly. SMA and SMV at the anteromedial edge of the fossa the jejunal branches of SMA and SMV may be seen coursing posteriorly and to the right of the superior mesenteric vessels location of SMV to the left of and ventral to SMA if malrotation is present	rarely ureter displacement and compression
FORAMEN OF WINSLOW HERNIA	bowel loops in lesser sac between liver hilum and IVC, posterior to the stomach	convergence of engorged vessels grouped together at the entrance of the hernia orifice, elongated in front of IVC and posterior to main portal vein	displacement of the stomach antero-laterally anterior compression of main portal vein
PERICECAL HERNIA	clustered small-bowel loops with a sac-like appearance lateral to the cecum and posterior to the ascending colon in right paracolic gutter	convergence of engorged vessels grouped together at the entrance of the hernia orifice	displacement of the ascending colon anteriorly or medially
SIGMOID-MESOCOLON RELATED HERNIA	clustered small-bowel loops (with a sac-like appearance in intra e inter-mesosigmoid types) posterior and lateral to the sigmoid colon	convergence of engorged vessels grouped together at the entrance of the hernia orifice	displacement of the sigmoid colon antero-medially
TRANSMESENTERIC HERNIA	dilatated small-bowel loops, directly abutting the abdominal wall without omental fat, lateral to colon	convergence of engorged vessels grouped together at the entrance of the hernia orifice displacement of the main mesenteric trunk to the right	central displacement of the colon segments
BROAD LIGAMENT INTERNAL HERNIA	cluster of dilated small bowel loops herniated in the pelvic cavity laterally to the uterus	convergence of engorged vessels grouped together at the entrance of the hernia orifice mesenteric vessels of herniated intestine penetrating the broad ligament	displacement of the rectosigmoid dorso-laterally and of the uterus ventrally enlargement of the distance between uterus and ovary deviating in opposite directions
SUPRAVESICAL INTERNAL HERNIA	cluster of bowel loops with a sac-like appearance in front of the bladder on the left or right	crowded and engorged mesenteric vessels may be seen	compression and displacement of bladder

Table 3. CT scanning protocol

Parameter	Details
Section thickness	Preferably submillimeter (0,5-1 mm)
Interval	Same as section thickness
Scan area	Abdomen (from the xiphoid process down to the symphysis pubis)
Contrast volume	100-150 ml
Contrast flow-rate	3-4 ml/sec
Scan acquisition	• Non-enhanced scan • Arterial phase at 35-40 sec • Venous phase at 70-75 sec
Image reconstruction	• Axial 2-5 mm thickness • Multiplanar reformats in the coronal and sagittal plane at 3 mm thickness

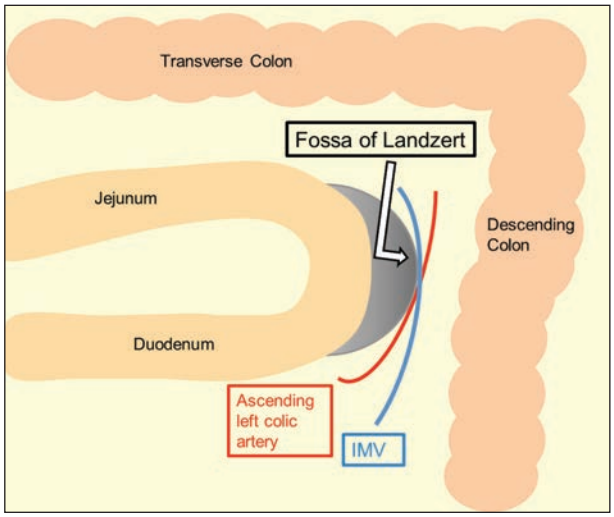

Figure 3. Graphic illustration of Landzert's fossa. The inferior mesenteric vein (IMV) and ascending left colic artery run at the anteromedial edge of the fossa

num as a result of abnormal rotation of the small intestine and failure of mesenteric fusion with the parietal peritoneum (2, 56)

Clinical findings

Patients often have a long standing history of indigestion or periodic cramps, vomiting and abdominal distention commonly dating back to the childhood; in particular postprandial pain which may be relieved by postural changes is a characteristic symptom (57). PDHs carry more than 50% lifetime risk of strangulation and intestinal infarction with a mortality rate of 20-50% (58, 59).

Left paraduodenal hernias (LPDHs)

Description

LPDHs occur when duodenal segments and jejunal loops, more often proximal, prolapse through *Landzert's fossa* (or *paraduodenal fossa*)(60), an aperture found in 2% of autopsy(32) located at the duodenojejunal junction (a zone of confluence of the descending mesocolon, transverse mesocolon and small bowel mesentery)(61), behind the descending mesocolon and to the left of the fourth part of the duodenum (33, 40). This peritoneal pocket is bordered anteriorly by a peritoneal fold lifted up by the inferior mesenteric vein (IMV) and ascending left colic artery that run at the anteromedial edge of the fossa (24, 32) (Fig. 3). In LPDHs bowel loops enter postero-inferiorly through the mesocolic defect, becoming entrapped in the Landzert's fossa, and then extend further into the descending mesocolon and the left portion of the transverse mesocolon (24, 54, 60). Since the afferent loop enters the sac from behind where the duodenum emerges from its fixed retroperitoneal position, only the efferent loop truly passes through the hernia orifice (32).

CT findings

The characteristic CT feature of LPDHs (Fig. 4) is an encapsulated cluster of commonly dilated bowel loops with a sac-like appearance in the left upper quadrant at the level of the anterior para-renal space (33). They can be noted either at the duodeno-jejunal junction between stomach and pancreas, at the level or just above and exterior to the ligament of Treitz, or behind the pancreatic tail or between transverse colon and the left adrenal gland, although these findings are non-specific (24, 60-62). Usually the herniated bowel loops cause mass effect with displacement of the posterior stomach wall anteriorly, the duodenal

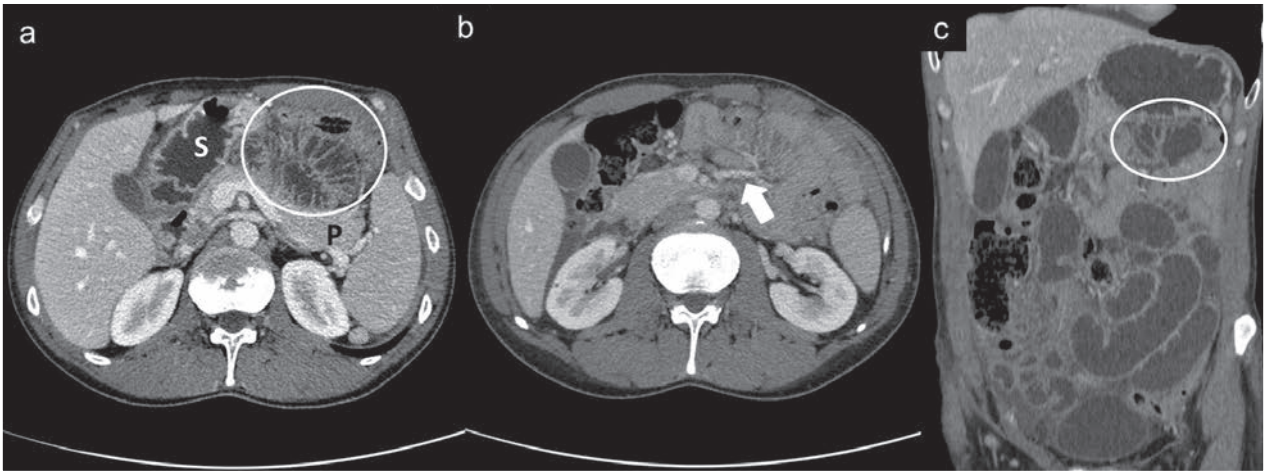

Figure 4. Left paraduodenal hernia in a 37-year-old man who presented with nausea and intense abdominal pain. Contrast-enhanced CT scans, axial (a) and (b) and coronal reformatted image (c), show a sac-like mass of clustered dilated small-bowel loops (white circles) between pancreas (P) and stomach (S) with multiple engorged and prominent vessels (white arrow) at the point of entry of the sac

flessure and the transverse colon inferiorly (1, 38, 40). CT demonstrated IMV and left colic artery as a key anatomic landmark at the anterior and medial border of the hernia orifice (33, 38). Abnormalities of the mesenteric vessel that supply the herniated loops, as crowding, stretching and enlargement at the entrance of the hernia sac as well as stretching and displacement of the IMV laterally to the left can also be observed (2, 38-40). Catalano et al. have reported a case of LPDH associated with volvulus, bowel wall ischemia and intussusception with additional CT findings like the target sign and a sausage-shaped mass composed of alternating high- and low-attenuation layers, indicative of intussusception (45, 63).

Right paraduodenal hernias (RPDHs)

Description

In RPDHs bowel's herniation occurs through the *Waldeyer's fossa* (or *mesentericoparietal fossa*), a congenital uncommon defect in the first part of the jejunal mesentery observed in no more than 1% of the population at autopsy (57). RPDHs occur most frequently in the setting of a non-rotated small intestine and a normally or incompletely rotated colon. The recess is located inferior to the third portion of duodenum, behind the root of the small bowel mesentery and extends rightward and downward into the ascending mesocolon. The superior mesenteric artery (SMA) along with the superior mesenteric vein (SMV), runs along the anteromedial edge of the fossa and represents the landmark for RPDHs (33, 61) (Fig. 5). In RPDHs the small bowel loops entrapped in this peritoneal pocket protrude through it toward the right half of the trans-

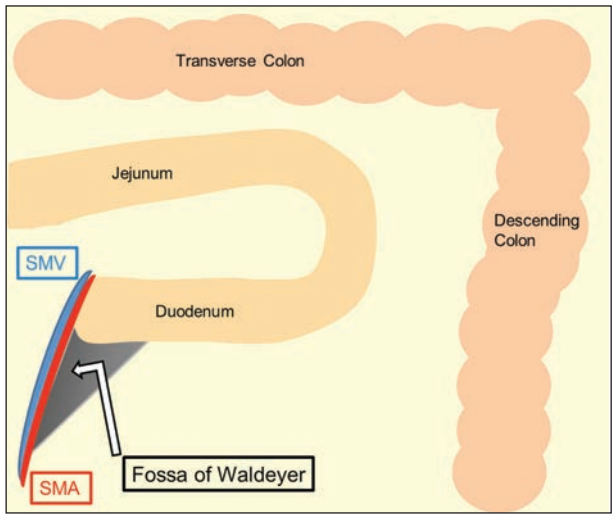

Figure 5. Graphic illustration of Waldeyer's fossa. The superior mesenteric artery (SMA) and the superior mesenteric vein (SMV) run along the anteromedial edge of the fossa

verse mesocolon behind the ascending mesocolon, lying posterior and to the right of the SMA that can be displaced anteriorly along with ileocolic artery and right colic vein, located in the anterior margin of the neck of the hernia sac (24, 38). Because both afferent and efferent loops pass through the hernia orifice where they are closely apposed and narrowed, RPDHs are usually larger and more often fixed than those occurring on the left side (32, 57).

CT findings

The characteristic CT feature of RPDHs (Fig. 6) is an encapsulated cluster of dilated small bowel loops located in the right mid abdomen, lateral and inferior to the descending duodenum (38). In addition, looping of the small intestine around the SMA and SMV at the root of the small bowel mesentery can be observed. In cases of intestinal non rotation the SMV is

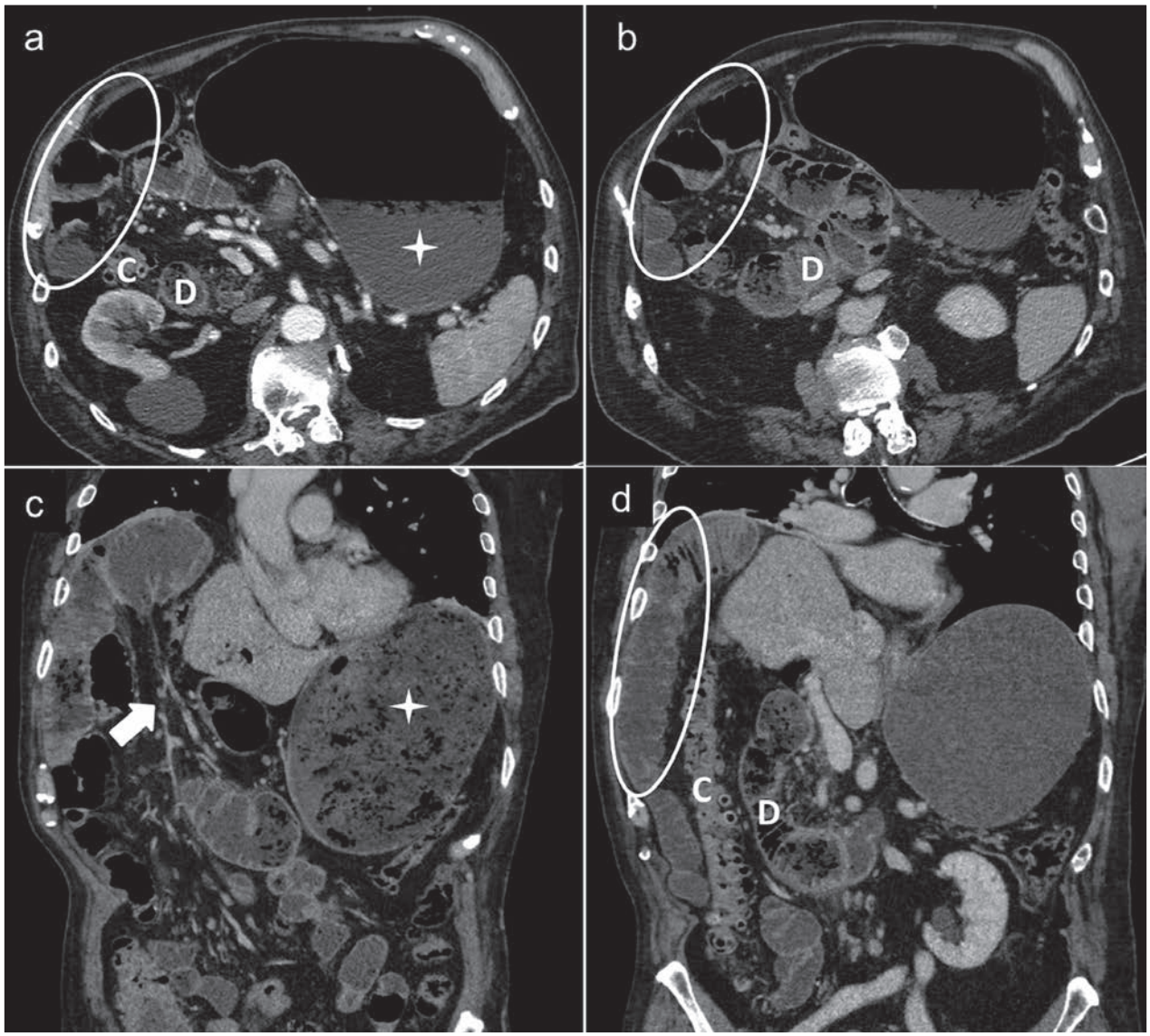

Figure 6. Right paraduodenal hernia in a 83-year-old man with mild abdominal pain and repeated episodes of vomiting for a few hours. Contrast enhanced CT scans, axial (a) and (b) and coronal reformatted image (c) and (d) show an encapsulated cluster of dilated jejunal loops in the right upper quadrant (white circles), lateral to the colon (C) and the II-III portion of duodenum (D) which appears located rightward. Gastric overdistention is also be observed (asterisks). Dilated and converging vessels (white arrow) are seen in the mesentery.

located in a more ventral and leftward position to the SMA and the horizontal duodenum is absent, with cecum in its normal position(61). Rare cases of right ureter displacement and compression have been reported, underlying the retroperitoneal location of this type of hernia (51).

Foramen of Winslow hernias (FWHs)

Background

In the classic literature FWHs constitutes 8% of all internal hernias. Foramen of Winslow hernias are the most common type of "lesser sac hernia", in which viscera enter the lesser sac (a unique remnant of the primitive right peritoneal space) through the foramen of Winslow (Fig. 7). Other types of "lesser sac hernia" include bowel herniation through abnormal aperture in only one leaf of the greater omentum or through the lesser omentum, composed of the gastrohepatic and hepatoduodenal ligaments (33). In 60%-70% of cases the herniated viscera are small bowel loops; the terminal ileum, cecum and ascending colon are involved in about 25-30%. The transverse colon, gallbladder and omentum account for the remainder (32). Several risk factors for this type of hernia have been described, including an enlarged foramen of Winslow, an usually long small bowel mesentery, common intestinal mesentery, an elongated right liver (such as Riedel lobe), persistence of the ascending mesocolon enabling increased mobility of the bowel (2, 64), a lack of fusion between cecum or ascending mesocolon to parietal peritoneum, a defect in the gastrohepatic ligament and finally an incomplete intestinal rotations or malrotations (65).

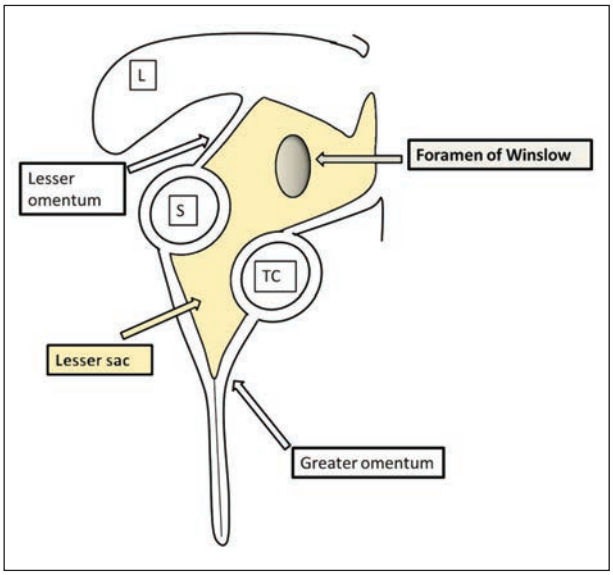

Figure 7. Graphic illustration of lesser sac and foramen of Winslow. L: liver; S:stomach; TC:transverse colon.

Clinical findings

The clinical findings of FWHs are often related to small bowel obstruction and occasionally to gastric outlet obstruction due to a compressive effect on the stomach by the herniated loops (66). Patients often present with an acute onset of a progressive abdominal pain, that can be preceded by a change in abdominal pressure, usually attenuated by forward flexion or in the position of the knee in the chest (32). An obstructive jaundice due to the compression of the hepatic pedicle by herniated gallbladder or bowel loops can also be observed, as reported by Numata et al. (67) and Welaratne et al. (68). Ye et al in 2002 have described the first case of obstructive jaundice and acute pancreatitis caused by a FWHs (69).

Since FWHs are often strangulated at presentation, they are associated with a high mortality rate of up to 49% (65).

Description

The epiploic foramen of Winslow is a congenital aperture located below the right border of the superior recess of the lesser sac, inferior to the caudate lobe of the liver, anterior to the inferior vena cava, superior to the second portion of the duodenum and posterior to the hepatoduodenal ligament (including hepatic artery, portal vein and bile duct). It represent the only communication between the greater and lesser peritoneal cavities (33).

CT findings

The characteristic CT findings of FWHs (Fig. 8) are the following: hydro-aerial levels in the lesser sac,

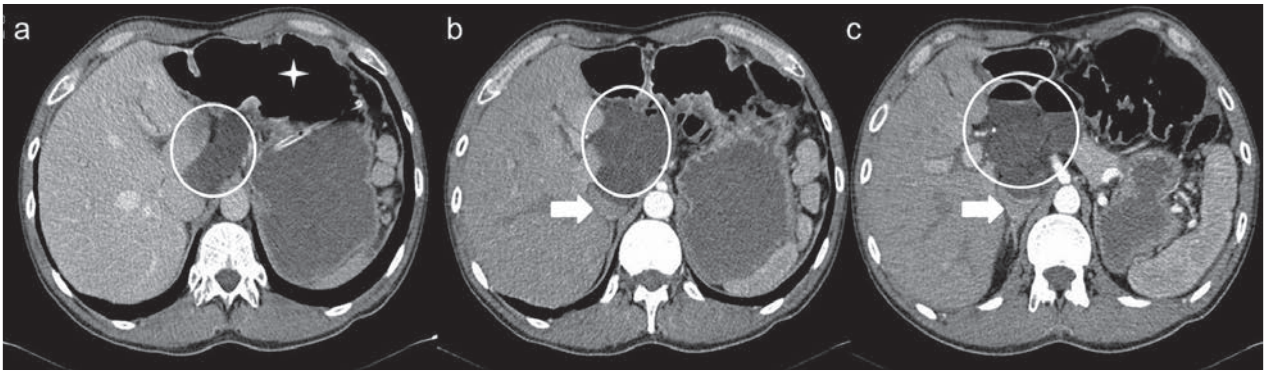

Figure 8. Foramen of Winslow hernia in a 72-year-old man with intermittent epigastric pain. Contrast-enhanced axial CT scans (a), (b) and (c) show cluster of small bowel loops located in the lesser sac (white circles) between liver and pancreas, posterior to stomach (displaced anteriorly) (asterisk) and anterior to inferior vena cava, which is compressed (white arrows)

posterior to the liver and between pancreas and stomach (which can be displaced antero-laterally) with a 'beak' directed toward the foramen of Winslow ('bird beak sign'); mesentery and associated vessels, often stretched through the foramen, located anterior to inferior vena cava and posterior to main portal vein, which can be compressed anteriorly; absence of the caecum and ascending colon in the right gutter; two or more bowel loops in the high sub hepatic space (2, 70). FWHs often presents similar radiographic features to that of left paraduodenal hernias; the absence of an encapsulated membrane is characteristic of the former, conversely a major mass effect on the transverse colon more commonly indicates a left paraduodenal hernia (24, 38).

Pericecal hernias (PCHs)

Background and Description

In the classic literature PCHs correspond of 13% of all internal hernias. Bowel loops, most commonly an ileal segment, herniate into the right paracolic gutter through a congenital or acquired (most commonly by adhesions) unusual defect in the cecal mesentery. Four different recesses in the pericecal region formed by folds of the peritoneum have been described: superior and inferior ileocecal recess, retrocecal recess and paracolic sulci (2, 33, 55). However, the diagnostic features and surgical management of the four subtypes do not differ (60).

Clinical findings

Patients commonly report recurrent episodes of colicky intense right lower abdominal pain. Chronic incarceration may produce symptoms compatible with appendiceal disordes, intestinal diseases or intestinal obstruction caused by adhesions (32). In PCHs however have been reported a higher incidence of occlusive symptoms (60) (71) with rapid progression to strangulation and a mortality rate that can be high as 75% (24, 72).

CT findings

With CT, a cluster of fixed and dilated small bowel loops with a sac-like appearance is noted, possibly extending into the right paracolic gutter, lateral to the cecum and posterior to the ascending colon, which can be displaced anteriorly or medially (2, 33, 60, 73) (Fig. 9).

Sigmoid-mesocolon related hernias (SMHs)

Background

In the classic literature SMHs account for 6% of all internal hernias. Historically Benson et al have described three many types of internal hernias involving the sigmoid mesocolon, a peritoneal fold that suspends the sigmoid colon from the posterior parietal perito-

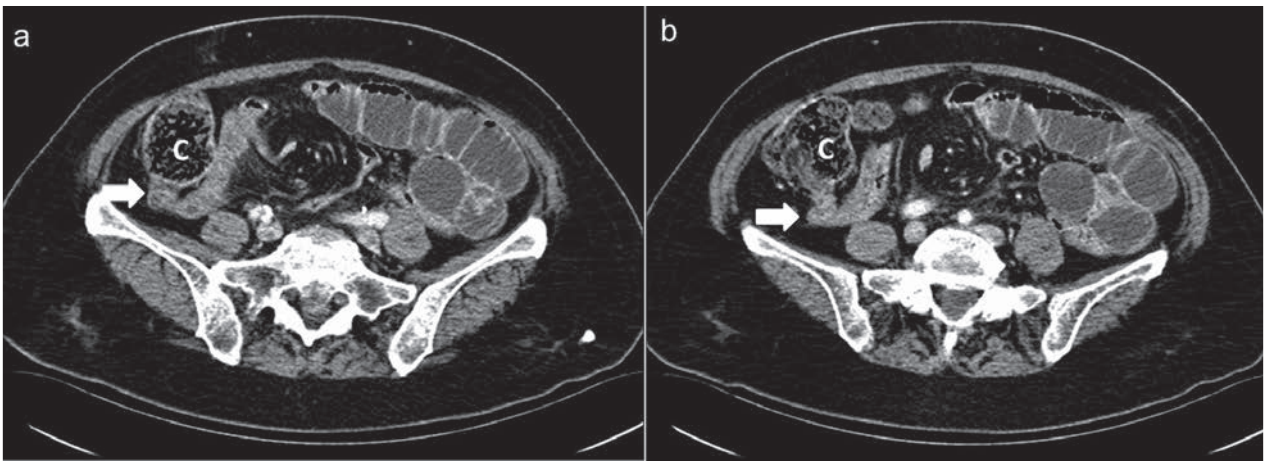

Figure 9. Pericecal hernia in a 80-year-old man with a 1- day history of right lower abdominal pain and vomiting. Contrast-enhanced axial CT scans (a) and (b) show small bowel loops (white arrows) posterior to cecum (C) in right paracolic gutter producing small bowel obstruction

neum: intersigmoid, transmesosigmoid and intramesosigmoid. The former have been reported as the most common (2, 24) (74), despite most Japanese studies have found intramesosigmoid hernias accounting for approximately half the cases (50%-57.3%), followed by intersigmoid hernia (24.5%-35%) and transmesosigmoid hernia (15%-18%)(75). These three categories are radiographically difficult to distinguish since they show similar CT findings, however not preoperative differentiation is required because surgical treatment is similar (24, 60).

Description

In the intersigmoid hernias small bowel, usually ileum, protrudes into the intersigmoid fossa, a congenital (found in 50-75% of autopsies) (74) unusual retroperitoneal recess formed between the adjacent sigmoid segments and their relative mesenteries, located above and behind the apex of the root of the sigmoid mesocolon (33, 60)In transmesosigmoid type bowel loops protrude without a hernia sac through a complete defect involving both of the peritoneal layers of the sigmoid mesentery, lying in a location lateral to the sigmoid itself. The third type, intramesosigmoid, is the herniation through only one peritoneal layer of the mesosigma (usually the left) so that the hernia sac lies within the sigmoid mesocolon (24, 60).

CT findings

CT findings in SMHs (Fig. 10) are a cluster of dilated small bowel loops entrapped posterior and lateral to the sigmoid colon, with the defect most commonly located between the sigmoid colon and the left psoas muscle, or between sigmoid loops in the intersigmoid type (24, 60, 76). In both inter- and intramesosigmoid types bowels show a sac-like appearance, absent in the transmesosigmoid type (33). Often a mass effect can be observed, with displacement of the sigmoid colon antero-medially (24, 76). Furthermore splaying of the sigmoid vessels, as if they are wrapping the hernia sac, may suggest an intramesosigmoid hernia (33, 77).

Transmesenteric and Roux-en-y anastomosis-related (TMHs) hernias

Background

A transmesenteric hernia occurs in presence of a congenital or acquired abnormal defect, involving both layers of the small bowel mesentery, usually located close the ligament of Treitz or the terminal ileum (33, 57). The small bowel mesentery is a voluminous, fat-laden peritoneal reflexion that fixes the loops of the small intestine to the posterior abdominal wall and

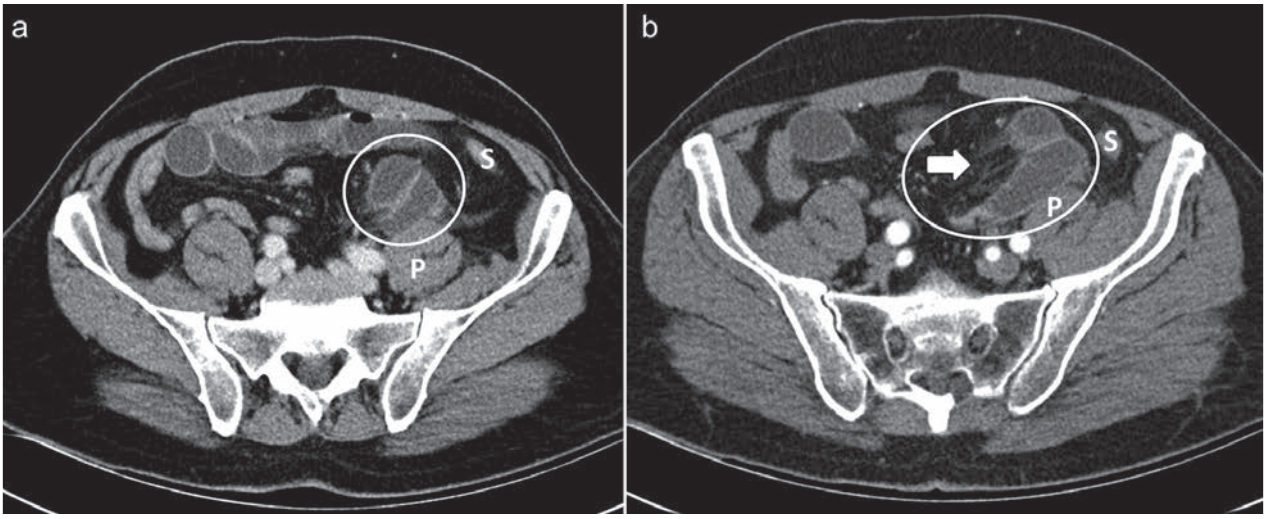

Figure 10. Sigmoid-mesocolon related hernia in a 80 year-old-man with acute left-sided abdominal pain. Contrast-enhanced axial CT scans (a) and (b) show encapsulated fluid-filled small bowel loops (white circles) protruding toward left lower abdomen through a defect in sigmoid mesocolon located near the left common iliac artery, between sigmoid colon (S) and the left psoas muscle (P). Convergence of engorged vessels grouped together at the entrance of the hernia orifice can also be seen (white arrow)

run obliquely down from its origin at the ligament of Treitz to the right toward the ileocecal junction (61). TMHs are the most common internal hernia in children. In fact almost 35% of cases occur in the pediatric age due to congenital defect in the small bowel mesentery close to the ileocecal region as a consequence of prenatal intestinal ischemia leading to thinning of the mesenteric leaves associated with bowel atresia in 5,5% of the pediatric population (78), partial regression of the dorsal mesentery, fenestration during the developmental enlargement of an inadequately vascularized area and an ileocecal mesentery with rapid and considerable lengthening in fetal life (2, 54). On the other hand, in the adult population TMHs are usually iatrogenic, being related to trauma, inflammation or previous abdominal surgery, in particular with Roux-en-Y anastomosis as in gastric by-pass or liver transplantation (2, 24, 60). In the classic literature TMHs account for approximately 8% of all internal hernias, although actually their incidence is increasing. Because of wide differences in the number of cases and follow-up time among existing research reports, the morbidity of internal hernia after laparoscopic Roux-en-Y gastric bypass fluctuates wildly between 0.2% and 9.0% (79).

Description

TMHs are difficult to detect due to the variability of their location since herniated bowel loops are not enveloped in a limiting sac and therefore can potentially be anywhere in the peritoneal cavity; however, they are detected more frequently in the right mid abdomen, usually adjacent to the abdominal wall (24, 39). Roux- en-Y anastomosis- related hernias usually occur more than one month after surgery and are more associated with the retrocolic procedure, in which the Roux limb passes through a complete defect created in the transverse mesocolon. After surgery, the defect can be incompletely closed or have a breakdown or a pulling of the suture material through the mesocolic fat; moreover enlargement of the mesenteric aperture can occur with repeated herniations or rapid weight loss and decreased peritoneal fat, common in bariatric patients, with consequent bowel herniation (24, 80-82). Furthermore, transmesenteric internal hernias in the adult postoperative patients more often occur after a laparoscopic rather than open approach because of lack of intra-abdominal adhesions required for fixation of the Roux-limb to prevent its displacement and to close mesenteric defects, as reported by Higa et al and Merkle et al. (83, 84).

Three types of Roux -en-Y related hernias have been described: '*transmesocolic*', the most common, in which bowel loops herniate through the surgical defect in the transverse mesocolon with possible mass effect on the stomach and displacement of the transverse colon anteriorly and inferiorly (24, 33); '*jejunostomy mesenteric*' if bowel prolapse through a defect in the small-bowel mesentery of the jejunojejunostomy site and finally the '*Petersen type*', in which bowel loops protrude behind the Roux loop before the small bowel eventually passes through the defect in the trasverse mesocolon in a space called Petersen defect, located between the jejunal mesentery of the Roux limb and transverse mesocolon (24, 81, 84). A deformed and displaced Roux limb, biliopancreatic limb and transverse colon may serve as landmarks of these hernias (33).

Clinical findings

Clinical findings of a TMHs often include signs of small bowel obstruction (60) with a more acute symptoms onset than other internal hernias (24, 40); vomiting is frequently absent because few secretions accumulate from the proximal gastric pouch or the Roux limb (84). A palpable abdominal mass representing "the Gordian knot of herniated intestine" may be present in a minority of patients (24). Due to the lack of delimitation which allow protrusion of a considerable length of bowel (25) and the small diameter of the mesenteric aperture (2-5 cm), transmesenteric hernias are more liable than other subtypes to develop volvulus and strangulation or ischemia, with an incidence of 30% and 40% respectively and high mortality rates reaching about of 50% for the treated groups and 100% for the non-treated groups (24, 40).

CT findings

Blachar et al. in 2001 have described the presence of clustered, compressed small bowel loops in the periphery of the abdominal cavity and the lack of omental fat between the loops and the abdominal wall as the most useful CT signs for the detection of a transmesenteric hernia. The herniated bowels appeared lateral to the colon (a reversal of the normal anatomic arrangement) with central, inferior and posterior displacement of the transverse colon and inferior and medial displacement of the hepatic flessure (40). Another study concluded that the only statistically significant CT signs predictors of a transmesenteric hernia are clustering of small bowel loops, especially those that are adjacent to the abdominal wall, mesenteric vessel abnormalities including stretching, crowding and engorgement, a displacement of the main mesenteric trunk to the right and signs of small bowel obstruction (39) (Fig. 11).

Dilauro et al. described the mesenteric swirl and small bowel obstruction as the CT signs with the highest accuracy for diagnosis of internal hernia after laparoscopic Roux-en-Y gastric bypass. The authors introduced two new signs: a 'SMV beaking' (a decreased calibre of SMV with beaked appearance), and 'criss cross appearance' of the second order mesenteric vessels with reversal of the SMV and SMA anatomic relationship (85). In literature other CT signs associated with internal mesenteric hernia following Roux-en-Y bypass gastric surgery have been described, like 'the mushroom sign' (a mushroom shaped mesenteric root between the SMA and the distal mesenteric arterial branch), the 'hurricane eye' sign (distal tubular mesentery with surrounding small bowel loops), a small bowel loop behind the SMA, abnormal position of the jejunojejunostomy, and 'weeping mesentery' (edematous mesentery with enlarged lymphnodes) (33, 85-87) (Tab. 4) (Fig. 12).

Transomental hernias (TOHs)

Background and Description

Traditionally, TOHs make up 1-4% of all IHs. The term "transomental hernia" usually refers to herniation, most commonly of small bowel loops, cecum and sigmoid colon, through or into a congenital or acquired abnormal defect of the greater omentum from 2 to 10 cm in diameter involving both leaves (four peritoneal layers) and located in the periphery near the free edge (2) .

CT findings

CT findings are often identical to those of a transmesenteric hernia, however characteristic features

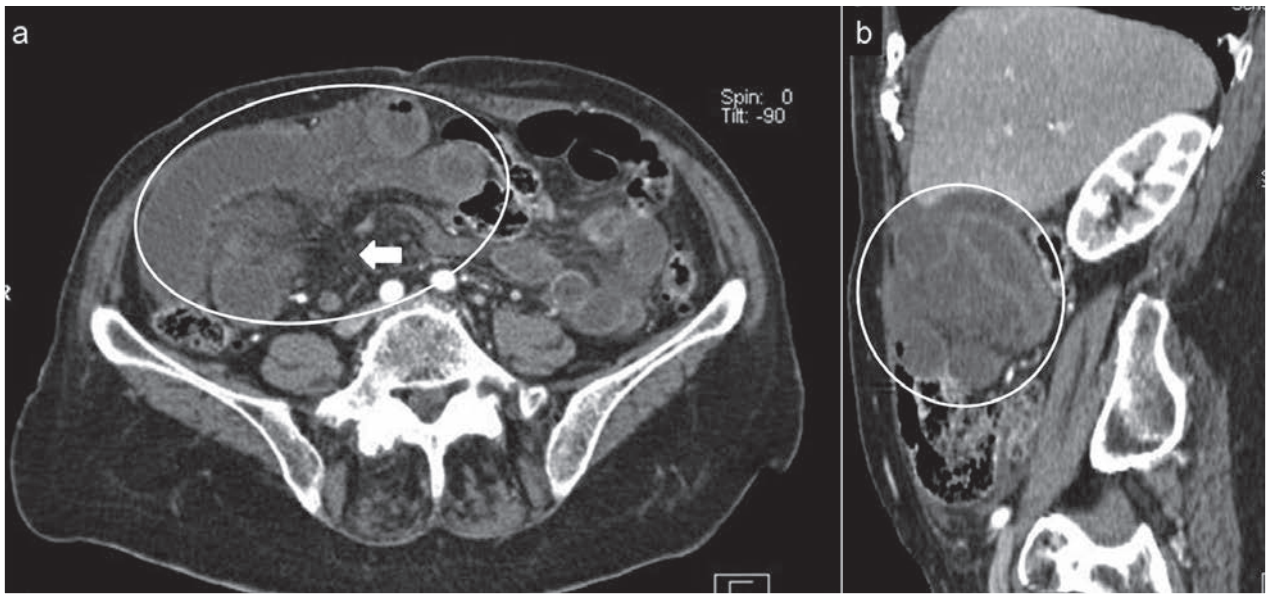

Figure 11. Transmesenteric hernia in a 28 year-old man with lower abdominal pain. Contrast-enhanced axial CT scan (a) and sagittal reformatted image (b) show distended ileal loops with poor enhancement of walls (white circles) adjacent to the right abdominal wall. The mesenteric vessels are engorged and crowded (white arrow)

Table 4. CT signs associated with Roux-en-Y anastomosis related hernia

- Swirled mesentery
- Small-bowel obstruction
- Hurricane eye
- SMV beaking
- Criss cross appearance
- Mushroom sign
- Small-bowel behind superior mesenteric artery
- Weeping mesentery
- Right-sided anastomosis

of TOHs are dilated bowel loops, without a sac-like appearance, located in the most anterior portion of the peritoneal cavity with omental vessels that run vertically around the hernia orifice (2, 24) (Fig. 13).

Supravesical and pelvic (PIHs) internal hernias

Background

Supravesical and pelvic internal hernias account for approximately 6% of all IHs. Broad ligament hernia is the most common type of pelvic internal hernias, a rare and heterogeneous group of IHs that occur in the pelvis, including also hernias through the perirectal fossa and fossa of Douglas (33). Bowel loops, usually small intestine, protrude through or into an abnormal aperture in the left or right broad ligament of the uterus, especially in multiparous middle-aged women as a consequence of developmental peritoneal defect around the uterus or acquired conditions such as pregnancy and birth trauma, injuries following vaginal manipulations or inflammatory pelvic diseases (2, 88). Herniation of colon, ovary and ureter have also been described (33, 89). Cameron et al. have reported the first case of SBO and ischemia secondary to an internal hernia due to both a defect in the broad ligament and wrapping of the fallopian tube around the bowel (90).

Description

According to the classification scheme proposed by Hunt, three categories of broad ligament hernias related to the degree of the defect have been described: '*fenestra type*', the most common, if both two peritoneal layers of the broad ligament are involved, '*pouch type*', if

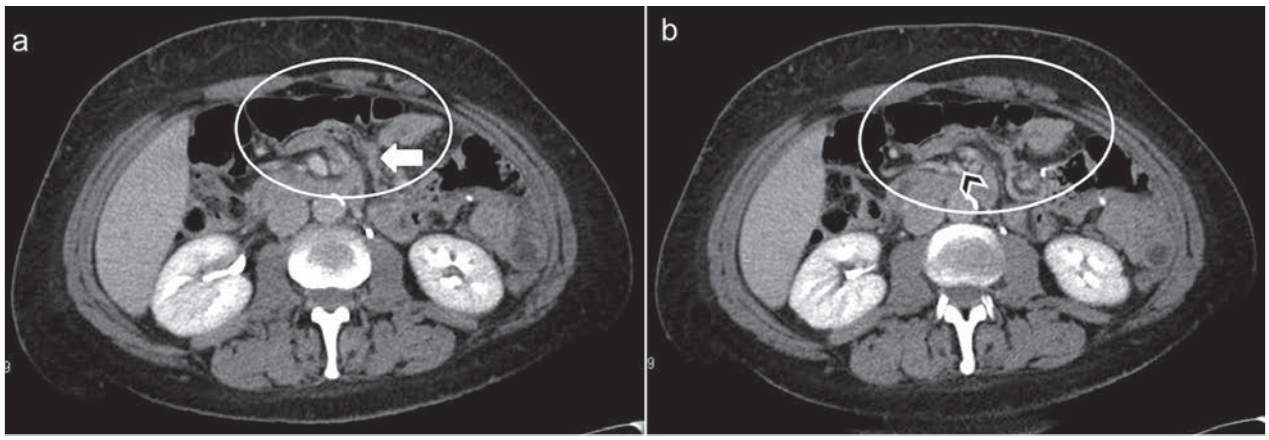

Figure 12. Petersen hernia in a 40 year-old-woman with nausea and vomiting 6 months after a Roux-en-Y gastric by-pass. Contrast-enhanced axial CT scans (a) and (b) show grouping of small bowel loops near anterior abdominal wall (white circles). A mushroom shape of the herniated mesenteric root (white arrow) and a decreased calibre of SMV with a beaked appearance are also seen (arrowhead)

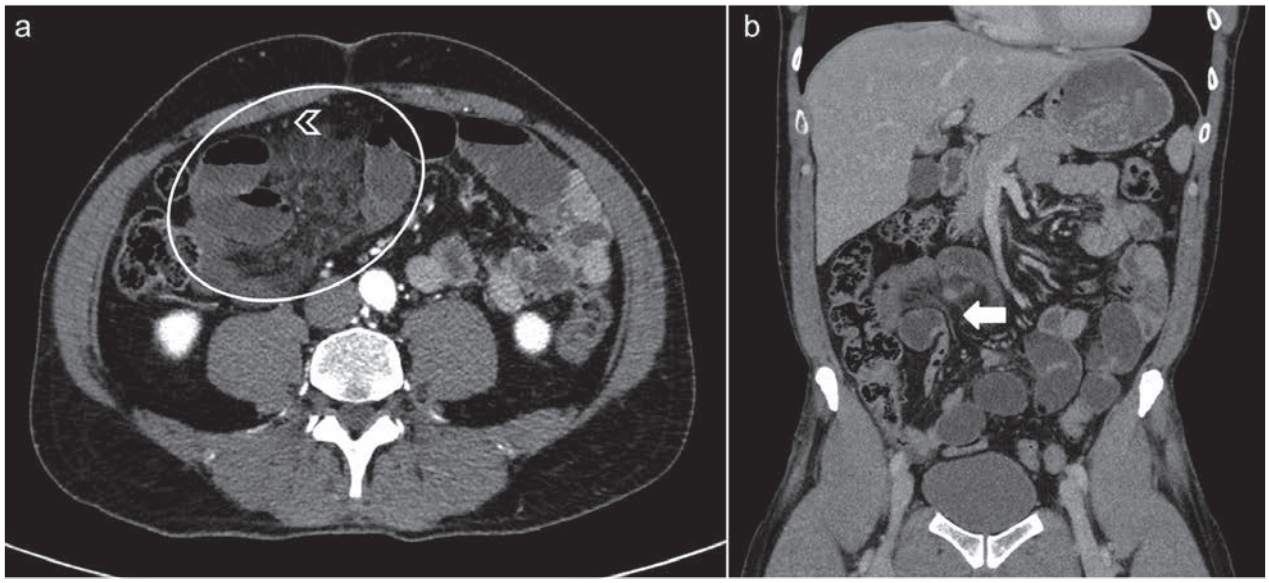

Figure 13. Transomental hernia in a 49 year-old man with diffuse abdominal pain. Contrast-enhanced axial CT scan (a) and coronal reformatted image (b) show small bowel loops (white circle) with converging mesenteric vessels and fat in the hernia orifice (white arrow). Omental vessels (arrowheads) running vertically are also seen

the defect is in only one of the two layers whereby the visceral structures would be entrapped within a sac in the parametrial tissue, and '*hernia sac type*', whereby a double layer of attenuated peritoneum lines the herniated bowel, forming a true internal hernia (88). Cilley et al. (91) introduced a new classification based on the anatomic position of the defect, which included three categories: type 1, defect caudal to the round ligament; type 2, defect above the broad ligament; and type 3, defect between the round ligament and remainder of the broad ligament, through the mesoligametum teres (88).

In internal supravesical hernias intestine protrude downward into a space around the bladder through

supravesical fossa, a triangular area bounded laterally by the left or right medial umbilical ligament, medially by the median umbilical ligament and inferiorly by the peritoneal reflection passing from the anterior abdominal wall to the dome of the urinary bladder (33, 92, 95-99). Skandalakis et al. proposed the terms "anterior supravesical", "right or left lateral supravesical", and "posterior supravesical" depending on whether the hernia passed in front of, beside or behind the bladder, respectively.

CT findings

CT findings of broad ligament hernias include a cluster of dilated small bowel loops herniated in the pelvic cavity laterally to the uterus with a displacement of the rectosigmoid dorso-laterally and of the uterus ventrally and enlargement of the distance between the uterus and the ovary deviating in opposite directions. Furthermore mesenteric vessels of herniated loops penetrating the broad ligament may be seen (33, 88). In supravesical internal hernia usually CT scans show bowel loops with a sac-like appearance pass into the space of Retzius and lay in front of the compressed bladder on the left or right. These patients can present with bladder irritation and dysuria, as the bladder is compressed by the small bowel (33, 93, 94) (Fig. 14).

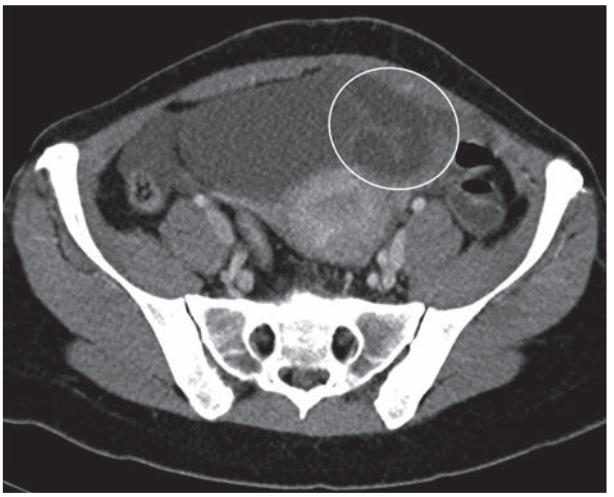

Figure 14. Internal supravesical hernia in a 67-year-old woman with a two-day history of lower abdominal pain. Contrast-enhanced axial CT scan shows intestine loops (white circle) to the left of the urinary bladder.

Conclusions

Although internal hernias are uncommon conditions, they must be considered in the differential diagnosis of acute abdominal pain, especially in presence of strangulated closed loop small bowel obstruction without external hernias or history of previous surgery or trauma and in gastric bypass patients. In the acute setting a prompt imaging diagnosis is mandatory in order to avoid intestinal ischemia and necrosis. Radiologists play a key role in detection of internal hernias and it is very important for them to be familiarized with the anatomy, aetiology and CT signs of these hernias to aid an accurate and quickly preoperative diagnosis and improve patient's outcome guiding surgeons to ensure the appropriate management in order to reduce morbidity and mortality rates.

Ethical approval: This article does not contain any studies with human participants performed by any of the authors.

Conflict of interest: None to declare

References

1. Miller PA, Mezwa DG, Feczko PJ, Jafri ZH, Madrazo BL. Imaging of abdominal hernias. Radiographics 1995; 15: 333-47.
2. Takeyama N, Gokan T, Ohgiya Y, et al. CT of internal hernias. Radiographics 2005; 25: 997-1015.
3. Akyildiz H, Artis T, Sozuer E, et al. Internal hernia: complex diagnostic and therapeutic problem. Int J Surg 2009; 7: 334-7.
4. Caranci F, Napoli M, Cirillo M, Briganti G, Brunese L, Briganti F. Basilar artery hypoplasia. Neuroradiol J 2012; 25: 739-43.
5. Cirillo M, Caranci F, Tortora F, et al. Structural neuroimaging in dementia. J Alzheimers Dis 2012; 29: 16-19.
6. di Giacomo V, Trinci M, van der Byl G, Catania VD, Calisti A, Miele V. Ultrasound in newborns and children suffering from non-traumatic acute abdominal pain: imaging with clinical and surgical correlation. J Ultrasound 2015; 18: 385-93.
7. Iacobellis F, Segreto T, Berritto D, et al. A rat model of acute kidney injury through systemic hypoperfusion evaluated by micro-US, color and PW-Doppler. Radiol Med 2018;
8. Barile A, Bruno F, Arrigoni F, et al. Emergency and Trauma of the Ankle. Semi Musc Rad 2017; 21: 282-89.
9. Barile A, Bruno F, Mariani S, et al. What can be seen after rotator cuff repair: a brief review of diagnostic imaging findings. Musculoskelet Surg 2017; 101: 3-14.

10. Cantisani V, Grazhdani H, Drakonaki E, et al. Strain US elastography for the characterization of thyroid nodules: Advantages and limitation. Int J Endocrinol 2015; 2015:
11. Mandato Y, Reginelli A, Galasso R, Iacobellis F, Berritto D, Cappabianca S. Errors in the Radiological Evaluation of the Alimentary Tract: Part I. Semin Ultrasound CT MR 2012; 33: 300-07.
12. Gatta G, Parlato V, Di Grezia G, et al. Ultrasound-guided aspiration and ethanol sclerotherapy for treating endometrial cysts. Radiol Med 2010; 115: 1330-39.
13. Scialpi M, Cappabianca S, Rotondo A, et al. Pulmonary congenital cystic disease in adults. Spiral computed tomography findings with pathologic correlation and management. Radiol Med 2010; 115: 539-50.
14. Sverzellati N, Calabrò E, Chetta A, et al. Visual score and quantitative CT indices in pulmonary fibrosis: Relationship with physiologic impairment. Radiol Med 2007; 112: 1160-72.
15. Vivarelli M, Vincenzi P, Montalti R, et al. ALPPS Procedure for Extended Liver Resections: A Single Centre Experience and a Systematic Review. PLoS One 2015; 10: e0144019.
16. Valeri G, Mazza FA, Maggi S, et al. Open source software in a practical approach for post processing of radiologic images. Radiol Med 2015; 120: 309-23.
17. Mocchegiani F, Vincenzi P, Coletta M, et al. Prevalence and clinical outcome of hepatic haemangioma with specific reference to the risk of rupture: A large retrospective cross-sectional study. Dig Liver Dis 2016; 48: 309-14.
18. Schicchi N, Valeri G, Moroncini G, et al. Myocardial perfusion defects in scleroderma detected by contrast-enhanced cardiovascular magnetic resonance. Radiol Med 2014; 119: 885-94.
19. Tarantini G, Favaretto E, Napodano M, et al. Design and methodologies of the postconditioning during coronary angioplasty in acute myocardial infarction (POST-AMI) trial. Cardiology 2010; 116: 110-16.
20. Salvolini L, Urbinati C, Valeri G, Ferrara C, Giovagnoni A. Contrast-enhanced MR cholangiography (MRCP) with GD-EOB-DTPA in evaluating biliary complications after surgery. Radiol Med 2012; 117: 354-68.
21. Sforza V, Martinelli E, Ciardiello F, et al. Mechanisms of resistance to anti-epidermal growth factor receptor inhibitors in metastatic colorectal cancer. World J Gastroenterol 2016; 22: 6345-61.
22. Maurizi N, Passantino S, Spaziani G, et al. Long-term Outcomes of Pediatric-Onset Hypertrophic Cardiomyopathy and Age-Specific Risk Factors for Lethal Arrhythmic Events. JAMA Cardiol 2018; 3: 520-25.
23. Di Pietto F, Chianca V, de Ritis R, et al. Postoperative imaging in arthroscopic hip surgery. Musculoskelet Surg 2017; 101: 43-49.
24. Martin LC, Merkle EM, Thompson WM. Review of internal hernias: radiographic and clinical findings. AJR Am J Roentgenol 2006; 186: 703-17.
25. Fan HP, Yang AD, Chang YJ, Juan CW, Wu HP. Clinical spectrum of internal hernia: a surgical emergency. Surg Today 2008; 38: 899-904.
26. Kar S, Mohapatra V, Rath PK. A Rare Type of Primary Internal Hernia Causing Small Intestinal Obstruction. Case Rep Surg 2016; 2016: 3540794.
27. Fujiwara T, Ohno Y, Sasaki A, Suzaki N, Matsuo Y. Internal hernia with triple hiatus of congenital origin: report of a case. Surg Today 2000; 30: 954-8.
28. Reginelli A, Mandato Y, Solazzo A, Berritto D, Iacobellis F, Grassi R. Errors in the Radiological Evaluation of the Alimentary Tract: Part II. Semin Ultrasound CT MR 2012; 33: 308-17.
29. Cappabianca S, Reginelli A, Monaco L, Del Vecchio L, Di Martino N, Grassi R. Combined videofluoroscopy and manometry in the diagnosis of oropharyngeal dysphagia: Examination technique and preliminary experience. Radiol Med 2008; 113: 923-40.
30. Blachar A, Federle MP. Internal hernia: an increasingly common cause of small bowel obstruction. Semin Ultrasound CT MR 2002; 23: 174-83.
31. Dionigi G, Dionigi R, Rovera F, et al. Treatment of high output entero-cutaneous fistulae associated with large abdominal wall defects: single center experience. Int J Surg 2008; 6: 51-6.
32. Gore RM, Levine MS, Textbook of Gastrointestinal Radiology E-Book, Elsevier Health Sciences2014.
33. Doishita S, Takeshita T, Uchima Y, et al. Internal Hernias in the Era of Multidetector CT: Correlation of Imaging and Surgical Findings. Radiographics 2016; 36: 88-106.
34. Maggialetti N, Capasso R, Pinto D, et al. Diagnostic value of computed tomography colonography (CTC) after incomplete optical colonoscopy. Int J Surg 2016; 33 Suppl 1: S36-44.
35. Di Cesare E, Patriarca L, Panebianco L, et al. Coronary computed tomography angiography in the evaluation of intermediate risk asymptomatic individuals. Radiol Med 2018; 123: 686-94.
36. Pradella S, Lucarini S, Colagrande S. Liver lesion characterization: The wrong choice of contrast agent can mislead the diagnosis of hemangioma. Am J Roentgenol 2012; 199:
37. Di Cesare E, Gennarelli A, Di Sibio A, et al. Assessment of dose exposure and image quality in coronary angiography performed by 640-slice CT: a comparison between adaptive iterative and filtered back-projection algorithm by propensity analysis. Radiol Med 2014; 119: 642-49.
38. Murali Appavoo Reddy UD, Dev B, Santosham R. Internal hernias: surgeons dilemma-unravelled by imaging. Indian J Surg 2014; 76: 323-8.
39. Blachar A, Federle MP, Brancatelli G, Peterson MS, Oliver JH, 3rd, Li W. Radiologist performance in the diagnosis of internal hernia by using specific CT findings with emphasis on transmesenteric hernia. Radiology 2001; 221: 422-8.
40. Blachar A, Federle MP, Dodson SF. Internal hernia: clinical and imaging findings in 17 patients with emphasis on CT criteria. Radiology 2001; 218: 68-74.

41. McDonagh T, Jelinek GA. Two cases of paraduodenal hernia, a rare internal hernia. J Accid Emerg Med 1996; 13: 64-8.
42. Regine G, Stasolla A, Miele V. Multidetector computed tomography of the renal arteries in vascular emergencies. Eur J Radiol 2007; 64: 83-91.
43. De Cecco CN, Buffa V, Fedeli S, et al. Preliminary experience with abdominal dual-energy CT (DECT): True versus virtual nonenhanced images of the liver. Radiol Med 2010; 115: 1258-66.
44. Buffa V, Solazzo A, D'Auria V, et al. Dual-source dual-energy CT: dose reduction after endovascular abdominal aortic aneurysm repair. Radiol Med 2014; 119: 934-41.
45. Valentini V, Buquicchio GL, Galluzzo M, et al. Intussusception in Adults: The Role of MDCT in the Identification of the Site and Cause of Obstruction. Gastroenterol Res Pract 2016; 2016: 5623718.
46. Zaiton F, Al-Azzazy MZ, Ahmed AS, Amr WM. MDCT signs predicting internal hernia and strangulation in patients presented to emergency department with acute small bowel obstruction. The Egyptian Journal of Radiology and Nuclear Medicine 2016; 47: 1185-94.
47. Boudiaf M, Soyer P, Terem C, Pelage JP, Maissiat E, Rymer R. Ct evaluation of small bowel obstruction. Radiographics 2001; 21: 613-24.
48. Pothiawala S, Gogna A. Early diagnosis of bowel obstruction and strangulation by computed tomography in emergency department. World J Emerg Med 2012; 3: 227-31.
49. Rosen MP, Siewert B, Sands DZ, Bromberg R, Edlow J, Raptopoulos V. Value of abdominal CT in the emergency department for patients with abdominal pain. Eur Radiol 2003; 13: 418-24.
50. Yaghmai V, Nikolaidis P, Hammond NA, Petrovic B, Gore RM, Miller FH. Multidetector-row computed tomography diagnosis of small bowel obstruction: can coronal reformations replace axial images? Emerg Radiol 2006; 13: 69-72.
51. Harbin WP. Computed tomographic diagnosis of internal hernia. Radiology 1982; 143: 736.
52. Pinto A, Miele V, Schilliro ML, et al. Spectrum of Signs of Pneumoperitoneum. Semin Ultrasound CT MR 2016; 37: 3-9.
53. Sessa B, Galluzzo M, Ianniello S, Pinto A, Trinci M, Miele V. Acute Perforated Diverticulitis: Assessment With Multidetector Computed Tomography. Semin Ultrasound CT MR 2016; 37: 37-48.
54. Shadhu K, Ramlagun D, Ping X. Para-duodenal hernia: a report of five cases and review of literature. BMC Surg 2018; 18: 32.
55. Selcuk D, Kantarci F, Ogut G, Korman U. Radiological evaluation of internal abdominal hernias. Turk J Gastroenterol 2005; 16: 57-64.
56. Zenitani M, Sasaki T, Tanaka N, Oue T. Strangulated right paraduodenal hernia successfully treated with single-incision transumbilical surgery. J Pediatr Surg Case Rep 2017; 22: 1-4.
57. Morton A. Meyers MDFF, Chusilp Charnsangavej MDF, Michael Oliphant MDF, Meyers' Dynamic Radiology of the Abdomen: Normal and Pathologic Anatomy, Springer New York2010.
58. Gusz JR, Wright LM. Intestinal obstruction secondary to left paraduodenal hernia. J Surg Case Rep 2015; 2015:
59. Barbosa L, Ferreira A, Povoa AA, Maciel JP. Left paraduodenal hernia: a rare cause of small bowel obstruction in the elderly. BMJ Case Rep 2016; 2016:
60. Mathieu D, Luciani A, Group G. Internal abdominal herniations. AJR Am J Roentgenol 2004; 183: 397-404.
61. Okino Y, Kiyosue H, Mori H, et al. Root of the small-bowel mesentery: correlative anatomy and CT features of pathologic conditions. Radiographics 2001; 21: 1475-90.
62. Suchato C, Pekanan P, Panjapiyakul C. CT findings in symptomatic left paraduodenal hernia. Abdom Imaging 1996; 21: 148-9.
63. Catalano OA, Bencivenga A, Abbate M, Tomei E, Napolitano M, Vanzulli A. Internal hernia with volvulus and intussusception: case report. Abdom Imaging 2004; 29: 164-5.
64. Erskine JM. Hernia through the foramen of Winslow. Surg Gynecol Obstet 1967; 125: 1093-109.
65. Sikiminywa-Kambale P, Anaye A, Roulet D, Pezzetta E. Internal hernia through the foramen of Winslow: a diagnosis to consider in moderate epigastric pain. J Surg Case Rep 2014; 2014:
66. Leung E, Bramhall S, Kumar P, Mourad M, Ahmed A. Internal Herniation Through Foramen of Winslow: A Diagnosis Not to Be Missed. Clinical medicine insights. Gastroenterology 2016; 9: 31-33.
67. Numata K, Kunishi Y, Kurakami Y, et al. Gallbladder herniation into the lesser sac through the foramen of Winslow: report of a case. Surg Today 2013; 43: 1194-8.
68. Welaratne I, Nasoodi A. A Rare Cause of Obstructive Jaundice: Cecal Herniation through the Foramen of Winslow. J Clin Imaging Sci 2018; 8: 24.
69. Joo YE, Kim HS, Choi SK, et al. Internal hernia presenting as obstructive jaundice and acute pancreatitis. Scand J Gastroenterol 2002; 37: 983-6.
70. Schuster MR, Tu RK, Scanlan KA. Caecal herniation through the foramen of Winslow: diagnosis by computed tomography. Br J Radiol 1992; 65: 1047-48.
71. Gullino D, Giordano O, Gullino E. [Internal hernia of the abdomen. Apropos of 14 cases]. J Chir (Paris) 1993; 130: 179-95.
72. Kleyman S, Ashraf S, Daniel S, Ananthan D, Sanni A, Khan F. Pericecal hernia: a rare form of internal hernias. J Surg Case Rep 2013; 2013:
73. Fu CY, Chang WC, Lu HE, Su CJ, Tan KH. Pericecal hernia of the inferior ileocecal recess: CT findings. Abdom Imaging 2007; 32: 81-3.
74. Benson JR, Killen DA. Internal Hernias Involving the Sigmoid Mesocolon. Ann Surg 1964; 159: 382-4.
75. Kayano H, Nomura E, Kuramoto T, et al. Two Cases of Laparoscopic Diagnosis and Treatment of Intersigmoid Hernia. Tokai J Exp Clin Med 2017; 42: 109-14.
76. Yu CY, Lin CC, Yu JC, Liu CH, Shyu RY, Chen CY. Stran-

gulated transmesosigmoid hernia: CT diagnosis. Abdom Imaging 2004; 29: 158-60.
77. Takeshita T, Ninoi T, Shigeoka H, Hirayama Y, Miki Y. Small bowel obstruction due to an intramesosigmoid hernia diagnosed by multidetector row computed tomography: a case report. Osaka city medical journal 2011; 56: 37-45.
78. Elmadi A, Lechqar M, El Biache I, et al. Trans-mesenteric hernia in infants: report of two cases. J Neonatal Surg 2014; 3: 29.
79. Farukhi MA, Mattingly MS, Clapp B, Tyroch AH. CT Scan Reliability in Detecting Internal Hernia after Gastric Bypass. JSLS 2017; 21: e2017.00054.
80. Blachar A, Federle MP. Bowel obstruction following liver transplantation: clinical and ct findings in 48 cases with emphasis on internal hernia. Radiology 2001; 218: 384-8.
81. Blachar A, Federle MP, Pealer KM, Ikramuddin S, Schauer PR. Gastrointestinal complications of laparoscopic Roux-en-Y gastric bypass surgery: clinical and imaging findings. Radiology 2002; 223: 625-32.
82. Filip JE, Mattar SG, Bowers SP, Smith CD. Internal hernia formation after laparoscopic Roux-en-Y gastric bypass for morbid obesity. Am Surg 2002; 68: 640-3.
83. Higa KD, Ho T, Boone KB. Internal hernias after laparoscopic Roux-en-Y gastric bypass: incidence, treatment and prevention. Obes Surg 2003; 13: 350-4.
84. Merkle EM, Hallowell PT, Crouse C, Nakamoto DA, Stellato TA. Roux-en-Y gastric bypass for clinically severe obesity: normal appearance and spectrum of complications at imaging. Radiology 2005; 234: 674-83.
85. Dilauro M, McInnes MD, Schieda N, et al. Internal Hernia after Laparoscopic Roux-en-Y Gastric Bypass: Optimal CT Signs for Diagnosis and Clinical Decision Making. Radiology 2017; 282: 752-60.
86. Lockhart ME, Tessler FN, Canon CL, et al. Internal hernia after gastric bypass: sensitivity and specificity of seven CT signs with surgical correlation and controls. AJR Am J Roentgenol 2007; 188: 745-50.
87. Iannuccilli JD, Grand D, Murphy BL, Evangelista P, Roye GD, Mayo-Smith W. Sensitivity and specificity of eight CT signs in the preoperative diagnosis of internal mesenteric hernia following Roux-en-Y gastric bypass surgery. Clin Radiol 2009; 64: 373-80.
88. Matsunami M, Kusanagi H, Hayashi K, Yamada S, Kano N. Broad ligament hernia successfully treated by laparoscopy: Case report and review of literature. Asian J Endosc Surg 2014; 7: 327-9.
89. Quiroga S, Sarrias M, Sanchez JL, Rivero J. Small bowel obstruction secondary to internal hernia through a defect of the broad ligament: preoperative multi-detector CT diagnosis. Abdom Imaging 2012; 37: 1089-91.
90. Cameron M, Janakan G, Birch D, Nazir S. A closed loop obstruction caused by entrapment of the fallopian tube and herniation through the broad ligament. Int J Surg 2015; 12: 57-59.
91. Cilley R, Poterack K, Lemmer J, Dafoe D. Defects of the broad ligament of the uterus. Am J Gastroenterol 1986; 81: 389-91.
92. Jan YT, Jeng KS, Liu YP, Yang FS. Internal supravesical hernia. Am J Surg 2008; 196: e27-8.
93. Morimoto M, Honjo S, Sakamoto T, et al. Internal supravesical hernia repaired via the anterior approach alone: A case report. Int J Surg Case Rep 2017; 39: 297-300.
94. Cisse M, Konate I, Ka O, Dieng M, Dia A, Toure CT. Internal supravesical hernia as a rare cauase of intestinal obstruction: a case report. J Med Case Rep 2009; 3: 9333.
95. Gafà G, Sverzellati N, Bonati E, et al (2012). Follow-up in pulmonary sarcoidosis: comparison between HRCT and pulmonary function tests. RAD. MED, vol. 117, p. 968-978, ISSN: 0033-8362, doi: 10.1007/s11547-012-0827-5
96. Bertolini L, Vaglio A, Bignardi L, et al (2011). Subclinical interstitial lung abnormalities in stable renal allograft recipients in the era of modern immunosuppression. Transplantation Proceedings, vol. 43, p. 2617-2623, ISSN: 0041-1345, doi: 10.1016/j.transproceed.2011.06.033
97. Palma BD, Guasco D, Pedrazzoni M, et al. Osteolytic lesions, cytogenetic features and bone marrow levels of cytokines and chemokines in multiple myeloma patients: Role of chemokine (C-C motif) ligand20. Leukemia. 2016 Feb;30(2):409-16. doi: 10.1038/leu.2015.259. Epub 2015 Sep 30.
98. Bozzetti C, Nizzoli R, Tiseo M, et al. ALK and ROS1 rearrangements tested by fluorescence in situ hybridization in cytological smears from advanced non-small cell lung cancer patients. Diagnostic Cytopathology, vol. 43, p. 941-946, ISSN: 8755-1039, doi: 10.1002/dc.23318
99. De Filippo M, Onniboni M, Rusca M, et al. (2008). Advantages of multidetector row CT with multiplanar reformation in guiding percutaneous lung biopsies. RAD. MED, vol. 113, p. 945-953, ISSN: 0033-8362, doi: 10.1007/s11547-008-0325-y

Received: 26 March 2019
Accepted: 4 April 2019
Correspondence:
Silvia Pradella
Department of Radiology – Careggi University Hospital
L.go G.A. Brambilla, 3 - 50134 Florence, Italy
E-mail: pradella3@yahoo.it

Acta Biomed 2019; Vol. 90, Supplement 5: 38-50 DOI: 10.23750/abm.v90i5-S.8337

Review

Magnetic resonance enterography (MRE) and ultrasonography (US) in the study of the small bowel in Crohn's disease: state of the art and review of the literature

Rosa Manetta[1], Ilaria Capretti[2], Noemi Belleggia[2], Claudia Marsecano[2], Angelo Viscido[3], Federico Bruno[2], Francesco Arrigoni[2], Liheng Ma[4], Giuseppe Guglielmi[5], Alessandra Splendiani[2], Ernesto Di Cesare[2], Carlo Masciocchi[2], Antonio Barile[2]

[1] Division of Radiology, S. Salvatore Hospital, L'Aquila, Italy; [2] Department of Biotechnology and Applied Clinical Sciences, University of L'Aquila, L'Aquila, Italy; [3]Department of Life, Health and Environmental Sciences, University of L'Aquila, L'Aquila, Italy; [4] Department of Radiology, GuangDong Pharmaceutical University, Guangzhou, Cina; [5] Department of Clinical and Experimental Medicine, Foggia University School of Medicine, Foggia, Italy

Summary. Crohn's disease (CD) is a chronic idiopathic disease and its diagnosis is based on a combination of clinical symptoms, laboratory tests and imaging data. There isn't a diagnostic gold standard: the ileocolonoscopy with mucosal biopsies represents the standard for luminal disease, while cross-sectional imaging such as Ultrasound (US), Computed Tomography (CT) or Magnetic Resonance Imaging (MRI) can show transmural alterations and extraintestinal manifestations. CD is usually diagnosed in the young age and after baseline diagnosis, the patients have to undergo to variable follow-up depending on remission or active disease. The aim of our review is to compare Magnetic Resonance Enterography (MRE) to Ultrasonography (US) in the follow-up of CD. (www.actabiomedica.it)

Key words: MR enterography, Crohn's disease, IBD, CEUS

Introduction

Crohn's disease (CD) is a chronic idiopathic disease that is commonly characterized by recurrent gastrointestinal tract inflammation. Patients affected by CD are mainly at reproductive ages and they need frequent follow-up (1)

The disease involves the whole gastrointestinal tract, in particular the small bowel (70%) in the tract of terminal ileum and colon (2); it is a pathology with multifactorial etiology and is more common in Europe and North America (3). It has an incidence in the U.K. of 83 per million people. Symptomatic manifestations may be unspecific. Danese et al. (4) have constructed the Red Flags index to individuate early symptoms and have established a value of 8 as highly predictive of CD diagnosis: chronic diarrhea (>3 bowel movements and >4-week duration); chronic abdominal pain (>3 months); rectal bleeding; extra-intestinal manifestations. There is a poor correlation between symptomatology and disease severity (5). Frequent complications are intestinal strictures (40% of cases) but also abscesses, phlegmons and fistulas (6). Diagnosis and staging of CD require different diagnostic exams: serological testing (C-reactive protein and fecal calprotectin), clinical and endoscopical evaluation (7, 8), video-capsule endoscopy for proximal small bowel. Endoscopy consists in ileocolonoscopy with biopsies from the terminal ileum and colon in order to confirm the diagnosis (9); esophagogastroduodenoscopy is used for suspected upper tract disease (10). The ileocolonoscopy represents the standard for luminal disease (11). Cross-sectional imaging (MRI, CT and US) techniques, gained large application in

gastrointestinal radiology (12-48); in the setting of inflammatory bowel diseases, they are is advised as first line techniques in the diagnosis, staging and follow-up (49, 50). An expert consensus committee from the European Society of Gastrointestinal and Abdominal Radiology (ESGAR) and European Society of Paediatric Radiology (ESPR) has established guidelines for performing these diagnostic techniques, including patient preparation, technical recommendations and scan protocol (51). Radiological examinations can evaluate accurately severity; they are non-invasive and not limited to the colon and terminal ileum (52) but can demonstrate complications of CD and extraintestinal manifestations. Aim of this review is to compare Magnetic Resonance Enterography (MRE) with Ultrasonography (US) as non-invasive, radiation-free and appropriate techniques for follow-up in patients affected by CD. In particular, dynamic imaging techniques can assess the degree of disease activity and the efficacy of treatment .

Magnetic resonance enterography

Magnetic resonance imaging is one of the most largely used imaging tool in many diagnostic (53-57) and interventional settings (58, 59) thanks to its intrinsic excellent soft tissue contrast and the absence of ionizing radiation compared to CT (55, 60-87). Magnetic resonance enterography (MRE) plays an important role in supporting the diagnosis, and in establishing severity and presence of penetrating or extra-intestinal disease. To date, MRE is the most employed technique to assess the response to medical or surgical treatment . Common complications of Crohn's disease are intestinal strictures that may be of fibrotic, inflammatory and mixed types (88). The distinction is important in treatment planning; therefore, an appropriate diagnosis of inflammatory stenosis is required. The inflammatory stenosis responds to medical therapy while the fibrotic one requires endoscopic approach or intestinal resection. The exact distinction is sometimes difficult to be determined (89, 90). In a recent review of 2016, Westerland et al (90) analyze advantages and appropriate sequences that allow evaluation of the intestinal wall and distinction between inflammatory or fibrotic component. MRE is a panoramic technique that shows intestinal wall layers, presence of penetrating disease and extraluminal complications such as fistulas or abscesses. Important factors during MRE are: optimal distension of the small bowel, obtained with biphasic agent (mannitol or polyethylene glycol); antiperistatical agent to minimize bowel peristalsis (91, 92). Conventional sequences, used to evaluate typical pathological alterations, are True-FISP or FIESTA (true fast imaging with steady-state free-precession), T2-weighted and T1- weighted fat-saturated sequences. FIESTA sequences are less sensible to motion artifact and show good contrast between the bowel wall, lumen and mesenteric fat. It is useful for a morphological evaluation of the bowel loops (93) (Fig. 1). T2-weighted sequences have a high sensitivity (83%-91%) and specificity (86%-100%) to detect inflamed bowel with a mural thickness greater than 3mm and T2-signal increased for the presence of mural and mesenteric edema. Other features of acute disease are: mesenteric vascular prominence (comb sign), hyperenhancing and enlarged lymph nodes (short axis up to 8 mm) (Fig. 2). In T1- weighted fat-saturated sequences acquired after contrast media, the active inflammatory appears with a stratified pattern of enhancement (hyper- intense mucosa and serosa and hypointense/edema submucosa) (Fig. 3). The chronic inflammation is characterized by T2 hypointense mural signal without adjacent mesenteric inflammation and homogeneous transmural enhancement on T1-weighted fat-saturated sequences (92) (Fig. 4). The distinction between inflammatory and fibrostenotic disease is facilitated by the peculiar tissue contrast obtained in MR images . Recently, Diffusion Weighted Imaging (DWI) has been added to conventional sequences and many studies (94) show that there is a restricted diffusion in active inflammation: the presence of a cellular inflammatory response in the bowel wall prevents the movement of water molecules, showing mucosal hyperintensity on DWI and corresponding low signal on the Apparent Diffusion Coefficient (ADC) map. A quantitative evaluation (for example through ADC) helps to determine the severity of the disease and to monitor treatment response: Rimola et al. (95, 96) have elaborated the MR index of activity (MaRIA), considering MR parameters such as wall thickness, relative contrast enhancement, presence

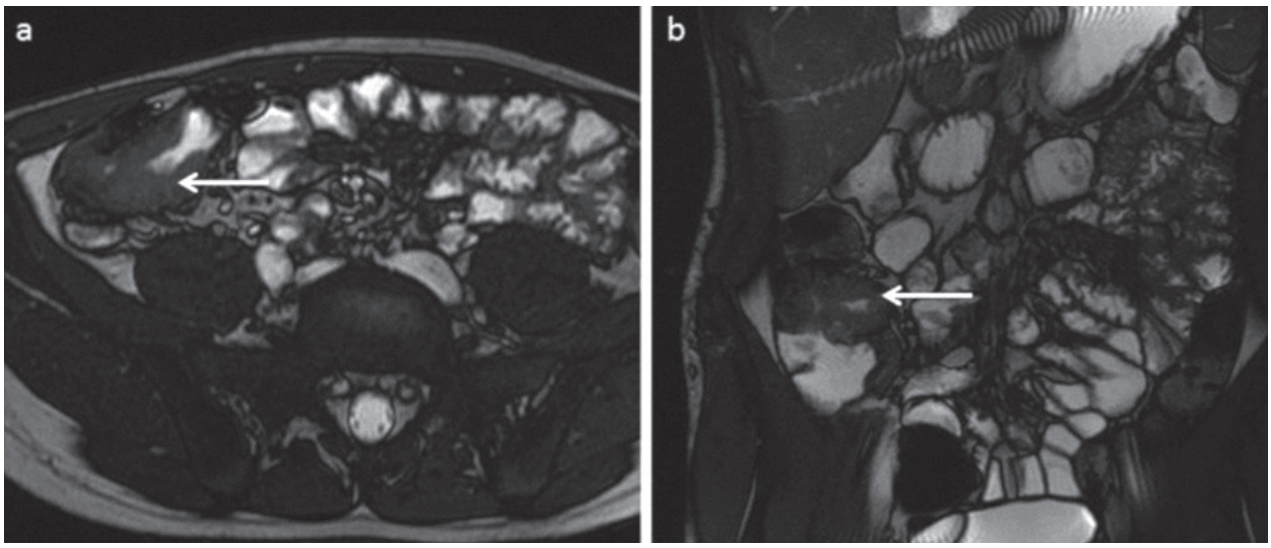

Figure 1. 14-year-old patient with abdominal pain, diarrhoea and elevated inflammatory biomarkers levels. Axial (a) and coronal (b) FIESTA sequences show active inflammation with increased wall thickness of the terminal ileum (arrows)

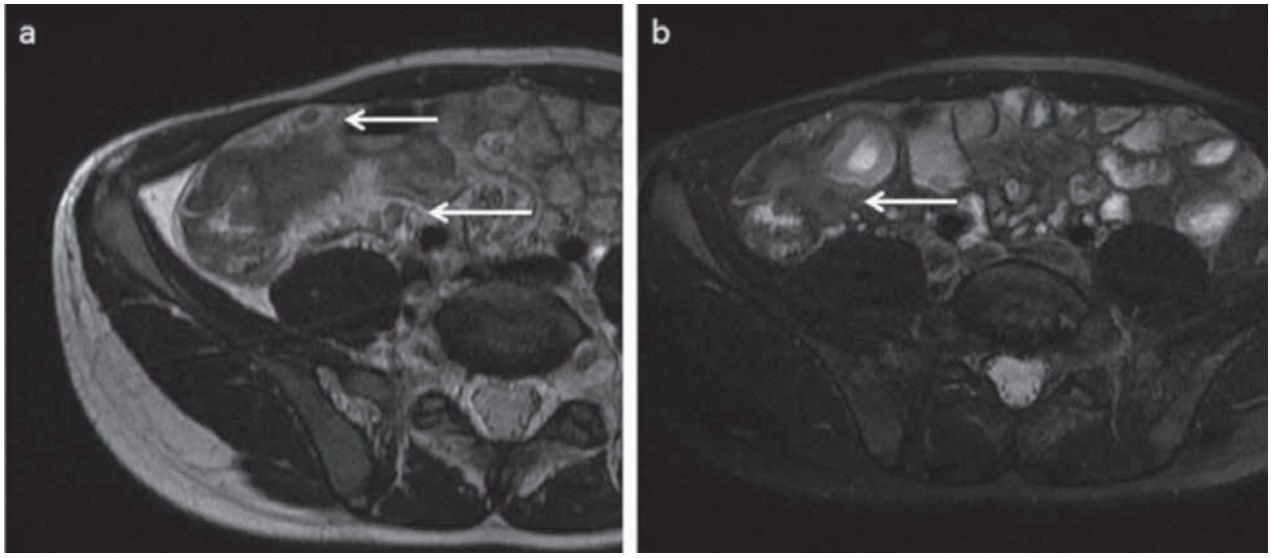

Figure 2. T2-weighted sequences show enlarged lymph nodes (a) and mural edema (b)

of edema, ulcers, pseudopolyps and enlarged lymph nodes. This index has a significant correlation with the endoscopic findings and, though being frequently quoted, it is not diffusely accepted in the clinical practice. In a study carried out in 2017, Kim et al (97) demonstrated that modified MaRIA scoring is quite accurate, because DWI, enteric and portal phase scans can improve reproducibility of the scoring system.

Ultrasonography

Ultrasonography (US) is the least invasive imaging examination, well tolerated by patients. This technique does not employ ionizing radiations, is repeatable with high diagnostic accuracy and is widely used in the diagnostic setting and as guidance in many interventional radiology procedures (61, 63, 98-105).

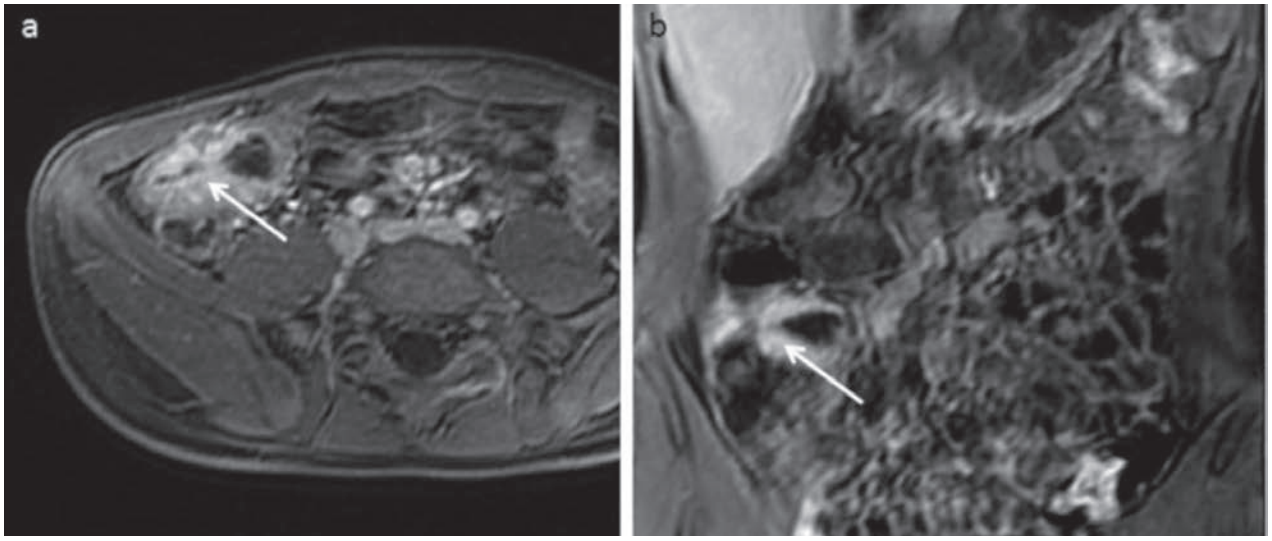

Figure 3. T1-w fat saturated images in axial (a) and coronal (b) planes, after contrast injection, show hyperintense mucosa (arrows) during the arterial phase

US can identify morphological features of bowel wall drawing the layer pattern and wall thickness (>3 mm in CD) (106) (Fig. 5). For this reasons, US is useful during active CD to show inflammatory processes of angiogenesis and hypervascularization into the intestinal wall (107); computed tomography (CT) and MR are unsuitable for repeated follow-up due to radiation exposure (CT) and high cost and complexity (MR) (108, 109). US can evaluate parietal vascularization using Color or Power Doppler: active disease is characterized by the increased number and caliber of vessels (110). Contrast-enhanced US is more accurate (111). The introduction of oral contrast solution (water and polyethylene glycol) to distend the bowel can improve the image quality and diagnostic accuracy in the evaluation of mild intestinal damage (112); the use of intravenous contrast media in US (CEUS) can emphasize the presence of an increased bowel wall vascularization that it is typical in the active form of CD. US with oral contrast agent (SICUS), as reported by Mocci et al. (113) in a review of 2017, has a sensitivity ranging from 96 to 100% if compared to that of conventional US (from 57 to 96%). Furthermore, it has been demonstrated that SICUS has high accuracy to identify complications and post-operative recurrence (114). An Italian group (115) has compiled a SICUS quantitative sonographic lesion index (SLIC) to study the evolution of the transmural bowel damage in CD patients in medical therapy. The index includes wall thickness, length of damaged intestinal tract, dilation and strictures. It identifies five classes of severity ranging from the lower (class A) to the higher score (class E). CEUS uses an intravenous contrast (Sonovue, at the recommended dose of 2.4-4.8 ml) and has a good ability to distinguish hypo- or hypervascularized intestinal strictures, identifying inflammation from fibrostenotic lesions (116) (Fig. 6). Active inflammation characteristics include rapid wash-in, when the microbubbles appear <20 second after infusion in bolus, and slow wash-out, when the microbubbles wash out in <80s (117). Some authors have shown that CEUS can be correlated with CD clinical activity (118). A quantitative method is proposed to evaluate vascularization of the intestinal wall in association with disease activity (the CD activity index, CDAI). Migaleddu et al. (119) have demonstrated that CEUS has the highest performance: 93.5% sensitivity, 93.7% specificity and 93.6% accuracy. In post-surgical recurrences, the values are 97%, 91%, 96%, respectively (120). The distinction between inflammatory and fibrotic lesions, as already mentioned, is very important for the therapeutic approach but some studies are controversial about this distinction: increased echogenicity of the submucosal layer results in inflammation while a clear visibility of all intestinal layers suggests fibrosis with reduced blood volume and flow (121, 122). The introduction of

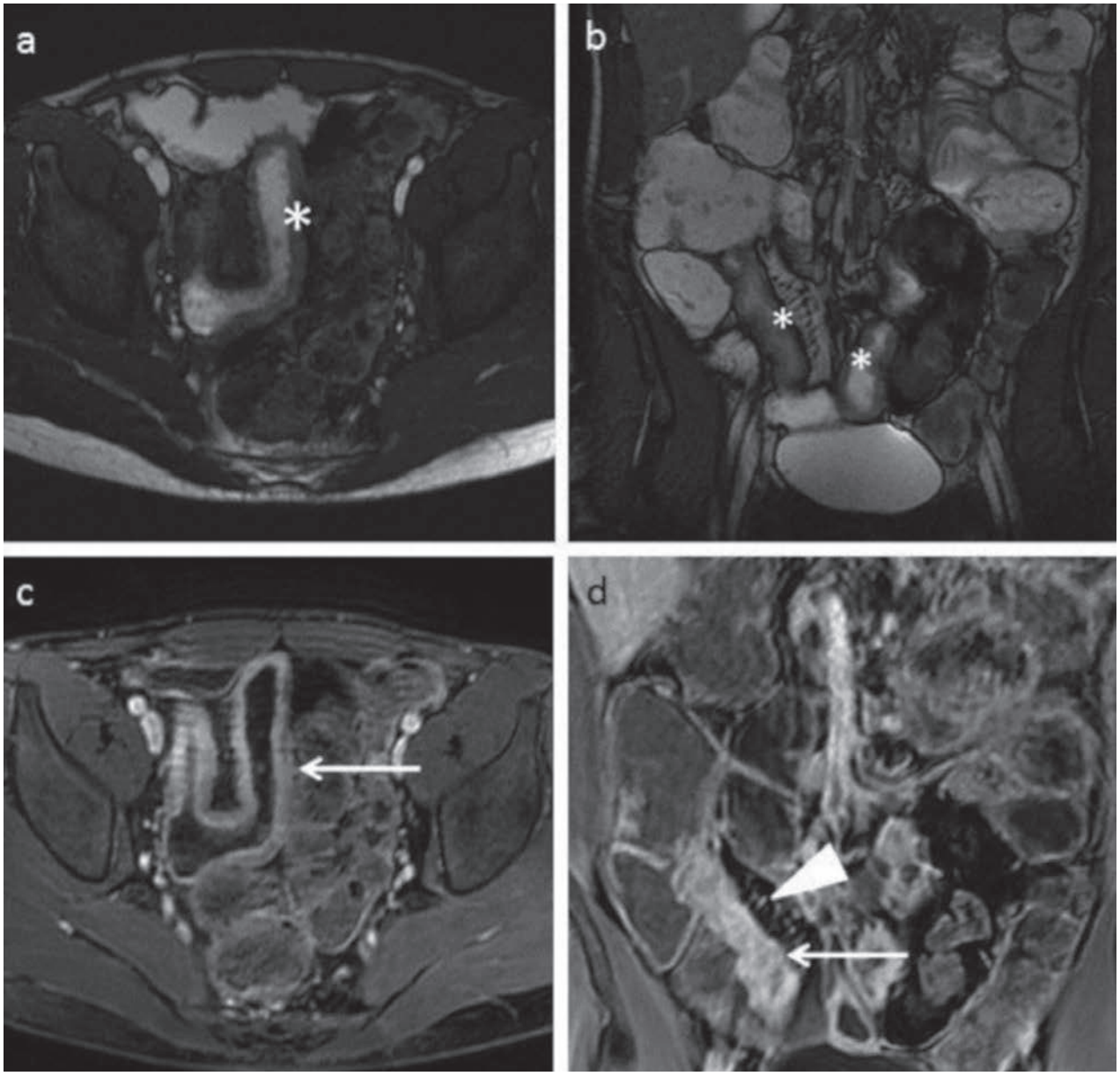

Figure 4. Follow-up at 5-years surgical treatment in 23-year-old patient. Images show, near ileum-ileal anastomosis, an inflamed loop, with increased thickness (*), vascular prominence (arrowhead), fibro-fatty proliferation and progressive transmural hyperenhancement (arrows). Early enhancement is showed in axial plane (a) and transmural enhancement in late venous phase (b)

a dedicated US software, the QLAB (Philips, Koninklijke, Belgium) and the Qontrast (Bracco, Milan, Italy) has allowed a quantitative and semi-quantitative analysis of contrast enhancement of the inflamed area. These data are derived from a selected "region of interest" (ROI) in which median values of the image intensity and a perfusion analysis are calculated to generate a time-intensity curve and obtain a good correlation between CD inflammatory activity and bowel wall vascularization (123, 124). In a recent study, Quaia (125) shows a positive correlation between contrast enhancement in affected tracts of small bowel and laboratory data in CD, so that the quantitative CEUS can define responder from non-responder patients affected by active disease and treated with immunosuppressive and biological therapies. The strain elastography (SE)

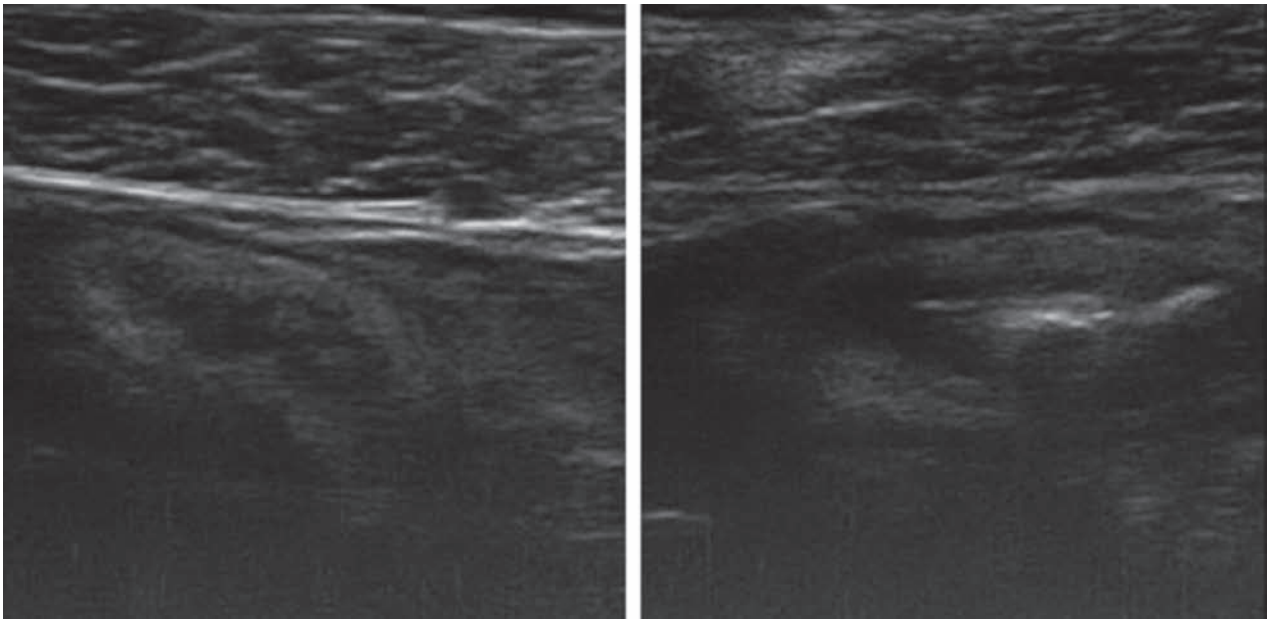

Figure 5. B-mode US with linear probe shows loop affected by CD and with increased mural thickness

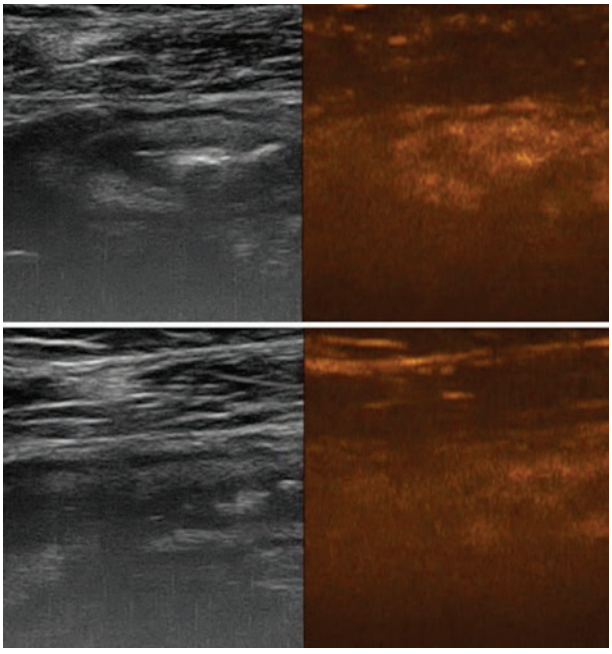

Figure 6. US after second-generation microbubble contrast shows slight enhancement, without signs of significant inflammation

is another diagnostic method useful but not routinely used for clinical management of inflammatory bowel diseases. It is a technique to evaluate the elasticity of the tissues as demonstrated in a case of ileum Crohn stricture by Giannetti (126) and confirmed by macroscopic and microscopic examination: the terminal ileum wall appears with abnormal elasticity and higher percentage of "blue" areas, suggesting stiffness.

Advantages and disadvatages of US

US has many advantages (127). It is widely used, low-cost, repeatable, noninvasive and radiation-free, all reasons that make of this technique one of the most tolerated by the patients. An experienced sonographer can find mural and extramural complications visualizing a good part of the small intestine and colon, in particular as the first approach in urgent assessment of complications. US is accurate in investigating stenosis, abscesses and fistulas; intraluminal oral contrast may improve image quality, but MR can show complicated fistulas better than US. Moreover, the use of intravenous contrast is necessary to distinguish CD strictures with predominantly inflammatory or fibrotic component especially when the stenosis is impassable with the endoscope. CEUS has an important role in revealing the presence and activity of CD in terminal ileum in particular in the follow-up of patients with known ileal localization of disease (128). Unfortunately, US

has some limitations: it is operator-dependent and the comparison or revision of images during the follow-up is not easy. Large body size, intestinal meteorism (in some cases it can be reduced by intraluminal solution) or depth of the region of interest can limit the exam. US cannot explore abdominal regions (retroperitoneum area) and intestinal tracts such as stomach, duodenum, jejunum, transverse colon, deep intrapelvic loops and rectum (129).

Advantages and disadvatages of MRE

MRE is another radiation-free diagnostic technique and represents the first choice in the pelvic localization of CD (11). It has high diagnostic accuracy and ability to investigate the complete bowel tract; it has multiplanar reconstructions, good visualization of soft tissues and easy detection of complications (strictures, abscess and fistulas) (Fig. 7) thus playing an important

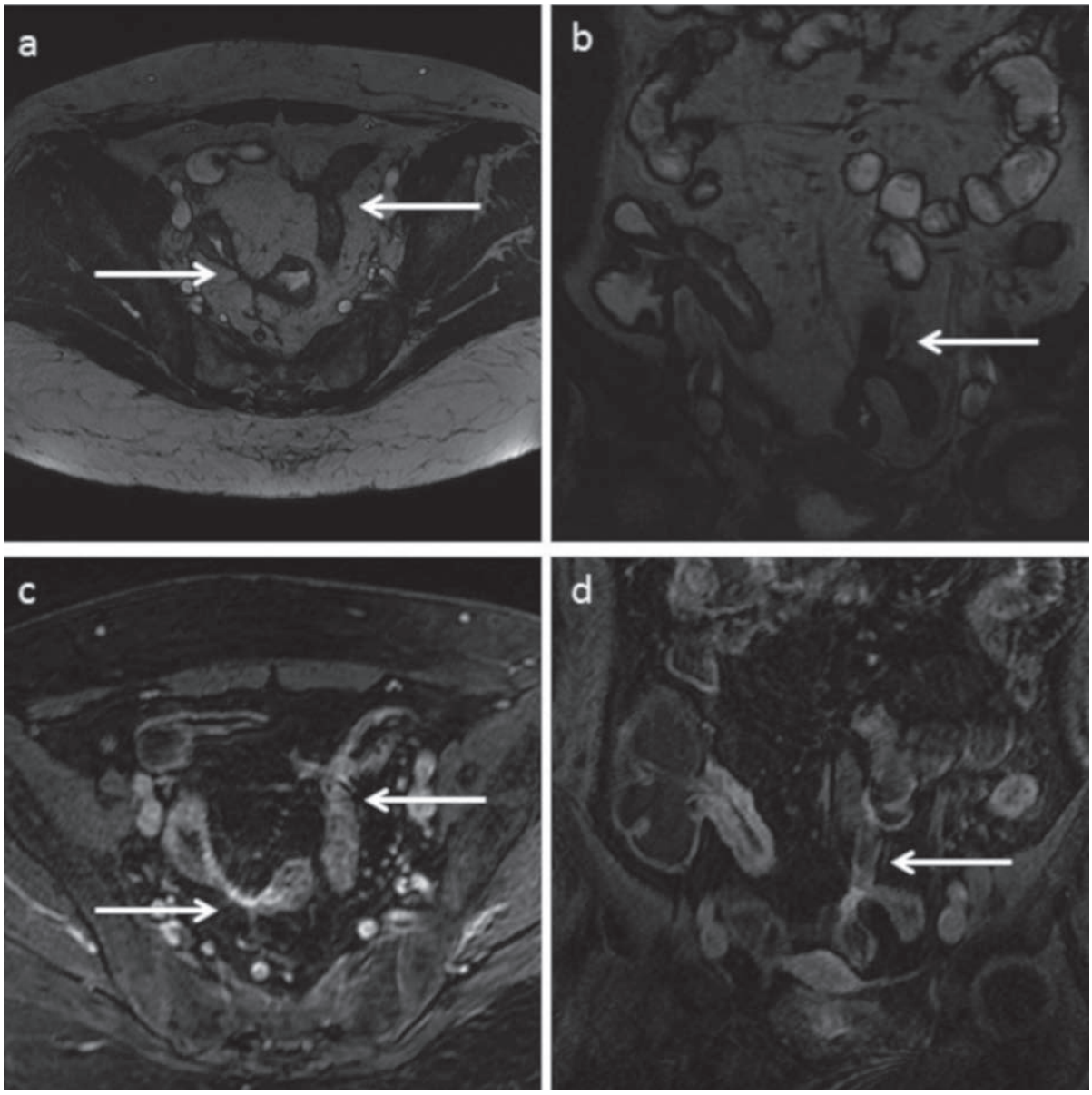

Figure 7. Example of enterocolic fistula formations (arrows) in a patient with CD for about 10 years. FIESTA images show «star sign» in axial (a) and coronal(b) planes and transmural enhancement appears in axial (c) and coronal (d) T1-weighted fat-saturated images

role in surgical planning (127). It provides a panoramic view of the entire abdominal region, mesenteric tissue and retroperitoneum area, allowing a good visualization also in patients in whom US is limited (e.g., overweight patients). Unfortunately, MRE is less used in clinical practice, because it is expensive, needs specific radiological competences and is time consuming (130). Other limitations include presence of metal devices, claustrophobia or sensitivity to MR contrast agents (131, 132).

CEUS vs MRE

A study by Malagò et al. (133) shows a good correlation between MRE and CEUS activity, with a Spearman's coefficient (rho) = 0.791 and a statistically significant p value (<0.0001). In particular, a high correlation was found in the study of the small bowel to evaluate wall thickness, lymph nodes and vasa recta (rho=0.926; p<0.0001); accurate correlation was obtained to assess layered wall appearance, disease extension and fibro adipose proliferation (rho=0.716; p<0.001). An excellent correlation between imaging and clinical laboratory data was achieved. MRE and CEUS are non-invasive techniques used in the diagnosis of CD, and in monitoring its activity. The affected loop and the main signs of the disease can be determined by both imaging modalities, despite different accuracy rates. In active disease, CEUS offers the possibility of recognizing all the characteristic signs, using intravenous contrast agent (gas microbubbles) that remains inside the microcirculation throughout the procedure, breaks up in the vascular system and is not retained in the fibrous tissue. This technique better shows the bowel-wall enhancement and the increased vascularization of the affected bowel loop (133). Conversely, MRI contrast agent has an initial vascular phase, tends to migrate and to accumulate in the interstitium. Therefore, gadolinium can detect also chronic lesions. Quaia et al. (134-137) demonstrated the accuracy of both techniques, with a quantitative analysis of enhancement patterns. Time intensity curves in CEUS and MRE are adequate for assessing intestinal-wall vascularity and for a more objective evaluation of the parietal enhancement compared with observer experience. In chronic lesions (133), which are fibrous scar tissue, MRE shows moderate enhancement in the venous phase with a pattern restricted to the mucosa, layered or homogeneous, while CEUS does not reveal any vascular enhancement.

Conclusions

An accurate diagnosis of CD is important to plan therapy and follow-up. The diagnosis is accomplished also by means of a bioptic extraction from the mucosal alteration performed during colonoscopy. In clinical practice, MRE is used as a first imaging exam to determine intestinal localization, extension and extra-intestinal complications. It can distinguish between inflamed and fibrotic component and helps in the therapeutic decision-making: medical therapy or surgical treatment. CEUS is useful in the explorable intestinal tracts, already visualized by previous MRI exams, and it is used in the follow-up after medical or surgical treatment or as fist-line exam in patients unsuitable to MR. Besides, CEUS can be helpful in emergency conditions as first approach examination in case of acute complications and recurrence. In conclusion, both techniques are useful and complementary in the study of CD evolution.

Ethical approval: This article does not contain any studies with human participants performed by any of the authors.

Conflict of interest: None to declare

References

1. Panes J. Inflammatory bowel disease: pathogenesis and targets for therapeutic interventions. Acta Physiol Scand 2001; 173: 159-65.
2. Martin DR, Lauenstein T, Sitaraman SV. Utility of Magnetic Resonance Imaging in Small Bowel Crohn's Disease. Gastroenterology 2007; 133: 385-90.
3. Marampon F, Gravina GL, Ju X, et al. Cyclin D1 silencing suppresses tumorigenicity, impairs DNA double strand break repair and thus radiosensitizes androgen-independent prostate cancer cells to DNA damage. Oncotarget 2016;
4. Danese S, Fiorino G, Mary JY, et al. Development of red flags index for early referral of adults with symptoms and

signs suggestive of Crohn's disease: An IOIBD initiative. J Crohns Colitis 2015; 9: 601-06.
5. Peyrin-Biroulet L, Reinisch W, Colombel JF, et al. Clinical disease activity, C-reactive protein normalisation and mucosal healing in Crohn's disease in the SONIC trial. Gut 2014; 63: 88-95.
6. Cosnes J, Gower-Rousseau C, Seksik P, Cortot A. Epidemiology and natural history of inflammatory bowel diseases. Gastroenterology 2011; 140: 1785-94.
7. Panes J, Bouhnik Y, Reinisch W, et al. Imaging techniques for assessment of inflammatory bowel disease: Joint ECCO and ESGAR evidence-based consensus guidelines. J Crohns Colitis 2013; 7: 556-85.
8. Porcile C, Di Zazzo E, Monaco ML, et al. Adiponectin as novel regulator of cell proliferation in human glioblastoma. J Cell Physiol 2014; 229: 1444-54.
9. Dalla Palma B, Guasco D, Pedrazzoni M, et al. Osteolytic lesions, cytogenetic features and bone marrow levels of cytokines and chemokines in multiple myeloma patients: Role of chemokine (C-C motif) ligand 20. Leukemia 2016; 30: 409-16.
10. Deepak P, Park SH, Ehman EC, et al. Crohn's disease diagnosis, treatment approach, and management paradigm: what the radiologist needs to know. Abdom Radiol (NY) 2017; 42: 1068-86.
11. Hommes DW, Van Deventer SJH. Endoscopy in inflammatory bowel diseases. Gastroenterology 2004; 126: 1561-73.
12. Iacobellis F, Berritto D, Fleischmann D, et al. CT findings in acute, subacute, and chronic ischemic colitis: suggestions for diagnosis. Biomed Res Int 2014; 2014: 895248.
13. Mazzei MA, Guerrini S, Squitieri NC, et al. The role of US examination in the management of acute abdomen. Crit Ultrasound J 2013; 5: 1-9.
14. Reginelli A, Iacobellis F, Del Vecchio L, et al. VFMSS findings in elderly dysphagic patients: Our experience. BMC Surg 2013; 13:
15. Somma F, Berritto D, Iacobellis F, et al. 7T μMRI of mesenteric venous ischemia in a rat model: Timing of the appearance of findings. Magn Reson Imaging 2013; 31: 408-13.
16. Berritto D, Somma F, Landi N, et al. Seven-Tesla micro-MRI in early detection of acute arterial ischaemia: evolution of findings in an in vivo rat model. Radiol Med 2011; 116: 829-41.
17. Grassi R, Lombardi G, Reginelli A, et al. Coccygeal movement: Assessment with dynamic MRI. Eur J Radiol 2007; 61: 473-79.
18. Iacobellis F, Berritto D, Somma F, et al. Magnetic resonance imaging: A new tool for diagnosis of acute ischemic colitis? World J Gastroenterol 2012; 18: 1496-501.
19. Mazzei MA, Mazzei FG, Marrelli D, et al. Computed tomographic evaluation of mesentery: Diagnostic value in acute mesenteric ischemia. J Comput Assist Tomogr 2012; 36: 1-7.
20. Cappabianca S, Granata V, Di Grezia G, et al. The role of nasoenteric intubation in the MR study of patients with Crohn's disease: Our experience and literature review. Radiol Med 2011; 116: 389-406.
21. Grassi R, Romano S, Micera O, Fioroni C, Boller B. Radiographic findings of post-operative double stapled trans anal rectal resection (STARR) in patient with obstructed defecation syndrome (ODS). Eur J Radiol 2005; 53: 410-16.
22. Grassi R, Di Mizio R, Pinto A, Romano L, Rotondo A. Serial plain abdominal film findings in the assessment of acute abdomen: spastic ileus, hypotonic ileus, mechanical ileus and paralytic ileus. Radiol Med 2004; 108: 56-70.
23. Buffa V, Solazzo A, D'Auria V, et al. Dual-source dual-energy CT: dose reduction after endovascular abdominal aortic aneurysm repair. Radiol Med 2014; 119: 934-41.
24. Grassi R, Pinto A, Mannelli L, Marin D, Mazzei MA, New Imaging in Gastrointestinal Tract, Gastroenterol Res Pract, 2016.
25. Di Cesare E, Gennarelli A, Di Sibio A, et al. Assessment of dose exposure and image quality in coronary angiography performed by 640-slice CT: a comparison between adaptive iterative and filtered back-projection algorithm by propensity analysis. Radiol Med 2014; 119: 642-49.
26. Mandato Y, Reginelli A, Galasso R, Iacobellis F, Berritto D, Cappabianca S. Errors in the Radiological Evaluation of the Alimentary Tract: Part I. Semin Ultrasound CT MR 2012; 33: 300-07.
27. Reginelli A, Russo A, Maresca D, Martiniello C, Cappabianca S, Brunese L. Imaging Assessment of Gunshot Wounds. Semin Ultrasound CT MR 2015; 36: 57-67.
28. Pinto A, Pinto F, Faggian A, et al. Sources of error in emergency ultrasonography. Crit Ultrasound J 2013; 5 Suppl 1: S1-S1.
29. Cappabianca S, Porto A, Petrillo M, et al. Preliminary study on the correlation between grading and histology of solitary pulmonary nodules and contrast enhancement and [18F] fluorodeoxyglucose standardised uptake value after evaluation by dynamic multiphase CT and PET/CT. J Clin Pathol 2011; 64: 114-19.
30. Miele V, Piccolo CL, Trinci M, Galluzzo M, Ianniello S, Brunese L. Diagnostic imaging of blunt abdominal trauma in pediatric patients. Radiol Med 2016; 121: 409-30.
31. Tamburrini S, Solazzo A, Sagnelli A, et al. Amyotrophic lateral sclerosis: Sonographic evaluation of dysphagia. Radiol Med 2010; 115: 784-93.
32. Pinto A, Reginelli A, Cagini L, et al. Accuracy of ultrasonography in the diagnosis of acute calculous cholecystitis: review of the literature. Crit Ultrasound J 2013; 5 Suppl 1: S11.
33. Pallotta N, Vincoli G, Montesani C, et al. Small intestine contrast ultrasonography (SICUS) for the detection of small bowel complications in crohn's disease: A prospective comparative study versus intraoperative findings. Inflamm Bowel Dis 2012; 18: 74-84.
34. De Cecco CN, Buffa V, Fedeli S, et al. Preliminary experience with abdominal dual-energy CT (DECT): True versus virtual nonenhanced images of the liver. Radiol Med 2010; 115: 1258-66.

35. di Giacomo V, Trinci M, van der Byl G, Catania VD, Calisti A, Miele V. Ultrasound in newborns and children suffering from non-traumatic acute abdominal pain: imaging with clinical and surgical correlation. J Ultrasound 2015; 18: 385-93.
36. Pinto A, Miele V, Laura Schillirò M, et al. Spectrum of Signs of Pneumoperitoneum. Semin Ultrasound CT MR 2016; 37: 3-9.
37. Sessa B, Galluzzo M, Ianniello S, Pinto A, Trinci M, Miele V. Acute Perforated Diverticulitis: Assessment With Multidetector Computed Tomography. Semin Ultrasound CT MR 2016; 37: 37-48.
38. Valentini V, Buquicchio GL, Galluzzo M, et al. Intussusception in Adults: The Role of MDCT in the Identification of the Site and Cause of Obstruction. Gastroenterol Res Pract 2016; 2016: 5623718-18.
39. Faggian A, Fracella MR, D'Alesio G, et al. Small-Bowel Neoplasms: Role of MRI Enteroclysis. Gastroenterol Res Pract 2016; 2016:
40. Valentini G, Marcoccia A, Cuomo G, et al. Early systemic sclerosis: marker autoantibodies and videocapillaroscopy patterns are each associated with distinct clinical, functional and cellular activation markers. Arthritis Res Ther 2013; 15: R63.
41. Reginelli A, Mandato Y, Solazzo A, Berritto D, Iacobellis F, Grassi R. Errors in the Radiological Evaluation of the Alimentary Tract: Part II. Semin Ultrasound CT MR 2012; 33: 308-17.
42. Dionigi G, Dionigi R, Rovera F, et al. Treatment of high output entero-cutaneous fistulae associated with large abdominal wall defects: single center experience. Int J Surg 2008; 6: 51-6.
43. Mocchegiani F, Vincenzi P, Coletta M, et al. Prevalence and clinical outcome of hepatic haemangioma with specific reference to the risk of rupture: A large retrospective cross-sectional study. Dig Liver Dis 2016; 48: 309-14.
44. Salvolini L, Urbinati C, Valeri G, Ferrara C, Giovagnoni A. Contrast-enhanced MR cholangiography (MRCP) with GD-EOB-DTPA in evaluating biliary complications after surgery. Radiol Med 2012; 117: 354-68.
45. Cappabianca S, Reginelli A, Monaco L, Del Vecchio L, Di Martino N, Grassi R. Combined videofluoroscopy and manometry in the diagnosis of oropharyngeal dysphagia: Examination technique and preliminary experience. Radiol Med 2008; 113: 923-40.
46. Maggialetti N, Capasso R, Pinto D, et al. Diagnostic value of computed tomography colonography (CTC) after incomplete optical colonoscopy. Int J Surg 2016; 33 Suppl 1: S36-44.
47. Sforza V, Martinelli E, Ciardiello F, et al. Mechanisms of resistance to anti-epidermal growth factor receptor inhibitors in metastatic colorectal cancer. World J Gastroenterol 2016; 22: 6345-61.
48. Valeri G, Mazza FA, Maggi S, et al. Open source software in a practical approach for post processing of radiologic images. Radiol Med 2015; 120: 309-23.
49. Grassi R, Rambaldi PF, Di Grezia G, et al. Inflammatory bowel disease: Value in diagnosis and management of MDCT-enteroclysis and 99mTc-HMPAO labeled leukocyte scintigraphy. Abdom Imaging 2011; 36: 372-81.
50. Lo Re G, Cappello M, Tudisca C, et al. CT enterography as a powerful tool for the evaluation of inflammatory activity in Crohn's disease: Relationship of CT findings with CDAI and acute-phase reactants. Radiol Med 2014; 119: 658-66.
51. Taylor SA, Avni F, Cronin CG, et al. The first joint ESGAR/ ESPR consensus statement on the technical performance of cross-sectional small bowel and colonic imaging. Eur Radiol 2017; 27: 2570-82.
52. Puylaert CAJ, Tielbeek JAW, Bipat S, Stoker J. Grading of Crohn's disease activity using CT, MRI, US and scintigraphy: a meta-analysis. Eur Radiol 2015; 25: 3295-313.
53. Di Cesare E, Cademartiri F, Carbone I, et al. Clinical indications for the use of cardiac MRI. by the SIRM Study Group on Cardiac Imaging. Radiol Med 2013; 118: 752-98.
54. Schicchi N, Valeri G, Moroncini G, et al. Myocardial perfusion defects in scleroderma detected by contrast-enhanced cardiovascular magnetic resonance. Radiol Med 2014; 119: 885-94.
55. Barile A, Arrigoni F, Bruno F, et al. Computed Tomography and MR Imaging in Rheumatoid Arthritis. Radiol Clin North Am 2017; 55: 997-1007.
56. Maurizi N, Passantino S, Spaziani G, et al. Long-term Outcomes of Pediatric-Onset Hypertrophic Cardiomyopathy and Age-Specific Risk Factors for Lethal Arrhythmic Events. JAMA Cardiol 2018; 3: 520-25.
57. Pradella S, Lucarini S, Colagrande S. Liver lesion characterization: The wrong choice of contrast agent can mislead the diagnosis of hemangioma. Am J Roentgenol 2012; 199:
58. Macchi M, Belfiore MP, Floridi C, et al. Radiofrequency versus microwave ablation for treatment of the lung tumours: LUMIRA (lung microwave radiofrequency) randomized trial. Med Oncol 2017; 34:
59. Tarantini G, Favaretto E, Napodano M, et al. Design and methodologies of the postconditioning during coronary angioplasty in acute myocardial infarction (POST-AMI) trial. Cardiology 2010; 116: 110-16.
60. Cazzato RL, Arrigoni F, Emanuele Boatta, et al. Percutaneous management of bone metastases: state of the art, interventional strategies and joint position statement of the Italian College of MSK Radiology (ICoMSKR) and the Italian College of Interventional Radiology (ICIR). Radiol Med 2018; 1: 3-3.
61. Barile A, Arrigoni F, Bruno F, et al. Present role and future perspectives of interventional radiology in the treatment of painful bone lesions. Future Oncol 2018; 14: 2945-55.
62. Bruno F, Barile A, Arrigoni F, et al. Weight-bearing MRI of the knee: A review of advantages and limits. Acta Biomed 2018; 89: 78-88.
63. Arrigoni F, Bruno F, Zugaro L, et al. Developments in the management of bone metastases with interventional radiology. Acta Biomed 2018; 89: 166-74.
64. Zoccali C, Arrigoni F, Mariani S, Bruno F, Barile A, Mas-

ciocchi C. An unusual localization of chondroblastoma: The triradiate cartilage; from a case report a reconstructive technique proposal with imaging evolution. J Clin Orthop Trauma 2017; 8: S48-S52.
65. Bruno F, Smaldone F, Varrassi M, et al. MRI findings in lumbar spine following O2-O3 chemiodiscolysis: A long-term follow-up. Interv Neuroradiol 2017; 23: 444-50.
66. Barile A, Bruno F, Arrigoni F, et al. Emergency and Trauma of the Ankle. Semi Musc Rad 2017; 21: 282-89.
67. Splendiani A, Bruno F, Patriarca L, et al. Thoracic spine trauma: advanced imaging modality. Radiol Med 2016; 121: 780-92.
68. Giordano AV, Arrigoni F, Bruno F, et al. Interventional Radiology Management of a Ruptured Lumbar Artery Pseudoaneurysm after Cryoablation and Vertebroplasty of a Lumbar Metastasis. Cardiovasc Intervent Radiol 2017; 40: 776-79.
69. Barile A, Bruno F, Mariani S, et al. What can be seen after rotator cuff repair: a brief review of diagnostic imaging findings. Musculoskelet Surg 2017; 101: 3-14.
70. Barile A, Bruno F, Mariani S, et al. Follow-up of surgical and minimally invasive treatment of Achilles tendon pathology: a brief diagnostic imaging review. Musculoskelet Surg 2017; 101: 51-61.
71. Splendiani A, Perri M, Grattacaso G, et al. Magnetic resonance imaging (MRI) of the lumbar spine with dedicated G-scan machine in the upright position: a retrospective study and our experience in 10 years with 4305 patients. Radiol Med 2016; 121: 38-44.
72. Arrigoni F, Barile A, Zugaro L, et al. Intra-articular benign bone lesions treated with Magnetic Resonance-guided Focused Ultrasound (MRgFUS): imaging follow-up and clinical results. Med Oncol 2017; 34: 55.
73. Zappia M, Castagna A, Barile A, Chianca V, Brunese L, Pouliart N. Imaging of the coracoglenoid ligament: a third ligament in the rotator interval of the shoulder. Skeletal Radiol 2017; 46: 1101-11.
74. Barile A, La Marra A, Arrigoni F, et al. Anaesthetics, steroids and platelet-rich plasma (PRP) in ultrasound-guided musculoskeletal procedures. Br J Radiol 2016; 89: 20150355.
75. Reginelli A, Zappia M, Barile A, Brunese L. Strategies of imaging after orthopedic surgery. Musculoskelet Surg 2017; 101: 1.
76. Maccioni F, Al Ansari N, Mazzamurro F, et al. Detection of Crohn disease lesions of the small and large bowel in pediatric patients: Diagnostic value of MR enterography versus reference examinations. Am J Roentgenol 2014; 203: W533-W42.
77. Michelini G, Corridore A, Torlone S, et al. Dynamic MRI in the evaluation of the spine: State of the art. Acta Biomed 2018; 89: 89-101.
78. Masciocchi C, Arrigoni F, Ferrari F, et al. Uterine fibroid therapy using interventional radiology mini-invasive treatments: current perspective. Med Oncol 2017; 34: 52.
79. Scialpi M, Cappabianca S, Rotondo A, et al. Pulmonary congenital cystic disease in adults. Spiral computed tomography findings with pathologic correlation and management. Radiol Med 2010; 115: 539-50.
80. Muccio CF, Di Blasi A, Esposito G, Brunese L, D'Arco F, Caranci F. Perfusion and spectroscopy magnetic resonance imaging in a case of lymphocytic vasculitis mimicking brain tumor. Pol J Radiol 2013; 78: 66-69.
81. Battipaglia G, Avilia S, Morelli E, Caranci F, Perna F, Camera A. Posterior reversible encephalopathy syndrome (PRES) during induction chemotherapy for acute myeloblastic leukemia (AML). Ann Hematol 2012; 91: 1327-28.
82. Briganti F, Leone G, Marseglia M, Cicala D, Caranci F, Maiuri F. P64 Flow Modulation Device in the treatment of intracranial aneurysms: Initial experience and technical aspects. J Neurointerv Surg 2016; 8: 173-80.
83. Cirillo M, Caranci F, Tortora F, et al. Structural neuroimaging in dementia. J Alzheimers Dis 2012; 29: 16-19.
84. Sverzellati N, Calabrò E, Chetta A, et al. Visual score and quantitative CT indices in pulmonary fibrosis: Relationship with physiologic impairment. Radiol Med 2007; 112: 1160-72.
85. Bertolini L, Vaglio A, Bignardi L, et al. Subclinical interstitial lung abnormalities in stable renal allograft recipients in the era of modern immunosuppression. Transplant Proc 2011; 43: 2617-23.
86. Di Cesare E, Gennarelli A, Di Sibio A, et al. Image quality and radiation dose of single heartbeat 640-slice coronary CT angiography: A comparison between patients with chronic Atrial Fibrillation and subjects in normal sinus rhythm by propensity analysis. Eur J Radiol 2015; 84: 631-36.
87. Masciocchi C, Conti L, D'Orazio F, Conchiglia A, Lanni G, Barile A, Errors in Musculoskeletal MRI, in: Romano L., Pinto A. (Eds.), Errors in Radiology, Springer Milan, Milano, 2012, pp. 209-17.
88. Lenze F, Wessling J, Bremer J, et al. Detection and differentiation of inflammatory versus fibromatous Crohn's disease strictures: Prospective comparison of18F-FDG-PET/CT, MR-enteroclysis, and transabdominal ultrasound versus endoscopic/histologic evaluation. Inflamm Bowel Dis 2012; 18: 2252-60.
89. Bettenworth D, Nowacki TM, Cordes F, Buerke B, Lenze F. Assessment of stricturing Crohn's disease: Current clinical practice and future avenues. World J Gastroenterol 2016; 22: 1008-16.
90. Westerland O, Griffin N. Magnetic Resonance Enterography in Crohn's Disease. Semin Ultrasound CT MR 2016; 37: 282-91.
91. Tolan DJM, Greenhalgh R, Zealley IA, Halligan S, Taylor SA. MR Enterographic Manifestations of Small Bowel Crohn Disease. RadioGraphics 2010; 30: 367-84.
92. Grand DJ, Guglielmo FF, Al-Hawary MM. MR enterography in Crohn's disease: current consensus on optimal imaging technique and future advances from the SAR Crohn's disease-focused panel. Abdom Imaging 2015; 40: 953-64.
93. Iannicelli E, Martini I, Fantini C, et al. Magnetic resonance enterography in Crohn's disease: New simple proposal to assess disease activity. Clin Imaging 2016; 40: 492-97.

94. Dohan A, Taylor S, Hoeffel C, et al. Diffusion-weighted MRI in Crohn's disease: Current status and recommendations. Journal of magnetic resonance imaging : JMRI 2016; 44: 1381-96.
95. Rimola J, Rodriguez S, García-Bosch O, et al. Magnetic resonance for assessment of disease activity and severity in ileocolonic Crohn's disease. Gut 2009; 58: 1113-20.
96. Rimola J, Ordás I, Rodriguez S, et al. Magnetic resonance imaging for evaluation of Crohn's disease: Validation of parameters of severity and quantitative index of activity. Inflamm Bowel Dis 2011; 17: 1759-68.
97. Kim JS, Jang HY, Park SH, et al. MR enterography assessment of bowel inflammation severity in Crohn disease using the MR index of activity score: Modifying roles of DWI and effects of contrast phases. Am J Roentgenol 2017; 208: 1022-29.
98. Arrigoni F, Bruno F, Zugaro L, et al. Role of interventional radiology in the management of musculoskeletal soft-tissue lesions. Radiol Med 2018; 1-6.
99. Barile A, Quarchioni S, Bruno F, et al. Interventional radiology of the thyroid gland: Critical review and state of the art. Gland Surg 2018; 7: 132-46.
100. Brunese L, Romeo A, Iorio S, et al. Thyroid B-flow twinkling sign: a new feature of papillary cancer. Eur J Endocrinol 2008; 159: 447-51.
101. Cantisani V, Grazhdani H, Drakonaki E, et al. Strain US elastography for the characterization of thyroid nodules: Advantages and limitation. Int J Endocrinol 2015; 2015:
102. Gatta G, Parlato V, Di Grezia G, et al. Ultrasound-guided aspiration and ethanol sclerotherapy for treating endometrial cysts. Radiol Med 2010; 115: 1330-39.
103. Regine G, Atzori M, Miele V, et al. Second-generation sonographic contrast agents in the evaluation of renal trauma. Radiol Med 2007; 112: 581-87.
104. Iacobellis F, Segreto T, Berritto D, et al. A rat model of acute kidney injury through systemic hypoperfusion evaluated by micro-US, color and PW-Doppler. Radiol Med 2018;
105. Perrotta FM, Astorri D, Zappia M, Reginelli A, Brunese L, Lubrano E. An ultrasonographic study of enthesis in early psoriatic arthritis patients naive to traditional and biologic DMARDs treatment. Rheumatol Int 2016; 36: 1579-83.
106. Wale A, Pilcher J. Current Role of Ultrasound in Small Bowel Imaging. Semin Ultrasound CT MR 2016; 37: 301-12.
107. De Franco A, Di Veronica A, Armuzzi A, et al. Ileal Crohn disease: mural microvascularity quantified with contrast-enhanced US correlates with disease activity. Radiology 2012; 262: 680-8.
108. Allen BC, Baker ME, Einstein DM, et al. Effect of altering automatic exposure control settings and quality reference mAs on radiation dose, image quality, and diagnostic efficacy in MDCT enterography of active inflammatory Crohn's disease. AJR Am J Roentgenol 2010; 195: 89-100.
109. Taylor SA, Punwani S, Rodriguez-Justo M, et al. Mural Crohn disease: correlation of dynamic contrast-enhanced MR imaging findings with angiogenesis and inflammation at histologic examination--pilot study. Radiology 2009; 251: 369-79.
110. Esteban JM, Maldonado L, Sanchiz V, Minguez M, Benages A. Activity of Crohn's disease assessed by colour Doppler ultrasound analysis of the affected loops. Eur Radiol 2001; 11: 1423-28.
111. Manetta R, Pistoia ML, Bultrini C, Stavroulis E, Di Cesare E, Masciocchi C. Ultrasound enhanced with sulphur-hexafluoride-filled microbubbles agent (SonoVue) in the follow-up of mild liver and spleen trauma. Radiol Med 2009; 114: 771-9.
112. Nylund K, Hausken T, Gilja OH. Ultrasound and inflammatory bowel disease. Ultrasound Q 2010; 26: 3-15.
113. Mocci G, Migaleddu V, Cabras F, et al. SICUS and CEUS imaging in Crohn's disease: an update. J Ultrasound 2017; 20: 1-9.
114. Onali S, Calabrese E, Petruzziello C, et al. Endoscopic vs ultrasonographic findings related to Crohn's disease recurrence: a prospective longitudinal study at 3 years. J Crohns Colitis 2010; 4: 319-28.
115. Calabrese E, Zorzi F, Zuzzi S, et al. Development of a numerical index quantitating small bowel damage as detected by ultrasonography in Crohn's disease. J Crohns Colitis 2012; 6: 852-60.
116. Kratzer W, von Tirpitz C, Mason R, et al. Contrast-enhanced power Doppler sonography of the intestinal wall in the differentiation of hypervascularized and hypovascularized intestinal obstructions in patients with Crohn's disease. J Ultrasound Med 2002; 21: 149-57.
117. Romanini L, Passamonti M, Navarria M, et al. Quantitative analysis of contrast-enhanced ultrasonography of the bowel wall can predict disease activity in inflammatory bowel disease. Eur J Radiol 2014; 83: 1317-23.
118. Robotti D, Cammarota T, Debani P, Sarno A, Astegiano M. Activity of Crohn disease: value of Color-Power-Doppler and contrast-enhanced ultrasonography. Abdom Imaging 2004; 29: 648-52.
119. Migaleddu V, Scanu AM, Quaia E, et al. Contrast-enhanced ultrasonographic evaluation of inflammatory activity in Crohn's disease. Gastroenterology 2009; 137: 43-52.
120. Paredes JM, Ripolles T, Cortes X, et al. Contrast-enhanced ultrasonography: usefulness in the assessment of postoperative recurrence of Crohn's disease. J Crohns Colitis 2013; 7: 192-201.
121. Parente F, Maconi G, Bollani S, et al. Bowel ultrasound in assessment of Crohn's disease and detection of related small bowel strictures: a prospective comparative study versus x ray and intraoperative findings. Gut 2002; 50: 490-5.
122. Nylund K, Jirik R, Mezl M, et al. Quantitative contrast-enhanced ultrasound comparison between inflammatory and fibrotic lesions in patients with Crohn's disease. Ultrasound Med Biol 2013; 39: 1197-206.
123. Girlich C, Jung EM, Iesalnieks I, et al. Quantitative as-

sessment of bowel wall vascularisation in Crohn's disease with contrast-enhanced ultrasound and perfusion analysis. Clin Hemorheol Microcirc 2009; 43: 141-8.
124. Girlich C, Jung EM, Huber E, et al. Comparison between preoperative quantitative assessment of bowel wall vascularization by contrast-enhanced ultrasound and operative macroscopic findings and results of histopathological scoring in Crohn's disease. Ultraschall Med 2011; 32: 154-9.
125. Quaia E, Sozzi M, Angileri R, Gennari AG, Cova MA. Time-Intensity Curves Obtained after Microbubble Injection Can Be Used to Differentiate Responders from Nonresponders among Patients with Clinically Active Crohn Disease after 6 Weeks of Pharmacologic Treatment. Radiology 2016; 281: 606-16.
126. Giannetti A, Biscontri M, Matergi M, Stumpo M, Minacci C. Feasibility of CEUS and strain elastography in one case of ileum Crohn stricture and literature review. J Ultrasound 2016; 19: 231-7.
127. Spinelli A, Allocca M, Jovani M, Danese S. Review article: optimal preparation for surgery in Crohn's disease. Aliment Pharmacol Ther 2014; 40: 1009-22.
128. Horjus Talabur Horje CS, Bruijnen R, Roovers L, Groenen MJ, Joosten FB, Wahab PJ. Contrast Enhanced Abdominal Ultrasound in the Assessment of Ileal Inflammation in Crohn's Disease: A Comparison with MR Enterography. PLoS One 2015; 10: e0136105.
129. Wilson SR, Burns PN. Microbubble-enhanced US in body imaging: what role? Radiology 2010; 257: 24-39.
130. Spinelli A, Allocca M, Jovani M, Danese S, Review article: Optimal preparation for surgery in Crohn's disease, 2014, pp. 1009-22.
131. Splendiani A, Perri M, Marsecano C, et al. Effects of serial macrocyclic-based contrast materials gadoterate meglumine and gadobutrol administrations on gadolinium-related dentate nuclei signal increases in unenhanced T1-weighted brain: a retrospective study in 158 multiple sclerosis (MS) patients. Radiol Med 2018; 123: 125-34.
132. Tedeschi E, Caranci F, Giordano F, Angelini V, Cocozza S, Brunetti A. Gadolinium retention in the body: what we know and what we can do. Radiol Med 2017; 122: 589-600.
133. Malago R, D'Onofrio M, Mantovani W, et al. Contrast-enhanced ultrasonography (CEUS) vs. MRI of the small bowel in the evaluation of Crohn's disease activity. Radiol Med 2012; 117: 268-81.
134. Quaia E, Migaleddu V, Baratella E, et al. The diagnostic value of small bowel wall vascularity after sulfur hexafluoride-filled microbubble injection in patients with Crohn's disease. Correlation with the therapeutic effectiveness of specific anti-inflammatory treatment. Eur J Radiol 2009; 69: 438-44.
135. Bozzetti C, Nizzoli R, Tiseo M, et al. ALK and ROS1 rearrangements tested by fluorescence in situ hybridization in cytological smears from advanced non-small cell lung cancer patients. Diagnostic Cytopathology, vol. 43, p. 941-946, ISSN: 8755-1039, doi: 10.1002/dc.23318.
136. De Filippo M, Gira F, Corradi D, Sverzellati N, Zompatori M, Rossi C. (2011). Benefits of 3D technique in guiding percutaneous retroperitoneal biopsies. RAD. MED, vol. 116(3), p. 407-416, ISSN: 0033-8362, doi: 10.1007/s11547-010-0604-2
137. De Filippo M, Onniboni M, Rusca M, et al. (2008). Advantages of multidetector row CT with multiplanar reformation in guiding percutaneous lung biopsies. RAD. MED, vol. 113, p. 945-953, ISSN: 0033-8362, doi: 10.1007/s11547-008-0325-y

Received: 26 March 2019
Accepted: 4 April 2019
Correspondence:
Antonio Barile M.D.
Department of Biotechnology and Applied Clinical Sciences
University of L'Aquila, Vetoio Street, 1 - 67100 L'Aquila, Italy
Tel. +390862414258
E-mail: antonio.barile@cc.univaq.it

Acta Biomed 2019; Vol. 90, Supplement 5: 51-61 DOI: 10.23750/abm.v90i5-S.8346

Review

Diagnostic value/performance of radiological liver imaging during chemoterapy for gastrointestinal malignancy: a critical review

Alfonso Reginelli[1], Giovanna Vacca[1], Nicoletta Zanaletti[2], Teresa Troiani [2], Raffaele Natella[1], Nicola Maggialetti[3], Pierpaolo Palumbo[4], Andrea Giovagnoni[5], Fortunato Ciardiello[2], Salvatore Cappabianca[1]

[1] Department of Precision Medicine, University of Campania "L. Vanvitelli", Naples, Italy; [2] Medical Oncology, University of Campania "Luigi Vanvitelli", Naples, Italy; [3] Department of Medicine and Health Sciences "V. Tiberio", University of Molise, Campobasso, Italy; [4] Department of Biotechnology and Applied Clinical Sciences, University of L'Aquila, S. Salvatore Hospital, L'Aquila, Italy; [5] Department of Radiology, Università Politecnica delle Marche, Ancona, Italy

Summary. This article reviews the main toxic effect, complications and relative imaging findings of the liver that may appear during the oncologic follow up among patients affected by gastrointestinal malignancy. Awareness of the causative chemotherapeutic agent and regimens, pathophysiology and relative characteristic imaging findings of hepatic injuries is critical in order to obtain an accurate diagnosis especially when these parenchymal lesions are focal. An accurate synergic radiological diagnosis with Computed Tomography (CT) and Magnetic Resonance (MR) techniques may induce a potential termination of ineffective/toxic chemotherapy during early phases of treatment, changing the therapeutic plan in order to avoid first unnecessary liver biopsy and then invasive treatment as hepatic resection if not required. (www.actabiomedica.it)

Key words: colorectal cancer-chemotherapy-induced focal hepatopathy, steatosis, steatohepatitis, sinusoidal obstruction syndrome, liver MR - hepatobiliary phase-Liver CT

1. Introduction

Nearly one in two men and one in three women in the United States will be affected by cancer during the lifetime (1). Colorectal cancer is the third most common type of cancer diagnosed in men and the second in women. The liver is the most frequent site of colorectal cancer metastases and up to 25% of patients present hepatic metastases at the time of diagnosis of the primary tumour (synchronous); another 25% will develop metachronous ones during the follow up (2) (3-6).

Ultrasonography (US), Magnetic Resonance Imaging (MRI) (7-17) and computed tomography (CT) (18-30) are widely used in the diagnostic setting, with or without the use of contrast agents (23, 31-33), and as guidance in many interventional radiology procedures (34-40). US is the least invasive imaging examination, well tolerated by patients (41-43).

Liver hepatectomy still represents the best curative therapeutic option for patients with colorectal metastases even if it is often preceded by chemotherapy in the preoperative setting (neoadjuvant chemotherapy) because only 15-25% of patients are fit for the curative metastasectomy at the time of presentation (44).

This medical treatment can reduce the size of colorectal liver metastases, downsize the present metastases and may provide to a presumptive treatment of micro metastases (45).

Unfortunately, micro metastases (less than 10 mm) are nearly undetectable using radiological imaging being the major cause of recurrence during follow up. Differentiation of small haemangiomas and cysts

smaller than 1 cm from metastases can be difficult due to volume averaging. The sensitivity of CT for detecting lesions less than 1 cm decreases from 65%-95% to 31%-38% (46, 47).

This article reviews the toxic effect, complications and relative imaging findings of the liver that may appear during the oncologic follow up among patients affected by gastrointestinal malignancy. Radiologists should know that in addition to the desired effects on malignancy, systemic oncological therapy could determine toxic effects whose are often visible first at imaging (48, 49).

2. Background

Any type of drug is able to induce changes in biological function and so to modify cell and organs function.

This modify can be positive or negative/toxic: it depends on concentration, dose and patient's own characteristics determining eventually drug adverse reaction that are predictable in most of cases.

Drug arrive to the target organs by steps. Pharmacokinetics studies processes that follow the administration of the drugs: absorption, metabolism and excretion. Through distribution, drugs arrive to the target organs to make its pharmacological effect (50).

Each of these steps is influenced by drug molecular structure (e.g. lipophilia), physiological characteristic such as pregnancy, age or nutritional state and patient pathologies such as hepatic or kidney's injury, cardiovascular disease or neoplastic ones.

Hepatic metabolism represents a crucial step because in most of cases drugs have to be transformed into more hydrophilic compounds in order to be eliminated easily by kidney and/or liver.

Chemotherapy traditionally includes cytotoxic agents because their own mechanism of action consists in the capacity of induction a cell damage that can be lethal for sensible cells, through a direct damn or interference in the replicative process of the proliferating cells. These agents have low therapeutic index because they're not specific for tumoral cells and they can cause toxicity especially to normal proliferating tissues (e.g. bone marrow).

Unfortunately, solid tumors (like colorectal malignancy) aren't sensible to these types of drugs compared with lymphoma or testis tumor so they should be associated to others in order to improve the therapeutic effect.

Nowadays newer agents such as molecular targeted therapies and immunological agents are available in clinical practice as monotherapy or in combination with each other.

2.1 Chemotherapy for gastrointestinal malignancy

Patients with advanced stage disease could require different types of chemotherapy (preoperative, postoperative or palliative chemotherapy) (51). Preoperative therapy, so called neoadjuvant chemotherapy, offers the potential advantage of eradicating micro metastatic disease preoperatively improving progression free survival especially through innovative associations of agents with the aim to ensure a multimodal treatment for colorectal liver metastases (2). In selected patients, unresectable metastatic disease can be rendered resettable by administering "conversion chemotherapy" in order to downsize the tumor and make possible a surgical resection increasing the number of patients undergoing curative hepatectomy. The duration of both these regimens of chemotherapy should be assessed as short as possible because of the risk of hepatic injury associated (52).

2.1.1 Alchilant agents (oxaliplatin)

They have the ability to react with DNA creating irreversible damage and lethal effect to the cell. One of these drugs called oxaliplatin is frequently used in combination with 5-FU/leucovorin or capecitabine for the treatment of gastrointestinal tumors. Toxicity, generally dose dependent, is represented by peripheral neuropathy and impose dose reduction. Oxaliplatin-based chemotherapy regimens (FOLFOX, CapeOX and FLOX) are recommended by NCCN for adjuvant treatment in colorectal cancer patients (8) and as neoadjuvant therapy in combination with 5-FU in patients with colorectal liver metastases.

2.1.2 Antimetabolite agents (fluorouracil and capecitabine)

Because of their similitude with physiological

metabolites, fluoropyrimidine such as fluorouracil (5-FU) can interfere with RNA synthesis and function and determine myelotoxicity as adverse reaction. 5-FU is administrated intravenously while capecitabine is a prodrug that is converted in the intestine into the active 5-FU and it's given orally (53).

2.1.3 Topoisomerase inhibitor (irinotecan)

Irinotecan reversibly stabilizes the topoisomerase. I complex, blocking DNA synthesis with a double-strand DNA break. This event induces arrest of the cell cycle in the S-G2 phase and ultimately cause cell death (53).

2.1.4 Target therapy (bevacizumab)

Bevacizumab is a monoclonal antibody that binds to vascular endothelial growth factor (VEGF) in the circulation and inhibits its connection to the receptor VEGFR. This complex prevents new vessel formation, reduces capillary leak and normalizes tumour vasculature (54).

3. Hepatic adverse injuries

Chemotherapy induces many undesirable effects against the hepatic parenchyma that may reduce and/or make difficult the detection of the hepatic tumor burden in patients with liver metastases. As patients with metastatic tumors undergo chemotherapy with curative intent with increasing frequency, it is mandatory therefore to understand the pathophysiology of these therapy-induced liver injury in order to be familiar with their imaging features .

3.1 Sinusoidal obstruction syndrome (SOS): pathophysiology and imaging features

Rubbia et al. observed that the neoadjuvant administration of oxaliplatin in patients with colorectal liver metastases was a risk factor for the development of a specific liver injury called sinusoidal obstruction syndrome (55, 56). Bevacizumab seems to have a protective effect against oxaliplatin-related sinusoidal lesions(57). This sinusoidal injury occurred for 19–52% of patients treated by oxaliplatin-based chemotherapy (58-61). Patients could present abdominal pain, swelling, and weight gain, with or without elevation in serum enzyme levels (62).

SOS includes several pathologic conditions such as sinusoidal dilatation, peliosis, and nodular regenerative hyperplasia.

The major component initiating SOS seems to be the depolymerization of the F-actin and the increased expression of matrix metalloproteinase-9 in sinusoidal endothelial cells.

The sinusoidal wall integrity is then disrupted causing red blood cells migration into the space of Disse and deposition of collagens determining respectively peliosis and perisinusoidal fibrosis (63-66). Furthermore, the obstruction and increased pressure in the sinusoid determine presence of atrophic hepatocytes and also enlarged ones forming nodular regenerative hyperplasia (67). The discover and relative diagnosis of SOS could be important clinically for at least three reasons. First it is associated with an increased risk of morbidity after liver resection and bleeding. Particularly SOS has been associated with an increased risk for intraoperative blood transfusions, early recurrence after resection and a short overall survival after resection due to liver insufficiency (60, 68). Recently another interesting reported side effect is the development of liver nodules mimicking liver metastases (69, 70) misinterpreted as hepatic metastasis (71). Finally radiologists have to consider the development of oxaliplatin-induced SOS to avoid mistaking new-onset ascites for evidence of recurrent disease (72).

However, US findings include ascites, gallbladder wall thickening, and hepatosplenomegaly. Doppler US may show decreased flow in the portal vein (73). Common signs of a new-onset portal hypertension on CT examination could appear, including ascites, splenomegaly, periesophageal varices, and recanalization of the umbilical vein. Increased volume of the spleen has been reported to suggest sinusoidal injury(74-76); however, increased spleen size indicates portal hypertension and it is not specific for SOS(77). Han et al. reported that post-oxaliplatin "heterogeneity" of liver parenchyma, appearing as diffuse and heterogeneous hypoattenuation of the hepatic parenchyma on contrast-enhanced CT, is frequently observed in patients treated with oxaliplatin (45, 77). These findings are

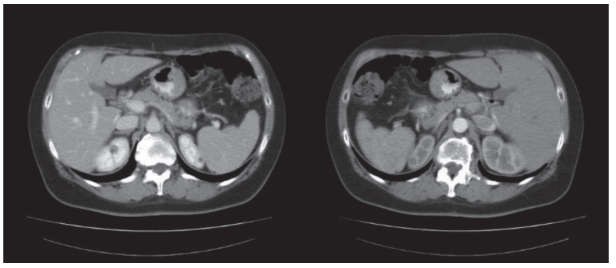

Figure 1. 55-year old woman affected by left colon adenocarcinoma who undergoes to left hemicolectomy. We may observe in this preoperative CT diffuse low attenuation of the liver

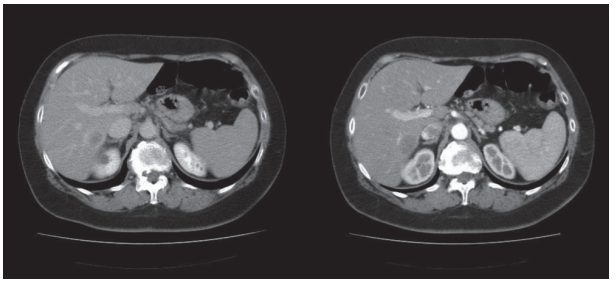

Figure 2. After the surgical resection of the primary tumor, the histological staging is pT3N1M1 for the presence, in the first post-operative CT, of a nodular hypodense lesion surrounded by rim enhancement with the appereance of a colorectal liver metastases

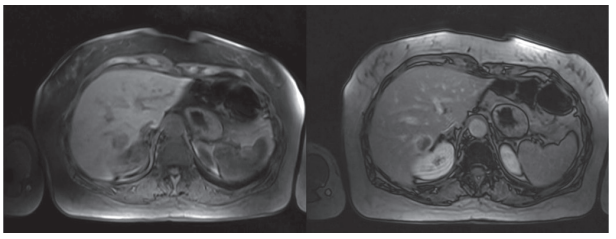

Figure 3. MR dynamic imaging confirms CT diagnosis of a colorectal metastase. This lesion is hypointense in T1w images before and after administration of contrast agent compared to the surrounding liver

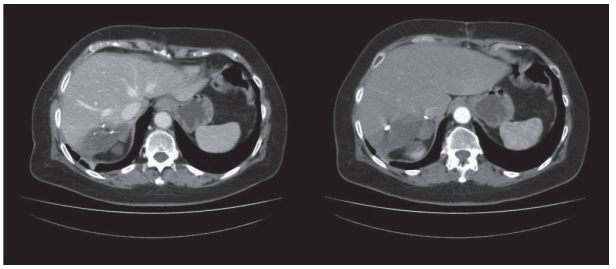

Figure 4. After a six-cycles-Folfox neoadjuvant regimen, these CT post-operative imaging shows common findings after surgical resection. The hepatic malignant lesion is confermed with the addiction of "blue liver" as chemotherapeutic liver adverse reaction

especially observed at the peripheral area and right hepatic lobe. At MR, diffused SOS is detectable by T2-weighted images showing a heterogeneous liver with areas of increased signal intensity corresponding to edema (47). Heterogeneous reticular pattern are also found in the hepatic parenchyma on hepatobiliary phase (HBP) MRI of the liver using gadoxetate disodium (78, 79) . However morphological imaging modalities, such as CT or US, are not enough suitable for the diagnosis of a pseudotumor caused by SOS (80). Focally lesions of SOS show an ill-defined margin (considered as the most valuable feature), nonspherical shape, isointensity on T1- weighted images, iso or hyper-signal intensity on T2-weighted images, unlike of a metastatic nodule. Gd-EOB MRI nevertheless displays a defect in the hepatocyte phase, similar to imaging findings of colorectal liver metastasis(47). Therefore, diffusion-weighted MRI, may be fundamental because the cellular density is higher in cancer than in pseudotumor (81).

3.2 Focal nodular hyperplasia-like lesions

Chemotherapeutic regimens with OXP may lead to the appearance of focal nodule hyperplasia (FNH) like lesions. It is very important to differentiate this type of pseudo metastases from the real ones during follow-up. This kind of diagnosis seems to be more suitable with MR images. Commonly FNK-like lesions appear as solitary or multiple nodular and well demarcated peripherally located liver lesions exhibiting significant contrast enhancement on hepatobiliary phase (77).

Images similarly to FNH ones, representing a benign hyperplasia of the hepatic parenchyma, maybe linked to a vascular injury with increased arterial perfusion in areas with absent portal blood flow (77). In these lesions' overexpression of OATP8 that is the uptake transporter of gadoxetic acid may be due to increased hepatocyte function to compensate diffuse liver injury (82, 83).

3.3 Pseudocirrhosis: pathophysiology and imaging features

Pseudocirrhosis describes diffuse and heterogenic hepatic parenchyma due to the contemporary presence

of capsular retraction and nodular regenerative hyperplasia. This setting is however more common in patients undergoing chemotherapy for breast cancer (up to 50%) of patients (84-87). CT imaging shows first initial loss of the normal convex edge of the liver, with the presence of metastases followed by capsular retraction. It is very important to discontinue therapy in order to avoid progression in fibrosis, especially when this structural liver morphological change becomes severe with the occurrence of ascites, varices and splenomegaly, similar to true cirrhosis signs of portal hypertension. A recent case report shows the singular diagnosis of esophageal varices without liver dysfunction, after 3.5-year follow-up of the oxaliplatin-based chemotherapy (88).

3.4 Portal vein thrombosis

Portal vein branch thrombosis may appear after chemotherapy regimens with 5-FU and irinotecan (FOLFIRI) and bevacizumab (89, 90).The latter binds to the VEGF receptor and decreases the healing capacity of endothelial cells, determining bleeding and thrombosis. The mechanism by which irinotecan may determine thrombosis is not known. Patients with portal vein thrombosis are usually asymptomatic so the first diagnosis is often reached by imaging. Portal vein thrombosis is seen as a filling defect in the portal vein branch. In the arterial phase this wedge-shaped area shows increased enhancement that becomes isoattenuating compared to the liver in the further phases (90).

3.5 Steathosis and steatohepatitis: pathophysiology and imaging features

Many studies show that some chemotherapeutic agents, such as 5-FU and irinotecan, may determine chemotherapy-induced steatosis (51). The form of nonalcoholic steatohepatitis linked to chemotherapy is called chemotherapy-associated steatohepatitis (CASH) (91). The frequency of this occurrence is unknown (65, 92, 93).The combination of irinotecan and 5-fluorouracil (FOLFIRI) should be used carefully therefore in patients who are predisposed to fatty liver, mainly for those who can be eligible for liver resection. Hepatic steatosis increases morbidity after liver resection and the presence of steatohepatitis has been associated with a higher 90-day mortality rate (93, 94). It is difficult to distinguish between steatosis and steatohepatitis through imaging features. However hepatic steatosis is characterized by deposition of lipid vesicles in hepatocytes while steatohepatitis is marked by ballooning of hepatocytes, lobular inflammation, or degeneration of hepatocytes(95). At imaging, steatosis can be focal or diffuse. At ultrasonography (US), the hepatic parenchyma shows increased echogenicity while at CT low attenuation compared to the spleen (at least 10 HU at unenhanced CT) (90). At MR imaging with in-phase and out-of-phase gradient-echo sequences, the presence of signal loss (dropout) on out-of-phase images when compared with in-phase images confirms the presence of steatosis. The pattern of fatty deposition may be also focal mimicking metastases. However, in this case MRI allows to obtain a more reliable diagnosis because unlike steatosis there is no signal drop on the opposed phase in the images of metastasis (95). According to Unal et al., focal steatosis liver parenchyma may show decreased hepatocyte function and signal on MRI Gd-EOB-DTPA-enhanced liver while fat spared areas may demonstrate compensatory increased hepatocyte function on the same phase similarly to FNH-like lesions. Anyway, in the latter case diagnosis could be easily reached with T1w in- and out-of-phase (77)

4. Discussion

Follow up in oncology represents the period of time that starts after the first treatment with a curative intent. Follow up for colorectal cancer has become much longer because of the increased median overall survival of these patients due principally to the improving efficacy of modern chemotherapeutic regimens (96).

The current concept of multidisciplinary treatment and management of patient affected by colorectal malignancy has been decisive to reach optimal outcomes.

In this team, radiologists must be aware of their crucial role. Mainly during chemotherapy, imaging diagnosis is necessary to evaluate:

- treatment response;
- detection of metastases and recurrence;

- restaging of the malignancy.

CT is currently the most commonly used first-line imaging modality for oncologic monitoring because of its wide availability and reproducibility (97). CT, is also a valuable diagnostic tool for the diagnosis and the guidance of interventional procedures in a wide range of organs and in the in gastrointestinal systems (98-103).

Regarding treatment response during follow up, the effects of conventional chemotherapeutic agents are assessed generally after three to four cycles of chemotherapy (after about 1 to 2 months into the therapy) and changes in lesion sizes, as classified according to Response Evaluation Criteria in Solid Tumor (RECIST) are used to planning further decision (104, 105). However, it is already known that new imaging criteria are needed to better characterize tumor response actually. Hepatic lesions, when treated through regimens with molecularly targeted therapeutic agents, may be responding to treatment even without change in size .

Regarding the detection of metastases (hepatic tumor burden) , we should remember indeed the effect of chemotherapy first on the hepatic metastases itself and then on the surrounding liver parenchymal.

Han et al demonstrated a correlation between treatment response of colorectal liver metastases and SOS in patient who have undergone oxaliplatin-based chemotherapy: the more severe is SOS, evaluated by CT parenchymal heterogeneity, the worse the tumor response is expected to be (45).

Hepatic hypoperfusion due to sinusoidal obstruction syndrome might induce hepatic hypoxia, reducing the response to chemotherapy and increasing instead the invasiveness of the tumor in the surrounding stroma (106).

Until now, in a patient with a story of gastrointestinal malignancy, radiologists have considered the appearance of each new hepatic nodule first as a new metastatic lesionn(51). This possible setting could indicate progression disease and change in therapeutic planning. It is important to recognize therefore parenchymal changes due to systemic therapy in order to make differential diagnosis especially from metastases when these structural changes are focal (pseudo metastases) (96).

During follow up with CT examination it might be possible to discover new indeterminate hepatic lesion or diffuse changes in the hepatic parenchyma that make difficult the detection of malignancy. Radiologists should be aware of the possibility that a new developing liver lesion is not always a new metastasis.

Multi-detector row CT represents the modality of choice for oncologic surveillance thanks to its availability and efficiency (23, 97, 107, 108); nowadays, for the complexity of the questions that radiologists have to answer, morphological CT study should be more often associated with other emerging functional and molecular imaging techniques.

CT perfusion parameters for example seems to predict properly the presence and extent of tumor vessels (109-112). Even if CT perfusion is a technique actually available mainly in research studies, it should be considered in future to improve earlier detection of liver malignancies and more individualized monitoring of patients during treatment, especially for molecular targeted therapies that act on on tumor perfusion.

In order to assess a better diagnosis and to quantify properly the hepatic tumor burden, liver dynamic MR examination with DWI/ADC (113) and contrast-hepatobiliary phase should be recommended. Multidetector CT has a specificity of 67% in characterizing lesions as benign or malignant, compared with 81% for MR imaging (47).The use of heavily T2-weighted images may help differentiate solid malignant lesions from hemangiomas and cysts (46).

Furthermore hepatocyte-specific contrast-enhanced MR imaging detects more metastatic lesions than does conventional MR imaging and should be used particularly for the follow-up of metastases after systemic or liver-directed therapies (114). Hepatic metastases typically appear hypointense relative to the surrounding liver parenchyma on delayed images, whereas “pseudo metastases” lesions such as focal nodular hyperplasia are visible as iso- or hyperintense. DW imaging helps the detection of small lesions and apparent diffusion coefficient (ADC) values can be useful to estimate diffusion restriction, differentiating metastatic lesions whose show high-signal-intensity with low ADC values (46, 114). Multiparametric MR examination seems to be necessary also for the preoperative planning after neoadjuvant chemotherapy

regimens with the aim to obtain the most reliable re-staging of the hepatic tumor burden. Systemic chemotherapy in the preoperative setting improves the potential benefit of surgery (115, 116) and this downsizing therapy represent the major reason for the yearly increase in the number of liver resections for colorectal liver metastases (44). Nowadays surgeons estimate that future liver remnant volume after hepatectomy can be as low as 20% if there is no evidence of injury in the remaining liver tissue (117). MR should be recommended therefore also to estimate the quality of the future remnant parenchyma.

MR pre-operative imaging features should be accurately considered because after curative resection in the context of liver surgery, chemotherapy-induced liver injury could increase the risks of intra- and postoperative complications and postoperative liver insufficiency (118). Preoperative diagnosis of these hepatic injuries seems to be important in order to choose the optimal timing for hepatic resection. Karoui et al. demonstrated that morbidity after liver resection was associated with the number of preoperative chemotherapy cycles: patients who received more than 6 cycles of chemotherapy increased morbidity (61). Another issue to consider is that the time interval between cessation of last chemotherapy predicts the possibility to have post-operative liver failure: an interval of less than four weeks was associated with more complications (59, 119).

The desirable aim would be avoiding liver needle biopsy as much as possible because of its invasive nature of carries inherent risks such as infection, requiring local anesthesia or patient sedation (104). In addition, biopsies can potentially stimulate neoangiogenesis by damaging tumor tissue and increase metastatic risk by increasing the number of circulating tumor cells (120).

5. Conclusion

It seems to be necessary to establish common standard radiological findings criteria first to recognize and assess chemotherapy liver adverse injuries (121-125) with the aim to achieve early and accurate diagnosis, especially when these parenchymal lesions are focal. An accurate synergic radiological diagnosis with CT and MR techniques may induce a potential termination of ineffective/toxic chemotherapy during early phases of treatment, changing the therapeutic plan in order to avoid first unnecessary liver biopsy and then invasive treatment as hepatic resection if not required. A more personalized approach of cancer treatment would be desirable by assessment of CT/MR imaging biomarker determining treatment response where the aim is to demonstrate that drugs may have an effect on tumor biology.

Conflict of interest: None to declare

Reference

1. Birch JC, Khatri G, Watumull LM, Arriaga YE, Leyendecker JR. Unintended Consequences of Systemic and Ablative Oncologic Therapy in the Abdomen and Pelvis. Radiographics 2018; 38: 1158-79.
2. Duwe G, Knitter S, Pesthy S, et al. Hepatotoxicity following systemic therapy for colorectal liver metastases and the impact of chemotherapy-associated liver injury on outcomes after curative liver resection. Eur J Surg Oncol 2017; 43: 1668-81.
3. Siegel R, Desantis C, Jemal A. Colorectal cancer statistics, 2014. CA Cancer J Clin 2014; 64: 104-17.
4. Ferlay J, Steliarova-Foucher E, Lortet-Tieulent J, et al. Cancer incidence and mortality patterns in Europe: estimates for 40 countries in 2012. Eur J Cancer 2013; 49: 1374-403.
5. Leporrier J, Maurel J, Chiche L, Bara S, Segol P, Launoy G. A population-based study of the incidence, management and prognosis of hepatic metastases from colorectal cancer. Br J Surg 2006; 93: 465-74.
6. Manfredi S, Lepage C, Hatem C, Coatmeur O, Faivre J, Bouvier AM. Epidemiology and management of liver metastases from colorectal cancer. Ann Surg 2006; 244: 254-9.
7. Muccio CF, Di Blasi A, Esposito G, Brunese L, D'Arco F, Caranci F. Perfusion and spectroscopy magnetic resonance imaging in a case of lymphocytic vasculitis mimicking brain tumor. Pol J Radiol 2013; 78: 66-69.
8. Cirillo M, Caranci F, Tortora F, et al. Structural neuroimaging in dementia. J Alzheimers Dis 2012; 29: 16-19.
9. Di Cesare E, Cademartiri F, Carbone I, et al. Clinical indications for the use of cardiac MRI. by the SIRM Study Group on Cardiac Imaging. Radiol Med 2013; 118: 752-98.
10. Schicchi N, Valeri G, Moroncini G, et al. Myocardial perfusion defects in scleroderma detected by contrast-enhanced cardiovascular magnetic resonance. Radiol Med 2014; 119: 885-94.
11. Tarantini G, Favaretto E, Napodano M, et al. Design and methodologies of the postconditioning during coronary angioplasty in acute myocardial infarction (POST-AMI) trial. Cardiology 2010; 116: 110-16.
12. Iacobellis F, Berritto D, Somma F, et al. Magnetic resonance

imaging: A new tool for diagnosis of acute ischemic colitis? World J Gastroenterol 2012; 18: 1496-501.
13. Cappabianca S, Granata V, Di Grezia G, et al. The role of nasoenteric intubation in the MR study of patients with Crohn's disease: Our experience and literature review. Radiol Med 2011; 116: 389-406.
14. Zappia M, Capasso R, Berritto D, et al. Anterior cruciate ligament reconstruction: MR imaging findings. Musculoskelet Surg 2017; 101: 23-35.
15. Barile A, Arrigoni F, Bruno F, et al. Computed Tomography and MR Imaging in Rheumatoid Arthritis. Radiol Clin North Am 2017; 55: 997-1007.
16. Francone M, Di Cesare E, Cademartiri F, et al. Italian registry of cardiac magnetic resonance. Eur J Radiol 2014; 83: e15-e22.
17. Maurizi N, Passantino S, Spaziani G, et al. Long-term Outcomes of Pediatric-Onset Hypertrophic Cardiomyopathy and Age-Specific Risk Factors for Lethal Arrhythmic Events. JAMA Cardiol 2018; 3: 520-25.
18. Grassi R, Rambaldi PF, Di Grezia G, et al. Inflammatory bowel disease: Value in diagnosis and management of MDCT-enteroclysis and 99mTc-HMPAO labeled leukocyte scintigraphy. Abdom Imaging 2011; 36: 372-81.
19. Scialpi M, Cappabianca S, Rotondo A, et al. Pulmonary congenital cystic disease in adults. Spiral computed tomography findings with pathologic correlation and management. Radiol Med 2010; 115: 539-50.
20. Gafà G, Sverzellati N, Bonati E, et al. Follow-up in pulmonary sarcoidosis: Comparison between HRCT and pulmonary function tests. Radiol Med 2012; 117: 968-78.
21. Bertolini L, Vaglio A, Bignardi L, et al. Subclinical interstitial lung abnormalities in stable renal allograft recipients in the era of modern immunosuppression. Transplant Proc 2011; 43: 2617-23.
22. Sverzellati N, Calabrò E, Chetta A, et al. Visual score and quantitative CT indices in pulmonary fibrosis: Relationship with physiologic impairment. Radiol Med 2007; 112: 1160-72.
23. Cappabianca S, Porto A, Petrillo M, et al. Preliminary study on the correlation between grading and histology of solitary pulmonary nodules and contrast enhancement and [18F] fluorodeoxyglucose standardised uptake value after evaluation by dynamic multiphase CT and PET/CT. J Clin Pathol 2011; 64: 114-19.
24. Maggialetti N, Ferrari C, Minoia C, et al. Role of WB-MR/DWIBS compared to 18F-FDG PET/CT in the therapy response assessment of lymphoma. Radiol Med 2016; 121: 132-43.
25. Di Cesare E, Gennarelli A, Di Sibio A, et al. Image quality and radiation dose of single heartbeat 640-slice coronary CT angiography: A comparison between patients with chronic Atrial Fibrillation and subjects in normal sinus rhythm by propensity analysis. Eur J Radiol 2015; 84: 631-36.
26. Buffa V, Solazzo A, D'Auria V, et al. Dual-source dual-energy CT: dose reduction after endovascular abdominal aortic aneurysm repair. Radiol Med 2014; 119: 934-41.
27. Valentini V, Buquicchio GL, Galluzzo M, et al. Intussusception in Adults: The Role of MDCT in the Identification of the Site and Cause of Obstruction. Gastroenterol Res Pract 2016; 2016: 5623718.
28. Di Cesare E, Patriarca L, Panebianco L, et al. Coronary computed tomography angiography in the evaluation of intermediate risk asymptomatic individuals. Radiol Med 2018; 123: 686-94.
29. Di Pietto F, Chianca V, de Ritis R, et al. Postoperative imaging in arthroscopic hip surgery. Musculoskelet Surg 2017; 101: 43-49.
30. Maggialetti N, Capasso R, Pinto D, et al. Diagnostic value of computed tomography colonography (CTC) after incomplete optical colonoscopy. Int J Surg 2016; 33 Suppl 1: S36-44.
31. Splendiani A, Perri M, Marsecano C, et al. Effects of serial macrocyclic-based contrast materials gadoterate meglumine and gadobutrol administrations on gadolinium-related dentate nuclei signal increases in unenhanced T1-weighted brain: a retrospective study in 158 multiple sclerosis (MS) patients. Radiol Med 2018; 123: 125-34.
32. Tedeschi E, Caranci F, Giordano F, Angelini V, Cocozza S, Brunetti A. Gadolinium retention in the body: what we know and what we can do. Radiol Med 2017; 122: 589-600.
33. Cappabianca S, Reginelli A, Monaco L, Del Vecchio L, Di Martino N, Grassi R. Combined videofluoroscopy and manometry in the diagnosis of oropharyngeal dysphagia: Examination technique and preliminary experience. Radiol Med 2008; 113: 923-40.
34. Barile A, Bruno F, Mariani S, et al. What can be seen after rotator cuff repair: a brief review of diagnostic imaging findings. Musculoskelet Surg 2017; 101: 3-14.
35. Ferrari F, Arrigoni F, Miccoli A, et al. Effectiveness of Magnetic Resonance-guided Focused Ultrasound Surgery (MRgFUS) in the uterine adenomyosis treatment: technical approach and MRI evaluation. Radiol Med 2016; 121: 153-61.
36. Gatta G, Parlato V, Di Grezia G, et al. Ultrasound-guided aspiration and ethanol sclerotherapy for treating endometrial cysts. Radiol Med 2010; 115: 1330-39.
37. Briganti F, Leone G, Marseglia M, Cicala D, Caranci F, Maiuri F. P64 Flow Modulation Device in the treatment of intracranial aneurysms: Initial experience and technical aspects. J Neurointerv Surg 2016; 8: 173-80.
38. Arrigoni F, Barile A, Zugaro L, et al. Intra-articular benign bone lesions treated with Magnetic Resonance-guided Focused Ultrasound (MRgFUS): imaging follow-up and clinical results. Med Oncol 2017; 34: 55.
39. Lagana D, Carrafiello G, Mangini M, et al. Radiofrequency ablation of primary and metastatic lung tumors: preliminary experience with a single center device. Surg Endosc 2006; 20: 1262-7.
40. Zappia M, Castagna A, Barile A, Chianca V, Brunese L, Pouliart N. Imaging of the coracoglenoid ligament: a third ligament in the rotator interval of the shoulder. Skeletal Radiol 2017; 46: 1101-11.

41. Brunese L, Romeo A, Iorio S, et al. Thyroid B-flow twinkling sign: a new feature of papillary cancer. Eur J Endocrinol 2008; 159: 447-51.
42. Cantisani V, Grazhdani H, Drakonaki E, et al. Strain US elastography for the characterization of thyroid nodules: Advantages and limitation. Int J Endocrinol 2015; 2015:
43. di Giacomo V, Trinci M, van der Byl G, Catania VD, Calisti A, Miele V. Ultrasound in newborns and children suffering from non-traumatic acute abdominal pain: imaging with clinical and surgical correlation. J Ultrasound 2015; 18: 385-93.
44. Stevenson HL, Prats MM, Sasatomi E. Chemotherapy-induced Sinusoidal Injury (CSI) score: a novel histologic assessment of chemotherapy-related hepatic sinusoidal injury in patients with colorectal liver metastasis. BMC cancer 2017; 17: 35-35.
45. Han NY, Park BJ, Yang KS, et al. Hepatic Parenchymal Heterogeneity as a Marker for Oxaliplatin-Induced Sinusoidal Obstruction Syndrome: Correlation With Treatment Response of Colorectal Cancer Liver Metastases. Am J Roentgenol 2017; 209: 1039-45.
46. Tirumani SH, Kim KW, Nishino M, et al. Update on the role of imaging in management of metastatic colorectal cancer. Radiographics 2014; 34: 1908-28.
47. Bajpai S, Sahani DV. Recent progress in imaging of colorectal cancer liver metastases. Curr Colorectal Cancer Rep 2009; 5: 99-107.
48. Grassi R, Cavaliere C, Cozzolino S, et al. Small animal imaging facility: New perspectives for the radiologist. Radiol Med 2009; 114: 152-67.
49. Iacobellis F, Segreto T, Berritto D, et al. A rat model of acute kidney injury through systemic hypoperfusion evaluated by micro-US, color and PW-Doppler. Radiol Med 2018;
50. Cortellini A, Verna L, Porzio G, et al. Predictive value of skeletal muscle mass for immunotherapy with nivolumab in non-small cell lung cancer patients: A "hypothesis-generator" preliminary report. Thorac Cancer 2019; 10: 347-51.
51. You S-H, Park BJ, Kim YH. Hepatic Lesions that Mimic Metastasis on Radiological Imaging during Chemotherapy for Gastrointestinal Malignancy: Recent Updates. Korean J Radiol 2017; 18: 413-26.
52. Adam R, De Gramont A, Figueras J, et al. The oncosurgery approach to managing liver metastases from colorectal cancer: a multidisciplinary international consensus. Oncologist 2012; 17: 1225-39.
53. Engstrom PF, Arnoletti JP, Benson AB, 3rd, et al. NCCN Clinical Practice Guidelines in Oncology: colon cancer. J Natl Compr Canc Netw 2009; 7: 778-831.
54. Benson AB, 3rd, Venook AP, Cederquist L, et al. Colon Cancer, Version 1.2017, NCCN Clinical Practice Guidelines in Oncology. J Natl Compr Canc Netw 2017; 15: 370-98.
55. Rubbia-Brandt L, Audard V, Sartoretti P, et al. Severe hepatic sinusoidal obstruction associated with oxaliplatin-based chemotherapy in patients with metastatic colorectal cancer. Ann Oncol 2004; 15: 460-6.
56. Rubbia-Brandt L, Lauwers GY, Wang H, et al. Sinusoidal obstruction syndrome and nodular regenerative hyperplasia are frequent oxaliplatin-associated liver lesions and partially prevented by bevacizumab in patients with hepatic colorectal metastasis. Histopathology 2010; 56: 430-9.
57. Hubert C, Sempoux C, Humblet Y, et al. Sinusoidal obstruction syndrome (SOS) related to chemotherapy for colorectal liver metastases: factors predictive of severe SOS lesions and protective effect of bevacizumab. HPB (Oxford) 2013; 15: 858-64.
58. Cayet S, Pasco J, Dujardin F, et al. Diagnostic performance of contrast-enhanced CT-scan in sinusoidal obstruction syndrome induced by chemotherapy of colorectal liver metastases: Radio-pathological correlation. Eur J Radiol 2017; 94: 180-90.
59. Aloia T, Sebagh M, Plasse M, et al. Liver histology and surgical outcomes after preoperative chemotherapy with fluorouracil plus oxaliplatin in colorectal cancer liver metastases. J Clin Oncol 2006; 24: 4983-90.
60. Nakano H, Oussoultzoglou E, Rosso E, et al. Sinusoidal injury increases morbidity after major hepatectomy in patients with colorectal liver metastases receiving preoperative chemotherapy. Ann Surg 2008; 247: 118-24.
61. Karoui M, Penna C, Amin-Hashem M, et al. Influence of preoperative chemotherapy on the risk of major hepatectomy for colorectal liver metastases. Ann Surg 2006; 243: 1-7.
62. Richardson P, Guinan E. The pathology, diagnosis, and treatment of hepatic veno-occlusive disease: current status and novel approaches. Br J Haematol 1999; 107: 485-93.
63. DeLeve LD, Shulman HM, McDonald GB. Toxic injury to hepatic sinusoids: sinusoidal obstruction syndrome (veno-occlusive disease). Semin Liver Dis 2002; 22: 27-42.
64. Robinson PJ. The effects of cancer chemotherapy on liver imaging. Eur Radiol 2009; 19: 1752-62.
65. Zorzi D, Laurent A, Pawlik TM, Lauwers GY, Vauthey JN, Abdalla EK. Chemotherapy-associated hepatotoxicity and surgery for colorectal liver metastases. Br J Surg 2007; 94: 274-86.
66. Deleve LD, Wang X, Tsai J, Kanel G, Strasberg S, Tokes ZA. Sinusoidal obstruction syndrome (veno-occlusive disease) in the rat is prevented by matrix metalloproteinase inhibition. Gastroenterology 2003; 125: 882-90.
67. Alexandrino H, Oliveira D, Cipriano MA, Ferreira L, Tralhão JG, Castro e Sousa F. Oxaliplatin toxicity presenting as a liver nodule – case report. BMC Cancer 2015; 15: 247.
68. Tamandl D, Klinger M, Eipeldauer S, et al. Sinusoidal obstruction syndrome impairs long-term outcome of colorectal liver metastases treated with resection after neoadjuvant chemotherapy. Ann Surg Oncol 2011; 18: 421-30.
69. Xiong WJ, Hu LJ, Jian YC, et al. Focal peliosis hepatis in a colon cancer patient resembling metastatic liver tumor. World J Gastroenterol 2012; 18: 5999-6002.
70. Nam SJ, Cho JY, Lee HS, et al. Chemotherapy-associated hepatopathy in korean colorectal cancer liver metastasis patients: oxaliplatin-based chemotherapy and sinusoidal injury. Korean J Pathol 2012; 46: 22-9.

71. Arakawa Y, Shimada M, Utsunomya T, et al. Oxaliplatin-related sinusoidal obstruction syndrome mimicking metastatic liver tumors. Hepatol Res 2013; 43: 685-9.
72. Tisman G, MacDonald D, Shindell N, et al. Oxaliplatin toxicity masquerading as recurrent colon cancer. J Clin Oncol 2004; 22: 3202-4.
73. Lassau N, Leclere J, Auperin A, et al. Hepatic veno-occlusive disease after myeloablative treatment and bone marrow transplantation: value of gray-scale and Doppler US in 100 patients. Radiology 1997; 204: 545-52.
74. Overman MJ, Maru DM, Charnsangavej C, et al. Oxaliplatin-mediated increase in spleen size as a biomarker for the development of hepatic sinusoidal injury. J Clin Oncol 2010; 28: 2549-55.
75. Iwai T, Yamada T, Koizumi M, et al. Oxaliplatin-induced increase in splenic volume; irreversible change after adjuvant FOLFOX. J Surg Oncol 2017; 116: 947-53.
76. Morine Y, Shimada M, Utsunomiya T. Evaluation and management of hepatic injury induced by oxaliplatin-based chemotherapy in patients with hepatic resection for colorectal liver metastasis. Hepatol Res 2014; 44: 59-69.
77. Unal E, Karaosmanoglu AD, Ozmen MN, Akata D, Karcaaltincaba M. Hepatobiliary phase liver MR imaging findings after Oxaliplatin-based chemotherapy in cancer patients. Abdom Radiol (NY) 2018; 43: 2321-28.
78. Salvolini L, Urbinati C, Valeri G, Ferrara C, Giovagnoni A. Contrast-enhanced MR cholangiography (MRCP) with GD-EOB-DTPA in evaluating biliary complications after surgery. Radiol Med 2012; 117: 354-68.
79. Mocchegiani F, Vincenzi P, Coletta M, et al. Prevalence and clinical outcome of hepatic haemangioma with specific reference to the risk of rupture: A large retrospective cross-sectional study. Dig Liver Dis 2016; 48: 309-14.
80. Kawai T, Yamazaki S, Iwama A, Higaki T, Sugitani M, Takayama T. Focal Sinusoidal Obstruction Syndrome Caused by Oxaliplatin-Induced Chemotherapy: A Case Report. Hepat Mon 2016; 16: e37572.
81. Namimoto T, Yamashita Y, Sumi S, Tang Y, Takahashi M. Focal liver masses: characterization with diffusion-weighted echo-planar MR imaging. Radiology 1997; 204: 739-44.
82. Donadon M, Di Tommaso L, Roncalli M, Torzilli G. Multiple focal nodular hyperplasias induced by oxaliplatin-based chemotherapy. World J Hepatol 2013; 5: 340-4.
83. Yoneda N, Matsui O, Kitao A, et al. Hepatocyte transporter expression in FNH and FNH-like nodule: correlation with signal intensity on gadoxetic acid enhanced magnetic resonance images. Jpn J Radiol 2012; 30: 499-508.
84. Blachar A, Federle MP, Brancatelli G. Hepatic capsular retraction: spectrum of benign and malignant etiologies. Abdom Imaging 2002; 27: 690-9.
85. Young ST, Paulson EK, Washington K, Gulliver DJ, Vredenburgh JJ, Baker ME. CT of the liver in patients with metastatic breast carcinoma treated by chemotherapy: findings simulating cirrhosis. AJR Am J Roentgenol 1994; 163: 1385-8.
86. Qayyum A, Lee GK, Yeh BM, Allen JN, Venook AP, Coakley FV. Frequency of hepatic contour abnormalities and signs of portal hypertension at CT in patients receiving chemotherapy for breast cancer metastatic to the liver. Clin Imaging 2007; 31: 6-10.
87. Shirkhoda A, Baird S. Morphologic changes of the liver following chemotherapy for metastatic breast carcinoma: CT findings. Abdom Imaging 1994; 19: 39-42.
88. Shigefuku R, Watanabe T, Mizukami T, et al. Esophagogastric varices were diagnosed in a non-cirrhotic liver case during long-term follow-up after oxaliplatin-based chemotherapy. Clin J Gastroenterol 2018; 11: 487-92.
89. Donadon M, Vauthey JN, Loyer EM, Charnsangavej C, Abdalla EK. Portal thrombosis and steatosis after preoperative chemotherapy with FOLFIRI-bevacizumab for colorectal liver metastases. World J Gastroenterol 2006; 12: 6556-8.
90. Viswanathan C, Truong MT, Sagebiel TL, et al. Abdominal and pelvic complications of nonoperative oncologic therapy. Radiographics 2014; 34: 941-61.
91. Khan AZ, Morris-Stiff G, Makuuchi M. Patterns of chemotherapy-induced hepatic injury and their implications for patients undergoing liver resection for colorectal liver metastases. J Hepatobiliary Pancreat Surg 2009; 16: 137-44.
92. McCullough AJ. Pathophysiology of Nonalcoholic Steatohepatitis. J Clin Gastroenterol 2006; 40 Suppl 1: S17-S29.
93. Vauthey JN, Pawlik TM, Ribero D, et al. Chemotherapy regimen predicts steatohepatitis and an increase in 90-day mortality after surgery for hepatic colorectal metastases. J Clin Oncol 2006; 24: 2065-72.
94. Maor Y, Malnick S. Liver injury induced by anticancer chemotherapy and radiation therapy. Int J Hepatol 2013; 2013: 815105-05.
95. Choi JS, Kim MJ. Education and imaging: hepatobiliary and pancreatic: focal steatohepatitis mimicking a metastasis. J Gastroenterol Hepatol 2011; 26: 415.
96. Han NY, Park BJ, Sung DJ, et al. Chemotherapy-induced focal hepatopathy in patients with gastrointestinal malignancy: gadoxetic acid--enhanced and diffusion-weighted MR imaging with clinical-pathologic correlation. Radiology 2014; 271: 416-25.
97. Han NY, Park BJ, Kim MJ, Sung DJ, Cho SB. Hepatic Parenchymal Heterogeneity on Contrast-enhanced CT Scans Following Oxaliplatin-based Chemotherapy: Natural History and Association with Clinical Evidence of Sinusoidal Obstruction Syndrome. Radiology 2015; 276: 766-74.
98. Ierardi AM, Lucchina N, Petrillo M, et al. Systematic review of minimally invasive ablation treatment for locally advanced pancreatic cancer. Radiol Med 2014; 119: 483-98.
99. Carrafiello G, Dionigi G, Ierardi AM, et al. Efficacy, safety and effectiveness of image-guided percutaneous microwave ablation in cystic renal lesions Bosniak III or IV after 24 months follow up. Int J Surg 2013; 11 Suppl 1: S30-5.
100. Macchi M, Belfiore MP, Floridi C, et al. Radiofrequency versus microwave ablation for treatment of the lung tumours: LUMIRA (lung microwave radiofrequency) randomized trial. Med Oncol 2017; 34: 96.

101. Cappabianca S, Scuotto A, Iaselli F, et al. Computed tomography and magnetic resonance angiography in the evaluation of aberrant origin of the external carotid artery branches. Surg Radiol Anat 2012; 34: 393-99.
102. Reginelli A, Capasso R, Ciccone V, et al. Usefulness of triphasic CT aortic angiography in acute and surveillance: Our experience in the assessment of acute aortic dissection and endoleak. Int J Surg 2016; 33 Suppl 1: S76-84.
103. Dialetto G, Reginelli A, Cerrato M, et al. Endovascular stent-graft treatment of thoracic aortic syndromes: A 7-year experience. Eur J Radiol 2007; 64: 65-72.
104. Kim SH, Kamaya A, Willmann JK. CT perfusion of the liver: principles and applications in oncology. Radiology 2014; 272: 322-44.
105. Eisenhauer EA, Therasse P, Bogaerts J, et al. New response evaluation criteria in solid tumours: revised RECIST guideline (version 1.1). Eur J Cancer 2009; 45: 228-47.
106. Vreuls CP, Van Den Broek MA, Winstanley A, et al. Hepatic sinusoidal obstruction syndrome (SOS) reduces the effect of oxaliplatin in colorectal liver metastases. Histopathology 2012; 61: 314-8.
107. Pradella S, Lucarini S, Colagrande S. Liver lesion characterization: The wrong choice of contrast agent can mislead the diagnosis of hemangioma. Am J Roentgenol 2012; 199:
108. Mandato Y, Reginelli A, Galasso R, Iacobellis F, Berritto D, Cappabianca S. Errors in the Radiological Evaluation of the Alimentary Tract: Part I. Semin Ultrasound CT MR 2012; 33: 300-07.
109. Goh V, Halligan S, Daley F, Wellsted DM, Guenther T, Bartram CI. Colorectal tumor vascularity: quantitative assessment with multidetector CT--do tumor perfusion measurements reflect angiogenesis? Radiology 2008; 249: 510-7.
110. Ash L, Teknos TN, Gandhi D, Patel S, Mukherji SK. Head and neck squamous cell carcinoma: CT perfusion can help noninvasively predict intratumoral microvessel density. Radiology 2009; 251: 422-8.
111. Kim JW, Jeong YY, Chang NK, et al. Perfusion CT in colorectal cancer: comparison of perfusion parameters with tumor grade and microvessel density. Korean J Radiol 2012; 13 Suppl 1: S89-97.
112. Sforza V, Martinelli E, Ciardiello F, et al. Mechanisms of resistance to anti-epidermal growth factor receptor inhibitors in metastatic colorectal cancer. World J Gastroenterol 2016; 22: 6345-61.
113. Cappabianca S, Iaselli F, Reginelli A, et al. Value of diffusion-weighted magnetic resonance imaging in the characterization of complex adnexal masses. Tumori 2013; 99: 210-17.
114. Lowenthal D, Zeile M, Lim WY, et al. Detection and characterisation of focal liver lesions in colorectal carcinoma patients: comparison of diffusion-weighted and Gd-EOB-DTPA enhanced MR imaging. Eur Radiol 2011; 21: 832-40.
115. Bartlett DL, Chu E. Can metastatic colorectal cancer be cured? Oncology 2012; 26: 266-75.
116. Folprecht G, Gruenberger T, Bechstein W, et al. Survival of patients with initially unresectable colorectal liver metastases treated with FOLFOX/cetuximab or FOLFIRI/cetuximab in a multidisciplinary concept (CELIM study). Ann Oncol 2014; 25: 1018-25.
117. Abdalla EK, Adam R, Bilchik AJ, Jaeck D, Vauthey JN, Mahvi D. Improving resectability of hepatic colorectal metastases: expert consensus statement. Ann Surg Oncol 2006; 13: 1271-80.
118. Kneuertz PJ, Maithel SK, Staley CA, Kooby DA. Chemotherapy-associated liver injury: impact on surgical management of colorectal cancer liver metastases. Ann Surg Oncol 2011; 18: 181-90.
119. Welsh FKS, Tilney HS, Tekkis PP, John TG, Rees M. Safe liver resection following chemotherapy for colorectal metastases is a matter of timing. Br J Cancer 2007; 96: 1037-42.
120. Kim H, Folks KD, Guo L, et al. Early therapy evaluation of combined cetuximab and irinotecan in orthotopic pancreatic tumor xenografts by dynamic contrast-enhanced magnetic resonance imaging. Mol Imaging 2011; 10: 153-67.
121. Torrisi JM, Schwartz LH, Gollub MJ, Ginsberg MS, Bosl GJ, Hricak H. CT findings of chemotherapy-induced toxicity: what radiologists need to know about the clinical and radiologic manifestations of chemotherapy toxicity. Radiology 2011; 258: 41-56.
122. De Filippo M, Onniboni M, Rusca M, et al. (2008). Advantages of multidetector row CT with multiplanar reformation in guiding percutaneous lung biopsies. RAD. MED, vol. 113, p. 945-953, ISSN: 0033-8362, doi: 10.1007/s11547-008-0325-y
123. Palma BD, Guasco D, Pedrazzoni M, et al. Osteolytic lesions, cytogenetic features and bone marrow levels of cytokines and chemokines in multiple myeloma patients: Role of chemokine (C-C motif) ligand20. Leukemia. 2016 Feb;30(2):409-16. doi: 10.1038/leu.2015.259. Epub 2015 Sep 30.
124. Bozzetti C, Nizzoli R, Tiseo M, et al. ALK and ROS1 rearrangements tested by fluorescence in situ hybridization in cytological smears from advanced non-small cell lung cancer patients. Diagnostic Cytopathology, vol. 43, p. 941-946, ISSN: 8755-1039, doi: 10.1002/dc.23318.
125. De Filippo M, Gira F, Corradi D, Sverzellati N, Zompatori M, Rossi C. (2011). Benefits of 3D technique in guiding percutaneous retroperitoneal biopsies. RAD. MED, vol. 116(3), p. 407-416, ISSN: 0033-8362, doi: 10.1007/s11547-010-0604-2

Received: 26 March 2019
Accepted: 4 April 2019
Correspondence:
Alfonso Reginelli
Department of Precision Medicine,
University of Campania “L. Vanvitelli”, Naples, Italy
Piazza Luigi Miraglia, 2 - 80138 Napoli NA
E-mail: alfonsoreginelli@hotmail.com

Acta Biomed 2019; Vol. 90, Supplement 5: 62-67 DOI: 10.23750/abm.v90i5-S.8331

Review

Percutaneous needle biopsy of retroperitoneal lesions: technical developments

Andrea Bevilacqua[1], Fabiano Vito D'Amuri[1], Francesco Pagnini[1], Vittorio Sabatino[1], Umberto Russo[1], Nicola Maggialetti[2], Pierpaolo Palumbo[3], Silvia Pradella[4], Andrea Giovagnoni[5], Vittorio Miele[4], Massimo De Filippo[1]

[1] Department of Medicine and Surgery, Unit of Radiologic Science, University of Parma, Maggiore Hospital, Parma, Italy; [2] Department of Medicine and Health Sciences "V. Tiberio", University of Molise, Campobasso, Italy; [3] Department of Biotechnology and Applied Clinical Sciences, University of L'Aquila, S. Salvatore Hospital, L'Aquila, Italy; [4] Department of Radiology - Careggi University Hospital, Florence, Italy; [5] Department of Radiology, Università Politecnica delle Marche, Ancona, Italy

Summary. Percutaneous Needle Biopsy (PNB) is the insertion of a needle into a suspected lesion or an organ with the aim to obtain cells or tissue for diagnosis. It's a relatively non-invasive procedure and is performed by radiologist under guidance of imaging techniques such as ultrasound (US), computed tomography (CT), fluoroscopy, magnetic resonance imaging (MRI), and positron emission tomography CT (PET-CT). The choice of imaging technique depends on the evaluation of the target lesion and patient compliance. PNB includes two categories: fine-needle aspiration biopsy (FNAB) that is the use of a thin needle (18-25 gauge) to extract cells for cytological evaluation; and core needle biopsy (CNB) that is the use of a larger needle (9-20 gauge) to extract a piece of tissue for histological evaluation. The indications for biopsy are the characterization of nature (benign or malignant) of a lesion, diagnosis and staging of tumor, and biological or immunohistochemical/genetic analisys on tissue. Success of PNB is the procurement of sufficient material to characterize lesions and to guide the patient outcome. Major complications are rare. PNB became a useful technique in diagnosis and study of retroperitoneal lesions, because of a more suitable access to specific intra-abdominal structures, lowering the risk of injury of interposed structures (such as bowel, great vessels).(www.actabiomedica.it)

Key words: biopsy, retroperitoneum, tumor, computed tomography

Introduction

Image-guided Percutaneous Needle Biopsy (PNB) is an interventional procedure performed by radiologists (1-5) with the aim to obtain cells or tissue for diagnosis by the insertion of a needle into a suspected lesion.

It's a relatively non-invasive procedure, and it has absolute advantages compared to open or excisional biopsy.

Success of PNB is related to proper patient selection, preparation and adequate procedural planning (6-8).

Planning and procedural phases

PNB implicates the involvement of interventional radiologists in multidisciplinary boards (9-21). The radiologyst has a key role in the pre-procedural phase: to evaluate potential contraindications and risks of PNB, to confirm the indications for PNB and to identify the optimal target and the selection of the proper imaging guidance.

Indications to PNB are the characterization of nature (benign or malignant) of a lesion (22), the diagnosis and staging of a tumor, and biological or immunohistochemical/genetic analisys on tissue (7, 23).

Although PNB is a relatively non-invasive procedure, there are some contraindications, such as the alteration of coagulation status (specially if it can't be correctable) and bleeding risk, the patient's clinical status (to tolerate bleeding or anesthesia) and cooperation.

The main imaging-guide modalities are ultrasound (US) (24-26) and computed tomography (CT) (27-35); other uncommon imaging techniques are fluoroscopy, magnetic resonance imaging (MRI) (36-47), and positron emission tomography CT (PET-CT) (6, 7, 48).

US guidance has a wide use because of portability, lack of ionizing radiation, and low operating cost. Real time imaging allows to visualize and track the needle throughout its entire pathway and is useful even in lesions moving on respiratory motion; Color-Doppler (24) aid in vascular structures visualization. Furthermore, in selected patients, US contrast-injection increases lesion characterization on the surrounding tissue. Freehand or needle-guided technique are both suitable. Compared to the freehand technique, the guided technique is limited by a fixed angle. Limits of the US-guidance technique are the operator experience and the appropriate acoustic window view, such as the difficulty to penetrate air-filled structures and bone(49).

Compared to US, CT has a better preprocedural planning of PNB, because of its high spatial resolution and large field of view. It permits multiplanar reformations (MPR) to obtain a more adequate path of needle. An intravenous contrast injection may be required to increase accuracy on lesion visualization.

Other imaging guidance modalities are: CT-fluoroscopy, that allows a real-time visualization of the needle, advancement reducing procedural time, but it exposes operators and patients to radiation doses; MR-guidance, despite excellent soft tissue contrast and lack of ionizing radiation, isn't currently feasible because of increased costs and procedure time, the lack in appropriate open-scanner and MRI-compatible instruments;

PNB includes two basic techniques for sample acquisition: fine needle aspiration biopsy (FNAB) and core needle biopsy (CNB) (Figg. 1-6) (50, 51).

FNAB device extracts individual cells for cytological evaluation using a small needle (18-25G) with inner stylet. Once in place, the stylet is removed, a syringe is attached to the needle, and cells are aspirated. Small lesions, necrotic tumors or lesions close to critical structures are its main targets. The most commonly devices used in retroperitoneal biopsies are the spinal needles and the Chiba needles (52).

CNB devices use larger needles (9-20G) with different mechanisms (manually or automatically cutting systems) to extract a piece of tissue for complete histologic evaluation (53).

A safe and proven technique is the use of coaxial needle: the biopsy needle is introduced coaxially into

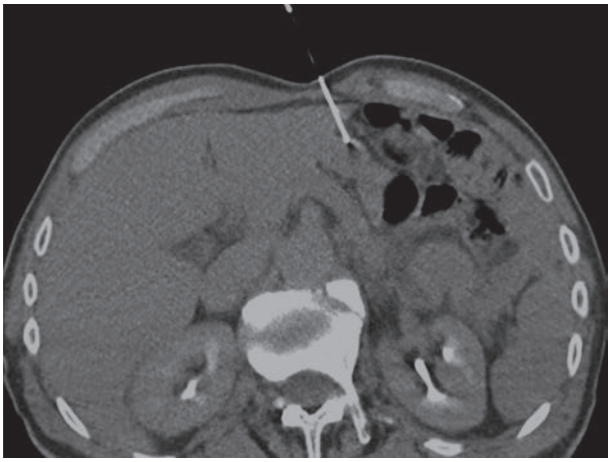

Figure 1. A 72 years old man with history of total gastrectomy for ADK. CT-guided CNB on supine patient for histological evaluation of epigastric solid lesion

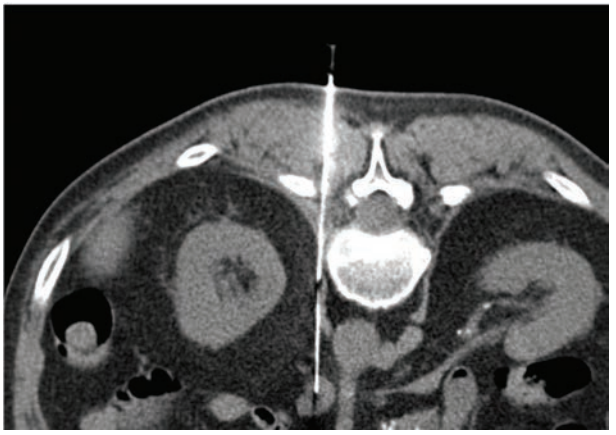

Figure 2. A 64 years old man with outcome of pulmonary lobectomy for primitive lung cancer. CT-guided CNB on prone position of retroperitoneal node: the sample permitted to confirm the metastatic nature

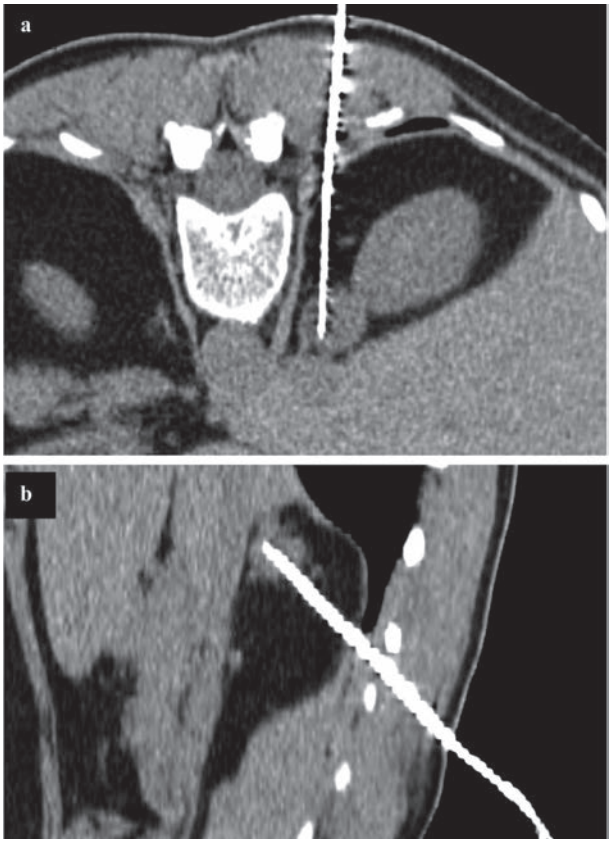

Figure 3. 54 years old woman with previous cervical and endometrial squamous cells carcinoma, with indeterminate right adrenal solid lesion having elevated metabolic activity at PET examination. CT guided CNB on prone position in axial view (a) and parasagittal reconstruction (b), permitted the histological diagnosis of adenoma

Figure 4. An 81 years old woman with outcome of anterior resection of the rectum for ADK with focal thickening of posterior wall. CT-guided FNAB on prone position of the lesion confirmed recurrence of the tumor

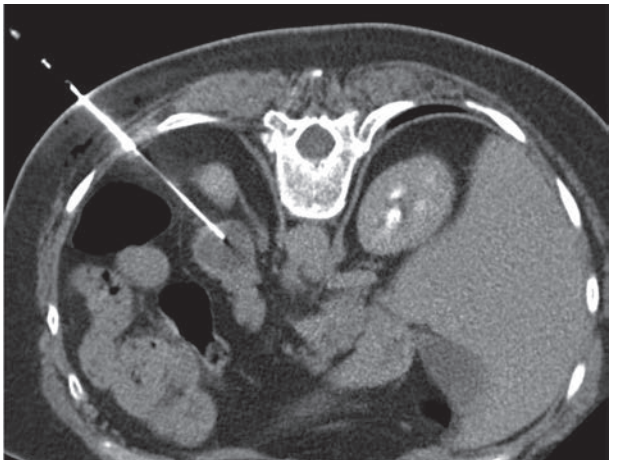

Figure 5. A 65 years old woman with abdominal pain; the abdominal CT demonstrate a pancreatic tail lesion. CT-guided PNB on prone position of pancreatic tail lesion showed a neuroendocrine tumor

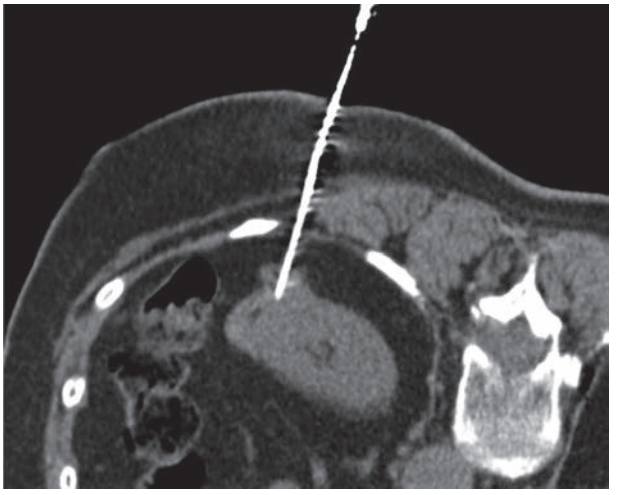

Figure 6. A 75 years old woman with solid exophytic lesion of left kidney. CT-guided CNB on prone position showed a renal cell carcinoma

a guide needle (9-19G), previously advanced nearby the target. It doesn't increase the recurrence of complications and allow multiple specimen samples in a single puncture and decrease the tumor cells seeding risk along the needle tract (48, 54-58).

The extracted samples are then smeared on glass slides and fixed (FNAB) or placed in formalin (CNB); for bacteriological analysis the sample is sent in saline for culture(59, 60).

Post-procedural phase

Retroperitoneal PNB is considered a minimally invasive and safe procedure.

There are major and minor complications, related to the technique (bleeding, infection, perforation, tract seeding) or to organ specific injury (such as haematuria, pneumothorax, haemoptysis, air embolism).

After the procedure and before discharge, imaging control is generally obtained and documented to detect immediate possible complications; equally, vital signs monitoring and clinical observation are required for a few hours following the procedure. In case of major complications, hospitalization in appropriate environment should be guaranteed.

Technical success of PNB varies greatly depending upon the size and location of the target, benign or malignant nature of the lesion, number of samples obtained, availability of an onsite cytopathologist, IRs' and pathologists' experience, equipment availability (61).

Clinical success of PNB is the usefulness of the procedure in terms of improvement of patient care.

In case of non-diagnostic biopsy a repeated biopsy should be considered, such as different techniques or approaches modalities (surgical biopsy or open access) (62-67).

Conclusions

Retroperitoneal Percutaneous Needle Biopsy is a minimally invasive, well established and safe procedure, with a low rate of complications and high diagnostic yield.

Radiologist plays a critical role in the entire management of the patient, since the procedure planning until the patient discharge.

PNB is gaining an even more crucial role, specially with the development of molecular personalized treatment, so avoiding in several patients more invasive diagnostic procedure.

Ethical approval: This article does not contain any studies with human participants performed by any of the authors.

Conflict of interest: None to declare

References

1. Giordano AV, Arrigoni F, Bruno F, et al. Interventional Radiology Management of a Ruptured Lumbar Artery Pseudoaneurysm after Cryoablation and Vertebroplasty of a Lumbar Metastasis. Cardiovasc Intervent Radiol 2017; 40: 776-79.
2. Barile A, Arrigoni F, Bruno F, et al. Present role and future perspectives of interventional radiology in the treatment of painful bone lesions. Future Oncol 2018; 14: 2945-55.
3. Arrigoni F, Bruno F, Zugaro L, et al. Developments in the management of bone metastases with interventional radiology. Acta Biomed 2018; 89: 166-74.
4. Barile A, Arrigoni F, Zugaro L, et al. Minimally invasive treatments of painful bone lesions: state of the art. Med Oncol 2017; 34: 53.
5. Barile A, La Marra A, Arrigoni F, et al. Anaesthetics, steroids and platelet-rich plasma (PRP) in ultrasound-guided musculoskeletal procedures. Br J Radiol 2016; 89: 20150355.
6. Veltri A, Bargellini I, Giorgi L, Almeida P, Akhan O. CIRSE Guidelines on Percutaneous Needle Biopsy (PNB). Cardiovasc Intervent Radiol 2017; 40: 1501-13.
7. Carberry GA, Lubner MG, Wells SA, Hinshaw JL. Percutaneous biopsy in the abdomen and pelvis: a step-by-step approach. Abdom Radiol (NY) 2016; 41: 720-42.
8. Shao H, McCarthy C, Wehrenberg-Klee E, et al. CT-Guided Percutaneous Needle Biopsy of Retroperitoneal and Pelvic Lymphadenopathy: Assessment of Technique, Diagnostic Yield, and Clinical Value. J Vasc Interv Radiol 2018; 29: 1429-36.
9. Basile A, Carrafiello G, Ierardi AM, Tsetis D, Brountzos E. Quality-improvement guidelines for hepatic transarterial chemoembolization. Cardiovasc Intervent Radiol 2012; 35: 765-74.
10. Carrafiello G, Mangini M, Fontana F, et al. Single-antenna microwave ablation under contrast-enhanced ultrasound guidance for treatment of small renal cell carcinoma: Preliminary experience. Cardiovasc Intervent Radiol 2010; 33: 367-74.
11. Laganà D, Carrafiello G, Mangini M, et al. Indications for the use of the Amplatzer vascular plug in interventional radiology. Radiol Med 2008; 113: 707-18.
12. Carrafiello G, Laganà D, Nosari AM, et al. Utility of computed tomography (CT) and of fine needle aspiration biopsy (FNAB) in early diagnosis of fungal pulmonary infections. Study of infections from filamentous fungi in haematologically immunodeficient patients. Radiol Med 2006; 111: 33-41.
13. Mangini M, Laganà D, Fontana F, et al. Use of Amplatzer Vascular Plug (AVP) in emergency embolisation: Preliminary experience and review of literature. Emergency Radiology 2008; 15: 153-60.
14. Laganà D, Carrafiello G, Mangini M, et al. Radiofrequency ablation of primary and metastatic lung tumors: Preliminary experience with a single center device. Surgical Endoscopy and Other Interventional Techniques 2006; 20: 1262-67.

15. Dionigi G, Dionigi R, Rovera F, et al. Treatment of high output entero-cutaneous fistulae associated with large abdominal wall defects: single center experience. Int J Surg 2008; 6: 51-6.
16. De Filippo M, Onniboni M, Rusca M, et al. Advantages of multidetector-row CT with multiplanar reformation in guiding percutaneous lung biopsies. Radiol Med 2008; 113: 945-53.
17. Ierardi AM, Lucchina N, Petrillo M, et al. Systematic review of minimally invasive ablation treatment for locally advanced pancreatic cancer. Radiol Med 2014; 119: 483-98.
18. Carrafiello G, Dionigi G, Ierardi AM, et al. Efficacy, safety and effectiveness of image-guided percutaneous microwave ablation in cystic renal lesions Bosniak III or IV after 24 months follow up. Int J Surg 2013; 11 Suppl 1: S30-5.
19. Macchi M, Belfiore MP, Floridi C, et al. Radiofrequency versus microwave ablation for treatment of the lung tumours: LUMIRA (lung microwave radiofrequency) randomized trial. Med Oncol 2017; 34: 96.
20. Vivarelli M, Vincenzi P, Montalti R, et al. ALPPS Procedure for Extended Liver Resections: A Single Centre Experience and a Systematic Review. PLoS One 2015; 10: e0144019.
21. Dialetto G, Reginelli A, Cerrato M, et al. Endovascular stent-graft treatment of thoracic aortic syndromes: A 7-year experience. Eur J Radiol 2007; 64: 65-72.
22. Pradella S, Lucarini S, Colagrande S. Liver lesion characterization: the wrong choice of contrast agent can mislead the diagnosis of hemangioma. AJR Am J Roentgenol 2012; 199: W662.
23. Cortellini A, Verna L, Porzio G, et al. Predictive value of skeletal muscle mass for immunotherapy with nivolumab in non-small cell lung cancer patients: A "hypothesis-generator" preliminary report. Thorac Cancer 2019; 10: 347-51.
24. Iacobellis F, Segreto T, Berritto D, et al. A rat model of acute kidney injury through systemic hypoperfusion evaluated by micro-US, color and PW-Doppler. Radiol Med 2018;
25. Gatta G, Parlato V, Di Grezia G, et al. Ultrasound-guided aspiration and ethanol sclerotherapy for treating endometrial cysts. Radiol Med 2010; 115: 1330-39.
26. Grassi R, Cavaliere C, Cozzolino S, et al. Small animal imaging facility: New perspectives for the radiologist. Radiol Med 2009; 114: 152-67.
27. Barile A, Bruno F, Arrigoni F, et al. Emergency and Trauma of the Ankle. Semi Musc Rad 2017; 21: 282-89.
28. Scialpi M, Cappabianca S, Rotondo A, et al. Pulmonary congenital cystic disease in adults. Spiral computed tomography findings with pathologic correlation and management. Radiol Med 2010; 115: 539-50.
29. Maggialetti N, Capasso R, Pinto D, et al. Diagnostic value of computed tomography colonography (CTC) after incomplete optical colonoscopy. Int J Surg 2016; 33 Suppl 1: S36-44.
30. Di Cesare E, Gennarelli A, Di Sibio A, et al. Image quality and radiation dose of single heartbeat 640-slice coronary CT angiography: A comparison between patients with chronic Atrial Fibrillation and subjects in normal sinus rhythm by propensity analysis. Eur J Radiol 2015; 84: 631-36.
31. Regine G, Stasolla A, Miele V. Multidetector computed tomography of the renal arteries in vascular emergencies. Eur J Radiol 2007; 64: 83-91.
32. De Cecco CN, Buffa V, Fedeli S, et al. Preliminary experience with abdominal dual-energy CT (DECT): True versus virtual nonenhanced images of the liver. Radiol Med 2010; 115: 1258-66.
33. Buffa V, Solazzo A, D'Auria V, et al. Dual-source dual-energy CT: dose reduction after endovascular abdominal aortic aneurysm repair. Radiol Med 2014; 119: 934-41.
34. Valentini V, Buquicchio GL, Galluzzo M, et al. Intussusception in Adults: The Role of MDCT in the Identification of the Site and Cause of Obstruction. Gastroenterol Res Pract 2016; 2016: 5623718.
35. Di Cesare E, Patriarca L, Panebianco L, et al. Coronary computed tomography angiography in the evaluation of intermediate risk asymptomatic individuals. Radiol Med 2018; 123: 686-94.
36. Masciocchi C, Arrigoni F, Ferrari F, et al. Uterine fibroid therapy using interventional radiology mini-invasive treatments: current perspective. Med Oncol 2017; 34: 52.
37. Splendiani A, D'Orazio F, Patriarca L, et al. Imaging of post-operative spine in intervertebral disc pathology. Musculoskelet Surg 2017; 101: 75-84.
38. Arrigoni F, Gregori LM, Zugaro L, Barile A, Masciocchi C. MRgFUS in the treatment of MSK lesions: A review based on the experience of the university of L'aquila, Italy. Transl Cancer Res 2014; 3: 442-48.
39. Battipaglia G, Avilia S, Morelli E, Caranci F, Perna F, Camera A. Posterior reversible encephalopathy syndrome (PRES) during induction chemotherapy for acute myeloblastic leukemia (AML). Ann Hematol 2012; 91: 1327-28.
40. Tedeschi E, Caranci F, Giordano F, Angelini V, Cocozza S, Brunetti A. Gadolinium retention in the body: what we know and what we can do. Radiol Med 2017; 122: 589-600.
41. Briganti F, Leone G, Marseglia M, Cicala D, Caranci F, Maiuri F. P64 Flow Modulation Device in the treatment of intracranial aneurysms: Initial experience and technical aspects. J Neurointerv Surg 2016; 8: 173-80.
42. Arrigoni F, Barile A, Zugaro L, et al. Intra-articular benign bone lesions treated with Magnetic Resonance-guided Focused Ultrasound (MRgFUS): imaging follow-up and clinical results. Med Oncol 2017; 34: 55.
43. Cirillo M, Caranci F, Tortora F, et al. Structural neuroimaging in dementia. J Alzheimers Dis 2012; 29: 16-19.
44. Mocchegiani F, Vincenzi P, Coletta M, et al. Prevalence and clinical outcome of hepatic haemangioma with specific reference to the risk of rupture: A large retrospective cross-sectional study. Dig Liver Dis 2016; 48: 309-14.
45. Schicchi N, Valeri G, Moroncini G, et al. Myocardial perfusion defects in scleroderma detected by contrast-enhanced cardiovascular magnetic resonance. Radiol Med 2014; 119: 885-94.
46. Tarantini G, Favaretto E, Napodano M, et al. Design and

methodologies of the postconditioning during coronary angioplasty in acute myocardial infarction (POST-AMI) trial. Cardiology 2010; 116: 110-16.
47. Salvolini L, Urbinati C, Valeri G, Ferrara C, Giovagnoni A. Contrast-enhanced MR cholangiography (MRCP) with GD-EOB-DTPA in evaluating biliary complications after surgery. Radiol Med 2012; 117: 354-68.
48. De Filippo M, Saba L, Rossi E, et al. Curved Needles in CT-Guided Fine Needle Biopsies of Abdominal and Retroperitoneal Small Lesions. Cardiovasc Intervent Radiol 2015; 38: 1611-6.
49. Lorentzen T, Nolsoe CP, Ewertsen C, et al. EFSUMB Guidelines on Interventional Ultrasound (INVUS), Part I. General Aspects (long Version). Ultraschall Med 2015; 36: E1-14.
50. Gupta P, Rajwanshi A, Nijhawan R, et al. Fine needle aspiration in retroperitoneal lesions. APMIS 2017; 125: 16-23.
51. Tomozawa Y, Inaba Y, Yamaura H, et al. Clinical value of CT-guided needle biopsy for retroperitoneal lesions. Korean J Radiol 2011; 12: 351-7.
52. Brandt KR, Charboneau JW, Stephens DH, Welch TJ, Goellner JR. CT- and US-guided biopsy of the pancreas. Radiology 1993; 187: 99-104.
53. Misra RK, Mitra S, Jain RK, Vahikar S, Bundela A, Misra P. Image-guided fine needle cytology with aspiration versus non-aspiration in retroperitoneal masses: is aspiration necessary? J Pathol Transl Med 2015; 49: 129-35.
54. Gupta S, Wallace MJ, Cardella JF, et al. Quality improvement guidelines for percutaneous needle biopsy. J Vasc Interv Radiol 2010; 21: 969-75.
55. Shyn PB, Tatli S, Sahni VA, et al. PET/CT-guided percutaneous liver mass biopsies and ablations: targeting accuracy of a single 20 s breath-hold PET acquisition. Clin Radiol 2014; 69: 410-5.
56. Winter TC, Lee FT, Jr., Hinshaw JL. Ultrasound-guided biopsies in the abdomen and pelvis. Ultrasound Q 2008; 24: 45-68.
57. Sainani NI, Arellano RS, Shyn PB, Gervais DA, Mueller PR, Silverman SG. The challenging image-guided abdominal mass biopsy: established and emerging techniques 'if you can see it, you can biopsy it'. Abdom Imaging 2013; 38: 672-96.
58. Akan H, Ozen N, Incesu L, Gumus S, Gunes M. Are percutaneous transgastric biopsies using 14-, 16- and 18-G Tru-Cut needles safe? An experimental study in the rabbit. Australas Radiol 1998; 42: 99-101.
59. Stewart CJ, Coldewey J, Stewart IS. Comparison of fine needle aspiration cytology and needle core biopsy in the diagnosis of radiologically detected abdominal lesions. J Clin Pathol 2002; 55: 93-7.
60. Robertson EG, Baxter G. Tumour seeding following percutaneous needle biopsy: the real story! Clin Radiol 2011; 66: 1007-14.
61. Harisinghani MG, Gervais DA, Hahn PF, et al. CT-guided transgluteal drainage of deep pelvic abscesses: indications, technique, procedure-related complications, and clinical outcome. Radiographics 2002; 22: 1353-67.
62. Wittmann TA, Abel EJ. Percutaneous biopsy in large, locally advanced or metastatic renal tumors. Urol Oncol 2017; 35: 87-91.
63. Bertolini L, Vaglio A, Bignardi L, et al (2011). Subclinical interstitial lung abnormalities in stable renal allograft recipients in the era of modern immunosuppression. Transplantation Proceedings, vol. 43, p. 2617-2623, ISSN: 0041-1345, doi: 10.1016/j.transproceed.2011.06.033.
64. Palma BD, Guasco D, Pedrazzoni M, et al. Osteolytic lesions, cytogenetic features and bone marrow levels of cytokines and chemokines in multiple myeloma patients: Role of chemokine (C-C motif) ligand20. Leukemia. 2016 Feb;30(2):409-16. doi: 10.1038/leu.2015.259. Epub 2015 Sep 30.
65. Bozzetti C, Nizzoli R, Tiseo M, et al. ALK and ROS1 rearrangements tested by fluorescence in situ hybridization in cytological smears from advanced non-small cell lung cancer patients. Diagnostic Cytopathology, vol. 43, p. 941-946, ISSN: 8755-1039, doi: 10.1002/dc.23318.
66. De Filippo M, Gira F, Corradi D, Sverzellati N, Zompatori M, Rossi C. (2011). Benefits of 3D technique in guiding percutaneous retroperitoneal biopsies. RAD. MED, vol. 116(3), p. 407-416, ISSN: 0033-8362, doi: 10.1007/s11547-010-0604-2
67. Barile A, Bruno F, Mariani S, et al. What can be seen after rotator cuff repair: a brief review of diagnostic imaging findings. Musculoskelet Surg. 2017 Mar;101(Suppl 1):3-14. doi: 10.1007/s12306-017-0455-2. Epub 2017 Feb 13. Review.

Received: 26 March 2019
Accepted: 4 April 2019
Correspondence:
Pagnini Francesco,
Department of Medicine and Surgery,
Unit of Radiologic Science, University of Parma,
Maggiore Hospital, Via Gramsci 14 - Parma, Italy
E-mail: f.pagnini90@gmail.com

Acta Biomed 2019; Vol. 90, Supplement 5: 68-76 DOI: 10.23750/abm.v90i5-S.8326

Review

Application of diffusion tensor imaging (DTI) and MR-tractography in the evaluation of peripheral nerve tumours: state of the art and review of the literature

Federico Bruno[1], Francesco Arrigoni[1], Silvia Mariani[1], Lucia Patriarca[1], Pierpaolo Palumbo[1], Raffaele Natella[2], Liheng Ma[3], Giuseppe Guglielmi[4], Renato J Galzio[5], Alessandra Splendiani[1], Ernesto Di Cesare[1], Carlo Masciocchi[1], Antonio Barile[1]

[1] Department of Biotechnology and Applied Clinical Sciences, University of L'Aquila, L'Aquila, Italy; [2] Department of Precision Medicine, University of Campania "L. Vanvitelli", Napoli; [3] Department of Radiology, GuangDong Pharmaceutical University, Guangzhou, Cina; [4] Department of Clinical and Experimental Medicine, Foggia University School of Medicine, Foggia, Italy; [5] Neurosurgery, "San Salvatore" Hospital, L'Aquila

Summary. Peripheral nerves can be affected by a variety of benign and malignant tumour and tumour-like lesions. Besides clinical evaluation and electrophysiologic studies, MRI is the imaging modality of choice for the assessment of these soft tissue tumours. Conventional MR sequences, however, can fail to assess the histologic features of the lesions. Moreover, the precise topographical relationship between the peripheral nerve and the tumor must be delineated preoperatively for complete tumour resection minimizing nerve damage. Using Diffusion tensor imaging (DTI) and tractography, it is possible to obtain functional information on tumour and nerve structures, allowing the assess anatomy, function and biological features. In this article, we review the technical aspects and clinical application of DTI for the evaluation of peripheral nerve tumours. (www.actabiomedica.it)

Key words: peripheral nerve tumours, schwannoma, neurofibroma, diffusion imaging, dti, tractography

Introduction

Peripheral nerve tumors (PNTs) are rare (less than 5% of tumors of the hand and upper extremities) and include benign lesions (mainly schwannomas and neurofibromas) and malignant lesions (malignant neurofibromas, also termed as malignant peripheral nerve sheaths tumors, MPNSTs) (1-3). PNTs are usually slow-growing masses, and about six people out of 1 million undergo surgery for these tumors each year, with a risk of developing a malignant PNST of about 0.001% in the general population (8-13% in patients with neurofibromatosis Type 1) (2).

Tumors may be intraneural involving 1 or multiple nerve fascicles, splaying apart them, or may be attached to a superficial fascicle and thereby displacing the remainder of the nerve (4, 5).

The diagnosis of PNTs is based primarily on the clinical examination, and instrumental evaluation using ultrasound and electrophysiologic studies are the first steps for diagnosing PNTs (6). MRI, due to its intrinsic excellent soft tissue contrast and the absence of ionizing radiations compared to CT (7), is a valuable diagnostic tool for the diagnosis and the guidance of interventional procedures in a wide range of organs and systems (8-19), and in peripheral nerve imaging as well (20-22). In particular, imaging plays a key role for the preoperative and postoperative evaluation (21, 23-30). However, two main limitations of standard MRI sequences are the low specificity for the discrimina-

tion of benign and malignant PNSTs (even when MRI findings such as nerve thickening, necrosis, infiltration, hemorrhage, inhomogeneous enhancement, pose for malignant tumor lesions) and the challenging delineation of the tumor and healthy nerve fascicles involvement (31, 32). Histological confirmation is often necessary to make a definitive diagnosis (33-36). Interventional radiology procedures are widely used for the treatment of most soft tissue lesions (37-48), but surgical removal is the definitive treatment for peripheral nerve tumours. As surgery for PNTSTs may result in a considerable neurological deficit, the primary goal is the preservation of unaffected nerve fibers. Currently, appropriate surgical planning is mainly based on intraoperative findings of electrophysiological monitoring and high-resolution ultrasound (49), even if the resolution is not sufficient to identify relations between tumor and individual nerve fascicles (50). Many advanced MRI sequences have been developed to provide additional anatomical and functional information to standard MR examination (12, 51, 52), and in this scenario, DTI application with tractography, already studied in chronic compressive neuropathies and traumatic nerve injuries, is being applied with increasing frequency to allow the diagnosis and the preoperative assessment of peripheral nerve tumors (53).

The purpose of this article is to review the technical aspects of this advanced MR imaging technique, with a particular focus on its clinical application in patients with peripheral nerve tumors.

Basic principles of DTI imaging

Diffusion tensor imaging (DTI) is an extension of diffusion-weighted imaging (DWI), a well-known technique that measures the magnitude of random displacement of water molecules and that is widely used for the diagnosis of different pathologic entities across a range of organ systems (54). Diffusion tensor imaging (DTI) evaluates the direction of the diffusion as well, differentiating isotropic tissues - in which water molecules show equal diffusion in all directions - and anisotropic tissues (such as neural tissue or other tissues displaying ordered and oriented fibers), in which diffusion is predominant in one direction (principal eigenvector) (55). The sequence involves the application of diffusion-sensitizing gradients in multiple directions, allowing diffusion to be displayed as vectors representing the characteristics of diffusion and anisotropy along the spatial axes. Fractional anisotropy (FA) is the overall measure of tissue anisotropy with values between 0 to 1 (from complete isotropic diffusion to completely directional diffusion) (56, 57).

Other parameters derived from DTI are: the mean diffusivity (MD), that is the average of three diagonal elements of the diffusion tensor, the axial diffusivity (AD), that is the direction of the largest eigenvector, and the radial diffusivity (RD), that is an average of the two smaller tensor eigenvalues (4, 58). Several evidences demonstrated the correlation of DTI parameters with electrophysiology and histology and their validity in characterizing nerve injury. In particular, lower FA values represent nerve injury (due to loss of directional diffusion), AD reflects axon integrity, and RD (and FA) correlates with myelin sheath integrity (59) (Fig. 1). Tractography exploits DTI data to generate 3D representations based on voxel fractional anisotropy values. Using color maps, fibers extending superior-inferiorly are colored blue; those extending left-right are colored red, and those extending anterior-superiorly are colored green. Other directions are represented by a combination of these colors (50) (Fig. 2).

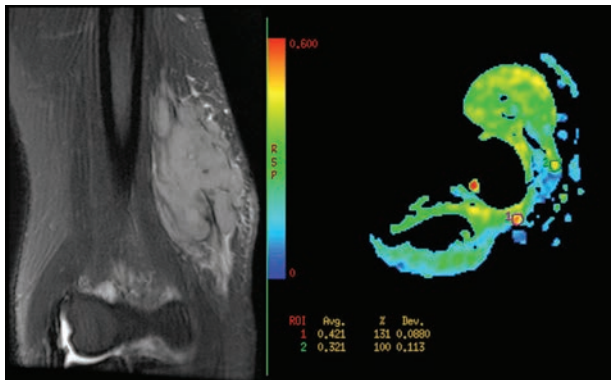

Figure 1. Coronal T2 fs sequence in a patient with a soft tissue mass involving the ulnar nerve . In the right picture, FA map of the DTI sequence with ROI positioning showing reduced FA values of the ulnar nerve at the level of the lesion, consistent with axonal damage

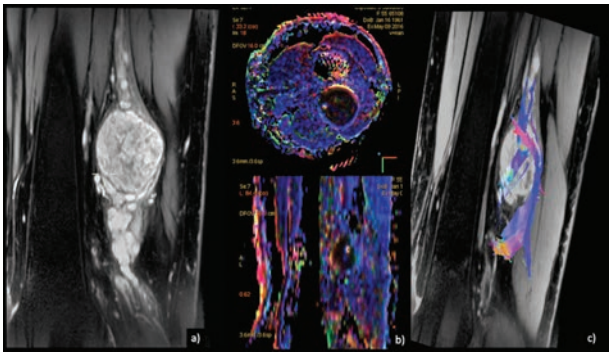

Figure 2. Sagittal contrast enhanced MR slice (a) showing a polylobate fusiform lesion between the biceps femuris and the semitendinosus muscles. FA colored maps in which diffusion vector directions are displayed in different colours (b). In c, tractographic 3D reconstruction

DTI imaging acquisition in peripheral nerve imaging: technical notes

Peripheral nerve DTI can be performed clinically without need of contrast medium administration (60-63), either with 1.5T and 3.0T scanners. Higher field strength, despite the higher SNR, exacerbates the effects of magnetic field inhomogeneities, so the use of localized shim regions is recommended (59). Experiences with peripheral nerve DTI at extremely high field strengths, such as 7.0T, are limited due to the need of specific transmit and receive coils, power deposition concerns, and susceptibility distortions in echo-planar imaging. Having MR imaging systems with a high slew rate is also important. High-channel surface phase-array *coils* can be used as close to the anatomy of interest for both upper and lower extremities. In our clinical practice, we use a multi-channel "flex" coil (small, medium, or large). Torso or spine coils can be used for the lumbosacral plexus (64, 65).

The most commonly DTI *sequence* is a single-shot, 2D EPI (SSEPI). This sequence allows obtaining high SNR with relatively short imaging and consequently few potential motion artifacts (6). Multishot sequences allow higher spatial resolution with higher SNR, with the drawback of more severe motion artifacts and increased scan time. EPI sequences can also be affected by other artifacts, such as chemical shift, ghost artifacts, T2-related blurring, and susceptibility artifacts due to magnetic field inhomogeneities. It is possible to minimize such artifacts using spectral fat suppression, shorter echo-train lengths, tighter echo spacing, higher bandwidth, shimming, and motion correction techniques. The number of acquisitions may be increased, but with consequent longer scanning time and possible motion artifacts (31).

Parallel imaging techniques can be used to reduce imaging time, but an acceleration factor of 2 is usually used, as higher acceleration factors can affect SNR and cause foldover artifacts.

The TR is in the order of 3000 to 4500 milliseconds, and it depends on the anatomic coverage. The TE ranges from 40 milliseconds to 80 milliseconds, depending on the b value and the gradient strength (66). The FOV is adjusted to the anatomy to be covered, typically 140 x 140 mm to 240 x 240 mm.

The *b value* is the main parameter of a diffusion-weighted sequence, representing the strength, duration, separation, and amplitude of the diffusion gradients (66-68). Several studies report the appropriate range of b values for peripheral nerve DTI, with values ranging from 400 to 1000s/mm. In our experience, a b-value of 600s/mm2 is sufficient to reliably track most peripheral nerves in the extremity and provides a good balance of diffusion weighting and SNR (69). Higher b-values increase the diffusion weighting but reduce the SNR. The images are also acquired with a b value of 0, before the application of diffusion gradients. Conversely, low b values can lead to erroneous tracking of low anisotropy structures (such as subcutaneous fat).

DTI of peripheral nerves requires at least six non-colinear *gradient directions*. A greater number of directions sampled increases the accuracy of diffusion measurements, but at the cost of increased imaging time. There is no universal agreement in the literature about the optimum number of gradient directions for the different peripheral nerves, with values ranging from a minimum of six directions at 1.5T to as many as 25 gradient directions at 3.0T (70).

Several stand-alone and vendors specific *dedicated software* can be used to evaluate DTI parameters (FA, ADC, MD) (56, 71). Tractographic images are created connecting adjacent voxels with similar anisotropy values. Measurements are made using regions of interest (ROI) positioning at specific sites along the nerve over the structure being investigated. The qual-

Table 1. Scanning parameters suggested for MR DTI sequence (ssEPI)

DTI PARAMETERS
▪ Spin-echo-single-shot EPI sequence
▪ Axial plane
▪ b-value: 0, 1000s/mm2
▪ 25 diffusion gradient orientations
▪ Slice 3 mm - no interslice gap
▪ TR: 8400ms
▪ TE: minumum
▪ NEX: 3
▪ FOV: 140x140 - 250x250mm
▪ Matrix: 96x96 - 256x256
▪ Shimming

ity of the tractography images partly depends on the thresholds that are applied for FA values and the turning angle of the eigenvectors between adjacent voxel, as optimal parameters vary depending on the geometry of the nerve studied (65). Usually, two thresholds are applied: minimum FA (typically >0.3) and turning angle of diffusion vectors (typically >278) to maintain optimal tracking of peripheral nerve bundles. Choosing the highest or lowest values can result in the tracking of adjacent anatomic structures (muscle or vessels) or the possible exclusion of nerve portions.

Acquisition parameters proposed from our experience are summarized in Table 1.

Clinical application of DTI in peripheral nerve tumours

In one of the first reports from Chabra et al. (58) on 29 patients with surgically proved peripheral nerve tumours, the FA of involved nerves was significantly lower than that of contralateral nerves (as a likely indirect sign of axonal degeneration and myelin loss) with excellent interobserver reliability. ADC values measured on DTI and DWI sequences in the same patients were comparable. DWI ADC was not able to differentiate benign and malignant lesions, while ADC on DTI resulted to be more useful for this discrimination; these findings may be explained by the higher number of directions in diffusion encoding and higher b-values used in their DTI technique (1000 s/mm2 versus 800 s/mm2). Additionally, among the benign lesions, ADC in 12-direction DTI was not statistically different from 20-direction DTI. On tractography, most benign lesions showed partial tract disruption or near-normal appearance except a degenerated schwannoma and a plexiform neurofibroma, in which there was complete tract disruption. They did not observe an isolated course deviation as a sign of BPNST as reported in a feasibility study by Vargas et al. (72-78), explaining these findings with the presence of axonal degeneration and/or myelin loss that result in local loss of fiber attenuation, even with intact anatomic fascicular architecture. Cases of MPNSTs showed partial and complete disruption of tracts, findings that were also confirmed surgically. The near-normal appearance of the tracts was also seen in lymphoma, CMT, and perineurioma; which are explainable by the permeative nature of lymphoma. 20% of the lesions could not be traced due to suboptimal SNR/ghosting artifacts. Higher ADC as an indicator of the benignity of lesions was also confirmed in other tumors, such as breast and prostate. They also suggested the use of ADC as a potential biomarker, due to its excellent interobserver reliability, to detect tumor response/necrosis during chemotherapy.

Also Schmidt et al. showed good preoperative nerve fascicle visualization using DTT scans in 83% of patients, with a good intraoperative correlation between DTT scans and surgical anatomy.

Cage et al. (50) evaluated the feasibility of DTI in 23 patients diagnosed with schwannomas and neurofibromas using intraoperative electrical stimulation as the reference standard. The authors found that DTI tractography identified the location of nerve fibers with a 95.7% sensitivity and 66.7% specificity (maybe due to the inability of intraoperative electrical stimulation to detect sensory nerve fibers, detected by DTI). They also reported a PPV of 75% for the mapping of anatomical fiber location. The NPV was also high (93.8%); this finding suggested that tractography may be suitable to identify a "window" from which to approach the tumor resection preoperatively. Regarding the accuracy of DTI concerning tumor size, pathologi-

cal diagnosis, and tumor location, they reported improved sensitivity, PPV, and NPV in tumours arising from a distal nerve branch rather than a more proximal nerve root and for larger tumours.

In a study of Kasprian et al. (6), the feasibility of DTI in identifying peripheral nerve infiltration in cases of soft tissue tumors near peripheral nerves was assessed. In cases of malignant infiltration of peripheral nerves by adjacent soft tissue tumors, the researchers demonstrated either a change in caliber or complete disruption of the nerve on tractography images. Moreover, they were able to localize the nerve on DTI images in cases of encasement by a tumour or, in cases of peripheral nerve sheath tumors, even when the nerve was not well delineated on T2-weighted imaging. In addition, a greater tendency toward lower FA and higher ADC values for neighboring nerve segments was found in malignant STTs than in benign STTs. As in the central nervous system, this may be explained by either the higher frequency and grade of regional nerve edema associated with more aggressive tumor expansion or by true infiltration by malignant cells.

In the author's experience evaluating DTI feasibility for preoperative evaluation of peripheral nerve tumours (mainly schwannomas and neurofibromas), we noticed, in accordance with previous literature data, a reduction in FA values (mean values 0.61±0.03, range 0.43-0.88) along the course of the nerve near and around the lesion (compared to the contralateral healthy nerve) as well as a variation of the ADC values, ranging between 0.81 and 1.87x10[-3] mm2/s (mean value 1.68+0.21x10[-3] mm2/s). In cases of malignant lesions, the FA and ADC values were lower. Tractographic reconstructions were able to predict tumour location with respect to nerve fiber bundles, with good intraoperative neurosurgical findings correlation (Fig. 3, Fig. 4). Complete disruption of the nerve bundle was observed only in malignant lesions. In one case the tractography could not be performed to the non-optimal SNR/artifacts from ghosting.

Conclusions

With preoperative DTI, the relationship of the nerve tumor to the axons and nerve fascicles can be visualized and studied. Although MR DTI with tractography alone should not replace a meticulous surgical technique and careful attention to the anatomy, DTI proves to be a reliable and useful technique in helping the surgeon to plan out the safest surgical approach providing a 3D-like map of the tumor in relation to the associated nerve from which it is arising, counseling the patient on the predicted extent of

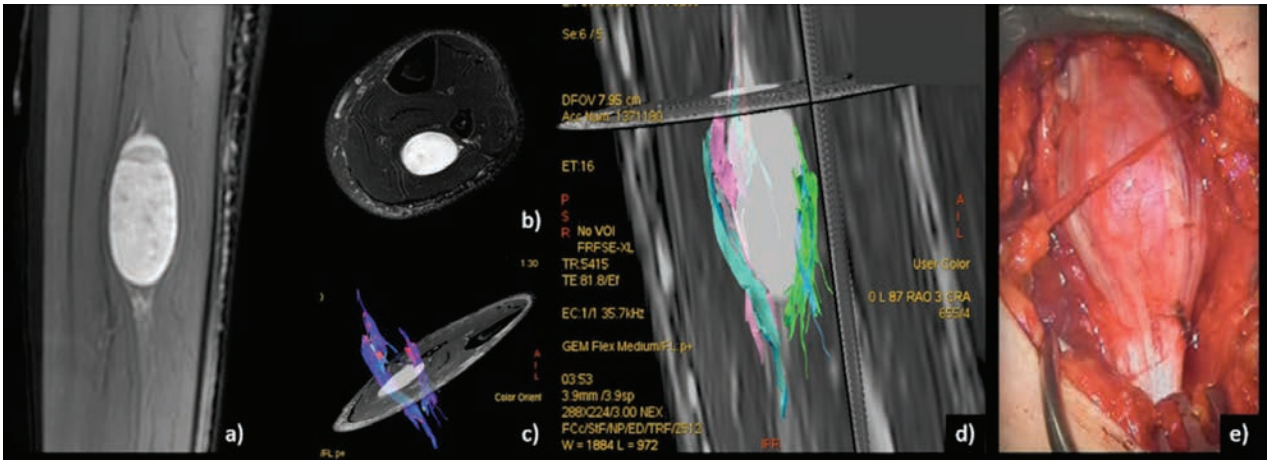

Figure 3. Post-contrast MR images (a, b) of an enhancing, fusiform lesion located at the lower third of the leg within flexor muscles. Tractography reconstructions (c, d) clearly depict in a 3D manner the relationship of the healthy nerve bundles splitted apart and arranged at the periphery of the lesion. Surgical finding (e)

Figure 4. Coronal contrast-enhanced MR slice (a) of an ovoid lesion involving the radial nerve showing inhomogeneous enhancement. 3D tractography fails to track fibers, showing a nerve fiber bundle in the lateral side of the lesion but marked nerve fiber discontinuation in the remainder, findings consistent with a neurofibroma or a degenerated schwannoma (b). Surgical finding (c)

resection and the possible compromise of nerve function.

Tractographic reconstructions provide information about neural integrity, while DTI imaging can indicate possible malignancy in neural masses evaluating diffusivity values. Thus, DTI with fiber tracking, with the functional and anatomical information provided, is a valuable tool to improve standard MR imaging techniques for the diagnosis and follow-up of nerve tumor and tumor-like conditions. Using tractography, the topographical relationship between the peripheral nerve and the tumor can be visualized unequivocally, even in the presence of marked alteration of regional anatomy where conventional sequences frequently fail to delineate clinically intact nerve structures from an encasing tumour.

The challenges of applying DTI with tractography to nerves include the relatively small size and complex course of these nerves, as well as the heterogeneity of tissues along the course of the nerves such as muscle, bone, and vasculature, which can cause an obscured background signal.

Ethical approval: This article does not contain any studies with human participants performed by any of the authors.

Conflict of interest: None to declare

References

1. Forthman CL, Blazar PE. Nerve tumors of the hand and upper extremity. Hand Clin 2004; 20: 233-42.
2. Abreu E, Aubert S, Wavreille G, Gheno R, Canella C, Cotten A. Peripheral tumor and tumor-like neurogenic lesions. Eur J Radiol 2013; 82: 38-50.
3. Stucky CC, Johnson KN, Gray RJ, et al. Malignant peripheral nerve sheath tumors (MPNST): the Mayo Clinic experience. Ann Surg Oncol 2012; 19: 878-85.
4. Ahlawat S, Chhabra A, Blakely J. Magnetic resonance neurography of peripheral nerve tumors and tumorlike conditions. Neuroimaging Clin N Am 2014; 24: 171-92.
5. Perrin RG, Guha A. Malignant peripheral nerve sheath tumors. Neurosurg Clin N Am 2004; 15: 203-16.
6. Kasprian G, Amann G, Panotopoulos J, et al. Peripheral nerve tractography in soft tissue tumors: A preliminary 3-tesla diffusion tensor magnetic resonance imaging study. Muscle Nerve 2015; 51: 338-45.
7. Di Cesare E, Patriarca L, Panebianco L, et al. Coronary computed tomography angiography in the evaluation of intermediate risk asymptomatic individuals. Radiol Med 2018; 123: 686-94.
8. Mariani S, La Marra A, Arrigoni F, et al. Dynamic measurement of patello-femoral joint alignment using weight-bearing magnetic resonance imaging (WB-MRI). Eur J Radiol 2015; 84: 2571-78.
9. Barile A, Bruno F, Arrigoni F, et al. Emergency and Trauma of the Ankle. Semi Musc Rad 2017; 21: 282-89.
10. Barile A, Bruno F, Mariani S, et al. What can be seen after rotator cuff repair: a brief review of diagnostic imaging findings. Musculoskelet Surg 2017; 101: 3-14.
11. De Filippo M, Pesce A, Barile A, et al. Imaging of postop-

erative shoulder instability. Musculoskelet Surg 2017; 101: 15-22.
12. Barile A, Arrigoni F, Bruno F, et al. Computed Tomography and MR Imaging in Rheumatoid Arthritis. Radiol Clin North Am 2017; 55: 997-1007.
13. Briganti F, Leone G, Marseglia M, Cicala D, Caranci F, Maiuri F. P64 Flow Modulation Device in the treatment of intracranial aneurysms: Initial experience and technical aspects. J Neurointerv Surg 2016; 8: 173-80.
14. Cirillo M, Caranci F, Tortora F, et al. Structural neuroimaging in dementia. J Alzheimers Dis 2012; 29: 16-19.
15. Di Cesare E, Cademartiri F, Carbone I, et al. Clinical indications for the use of cardiac MRI. by the SIRM Study Group on Cardiac Imaging. Radiol Med 2013; 118: 752-98.
16. Cappabianca S, Scuotto A, Iaselli F, et al. Computed tomography and magnetic resonance angiography in the evaluation of aberrant origin of the external carotid artery branches. Surg Radiol Anat 2012; 34: 393-99.
17. Barile A, La Marra A, Arrigoni F, et al. Anaesthetics, steroids and platelet-rich plasma (PRP) in ultrasound-guided musculoskeletal procedures. Br J Radiol 2016; 89: 20150355.
18. Zappia M, Castagna A, Barile A, Chianca V, Brunese L, Pouliart N. Imaging of the coracoglenoid ligament: a third ligament in the rotator interval of the shoulder. Skeletal Radiol 2017; 46: 1101-11.
19. Splendiani A, D'Orazio F, Patriarca L, et al. Imaging of post-operative spine in intervertebral disc pathology. Musculoskelet Surg 2017; 101: 75-84.
20. Walker EA, Fenton ME, Salesky JS, Murphey MD. Magnetic resonance imaging of benign soft tissue neoplasms in adults. Radiol Clin North Am 2011; 49: 1197-217.
21. Barile A, Regis G, Masi R, et al. Musculoskeletal tumours: Preliminary experience with perfusion MRI. Radiol Med 2007; 112: 550-61.
22. Caranci F, Briganti F, La Porta M, et al. Magnetic resonance imaging in brachial plexus injury. Musculoskelet Surg 2013; 97 Suppl 2: S181-90.
23. Reginelli A, Zappia M, Barile A, Brunese L. Strategies of imaging after orthopedic surgery. Musculoskelet Surg 2017; 101: 1.
24. Masciocchi C, Conti L, D'Orazio F, Conchiglia A, Lanni G, Barile A, Errors in Musculoskeletal MRI, in: Romano L., Pinto A. (Eds.), Errors in Radiology, Springer Milan, Milano, 2012, pp. 209-17.
25. Zappia M, Capasso R, Berritto D, et al. Anterior cruciate ligament reconstruction: MR imaging findings. Musculoskelet Surg 2017; 101: 23-35.
26. Barile A, Lanni G, Conti L, et al. Lesions of the biceps pulley as cause of anterosuperior impingement of the shoulder in the athlete: Potentials and limits of MR arthrography compared with arthroscopy. Radiol Med 2013; 118: 112-22.
27. Perrotta FM, Astorri D, Zappia M, Reginelli A, Brunese L, Lubrano E. An ultrasonographic study of enthesis in early psoriatic arthritis patients naive to traditional and biologic DMARDs treatment. Rheumatol Int 2016; 36: 1579-83.
28. Cuomo G, Zappia M, Iudici M, Abignano G, Rotondo A, Valentini G. The origin of tendon friction rubs in patients with systemic sclerosis: a sonographic explanation. Arthritis Rheum 2012; 64: 1291-93.
29. Di Pietto F, Chianca V, de Ritis R, et al. Postoperative imaging in arthroscopic hip surgery. Musculoskelet Surg 2017; 101: 43-49.
30. Perri M, Grattacaso G, Di Tunno V, et al. MRI DWI/ADC signal predicts shrinkage of lumbar disc herniation after O2-O3 discolysis. Neuroradiol J 2015; 28: 198-204.
31. Aszmann OC. Diffusion tensor tractography for the surgical management of peripheral nerve sheath tumors. Neurosurg Focus 2015; 39: 1-6.
32. Pilavaki M, Chourmouzi D, Kiziridou A, Skordalaki A, Zarampoukas T, Drevelengas A. Imaging of peripheral nerve sheath tumors with pathologic correlation: pictorial review. Eur J Radiol 2004; 52: 229-39.
33. Marampon F, Gravina G, Ju X, et al. Cyclin D1 silencing suppresses tumorigenicity, impairs DNA double strand break repair and thus radiosensitizes androgen-independent prostate cancer cells to DNA damage. Oncotarget 2016;
34. Berghmans S, Murphey RD, Wienholds E, et al. tp53 mutant zebrafish develop malignant peripheral nerve sheath tumors. Proc Natl Acad Sci U S A 2005; 102: 407-12.
35. Dalla Palma B, Guasco D, Pedrazzoni M, et al. Osteolytic lesions, cytogenetic features and bone marrow levels of cytokines and chemokines in multiple myeloma patients: Role of chemokine (C-C motif) ligand 20. Leukemia 2016; 30: 409-16.
36. Marampon F, Gravina GL, Popov VM, et al. Close correlation between MEK/ERK and Aurora-B signaling pathways in sustaining tumorigenic potential and radioresistance of gynecological cancer cell lines. Int J Oncol 2014; 44: 285-94.
37. Barile A, Quarchioni S, Bruno F, et al. Interventional radiology of the thyroid gland: Critical review and state of the art. Gland Surg 2018; 7: 132-46.
38. Barile A, Arrigoni F, Bruno F, et al. Present role and future perspectives of interventional radiology in the treatment of painful bone lesions. Future Oncol 2018; 14: 2945-55.
39. Giordano AV, Arrigoni F, Bruno F, et al. Interventional Radiology Management of a Ruptured Lumbar Artery Pseudoaneurysm after Cryoablation and Vertebroplasty of a Lumbar Metastasis. Cardiovasc Intervent Radiol 2017; 40: 776-79.
40. Arrigoni F, Bruno F, Zugaro L, et al. Role of interventional radiology in the management of musculoskeletal soft-tissue lesions. Radiol Med 2018; 1-6.
41. Cazzato RL, Arrigoni F, Emanuele Boatta, et al. Percutaneous management of bone metastases: state of the art, interventional strategies and joint position statement of the Italian College of MSK Radiology (ICoMSKR) and the Italian College of Interventional Radiology (ICIR). Radiol Med 2018; 1: 3-3.
42. Arrigoni F, Gregori LM, Zugaro L, Barile A, Masciocchi C. MRgFUS in the treatment of MSK lesions: A review based on the experience of the university of L'aquila, Italy. Transl Cancer Res 2014; 3: 442-48.

43. Ferrari F, Arrigoni F, Miccoli A, et al. Effectiveness of Magnetic Resonance-guided Focused Ultrasound Surgery (MRgFUS) in the uterine adenomyosis treatment: technical approach and MRI evaluation. Radiol Med 2016; 121: 153-61.
44. Arrigoni F, Bruno F, Zugaro L, et al. Developments in the management of bone metastases with interventional radiology. Acta Biomed 2018; 89: 166-74.
45. Arrigoni F, Barile A, Zugaro L, et al. Intra-articular benign bone lesions treated with Magnetic Resonance-guided Focused Ultrasound (MRgFUS): imaging follow-up and clinical results. Med Oncol 2017; 34: 55.
46. Tarantini G, Favaretto E, Napodano M, et al. Design and methodologies of the postconditioning during coronary angioplasty in acute myocardial infarction (POST-AMI) trial. Cardiology 2010; 116: 110-16.
47. Barile A, La Marra A, Arrigoni F, et al. Anaesthetics, steroids and platelet-rich plasma (PRP) in ultrasound-guided musculoskeletal procedures. British Journal of Radiology 2016; 89:
48. Barile A, Arrigoni F, Zugaro L, et al. Minimally invasive treatments of painful bone lesions: state of the art. Med Oncol 2017; 34: 53.
49. Gruber H, Glodny B, Bendix N, Tzankov A, Peer S. High-resolution ultrasound of peripheral neurogenic tumors. Eur Radiol 2007; 17: 2880-8.
50. Cage TA, Yuh EL, Hou SW, et al. Visualization of nerve fibers and their relationship to peripheral nerve tumors by diffusion tensor imaging. Neurosurg Focus 2015; 39: E16-E16.
51. Bruno F, Barile A, Arrigoni F, et al. Weight-bearing MRI of the knee: A review of advantages and limits. Acta Biomed 2018; 89: 78-88.
52. Michelini G, Corridore A, Torlone S, et al. Dynamic MRI in the evaluation of the spine: State of the art. Acta Biomed 2018; 89: 89-101.
53. Zhang Y, Mao Z, Wei P, et al. Preoperative Prediction of Location and Shape of Facial Nerve in Patients with Large Vestibular Schwannomas Using Diffusion Tensor Imaging–Based Fiber Tracking. World Neurosurg 2017; 99: 70-78.
54. Simon NG, Lagopoulos J, Gallagher T, Kliot M, Kiernan MC. Peripheral nerve diffusion tensor imaging is reliable and reproducible. J Magn Reson Imaging 2016; 43: 962-9.
55. Hiltunen J, Suortti T, Arvela S, Seppä M, Joensuu R, Hari R. Diffusion tensor imaging and tractography of distal peripheral nerves at 3 T. Clinical neurophysiology : official journal of the International Federation of Clinical Neurophysiology 2005;
56. Jeon T, Fung MM, Koch KM, Tan ET, Sneag DB. Peripheral nerve diffusion tensor imaging: Overview, pitfalls, and future directions. J Magn Reson Imaging 2018;
57. Skorpil M, Engstrom M, Nordell A. Diffusion-direction-dependent imaging: a novel MRI approach for peripheral nerve imaging. Magn Reson Imaging 2007; 25: 406-11.
58. Chhabra A, Thakkar RS, Andreisek G, et al. Anatomic MR imaging and functional diffusion tensor imaging of peripheral nerve tumors and tumorlike conditions. AJNR Am J Neuroradiol 2013; 34: 802-7.
59. Kronlage M, Schwehr V, Schwarz D, et al. Peripheral nerve diffusion tensor imaging (DTI): normal values and demographic determinants in a cohort of 60 healthy individuals. Eur Radiol 2018; 28: 1801-08.
60. Splendiani A, Perri M, Marsecano C, et al. Effects of serial macrocyclic-based contrast materials gadoterate meglumine and gadobutrol administrations on gadolinium-related dentate nuclei signal increases in unenhanced T1-weighted brain: a retrospective study in 158 multiple sclerosis (MS) patients. Radiol Med 2018; 123: 125-34.
61. Tedeschi E, Caranci F, Giordano F, Angelini V, Cocozza S, Brunetti A. Gadolinium retention in the body: what we know and what we can do. Radiol Med 2017; 122: 589-600.
62. Schicchi N, Valeri G, Moroncini G, et al. Myocardial perfusion defects in scleroderma detected by contrast-enhanced cardiovascular magnetic resonance. Radiol Med 2014; 119: 885-94.
63. Salvolini L, Urbinati C, Valeri G, Ferrara C, Giovagnoni A. Contrast-enhanced MR cholangiography (MRCP) with GD-EOB-DTPA in evaluating biliary complications after surgery. Radiol Med 2012; 117: 354-68.
64. Partovi S, von Tengg-Kobligk H, Bhojwani N, Karmonik C, Maurer M, Robbin MR. Advanced Noncontrast MR Imaging in Musculoskeletal Radiology. Radiol Clin North Am 2015; 53: 549-67.
65. Rangavajla G, Mokarram N, Masoodzadehgan N, Pai SB, Bellamkonda RV. Noninvasive imaging of peripheral nerves. Cells Tissues Organs 2014; 200: 69-77.
66. Chhabra A, Madhuranthakam AJ, Andreisek G. Magnetic resonance neurography: current perspectives and literature review. Eur Radiol 2018; 28: 698-707.
67. Cauley KA, Filippi CG. Diffusion-tensor imaging of small nerve bundles: Cranial nerves, peripheral nerves, distal spinal cord, and lumbar nerve roots- Clinical applications. Am J Roentgenol 2013; 201: 326-35.
68. Jambawalikar S, Baum J, Button T, Li H, Geronimo V, Gould ES. Diffusion tensor imaging of peripheral nerves. Skeletal Radiol 2010; 39: 1073-79.
69. Eppenberger P, Andreisek G, Chhabra A. Magnetic resonance neurography. Diffusion tensor imaging and future directions. Neuroimaging Clin N Am 2014; 24: 245-56.
70. Khalil C, Budzik JF, Kermarrec E, Balbi V, Le Thuc V, Cotten A. Tractography of peripheral nerves and skeletal muscles. Eur J Radiol 2010; 76: 391-97.
71. Valeri G, Mazza FA, Maggi S, et al. Open source software in a practical approach for post processing of radiologic images. Radiol Med 2015; 120: 309-23.
72. Vargas MI, Viallon M, Nguyen D, Delavelle J, Becker M. Diffusion tensor imaging (DTI) and tractography of the brachial plexus: Feasibility and initial experience in neoplastic conditions. Neuroradiology 2010.
73. De Filippo M, Onniboni M, Rusca M, et al. (2008). Advantages of multidetector row CT with multiplanar reformation in guiding percutaneous lung biopsies. RAD. MED, vol.

113, p. 945-953, ISSN: 0033-8362, doi: 10.1007/s11547-008-0325-y
74. Bertolini L, Vaglio A, Bignardi L, et al (2011). Subclinical interstitial lung abnormalities in stable renal allograft recipients in the era of modern immunosuppression. Transplantation Proceedings, vol. 43, p. 2617-2623, ISSN: 0041-1345, doi: 10.1016/j.transproceed.2011.06.033.
75. Palma BD, Guasco D, Pedrazzoni M, et al. Osteolytic lesions, cytogenetic features and bone marrow levels of cytokines and chemokines in multiple myeloma patients: Role of chemokine (C-C motif) ligand20. Leukemia. 2016 Feb;30(2):409-16. doi: 10.1038/leu.2015.259. Epub 2015 Sep 30.
76. Bozzetti C, Nizzoli R, Tiseo M, et al. ALK and ROS1 rearrangements tested by fluorescence in situ hybridization in cytological smears from advanced non-small cell lung cancer patients. Diagnostic Cytopathology, vol. 43, p. 941-946, ISSN: 8755-1039, doi: 10.1002/dc.23318.
77. De Filippo M, Gira F, Corradi D, Sverzellati N, Zompatori M, Rossi C. (2011). Benefits of 3D technique in guiding percutaneous retroperitoneal biopsies. RAD. MED, vol. 116(3), p. 407-416, ISSN: 0033-8362, doi: 10.1007/s11547-010-0604-2.
78. Barile A, Bruno F, Mariani S, et al. What can be seen after rotator cuff repair: a brief review of diagnostic imaging findings. Musculoskelet Surg. 2017 Mar;101(Suppl 1):3-14. doi: 10.1007/s12306-017-0455-2. Epub 2017 Feb 13. Review.

Received: 26 March 2019
Accepted: 4 April 2019
Correspondence:
Federico Bruno, M.D.
Department of Biotechnology and Applied Clinical Sciences
University of L'Aquila,
Vetoio Street 1 - 67100 L'Aquila, Italy
Tel. +390862368512
E-mail: federico.bruno.1988@gmail.com

Acta Biomed 2019; Vol. 90, Supplement 5: 77-83 DOI: 10.23750/abm.v90i5-S.8328

Review

Radiation-induced brain cavernomas in elderly: review of the literature and a rare case report

Giuseppe Mariniello[1], Maria De Liso[2], Camilla Russo[2], Walter Del Vecchio[3], Oreste De Divitiis[1], Federico Bruno[4], Nicola Maggialetti[5], Francesco Arrigoni[4], Luca Brunese[5], Ferdinando Caranci[5]

[1] Department of Neurosciences, Reproductive Sciences and Odontostomatology, Neurosurgical Clinic, University of Naples Federico II, Naples, Italy; [2] Department of Advanced Biomedical Sciences, University of Naples Federico II, Naples, Italy; [3] Istitute of Biostructure and Bioimages IBB-CNR, Naples Italy; [4] Department of Biotechnological and Applied Clinical Sciences, University of L'Aquila; [5] Department of Medicine and Health Sciences "V. Tiberio", University of Molise, Campobasso, Italy

Summary. Radiation-induced brain cavernomas have been mainly reported in children who underwent radiotherapy for medulloblastoma, leukemia, or low-grade glioma. Otherwise, the "de novo" appearance of a cavernoma in an elderly long-survivor patient after resection and radiotherapy of a glioblastoma is a rare event. We report the case of a 62-year-old female patient who underwent surgical resection of a right temporal glioblastoma, followed by radiation therapy of the operative field and surrounding brain and concomitant adjuvant temozolomide. Four years after the operation, a follow-up Magnetic Resonance revealed a good tumor control and a small round lesion at the superior surface of the right cerebellar hemisphere, close to the margins of the previous irradiation field. The radiological items were consistent with a cavernous angioma. Because of the small size of the malformation and the absence of related symptoms, no treatment was performed. The patient died for tumor progression 86 months after the initial operation, with unchanged cerebellar cavernoma. The occurrence of a cavernous angioma in an elderly patient after radiotherapy for brain glioblastoma is an exceptional event; the distribution of radiotherapy-induced cavernous malformations reported in current literature is presented and the mechanism of their formation is discussed. (www.actabiomedica.it)

Key words: glioblastoma, cavernous angioma, radiotherapy

Abbreviations:
CAs - Cavernous angiomas; CNS - Central Nervous System; HGG - High Grade Glioma; MRI - Magnetic Resonance Imaging; LGG - Low Grade Glioma; RICM - Radiotherapy-Induced Cavernous Malformations.

Introduction

Cavernous angiomas (CAs) are well-circumscribed vascular lesions composed of dilated thin walled venous channels without intervening normal brain tissue (1). Although benignant, CAs can be responsible for disabling neurological symptoms depending on their localization within the Central Nervous System (CNS). These lesions can be either acquired or congenital; multiple CAs (10% to 20%) are typically familiar or secondary to radiation therapy.

Acquired CAs may occasionally occur after radiotherapy, generally in addition to other more common complications such as white matter leukoencephalopathy, atrophy and dystrophic mineralization. The "de novo" presentation of CAs after radiation therapy is a relatively rare event, which may occur even after several years after the treatment, irrespective of the radiation dose and type of malignancy. Most of the reported cases (2, 3) mainly concern children (mean

age 12 years) who underwent radiotherapy for medulloblastoma, leukemia or low-grade glioma (LGA); induced CAs after radiotherapy for high grade gliomas (HGG) are less common across older age groups.

We describe the unusual case of a cerebellar CA observed after radiation therapy for temporal glioblastoma in an elderly patient, reviewing current literature on the topic.

Case Report

A 62-year-old female patient was admitted to hospital because of a 2-month history of temporal lobe epilepsy. After a first-level neurological examination, further diagnostic investigations were required to exclude secondary epilepsy causes. Magnetic Resonance Imaging (MRI) showed the presence of a large right intracerebral temporal mass with intense and inhomogeneous contrast enhancement and perilesional oedema, suggestive for a HGG (Figure 1a). A gross total tumor resection was performed through a right temporal craniotomy. Histology was consistent with glioblastoma (WHO IV). Subsequent radiation therapy of the operative field and surrounding brain (60Gy for 30 days, 2Gy per daily fraction) and concomitant adjuvant therapy with multiple temozolomide administrations (during radiotherapy: 75 mg/m² per day, 7 days per week; post-radiotherapy: 150-200 mg/m² for 5 days during each 28-day cycle) were performed.

After 26 months the patient came to our attention because of tumor recurrence (Figure 1b). Thus, she underwent re-intervention remaining symptom-free for the following 2 years. Following examinations (4) did not show significant tumor recurrence, with a good disease control.

Almost 4 years after the initial diagnosis, a follow-up MRI confirmed the absence of recurrent disease; nevertheless a new round small lesion of the right cerebellar convexity was observed close to the margins of

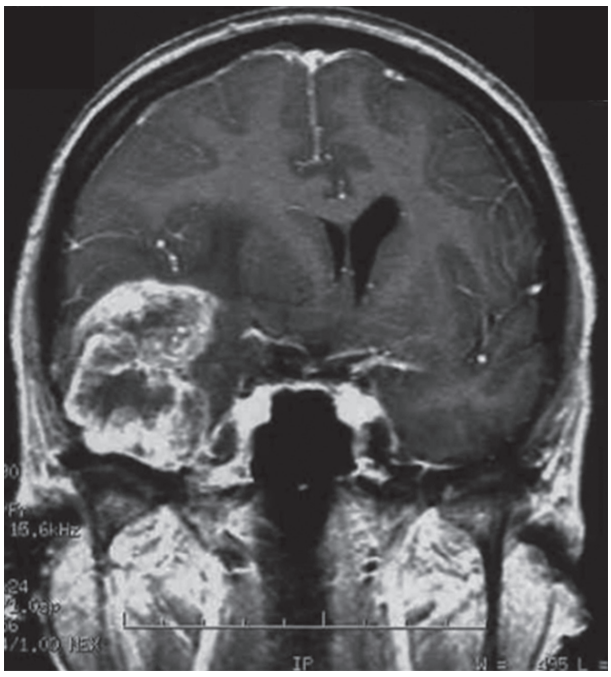

Figure 1a. Coronal contrast-enhanced T1 weighted image showing a large intra-axial right temporal lesion with intense and inhomogeneous contrast enhancement due to the presence of necrotic areas, strongly suggestive for a high-grade glioma. The lesion is surrounded by a large amount of perifocal oedema, with subsequent compressive effect on the right lateral ventricle and contralateral shift of the midline structures

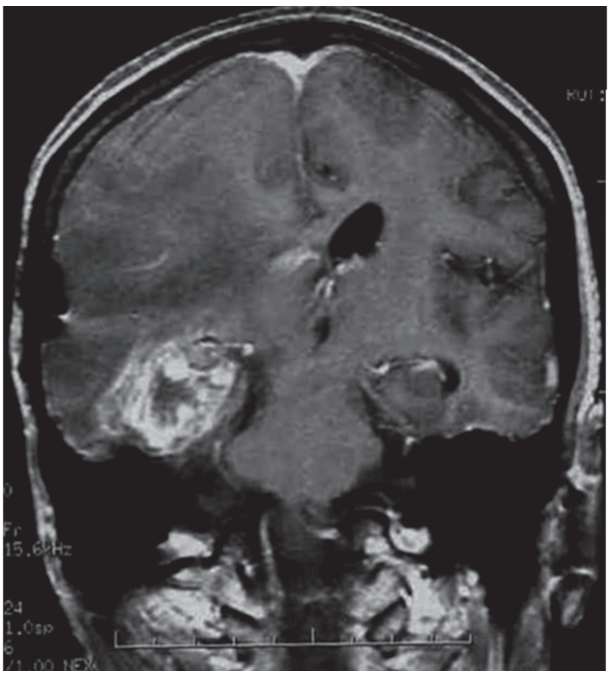

Figure 1b. Coronal contrast-enhanced T1 weighted image showing the presence of an area of intense enhancement in the right temporal region, peripherally to the surgical cavity, consistent with tumor recurrence

the previous irradiation field, showing central hyperintensity with a rim of signal loss due to hemosiderin (Figure 2b); this asymptomatic lesion was not visible in the previous MRI control (Figure 2a). Radiological findings were strongly suggestive for CA, due to the typical berry appearance on unenhanced sequences.

Because of the small size of the malformation and the absence of related symptoms, no treatment was performed. After 1 year, a further follow-up MRI showed no tumor recurrence, as well as the unchanged right cerebellar CA. The patient died for tumor progression after a 7-year disease-free survival.

Discussion

CA is one of the possible complications of high dose radiation therapy, with a large number of cases reported in scientific literature at present (2, 3, 5). Almost all reported cases were described in paediatric population, whereas only a minority of case concerned adult patients. The most common primitive neoplasms associated with radiation-induced CAs include medulloblastoma and malignant hematopoietic neoplasms (2-5) as well as low grade gliomas (LGG) (3), whereas only anedoctal observations of CA in HGG are reported. The distribution of radiotherapy-induced cavernous malformations (RICMs) reported in current literature is represented in Figure 3. The radiation dose was very variable, ranging from 18 to 90 Gy; most patients (57%) received a high radiation dose of 40 up to 60 Gy. The time interval between the irradiation and the diagnosis of CAs was very variable (1 to 52 years), with most cases (65%) occurring within 10 years after irradiation. A correlation has been found between a radiation dose >30Gy and a shorter

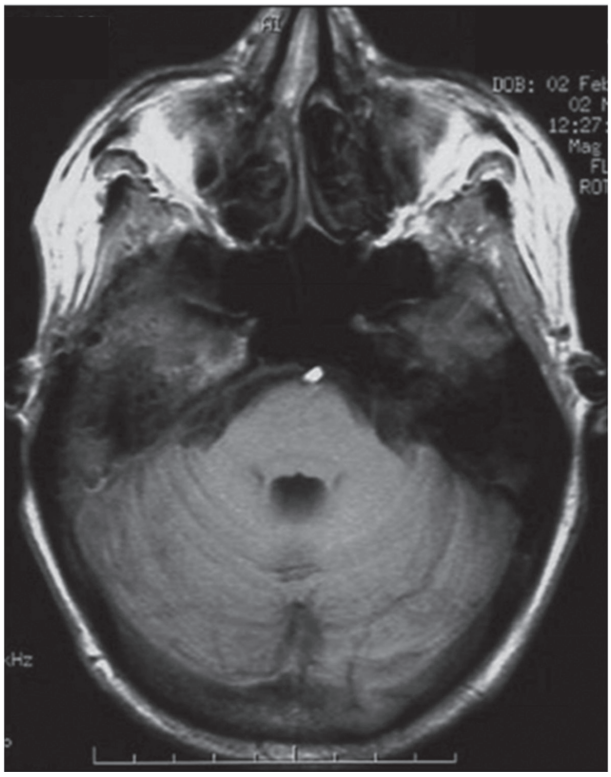

Figure 2a. Axial T1 weighted image showing regular morphology and signal of the posterior fossa structures, with no evidence of focal lesions of the cerebellar hemispheres

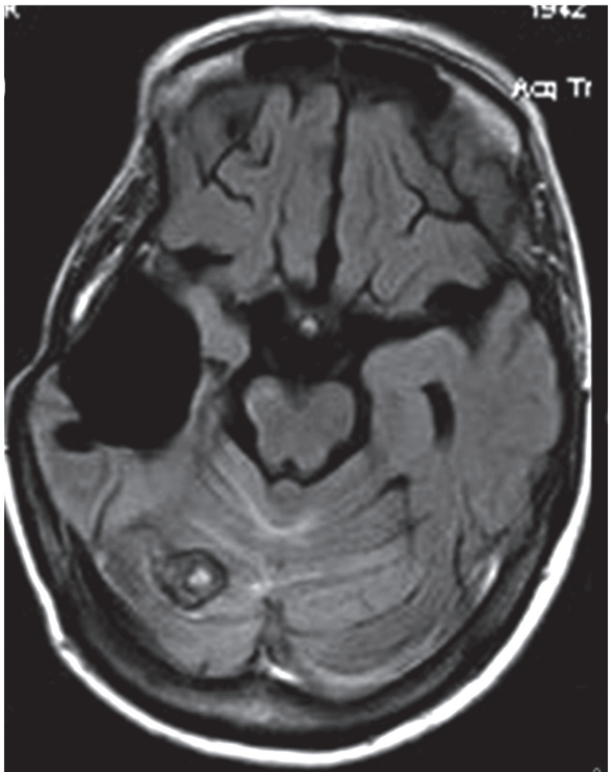

Figure 2b. Axial FLAIR image revealing surgical cavity in the right temporal region with no sign of tumor recurrence; presence of a round small lesion (transverse diameter: 1 cm) in the upper convexity of the right cerebellar hemisphere showing central hyperintensity with a rim of signal loss due to the presence of hemosiderin, consistent with CA

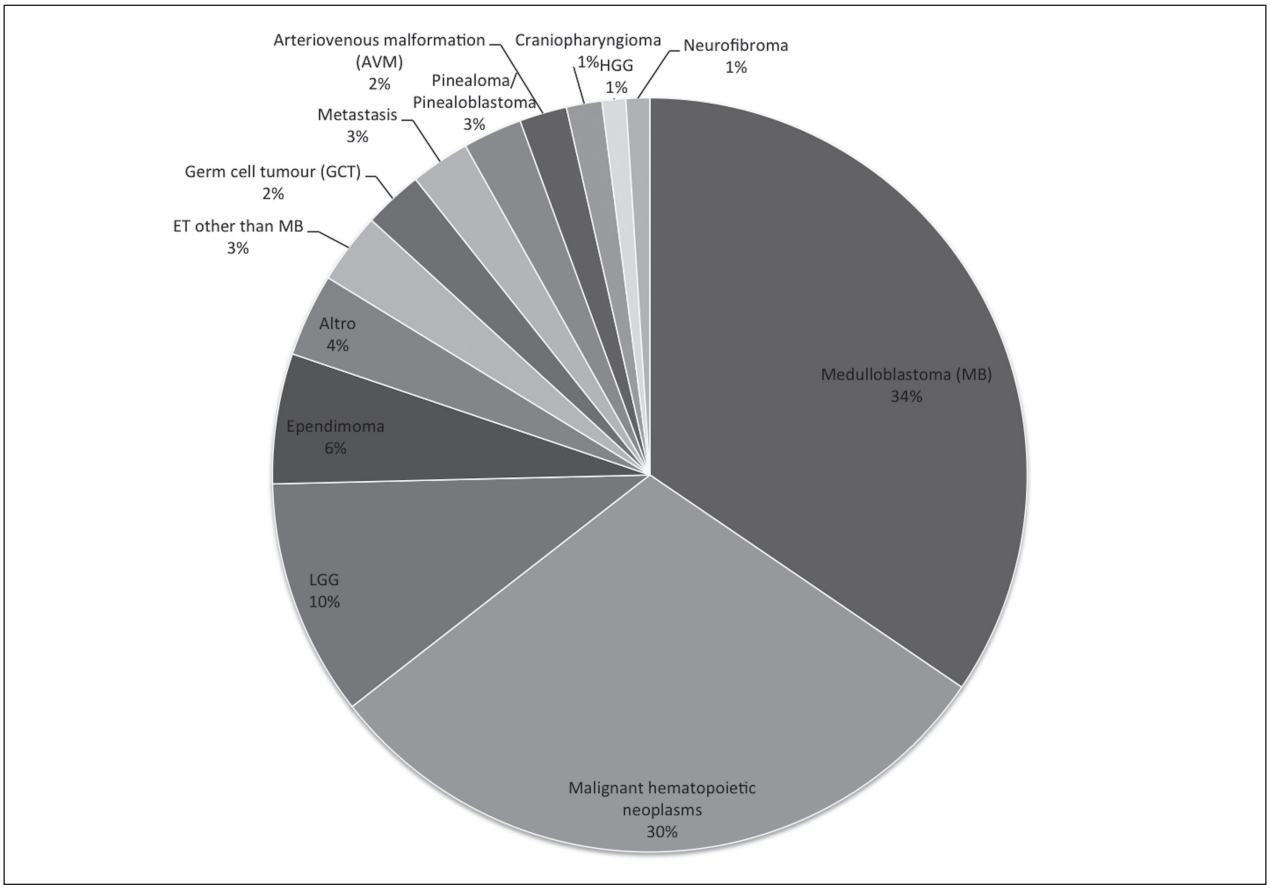

Figure 3. Distribution of CNS radiotherapy-induced cavernous malformations, according to primary tumours

latency to development of cavernomas (1). Multiple CAs were found in 36% patients, and clinical and/or radiological evidence of haemorrhage was reported in 38% of the radiation-induced cases, a significantly higher incidence compared with sporadic cavernomas (3, 6-8).

Our case presents several elements of distinctiveness being unusual due to the patient age, type of radio-treated tumour and CA location in the posterior fossa. The age of our patient, both at the irradiation (62 years) and at the appearance of the cavernoma (66 years), is very atypical. Indeed, among the 100 reviewed patients, at the diagnosis only 5 were older than 40 years (9), and none was older than 50 years. Moreover, at the CAs appearance only 5 patients (10) were older than 50 years and none was older than 60 years. Interestingly, all but one of these adult patients had received radiation doses greater than 60 Gy. On the other hand, the median latency time to diagnosis was 8.2 years, similarly in younger patients reports.

The present case is only the third reported in the literature of a brain cavernoma after HGG irradiation (11-19), although it is the first report of "de novo" appearance of a cavernous malformation in a patient who had radiation therapy for glioblastoma in such an advanced age (>60 years of age). Indeed, the higher incidence observed in LGGs is probably due to the longer mean survival of these patients compared with HGGs.

The infratentorial location of CAs at the superior surface of cerebellar hemispheres is unusual as well, being this region close to the margins but not included within the irradiation field. It has been suggested that low radiation doses are more efficient to induce CAs; indeed, higher radiation dose delivered at the centre of the field of irradiation may result in extensive cellular apoptosis, thus preventing the CA formation. Con-

versely, the periphery of the field is at higher risk, as the radiation may modify the genetic stability, inducing abnormal vascular proliferation without substantial cell apoptosis (2).

The management of the radiation-induced CAs mainly depends on clinical manifestations and mean survival time associated with the primary lesion. Generally, when clinically silent, CAs may benefit from a regular MRI follow-up, especially in patients with small CAs and short life expectancy, as in the present case. Surgical treatment is indicated in cases with conspicuous haemorrhage or should be limited to younger patients with stable disease, low grade lesions and/or and long life expectancy.

Imaging plays a key role in the evaluation of different pathologic conditions, both for diagnostic and interventional purposes (20-33). In neuroradiology, the combined use of CT and MRI imaging is the approach of choice (34-43), while angiography is the primary modality used for interventional neuroradiology procedures (44, 45).

On imaging, CAs have a distinctive appearance of the nidus with little or no surrounding edema (1). CT may show ring-like calcification with a core reticulation of variable attenuation, with usually no contrast enhancement (1, 13). MRI imaging shows a reticulated core of heterogeneous signal intensity giving a typical "popcorn" appearance, with a dark peripheral rim of hemosiderin (14, 15).

A comparison between patients with RICMs and those with non-radiotherapy-induced lesions showed that there are no significant differences in size, location and imaging appearance, although RICMs are more often multiple and present some different histologic features (13, 16, 46-48).

Another difference lies in the possible clinical-radiological progression; variation in size and imaging characteristics is a more frequent feature of "de novo" cavernomas, that have significantly higher VEGF, MIB-1 and Ki-67 expression compared to congenital stable and indolent ones (17-19). Therefore, it may be suggested that the production of the angiogenic factors such as VEGF and TGF may play a crucial role in the formation of radiation-induced Cas (49-54).

The mechanism of CAs formation is not completely defined. It is controversial whether radiation therapy causes enlargement of a pre-existing small cavernoma, or induces a "de-novo" cavernous malformation due to direct radiation-induced damage in blood vessels and DNA injury in predisposed pa-tients (13).

In conclusion, the occurrence of CAs in elderly patients after glioblastoma radiotherapy is exceptional, although its prevalence may change over time. In fact, this kind of complication could become more frequent because of new treatment lines with progressively increasing survival time of patients with HGG; in this light radiation field margins should be considered particularly susceptible to this kind of vascular damage.

Ethical approval: This article does not contain any studies with human participants performed by any of the authors.

Conflict of interest: None to declare

References

1. Jain R, Robertson PL, Gandhi D, Gujar SK, Muraszko KM, Gebarski S. Radiation-induced cavernomas of the brain. AJNR Am J Neuroradiol 2005; 26: 1158-62.
2. Keezer MR, Del Maestro R. Radiation-induced cavernous hemangiomas: case report and literature review. Can J Neurol Sci 2009; 36: 303-10.
3. Nimjee SM, Powers CJ, Bulsara KR. Review of the literature on de novo formation of cavernous malformations of the central nervous system after radiation therapy. Neurosurg Focus 2006; 21: e4.
4. Caruso R, Colonnese C, Elefante A, Innocenzi G, Raguso M, Gagliardi FM. Use of spiral computerized tomography angiography in patients with cerebral aneurysm. Our experience. J Neurosurg Sci 2002; 46: 4-9.
5. Elefante A, Peca C, Del Basso De Caro ML, et al. Symptomatic spinal cord metastasis from cerebral oligodendroglioma. Neurol Sci 2012; 33: 609-13.
6. Larson JJ, Ball WS, Bove KE, Crone KR, Tew JM, Jr. Formation of intracerebral cavernous malformations after radiation treatment for central nervous system neoplasia in children. J Neurosurg 1998; 88: 51-6.
7. Capalbo D, Elefante A, Spagnuolo MI, et al. Posterior reversible encephalopathy syndrome in a child during an accelerated phase of a severe APECED phenotype due to an uncommon mutation of AIRE. Clin Endocrinol (Oxf) 2008; 69: 511-3.
8. Chai YH, Jung TY, Lee KH, Kim SK. Progressive Multiple Cavernous Angiomas after Radiotherapy in a Pediatric Patient with Medulloblastoma: A Case Report. Pediatr Neurosurg 2015; 50: 270-4.

9. Lew SM, Morgan JN, Psaty E, Lefton DR, Allen JC, Abbott R. Cumulative incidence of radiation-induced cavernomas in long-term survivors of medulloblastoma. J Neurosurg 2006; 104: 103-7.
10. Furuse M, Miyatake SI, Kuroiwa T. Cavernous malformation after radiation therapy for astrocytoma in adult patients: report of 2 cases. Acta Neurochir (Wien) 2005; 147: 1097-101.
11. Fukushima S, Narita Y, Miyakita Y, et al. A case of more than 20 years survival with glioblastoma, and development of cavernous angioma as a delayed complication of radiotherapy. Neuropathology 2013; 33: 576-81.
12. Noel L, Christmann D, Jacques C, et al. [Intracerebral radiation-induced cavernous angiomas]. J Neuroradiol 2002; 29: 49-56.
13. Martino A, Krainik A, Pasteris C, et al. Neurological imaging of brain damages after radiotherapy and/or chimiotherapy. J Neuroradiol 2014; 41: 52-70.
14. Rigamonti D, Drayer BP, Johnson PC, Hadley MN, Zabramski J, Spetzler RF. The MRI appearance of cavernous malformations (angiomas). J Neurosurg 1987; 67: 518-24.
15. Muccio CF, Tedeschi E, Elefante A, Caranci F, Cerase A. Primary central nervous system vasculitis mimicking a brain tumor on conventional magnetic resonance imaging: the usefulness of perfusion-weighted imaging. A case report. Acta Neurol Belg 2018;
16. Cutsforth-Gregory JK, Lanzino G, Link MJ, Brown RD, Jr., Flemming KD. Characterization of radiation-induced cavernous malformations and comparison with a nonradiation cavernous malformation cohort. J Neurosurg 2015; 122: 1214-22.
17. Maiuri F, Cappabianca P, Gangemi M, et al. Clinical progression and familial occurrence of cerebral cavernous angiomas: the role of angiogenic and growth factors. Neurosurg Focus 2006; 21: e3.
18. Schettino C, Caranci F, Lus G, et al. Diffuse glioblastoma resembling acute hemorrhagic leukoencephalitis. Quant Imaging Med Surg 2017; 7: 592-97.
19. Briganti F, Tortora F, Elefante A, Volpe A, Bruno MC, Panagiotopoulos K. An unusual case of vertebral arteriovenous fistula treated with electrodetachable coil embolization. Minim Invasive Neurosurg 2004; 47: 386-8.
20. Masciocchi C, Conti L, D'Orazio F, Conchiglia A, Lanni G, Barile A, Errors in Musculoskeletal MRI, in: Romano L., Pinto A. (Eds.), Errors in Radiology, Springer Milan, Milano, 2012, pp. 209-17.
21. Ferrari F, Arrigoni F, Miccoli A, et al. Effectiveness of Magnetic Resonance-guided Focused Ultrasound Surgery (MRgFUS) in the uterine adenomyosis treatment: technical approach and MRI evaluation. Radiol Med 2016; 121: 153-61.
22. Arrigoni F, Barile A, Zugaro L, et al. Intra-articular benign bone lesions treated with Magnetic Resonance-guided Focused Ultrasound (MRgFUS): imaging follow-up and clinical results. Med Oncol 2017; 34:
23. Mangini M, Lagana D, Fontana F, et al. Use of Amplatzer Vascular Plug (AVP) in emergency embolisation: preliminary experience and review of literature. Emerg Radiol 2008; 15: 153-60.
24. Valeri G, Mazza FA, Maggi S, et al. Open source software in a practical approach for post processing of radiologic images. Radiol Med 2015; 120: 309-23.
25. Mocchegiani F, Vincenzi P, Coletta M, et al. Prevalence and clinical outcome of hepatic haemangioma with specific reference to the risk of rupture: A large retrospective cross-sectional study. Dig Liver Dis 2016; 48: 309-14.
26. Schicchi N, Valeri G, Moroncini G, et al. Myocardial perfusion defects in scleroderma detected by contrast-enhanced cardiovascular magnetic resonance. Radiol Med 2014; 119: 885-94.
27. Tarantini G, Favaretto E, Napodano M, et al. Design and methodologies of the postconditioning during coronary angioplasty in acute myocardial infarction (POST-AMI) trial. Cardiology 2010; 116: 110-16.
28. Salvolini L, Urbinati C, Valeri G, Ferrara C, Giovagnoni A. Contrast-enhanced MR cholangiography (MRCP) with GD-EOB-DTPA in evaluating biliary complications after surgery. Radiol Med 2012; 117: 354-68.
29. Barile A, Regis G, Masi R, et al. Musculoskeletal tumours: Preliminary experience with perfusion MRI. Radiol Med 2007; 112: 550-61.
30. Di Cesare E, Gennarelli A, Di Sibio A, et al. Image quality and radiation dose of single heartbeat 640-slice coronary CT angiography: A comparison between patients with chronic Atrial Fibrillation and subjects in normal sinus rhythm by propensity analysis. Eur J Radiol 2015; 84: 631-36.
31. Buffa V, Solazzo A, D'Auria V, et al. Dual-source dual-energy CT: dose reduction after endovascular abdominal aortic aneurysm repair. Radiol Med 2014; 119: 934-41.
32. Barile A, Bruno F, Arrigoni F, et al. Emergency and Trauma of the Ankle. Semi Musc Rad 2017; 21: 282-89.
33. Barile A, Bruno F, Mariani S, et al. What can be seen after rotator cuff repair: a brief review of diagnostic imaging findings. Musculoskelet Surg 2017; 101: 3-14.
34. Splendiani A, D'Orazio F, Patriarca L, et al. Imaging of post-operative spine in intervertebral disc pathology. Musculoskelet Surg 2017; 101: 75-84.
35. Splendiani A, Perri M, Marsecano C, et al. Effects of serial macrocyclic-based contrast materials gadoterate meglumine and gadobutrol administrations on gadolinium-related dentate nuclei signal increases in unenhanced T1-weighted brain: a retrospective study in 158 multiple sclerosis (MS) patients. Radiol Med 2018; 123: 125-34.
36. Caranci F, Briganti F, La Porta M, et al. Magnetic resonance imaging in brachial plexus injury. Musculoskelet Surg 2013; 97: S181-S90.
37. Cicala D, Briganti F, Casale L, et al. Atraumatic vertebral compression fractures: Differential diagnosis between benign osteoporotic and malignant fractures by MRI. Musculoskelet Surg 2013; 97: S169-S79.
38. Muccio CF, Di Blasi A, Esposito G, Brunese L, D'Arco F,

Caranci F. Perfusion and spectroscopy magnetic resonance imaging in a case of lymphocytic vasculitis mimicking brain tumor. Pol J Radiol 2013; 78: 66-69.
39. Caranci F, Napoli M, Cirillo M, Briganti G, Brunese L, Briganti F. Basilar artery hypoplasia. Neuroradiol J 2012; 25: 739-43.
40. Battipaglia G, Avilia S, Morelli E, Caranci F, Perna F, Camera A. Posterior reversible encephalopathy syndrome (PRES) during induction chemotherapy for acute myeloblastic leukemia (AML). Ann Hematol 2012; 91: 1327-28.
41. Cirillo M, Caranci F, Tortora F, et al. Structural neuroimaging in dementia. J Alzheimers Dis 2012; 29: 16-19.
42. Cappabianca S, Scuotto A, Iaselli F, et al. Computed tomography and magnetic resonance angiography in the evaluation of aberrant origin of the external carotid artery branches. Surg Radiol Anat 2012; 34: 393-99.
43. Cappabianca S, Colella G, Russo A, et al. Maxillofacial fibrous dysplasia: Personal experience with gadoliniumenhanced magnetic resonance imaging. Radiol Med 2008; 113: 1198-210.
44. Briganti F, Leone G, Marseglia M, Cicala D, Caranci F, Maiuri F. P64 Flow Modulation Device in the treatment of intracranial aneurysms: Initial experience and technical aspects. J Neurointerv Surg 2016; 8: 173-80.
45. Dialetto G, Reginelli A, Cerrato M, et al. Endovascular stent-graft treatment of thoracic aortic syndromes: A 7-year experience. Eur J Radiol 2007; 64: 65-72.
46. Tedeschi E, Caranci F, Giordano F, Angelini V, Cocozza S, Brunetti A. Gadolinium retention in the body: what we know and what we can do. Radiol Med 2017; 122: 589-600.
47. Cocozza S, Russo C, Pontillo G, et al. Is advanced neuroimaging for neuroradiologists? A systematic review of the scientific literature of the last decade. Neuroradiology 2016; 58: 1233-39.
48. Cha YJ, Nahm JH, Ko JE, et al. Pathological Evaluation of Radiation-Induced Vascular Lesions of the Brain: Distinct from De Novo Cavernous Hemangioma. Yonsei Med J 2015; 56: 1714-20.
49. De Filippo M, Onniboni M, Rusca M, et al. (2008). Advantages of multidetector row CT with multiplanar reformation in guiding percutaneous lung biopsies. RAD. MED, vol. 113, p. 945-953, ISSN: 0033-8362, doi: 10.1007/s11547-008-0325-y
49. Bertolini L, Vaglio A, Bignardi L, et al (2011). Subclinical interstitial lung abnormalities in stable renal allograft recipients in the era of modern immunosuppression. Transplantation Proceedings, vol. 43, p. 2617-2623, ISSN: 0041-1345, doi: 10.1016/j.transproceed.2011.06.033.
50. Palma BD, Guasco D, Pedrazzoni M, et al. Osteolytic lesions, cytogenetic features and bone marrow levels of cytokines and chemokines in multiple myeloma patients: Role of chemokine (C-C motif) ligand20. Leukemia. 2016 Feb;30(2):409-16. doi: 10.1038/leu.2015.259. Epub 2015 Sep 30.
51. Bozzetti C, Nizzoli R, Tiseo M, et al. ALK and ROS1 rearrangements tested by fluorescence in situ hybridization in cytological smears from advanced non-small cell lung cancer patients. Diagnostic Cytopathology, vol. 43, p. 941-946, ISSN: 8755-1039, doi: 10.1002/dc.23318.
52. De Filippo M, Gira F, Corradi D, Sverzellati N, Zompatori M, Rossi C. (2011). Benefits of 3D technique in guiding percutaneous retroperitoneal biopsies. RAD. MED, vol. 116(3), p. 407-416, ISSN: 0033-8362, doi: 10.1007/s11547-010-0604-2
53. Quarrell OW, Handley O, O'Donovan K, et al. Discrepancies in reporting the CAG repeat lengths for Huntington's disease. Eur J Hum Genet 2012; 20: 20-26.
54. Perri M, Grattacaso G, Di Tunno V, et al. MRI DWI/ADC signal predicts shrinkage of lumbar disc herniation after O2-O3 discolysis. Neuroradiology Journal 2015; 28(2): 198-204.

Received: 26 March 2019
Accepted: 4 April 2019
Correspondence:
Prof. Ferdinando Caranci
Department of Medicine and
Health Sciences "V. Tiberio", University of Molise
Via Francesco De Sanctis 1 - 86100 Campobasso, Italy
E-mail: ferdinando.caranci@unimol.it

Acta Biomed 2019; Vol. 90, Supplement 5: 84-94 DOI: 10.23750/abm.v90i5-S.8351

Review

Imaging of long head biceps tendon. A multimodality pictorial essay

Marcello Zappia[1], Vito Chianca[2], Francesco Di Pietto[3], Alfonso Reginelli[4], Raffaele Natella[4], Nicola Maggialetti[1], Domenico Albano[2], Raffaele Russo[5], Luca Maria Sconfienza[2], Luca Brunese[1], Carlo Faletti[6]

[1] Department of Medicine and Health Sciences "V. Tiberio", University of Molise, Campobasso, Italy; [2] IRCCS Istituto Ortopedico Galeazzi, Milano, Italy; [3] Dipartimento di Diagnostica per Immagini, Pineta Grande Hospital, Castel Volturno (CE), Italy; [4] Department of Precision Medicine, University of Campania "L. Vanvitelli", Naples, Italy; [5] Dipartmento di ortopedia, Pineta Grande Hospital, Castel Volturno; [6] Unità di Diagnostica per Immagini, Casa di cura Fornaca, Torino, Italy

Summary. The aim of this is article is to provide an imaging review of normal anatomy, most common anatomical variants and pathologies of the long head of the biceps tendon (LHB) encountered during the daily practice. (www.actabiomedica.it)

Key words: LHB, MR, MR-Arthrography

Anatomy

The term "biceps brachii" derives from the Latin Language and it stands for the "two heads of the arm". As the same name suggests, this muscle has two separate origins, but both are innervated by the musculocutaneous nerve, a mixed nerve originating from the lateral cord (C5-C7) (1). The short head has an extraarticular localization and it has origin from the coracoid process of the scapula blending with the coracobrachial tendon. LHB is long about 9 cm and has partially origin from the tubercle; at first, it passes in the intraarticular location to leave then the capsule and enter its bone groove (2-4). The LHB tendon is innervated by a network of sensory sympathetic fibers with a higher degree of innervation at the origin, and it explains the role in the genesis of anterior shoulder pain (5).

Intraarticular portion

During its intra-articular course, the long head of the biceps passes through the rotator interval, a triangle formed super-laterally from the anterior edge of the supraspinatus tendon and inferiorly from the upper edge of the subscapularis tendon. The base of the triangle corresponds to the base of the coracoid process and the apex of the transverse ligament. The rotator interval can be considered a rotator cuff defect formed by the protrusion of the coracoid process between the tendons of the supraspinatus and subscapularis (6). Along with its course in the rotator interval, the LHB tendon is stabilized by a capsule-ligamentous complex called the bicipital pulley, formed by the coracohumeral and superior glenohumeral ligaments (Fig. 1).

The coraco-humeral ligament originates from the postero-lateral portion of the base of the coracoid process and distally opens into two bands; the medial and smaller band pass over the LHB and look at the small tuberosity and the lateral and broader band pass on the great tuberosity and the anterior portion of the supraspinatus tendon. The superior glenohumeral ligament has origin from the superior glenoid tubercle, anteriorly to the biceps tendon, and it inserts on the lesser tuberosity (7). There is a third ligament in the

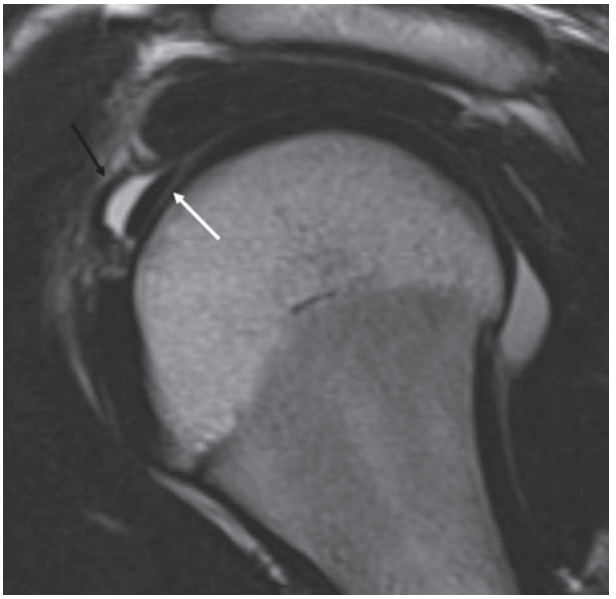

Figure 1. Oblique sagittal fat-saturated T1-weighted magnetic resonance arthrographic (MRA) image depicts biceps pulley (black arrow) forming a sling around LHB tendon (white arrow)

rotator interval of the shoulder, the coracoglenoid ligament (CGL),that forms a part of the anterosuperior capsuloligamentous complex of the shoulder (8) (Fig. 2).

Extra-articular portion

Distally to its pulley, the LHB tendon leaves the articular joint space entering the bicipital groove, formed by the greater and lesser humeral tuberosity. At the exit of the articular cavity, the LHB is covered by a sheath deriving from a synovial extroflection of the glenohumeral articular capsule. The LHB sheath inserts into the third proximal of the humerus.

Inside this synovial sheath we could find a structure called "vinculum", a membrane which develops from the humeral groove to the LHB, inserting superiorly on the rotator interval, contributing to the vascular supply of the tendon (Fig. 3). The integrity of this structure during the complete lesions of the LHB seems to prevent the "Popeye" deformity (9). The term vinculum has not to be confused with the mesotenon (some of mesotenons are called vincula, too) which connect the intraarticular portion of the LHB tendon with the superior capsular one (10).

In the proximal portion of the bicipital groove, the tendon appears to be covered by the transverse ligament. Described at the beginning of the XXth century, this structure does not play a significant role in LHB stability. However, today, the transverse ligament is not purely considered a ligament but represents the

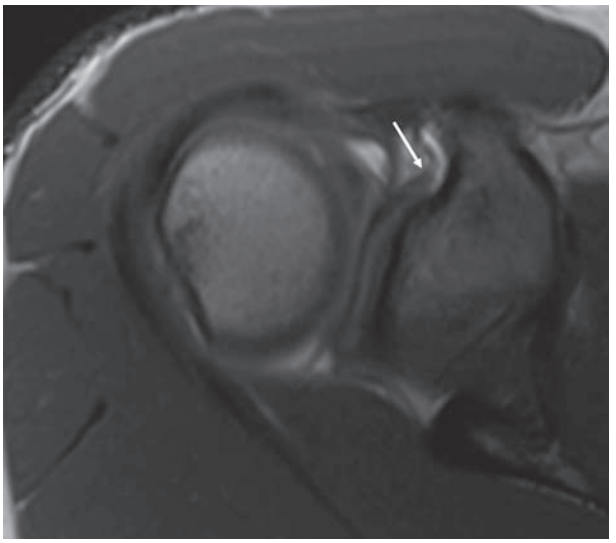

Figure 2. Axial T1w MRA image shows an independent course of coraco-glenoid ligament (arrow) from the anterior aspect of the glenoid to the proximal aspect of the coracoid

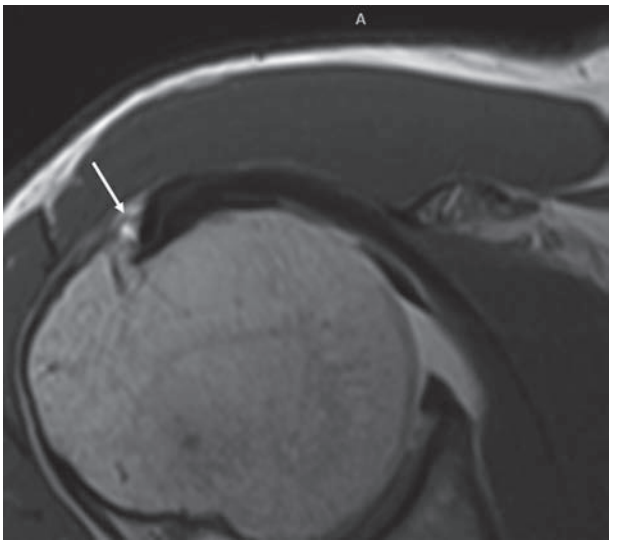

Figure 3. Axial T1w MRA image shows a vinculum (arrow) in the synovial sheath of LHB tendon

expansion of the subscapularis tendon joined with the supraspinatus tendon, the coracohumeral ligament (8) and, according to some authors, with the pectoralis minor too (11).

Anatomical variants

The LHB tendon shows a great variability among individuals and the radiological literature is rich of works about that.

A first element of this variability can be the number of tendons. The tendon and the muscular head can be absent (12). It is not uncommon the visualization of a double tendon of the LHB, both with Ultrasound (US) and Magnetic Resonance (MR) (Fig. 4a-b) (13).

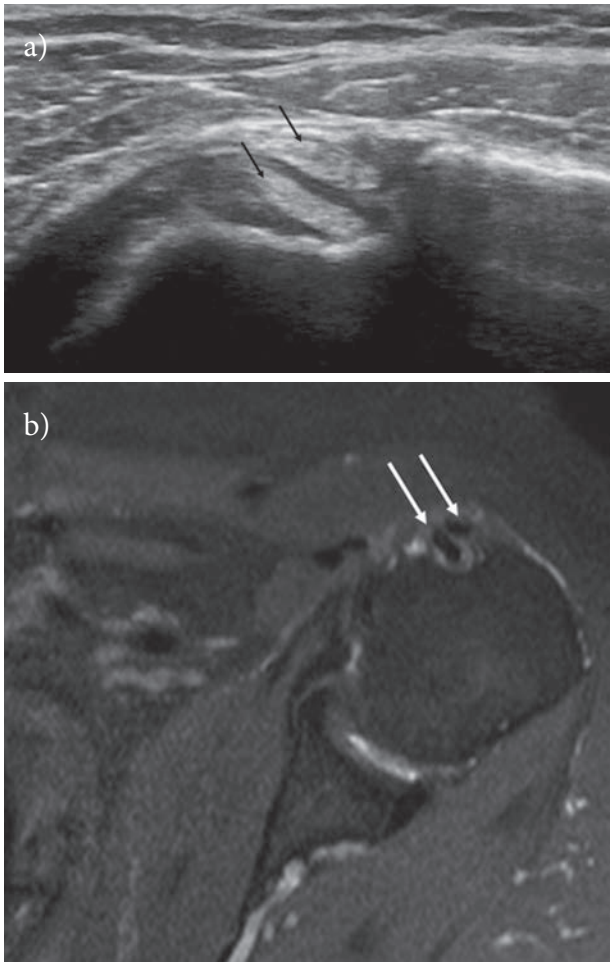

Figure 4. Two separate LHB tendons within the bicipital groove are demonstrated on US short scan image (a) (black arrows) and on axial PD fat-saturated image (b) (white arrows)

The two tendons could have a common origin from the supraglenoid tubercle splitting then later, or, as it more often happens, they could have a double origin (14). In the case of a double origin, a tendon has origin from the supraglenoid tubercle while the other one from the superior capsule (13, 15). Some authors think that in these cases, the second structure present in the bicipital sheath is not a second tendon but an aponeurotic expansion (16). In literature, some cases, where the brachial biceps appears with three or more heads, have been reported (17-19).

Even if there are few works about that, the presence of anatomical variants of the LHB are considered the cause of a pathology (10, 20).

The proximal insertion of the LHB represents a further site of variability. The presence of recesses or of a "meniscoid insertion" could be the cause of pitfalls in MR and MR-Arthrography. The last element of variability is represented by the presence of the mesotenon, that is the structure connecting the intraarticular portion of the LHB and the superior capsule. These structures, in according to our knowledge, have never been studied with imaging.

The presence of recesses or "meniscoid insertion" can represent a pitfall in MR and MR arthrography. The last element of variability is the presence of mesotenon, a synovial band connecting the rotator cuff with the intrarticular portion of LHB (10). According to our knowledge, the mesotenon has never been studied with imaging.

Biomechanics

The role of the LHB tendon is still controversial; many electromyographical studies demonstrate that it does not play an active role in shoulder movements but only in the elbow ones (21), while some authors assert that it has an active role in the depression of the humeral head during shoulder abduction (22, 23).

LHB tendon instabilities

The instabilities of the long head of the biceps are widely discussed in the radiological and orthopedic literature. For an educational purpose, it is possible to distinguish the microinstability forms of the LHB

characterized by the initial lesion of its pulley where the tendon appears instable only in its intraarticular portion, from the most severe and tardive forms which affect also the extraarticular portion of the tendon (24).

LHB pulley lesions

The lesions of the biceps pulley have been identified as "primum movens" of the LHB instability and they represent a cause of chronic shoulder pain, resistant to the conservative therapy.

These lesions could be caused by acute traumas, repeated microtraumas, degenerative causes, or they could be associated to lesions of the rotator cuff (7). Habermayer et al. have distinguished the pulley lesions in 4 groups (25): group 1 - isolated lesion of the superior glenohumeral ligament; group 2 - lesion of the superior glenohumeral ligament associated to a partial articular lesion of the supraspinatus tendon; group 3 - lesion of the superior glenohumeral ligament associated to a partial articular lesion of the subscapular; group 4 - lesion of the superior glenohumeral ligament associated to a partial articular lesion both of the supraspinatus tendon and the subscapularis one. These lesions were defined by Walch as "Hidden Lesions" because they were arthroscopically difficult to identify (26).

Imaging

Magnetic resonance (MR) and Ultrasonography (US) are the most largely used imaging tool in many diagnostic and interventional settings in radiology and particularly in musculoskeletal radiology (27-38).

In the isolated pulley lesions, although the LHB is unstable in its intraarticular portion, it may not show a clear instability in the extraarticular portion and for this reason there may be no contact loss between the tendon and its bone groove (39). Therefore, the radiological examination plays no role in this pathological phase.

Although it is possible to identify the LHB pulley with ultrasound, there are no studies in literature which demonstrate the possibility of directly assessing its lesions. However, it is possible to identify an indirect sign of pulley lesion, called "Chondral print" (40) (Fig. 5). As assessed by the arthroscopic studies of Castagna et al., the increase of the LHB intraarticular portion mobility caused by the lesion of its pulley, determines the erosion of the underlying cartilaginous humeral profile. With an accuracy of the 96%, the ultrasound identification of the chondral print can be used as an indirect sign to reveal also those early forms of the LHB instability caused by the pulley isolated lesions (41).

The standard MR images show only some parts of the LHB intracapsular portion and the ligaments of the bicipital pulley are poorly evaluable. Only on MR arthrography it is possible to directly evaluate the LHB pulley and its lesions (7, 42-44).

Barile et al. revealed a weak agreement between arthroscopy and MR imaging for Habermayer group 1 injury, an excellent agreement for group 2 and group 4 lesions and a good one for group 3 lesion (39).

On contrary, Schaeffeler et al. demonstrated high accuracy in the detection of the isolated pulley lesions using the "displacement sign" in the oblique sagittal sequences (45) (Fig. 6).

Chandiani et al. reported for the MR arthrography 100% sensitivity, 94% specificity and 94% diagnostic accuracy in the diagnosis of superior glenohumeral ligament lesions (46).

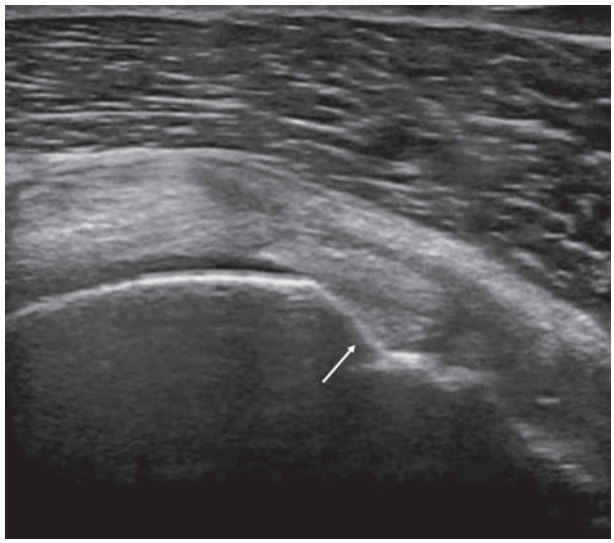

Figure 5. Short axis US scan of intrarticular portion of LHB shows a subchondral irregularity called "chondral print" (arrow) on humeral head at the level of the rotator interval

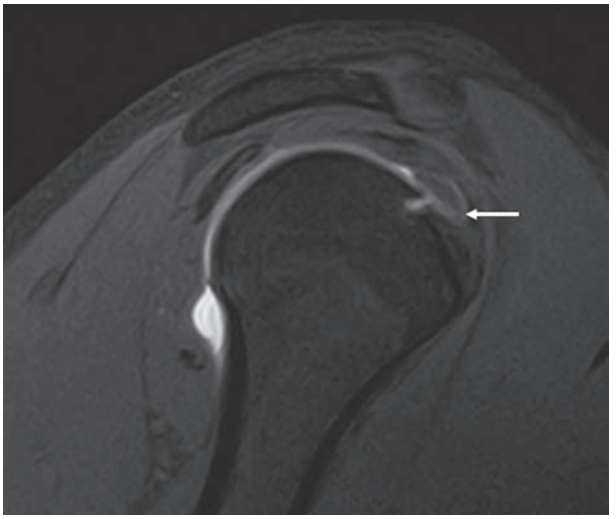

Figure 6. Sagittal PDw fat-saturated MRA image shows "displacement sign". The LHB tendon (arrow) is dislocated inferiorly, on the superior border of the SSC tendon

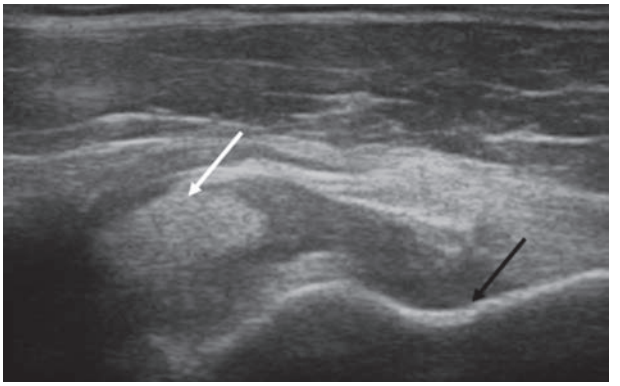

Figure 7. Short axis US scan of LHB shows medial dislocation of tendon (white arrow) inside subscapularis fibers. The LHB bone groove is empty (black arrow)

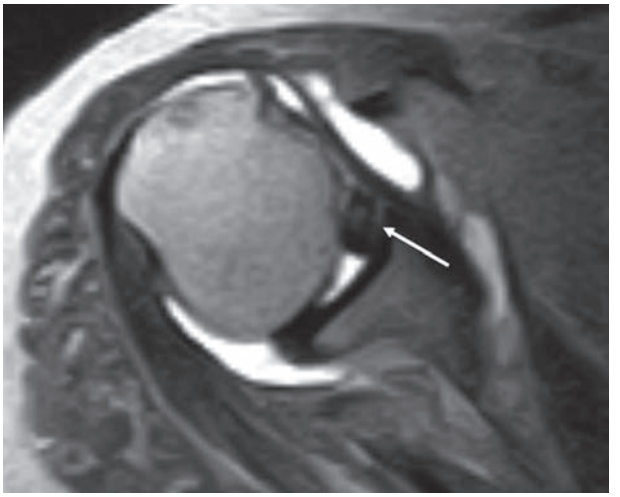

Figure 8. Axial T1w MRA image shows complete tear of subscapularis tendon. The LHB tendon is dislocated medially and it is incarcerated in the joint space (arrow)

Luxation and subluxation of LHB

The instabilities which involve also the extraarticular portion of the tendon could be considered an advanced stage of this pathology. The complete pulley lesion, associated or not with a rotator cuff lesion, determines a partial loss of contact (subluxation) or a complete one (dislocation) between the LHB tendon and its bone groove. The classification of Walch et al. is still among the most used (47). In their work Walch defines the LHB subluxation as a partial and reducible loss of the contact between the tendon and its bone groove. The dislocation was defined as a permanent loss of contact between the tendon and the intertubercular groove and it has been classified into four types:

- LHB tendon dislocation "inside" the subscapularis tendon (Fig. 7)
- intraarticular tendon dislocation with complete tearing of all anterior muscle and ligaments, but there is intact anterior fascia.
- intraarticular tendon dislocation with complete tear of both subscapularis tendon and the anterior fascia; rarely the LHB dislocated intraarticularly can be incarcerated in the gleno-humeral joint space (Fig. 8)
- extraarticular dislocation of the LHB tendon over the intact suprascapular tendon as a consequence of a supraspinatus lesion extending and involving the lateral band of the coraco-humeral ligament (Fig. 9).

The posterior dislocation of the LHB tendon as a consequence of the anterior dislocation of the humeral head has been described (48-51) (Fig. 10 a-b).

Imaging

The radiographic examination, through the modified projection of Fisk, allows a good evaluation of the characteristics of the bicipital bone sulcus (52) (Fig. 11). Cone et al. have highlighted as the presence of a

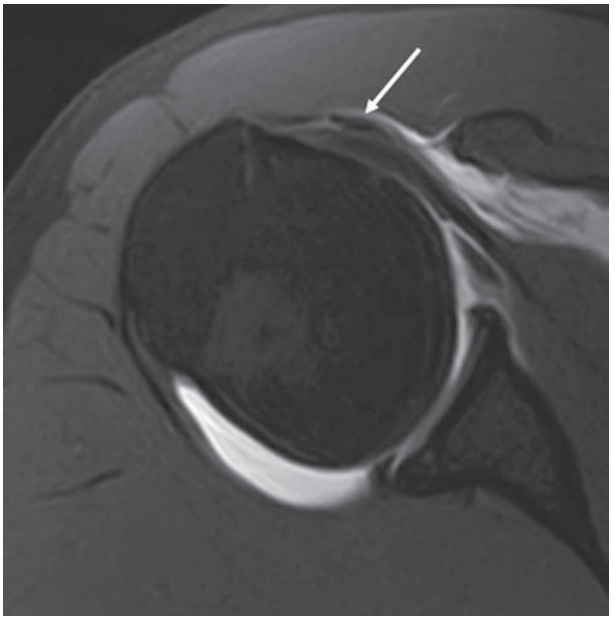

Figure 9. Axial PDw MRA image shows a dislocated LHB tendon (arrow) over the intact fibers of suprascapular tendon

bicipital groove less than 4 mm of depth on the radiographic examination represents one of the predisposing causes of bicipital dislocation (53). The presence of "geodes", sclerosis and osteophytes, on the other hand, represents the consequence of the pathological movements of the tendon, which will be more evident as the tendinous instability increases (Fig. 12).

Ultrasound shows an excellent diagnostic accuracy in detecting both the dislocations and subluxations of the LHB (54, 55). Also MR and MR arthrography can easily identify the various forms of dislocation and subluxation of LHBT (56, 57).

Tendinopathy and tendon tear

Tendinopathy of LHB tendon is caused by several pathologies such as subacromial impingement, tendon instability or tendon entrapment (hourglass biceps) (58, 59). These biomechanical alterations produce excessive traction, pressure and friction forces to the tendon (60, 61).

Tendon degeneration identifies a range of histopathologic changes. Tendinopathy is characterized by mucoid fibrous changes, increased vascularization and pallor, infiltration and replacement by adipocytes and

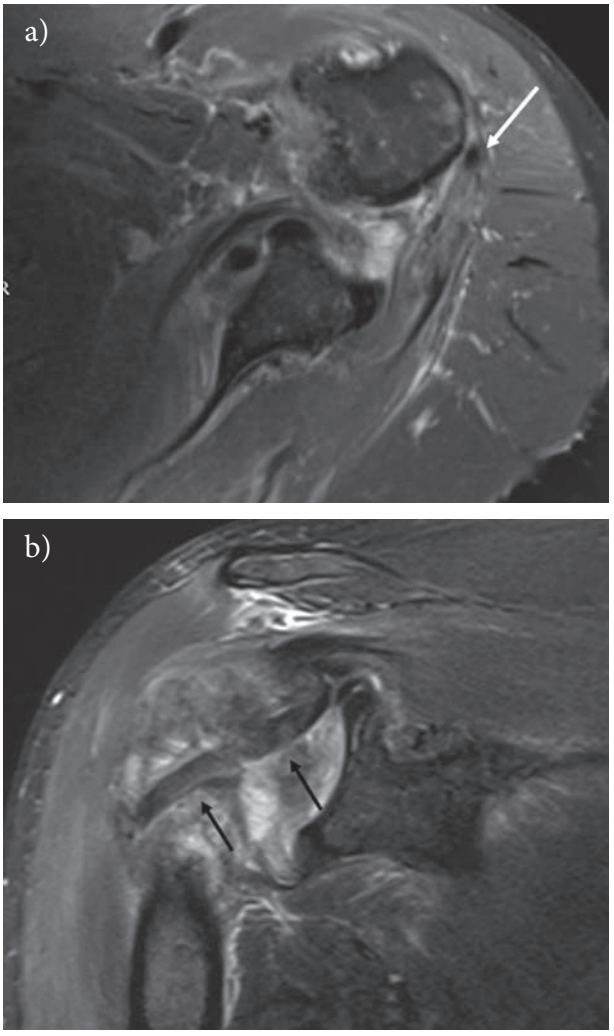

Figure 10. Axial PDw fat-saturated image (a) shows posterior dislocation of the humeral head. The LHB (white arrow) is dislocated posteriorly to the humeral head. Coronal oblique PDw fat-saturated image (b) shows the oblique course of the dislocated tendon.

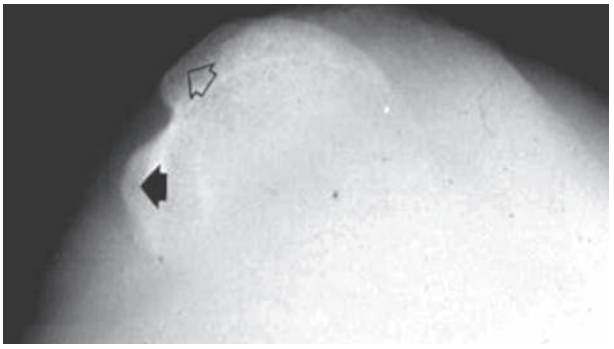

Figure 11. Fisk radiographic projection shows the normal aspect of the bicipital groove with regular medial (black arrowhead) and lateral (white arrowhead) contour.

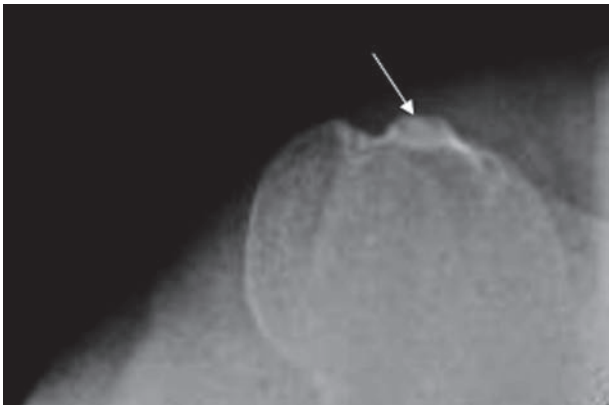

Figure 12. Fisk radiographic projection shows sclerosis (arrows) on the medial aspect of the bicipital groove

frequent chondrocytic/chondrometaplasia differentiations. Higher levels of inflammation may occur in the more proximal two-thirds of the LHB tendon (62).

Tendinopathy is associated with chronic pain that has an insidious onset and a progressive course. Repeated stress applied to a degenerate tendon can determine partial or complete tear (63).

Contrary to the tendon, in patients with anterior chronic pain the synovium of the sheath of the shoulder does not show significant inflammatory changes (62).

Imaging

Ultrasonography (US) is the least invasive imaging examination, well tolerated by patients. This technique does not employ ionizing radiations, as Magnetic Resonance (MR), and is widely used musculoskeletal radiology (64-73).

US is accurate to diagnose a normal biceps tendon or full-thickness tear, but it is less accurate in the identification of partial-thickness tear and tendinopathy (74). In tendinopathy the LHB may appear abnormally hypoechoic and possibly thickened and may eventually progress to longitudinal partial tear (Fig. 13). The use of Color-Doppler is useful for the evaluation of active inflammation of the tendon (75). A moderate tenosynovitis could be associated to the tendinopathy, and synovial hypoechoic fluid or synovial hyperechoic hypertrophy tissue around the LHB tendon could be detected (60, 76).

Using arthroscopy as reference standard, the MR has shown adequate accuracy in diagnosis of tendinopathy, partial and full thickness tears (77). On the contrary, MR does not correlate with histologic severity of tendinopathy. Higher levels of inflammatory and histopathologic changes have been found in tendons that had appeared normal in MR (62). The thickening of the intrarticular portion of the tendon on sagittal sequences is the most specific sign of tendinopathy (23, 77) (Fig. 14).

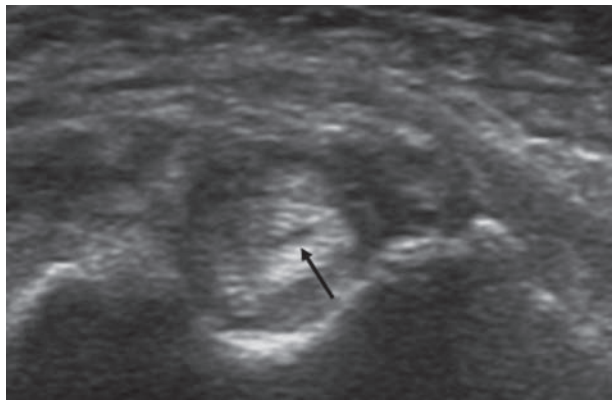

Figure 13. Short axis US scan of LHB shows a thickened tendon with a focal hypoechoic area due to a longitudinal tear (arrow)

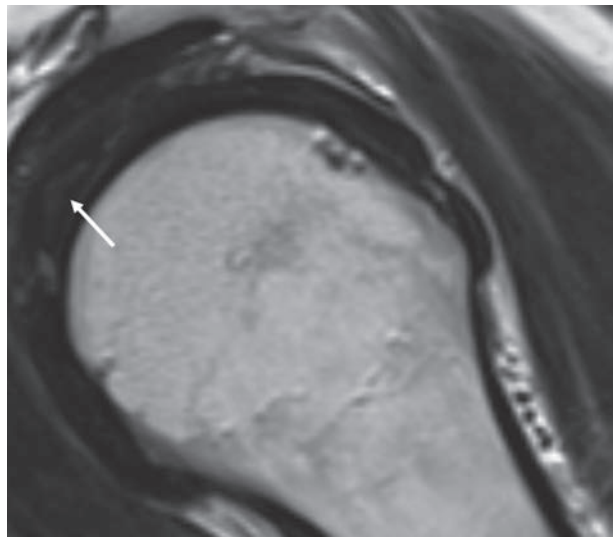

Figure 14. Oblique sagittal T2w image shows thickened and hyperintense LHB tendon (arrow)

Figure 15. Axial PDw fat-saturated MRI shows high signal (arrow) within the tendon, indicating partial-thickness tear

The presence of high signal within the tendon on T2w sequences indicates circumferential or longitudinal partial-thickness tear (Fig. 15). The absence of the LHB tendon in its bony groove indicates a complete rupture or a previous tenotomy (Fig. 16 a-b) (78) .

Conflict of interest: None to declare

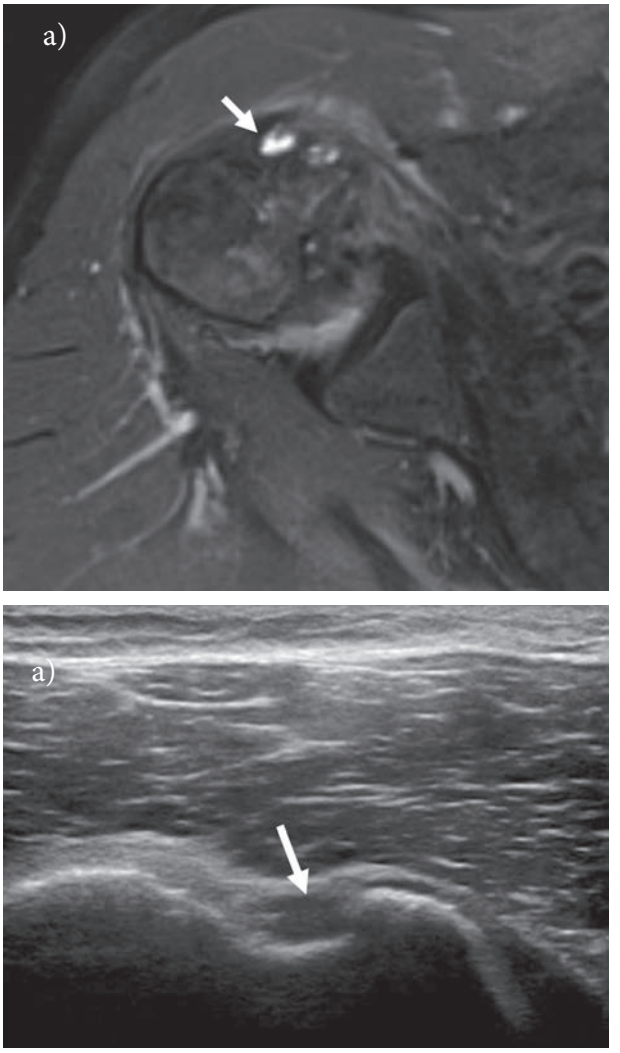

Figure 16. (a) Axial PDw fat-saturated MRI and (b) short axis US scan of LHB show the absence of the tendon and empty bicipital groove (arrow)

References

1. Sirico F, Castaldo C, Baioccato V, et al. Prevalence of musculocutaneous nerve variations: Systematic review and meta-analysis. Clin Anat 2019; 32: 183-95.
2. Beltran J, Jbara M, Maimon R. Shoulder: labrum and bicipital tendon. Top Magn Reson Imaging 2003; 14: 35-49.
3. Vangsness CT, Jr., Jorgenson SS, Watson T, Johnson DL. The origin of the long head of the biceps from the scapula and glenoid labrum. An anatomical study of 100 shoulders. J Bone Joint Surg Br 1994; 76: 951-4.
4. Elser F, Braun S, Dewing CB, Giphart JE, Millett PJ. Anatomy, function, injuries, and treatment of the long head of the biceps brachii tendon. Arthroscopy 2011; 27: 581-92.
5. Alpantaki K, McLaughlin D, Karagogeos D, Hadjipavlou A, Kontakis G. Sympathetic and sensory neural elements in the tendon of the long head of the biceps. J Bone Joint Surg Am 2005; 87: 1580-3.
6. Jost B, Koch PP, Gerber C. Anatomy and functional aspects of the rotator interval. J Shoulder Elbow Surg 2000; 9: 336-41.
7. Nakata W, Katou S, Fujita A, Nakata M, Lefor AT, Sugimoto H. Biceps pulley: normal anatomy and associated lesions at MR arthrography. Radiographics 2011; 31: 791-810.
8. Zappia M, Castagna A, Barile A, Chianca V, Brunese L, Pouliart N. Imaging of the coracoglenoid ligament: a third ligament in the rotator interval of the shoulder. Skeletal Radiol 2017; 46: 1101-11.
9. Gothelf TK, Bell D, Goldberg JA, et al. Anatomic and biomechanical study of the biceps vinculum, a structure within the biceps sheath. Arthroscopy 2009; 25: 515-21.
10. Dierickx C, Ceccarelli E, Conti M, Vanlommel J, Castagna A. Variations of the intra-articular portion of the long head of the biceps tendon: a classification of embryologically explained variations. J Shoulder Elbow Surg 2009; 18: 556-65.

11. MacDonald K, Bridger J, Cash C, Parkin I. Transverse humeral ligament: does it exist? Clin Anat 2007; 20: 663-7.
12. Kumar CD, Rakesh J, Tungish B, Singh DM. Congenital absence of the long head of biceps tendon & its clinical implications: a systematic review of the literature. Muscles Ligaments Tendons J 2017; 7: 562-69.
13. Gheno R, Zoner CS, Buck FM, et al. Accessory head of biceps brachii muscle: anatomy, histology, and MRI in cadavers. AJR Am J Roentgenol 2010; 194: W80-3.
14. Enad JG. Bifurcate origin of the long head of the biceps tendon. Arthroscopy 2004; 20: 1081-3.
15. Wittstein J, Lassiter T, Jr., Taylor D. Aberrant origin of the long head of the biceps: a case series. J Shoulder Elbow Surg 2012; 21: 356-60.
16. Moser TP, Cardinal E, Bureau NJ, Guillin R, Lanneville P, Grabs D. The aponeurotic expansion of the supraspinatus tendon: anatomy and prevalence in a series of 150 shoulder MRIs. Skeletal Radiol 2015; 44: 223-31.
17. Vazquez T, Rodriguez-Niedenfuhr M, Parkin I, Sanudo JR. A rare case of a four-headed biceps brachii muscle with a double piercing by the musculocutaneous nerve. Surg Radiol Anat 2003; 25: 462-4.
18. Nayak SR, Krishnamurthy A, Kumar M, Prabhu LV, Saralaya V, Thomas MM. Four-headed biceps and triceps brachii muscles, with neurovascular variation. Anat Sci Int 2008; 83: 107-11.
19. Battaglia PJ, Welk AB, Kettner NW. Ultrasound appearance and dynamic evaluation of variant long head of the biceps tendon anatomy with MRI correlation. J Ultrasound 2015; 18: 187-9.
20. Zhang AL, Gates CH, Link TM, Ma CB. Abnormal origins of the long head of the biceps tendon can lead to rotator cuff pathology: a report of two cases. Skeletal Radiol 2014; 43: 1621-6.
21. Yamaguchi K, Riew KD, Galatz LM, Syme JA, Neviaser RJ. Biceps activity during shoulder motion: an electromyographic analysis. Clin Orthop Relat Res 1997; 122-9.
22. Warner JJ, McMahon PJ. The role of the long head of the biceps brachii in superior stability of the glenohumeral joint. J Bone Joint Surg Am 1995; 77: 366-72.
23. Buck FM, Dietrich TJ, Resnick D, Jost B, Pfirrmann CW. Long biceps tendon: normal position, shape, and orientation in its groove in neutral position and external and internal rotation. Radiology 2011; 261: 872-81.
24. Zappia M, Reginelli A, Russo A, et al. Long head of the biceps tendon and rotator interval. Musculoskelet Surg 2013; 97 Suppl 2: S99-108.
25. Habermeyer P, Magosch P, Pritsch M, Scheibel MT, Lichtenberg S. Anterosuperior impingement of the shoulder as a result of pulley lesions: a prospective arthroscopic study. J Shoulder Elbow Surg 2004; 13: 5-12.
26. Walch G, Nove-Josserand L, Levigne C, Renaud E. Tears of the supraspinatus tendon associated with "hidden" lesions of the rotator interval. J Shoulder Elbow Surg 1994; 3: 353-60.
27. Barile A, Bruno F, Arrigoni F, et al. Emergency and Trauma of the Ankle. Semi Musc Rad 2017; 21: 282-89.
28. Barile A, Bruno F, Mariani S, et al. What can be seen after rotator cuff repair: a brief review of diagnostic imaging findings. Musculoskelet Surg 2017; 101: 3-14.
29. Splendiani A, D'Orazio F, Patriarca L, et al. Imaging of post-operative spine in intervertebral disc pathology. Musculoskelet Surg 2017; 101: 75-84.
30. Arrigoni F, Gregori LM, Zugaro L, Barile A, Masciocchi C. MRgFUS in the treatment of MSK lesions: A review based on the experience of the university of L'aquila, Italy. Transl Cancer Res 2014; 3: 442-48.
31. Reginelli A, Zappia M, Barile A, Brunese L. Strategies of imaging after orthopedic surgery. Musculoskelet Surg 2017; 101: 1.
32. Masciocchi C, Conti L, D'Orazio F, Conchiglia A, Lanni G, Barile A, Errors in Musculoskeletal MRI, in: Romano L., Pinto A. (Eds.), Errors in Radiology, Springer Milan, Milano, 2012, pp. 209-17.
33. Cicala D, Briganti F, Casale L, et al. Atraumatic vertebral compression fractures: Differential diagnosis between benign osteoporotic and malignant fractures by MRI. Musculoskelet Surg 2013; 97: S169-S79.
34. Barile A, Arrigoni F, Bruno F, et al. Present role and future perspectives of interventional radiology in the treatment of painful bone lesions. Future Oncol 2018; 14: 2945-55.
35. Arrigoni F, Bruno F, Zugaro L, et al. Developments in the management of bone metastases with interventional radiology. Acta Biomed 2018; 89: 166-74.
36. Arrigoni F, Barile A, Zugaro L, et al. Intra-articular benign bone lesions treated with Magnetic Resonance-guided Focused Ultrasound (MRgFUS): imaging follow-up and clinical results. Med Oncol 2017; 34: 55.
37. Tarantini G, Favaretto E, Napodano M, et al. Design and methodologies of the postconditioning during coronary angioplasty in acute myocardial infarction (POST-AMI) trial. Cardiology 2010; 116: 110-16.
38. Salvolini L, Urbinati C, Valeri G, Ferrara C, Giovagnoni A. Contrast-enhanced MR cholangiography (MRCP) with GD-EOB-DTPA in evaluating biliary complications after surgery. Radiol Med 2012; 117: 354-68.
39. Barile A, Lanni G, Conti L, et al. Lesions of the biceps pulley as cause of anterosuperior impingement of the shoulder in the athlete: Potentials and limits of MR arthrography compared with arthroscopy. Radiol Med 2013; 118: 112-22.
40. Zappia M, Carfora M, Romano AM, et al. Sonography of chondral print on humeral head. Skeletal Radiol 2016; 45: 35-40.
41. Castagna A, Mouhsine E, Conti M, et al. Chondral print on humeral head: an indirect sign of long head biceps tendon instability. Knee Surg Sports Traumatol Arthrosc 2007; 15: 645-8.
42. Chung CB, Dwek JR, Cho GJ, Lektrakul N, Trudell D, Resnick D. Rotator cuff interval: evaluation with MR imaging and MR arthrography of the shoulder in 32 cadavers. J Comput Assist Tomogr 2000; 24: 738-43.
43. Ho CP. MR imaging of rotator interval, long biceps, and

associated injuries in the overhead-throwing athlete. Magn Reson Imaging Clin N Am 1999; 7: 23-37.
44. Lee JC, Guy S, Connell D, Saifuddin A, Lambert S. MRI of the rotator interval of the shoulder. Clin Radiol 2007; 62: 416-23.
45. Schaeffeler C, Waldt S, Holzapfel K, et al. Lesions of the biceps pulley: diagnostic accuracy of MR arthrography of the shoulder and evaluation of previously described and new diagnostic signs. Radiology 2012; 264: 504-13.
46. Chandnani VP, Gagliardi JA, Murnane TG, et al. Glenohumeral ligaments and shoulder capsular mechanism: evaluation with MR arthrography. Radiology 1995; 196: 27-32.
47. Walch G, Nove-Josserand L, Boileau P, Levigne C. Subluxations and dislocations of the tendon of the long head of the biceps. J Shoulder Elbow Surg 1998; 7: 100-8.
48. Freeland AE, Higgins RW. Anterior shoulder dislocation with posterior displacement of the long head of the biceps tendon. Arthrographic findings. A case report. Orthopedics 1985; 8: 468-9.
49. Strobel K, Treumann TC, Allgayer B. Posterior entrapment of the long biceps tendon after traumatic shoulder dislocation: findings on MR imaging. AJR Am J Roentgenol 2002; 178: 238-9.
50. McArthur C, Welsh F, Campbell C. Posterior dislocation of long head of biceps tendon following traumatic anterior shoulder dislocation: imaging and intra-operative findings. J Radiol Case Rep 2013; 7: 19-26.
51. Mullaney PJ, Bleakney R, Tuchscherer P, Boynton E, White L. Posterior dislocation of the long head of biceps tendon: case report and review of the literature. Skeletal Radiol 2007; 36: 779-83.
52. Fisk C. Adaption of the technique for radiography of the bicipital groove. Radiol Technol 1965; 37: 47-50.
53. Cone RO, Danzig L, Resnick D, Goldman AB. The bicipital groove: radiographic, anatomic, and pathologic study. AJR Am J Roentgenol 1983; 141: 781-8.
54. Farin PU, Jaroma H, Harju A, Soimakallio S. Medial displacement of the biceps brachii tendon: evaluation with dynamic sonography during maximal external shoulder rotation. Radiology 1995; 195: 845-8.
55. Armstrong A, Teefey SA, Wu T, et al. The efficacy of ultrasound in the diagnosis of long head of the biceps tendon pathology. J Shoulder Elbow Surg 2006; 15: 7-11.
56. Chan TW, Dalinka MK, Kneeland JB, Chervrot A. Biceps tendon dislocation: evaluation with MR imaging. Radiology 1991; 179: 649-52.
57. Cervilla V, Schweitzer ME, Ho C, Motta A, Kerr R, Resnick D. Medial dislocation of the biceps brachii tendon: appearance at MR imaging. Radiology 1991; 180: 523-6.
58. Becker DA, Cofield RH. Tenodesis of the long head of the biceps brachii for chronic bicipital tendinitis. Long-term results. J Bone Joint Surg Am 1989; 71: 376-81.
59. Boileau P, Ahrens PM, Hatzidakis AM. Entrapment of the long head of the biceps tendon: the hourglass biceps--a cause of pain and locking of the shoulder. J Shoulder Elbow Surg 2004; 13: 249-57.
60. Skendzel JG, Jacobson JA, Carpenter JE, Miller BS. Long head of biceps brachii tendon evaluation: accuracy of preoperative ultrasound. AJR Am J Roentgenol 2011; 197: 942-8.
61. Joseph M, Maresh CM, McCarthy MB, et al. Histological and molecular analysis of the biceps tendon long head posttenotomy. J Orthop Res 2009; 27: 1379-85.
62. Nuelle CW, Stokes DC, Kuroki K, Crim JR, Sherman SL. Radiologic and Histologic Evaluation of Proximal Bicep Pathology in Patients With Chronic Biceps Tendinopathy Undergoing Open Subpectoral Biceps Tenodesis. Arthroscopy 2018; 34: 1790-96.
63. Ahrens PM, Boileau P. The long head of biceps and associated tendinopathy. J Bone Joint Surg Br 2007; 89: 1001-9.
64. Zappia M, Capasso R, Berritto D, et al. Anterior cruciate ligament reconstruction: MR imaging findings. Musculoskelet Surg 2017; 101: 23-35.
65. Masciocchi C, Zugaro L, Arrigoni F, et al. Radiofrequency ablation versus magnetic resonance guided focused ultrasound surgery for minimally invasive treatment of osteoid osteoma: a propensity score matching study. Eur Radiol 2016; 26: 2472-81.
66. Barile A, Regis G, Masi R, et al. Musculoskeletal tumours: Preliminary experience with perfusion MRI. Radiol Med 2007; 112: 550-61.
67. Barile A, Arrigoni F, Zugaro L, et al. Minimally invasive treatments of painful bone lesions: state of the art. Med Oncol 2017; 34: 53.
68. Barile A, Arrigoni F, Bruno F, et al. Computed Tomography and MR Imaging in Rheumatoid Arthritis. Radiol Clin North Am 2017; 55: 997-1007.
69. Perrotta FM, Astorri D, Zappia M, Reginelli A, Brunese L, Lubrano E. An ultrasonographic study of enthesis in early psoriatic arthritis patients naive to traditional and biologic DMARDs treatment. Rheumatol Int 2016; 36: 1579-83.
70. Barile A, La Marra A, Arrigoni F, et al. Anaesthetics, steroids and platelet-rich plasma (PRP) in ultrasound-guided musculoskeletal procedures. Br J Radiol 2016; 89: 20150355.
71. Cuomo G, Zappia M, Iudici M, Abignano G, Rotondo A, Valentini G. The origin of tendon friction rubs in patients with systemic sclerosis: a sonographic explanation. Arthritis Rheum 2012; 64: 1291-3.
72. Di Pietto F, Chianca V, de Ritis R, et al. Postoperative imaging in arthroscopic hip surgery. Musculoskelet Surg 2017; 101: 43-49.
73. Aliprandi A, Di Pietto F, Minafra P, Zappia M, Pozza S, Sconfienza LM. Femoro-acetabular impingement: What the general radiologist should know. Radiol Med 2014; 119: 103-12.
74. Sconfienza LM, Albano D, Allen G, et al. Clinical indications for musculoskeletal ultrasound updated in 2017 by European Society of Musculoskeletal Radiology (ESSR) consensus. Eur Radiol 2018;
75. Albano D, Chianca V, Tormenta S, Migliore A, Sconfienza LM. Old and new evidence concerning the crucial role of ultrasound in guiding intra-articular injections. Skeletal Radiol 2017; 46: 963-64.

76. Martinoli C, Bianchi S, Prato N, et al. US of the shoulder: non-rotator cuff disorders. Radiographics 2003; 23: 381-401; quiz 534.
77. Zanetti M, Weishaupt D, Gerber C, Hodler J. Tendinopathy and rupture of the tendon of the long head of the biceps brachii muscle: evaluation with MR arthrography. AJR Am J Roentgenol 1998; 170: 1557-61.
78. Albano D, Chianca V, Zappia M, et al. Imaging of Usual and Unusual Complication of Rotator Cuff Repair. J Comput Assist Tomogr 2019;

Received: 26 March 2019
Accepted: 4 April 2019
Correspondence:
Alfonso Reginelli
Department of Precision Medicine,
University of Campania "L. Vanvitelli",
Naples, Italy
E-mail: alfonsoreginelli@hotmail.com

Acta Biomed 2019; Vol. 90, Supplement 5: 95-100 DOI: 10.23750/abm.v90i5-S.8333

Review

Ultrasound-guided percutaneous irrigation of calcific tendinopathy: technical developments

Francesco Pagnini[1], Fabiano Vito D'Amuri[1], Andrea Bevilacqua[1], Vittorio Sabatino[1], Umberto Russo[1], Marcello Zappia[2], Raffaele Natella[3], Pierpaolo Palumbo[4], Silvia Pradella[5], Vittorio Miele[5], Massimo De Filippo[1]

[1] Department of Medicine and Surgery, Unit of Radiologic Science, University of Parma, Maggiore Hospital, Parma, Italy; [2] Department of Medicine and Health Sciences, University of Molise, Campobasso, Italy; [3] Department of Precision Medicine, University of Campania "L. Vanvitelli", Naples, Italy; [4] Department of Biotechnology and Applied Clinical Sciences, University of L'Aquila, S. Salvatore Hospital, L'Aquila, Italy; [5] Department of Radiology - Careggi University Hospital, Florence, Italy

Summary. Rotator cuff calcific tendinopathy (RCCT) is a common and painful shoulder disease characterised by deposition of calcium into the rotator cuff's tendond. Different therapeutic options have been proposed, but the ultrasound-guided percutaneous irrigation (US-PICT) is been proved as an effective and safe first-line treatment. It can be performed with a single- of a double-needle tecnique, using warm saline solution to improve the dissolution of the calcific deposit. The procedure is ended with an intrabursal injection of local anaesthetics and slow-release steroids to improve the pain relief and to prevent complications. US-PICT leads to significative improvement in the shoulder funtion and pain relief in the short and long term, with a low complications rate. (www.actabiomedica.it)

Key words: rotator cuff, shoulder, ultrasound-guided procedures, calcific tendinopathy, percutaneus treatments

Introduction

Rotator cuff calcific tendinopathy (RCCT) is a common disease, with a reported prevalence of 2.5% up to 7.5% of asymptomatic adults, and up to 30-40% of painful shoulders, tipically seen in women in the 4th or 5th decade and in sedentary workers (1-3).

Aetiology of this condition is still poorly understood, but the most convincing mechanism is that a decrease of intratendinous oxygen concentration may promote tendon fibrocartilaginous metaplasia and cellular necrosis, followed by deposition of calcium, mainly hydroxyapatite (4).

Diagnostic and interventional radiology in the musculoskeletal system are widely used (5-21). Regarding to the US imaging (22-24), three types of calcifications can be found: type I - a hyperechoic focus with a well defined shadow; type II - a hyperechoic focus with a faint shadow; Type III - a hyperecoic focus whithout an acoustic shadow (Fig. 1) (25).

In the RCCT's pathogenesis 4 stages are recognizable:

- Precalcific stage with fibrocartilaginous transformation within the tendon.
- Formative stage with calcium deposition
- Resorptive phase.
- Postcalcific phase, in which self-healing and repair of the affected tendon occurs.

The resorptive phase is characterized by hyperemia, edema, increased intratendinous pressure with possible etravasation of calcium crystals in the subacromial bursa. Usually this stage is associated with the development of acute pain, that can be very disabling (pseudoparalytic shoulder) and unresponsive to con-

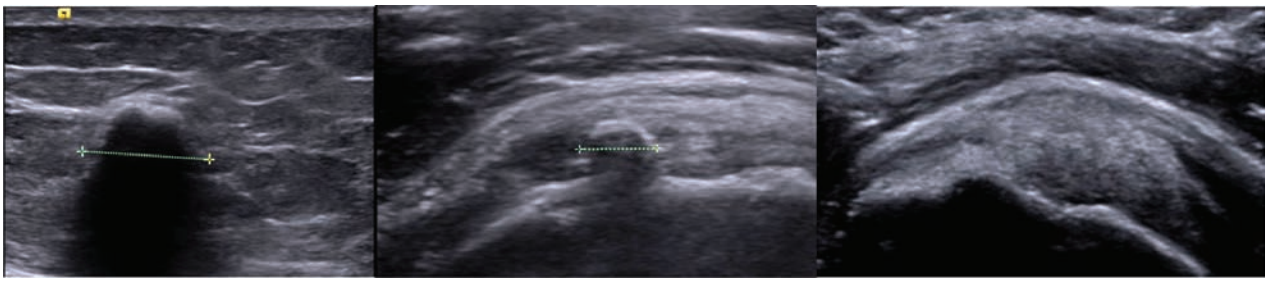

Figure 1. US findings of shoulder calcifications, as decribed by Farin et al.: (A) a hyperechoic focus with a well defined shadow (B) a hyperechoic focus with a faint shadow (C) a hyperecoic focus whithout an acoustic shadow

servative treatments such as nonsteroidal anti-inflammatory drugs (NSAIDs) (26).

The most affected tendon of the rotator cuff is the supraspinatus (80%), followed by the lower side of infraspinatus (15%) and the preinsertional area of the subscapularis tendon (5%) (8, 27-31).

Therapeutic options include subacromial steroid injections, arthroscopy, and extracorporeal shockwaves. Currently ultrasound-guided percutaneous irrigation of calcific tendinopathy (US-PICT) is accepted as the first-line safe and effective treatment for RCCT, wth significant pain improvement and a very low rate of minor complications (vasovagal reaction, bursitis) (32).

This procedure is also known as "barbotage" and "lavage", it does not require hospitalization, is performed under local anesthesia and there is no need of post-procedural immoblization. The patient can go home about 30 minutes after the procedure and return the day after the treatment to his daily activities.

Procedure details

- *Pretreatment evaluation:*

US-PICT is always indicated in the resorptive phase, in presence of soft or semi-fluid calcifications (type II or III). In case of hard calcification (type I) or mildly symptomatic patient, elective treatment should be considered. With very small calcifications (<5 mm) or migration into the bursal space the procedure is not indicated (33).

- *Patient positioning and antisepsis:*

The procedure is performed with the patient in semisupine position, the arm of the affected shoulder should lie completely extended along the body with a internal/external rotation according to the calcification's location.

Ordinary antisepsis is generally sufficient to guarantee a safe procedure for both the patient and the operator.

- *Local anaesthesia:*

A small amount of local anaesthetic (up to 10 ml of lidocaine) is injected along the path of the needles, into the subacromial-subdeltoid bursa (almost two thirds) and around the calcifications. In order to preserve the peripheral calcific rim, no anaesthetic solution should be injected directly within the calcification.

Positioning of the needles and irrigation procedure:

The procedure can be done with a single or double needle tecnique (Figg. 2, 3).

The size of the needle should be chosen in order to maximize calcium retriveal and avoid obstruction, in other published studies for RCCT treatment varies between 16 and 18 G. Every approach is done under continuous US monitoring, with a free-hand tecnique or with needle guidance kit, but the first one is faster and allows a more flexible approach. In the double-needle tecnique the needles are inserted depending on the location and accessibility to the calcification. Both needles should be as perpedicular as possible to the US beam so anisotropy artifacts are minimyzed and needles can be seen thoroughly (Fig. 4). The deeper needle is first inserted, taking care to preserve the integrity of the calcific shell, than the second needle is inserted su-

Figure 2. (A) US probe and needle positioning with the one-needle tecnique. (B) Ultrasound image of a soft-fluid calcification (type III). After the puncture and the washing, a leakage of toothpaste-like material is seen from the needle

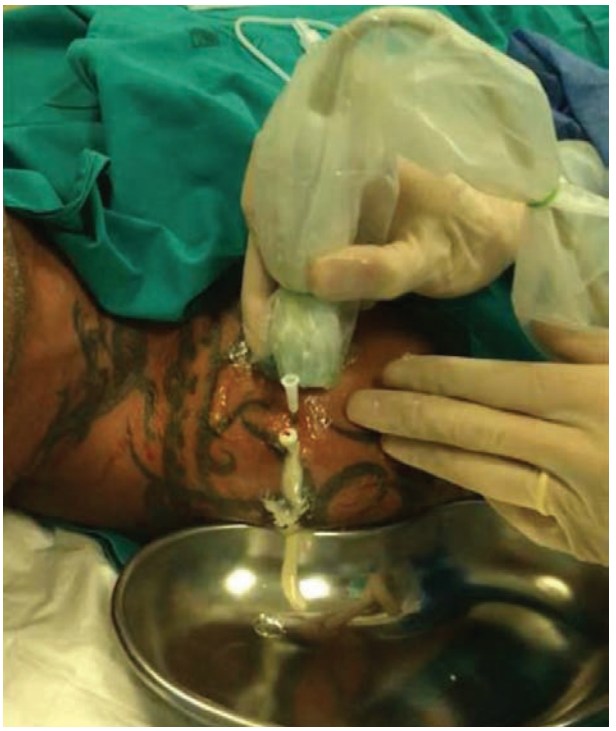

Figure 3. Image shows the needles positioning in the double-needle technique. The deeper needle (1) inserted first, than the second needle is inserted superficial to the first one. Is important to position the needles as much perpendicular as possible to the US beam to achieve optimal visualization under US guidance

perficially. The correct angulation of the needles's tips should be 25-30°, with both bevels facing each other, to allow a continuous flow of water that is injected from one needle and drained by the other (Fig. 5) (34). Saline solution is normally injected using 20/40-ml syringe in one needle, the plunger pushed repeatedly and when the calcification starts to dissolve, water and calcium debris are drained from the second needle.

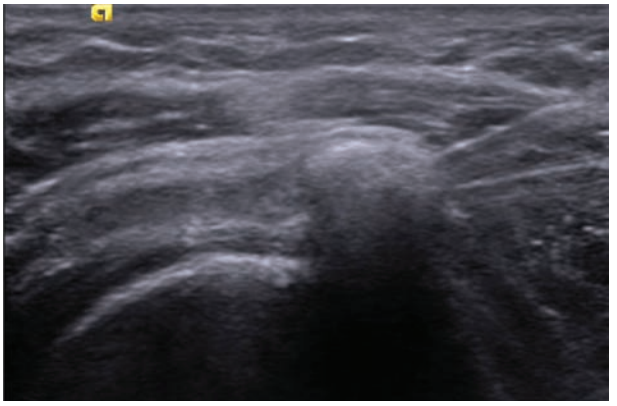

Figure 4. Ultrasound image of the double-needle technique. Both needles lay on the same coronal plane, with a correct angulation (25-30°) and both bevels facing each other

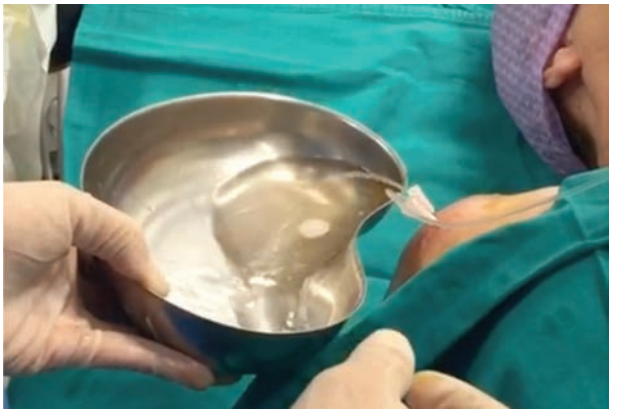

Figure 5. The flow of saline water, injected from one needle and drained by the other, using the double-needle technique.

During the irrigation procedure needles can be rotated and displaced to increase calcium disaggregation and fragmentation. The use of warm saline solution may shorten the procedure and improve calcification dissolution (Fig. 6) (2).

Postprocedural treatment

At the end of the procedure, to reduce the risk of postprocedural bursitis, US-guided intrabursal injection of local anaesthetics and slow-release steroids is indicated (35).

After the treatment a short course of nonsteroidal anti-inflammatory drugs (NSAIDs), a period of relative rest (~15 days), and physiokinetic therapy are recommended.

Figure 6. (A) Out-flow of calcium deposit with toothpaste-like consistency. (B) After few minutes the calcium tends to form aggregates.

Clinical outcome and complications

In the short-term period the worsening of symptoms is frequent, but normally followed by a quick resolution (~48 h). In the middle and long-term period many authors reported a greater reduction of pain, compared to patients who refused the treatment, and a significant improvement of shoulder function.

A recent sistematic review reported a 10% complication rate: bursitis was the most frequent, that occured in 7% of all procedures. Other complications included vasovagal reactions (2%), frozen shoulder (0,2%), seizures (0,2%), tenosynovitis of the bicipital long head (0,1%) (2) (36).

Conclusions

Magnetic Resonance Imaging (MRI), thanks to its excellent soft tissue contrast and multiplanar capability, is the primary imaging tool for a variety of conditions and diseases both for diagnostic and interventional purposes (37-48) but US-PICT has been demonstreted to be a quick, minimally invasive, low cost and effective procedure for treating RCCT, regardless of the use of a single- or double- needle tecnique. It lead to significant long term improvement in the shoulder function and is very effective in the short term with regard to pain relief.

Ethical approval: This article does not contain any studies with human participants performed by any of the authors.

Conflict of interest: None to declare

References

1. Speed CA, Hazleman BL. Calcific tendinitis of the shoulder. N Engl J Med 1999; 340: 1582-4.
2. Lanza E, Banfi G, Serafini G, et al. Ultrasound-guided percutaneous irrigation in rotator cuff calcific tendinopathy: what is the evidence? A systematic review with proposals for future reporting. Eur Radiol 2015; 25: 2176-83.
3. Sharma P, Maffulli N. Tendon injury and tendinopathy: healing and repair. J Bone Joint Surg Am 2005; 87: 187-202.
4. Uhthoff HK, Sarkar K. Calcifying tendinitis. Baillieres Clin Rheumatol 1989; 3: 567-81.
5. Mariani S, La Marra A, Arrigoni F, et al. Dynamic measurement of patello-femoral joint alignment using weight-bearing magnetic resonance imaging (WB-MRI). Eur J Radiol 2015; 84: 2571-78.
6. Barile A, Bruno F, Arrigoni F, et al. Emergency and Trauma of the Ankle. Semi Musc Rad 2017; 21: 282-89.
7. Splendiani A, D'Orazio F, Patriarca L, et al. Imaging of post-operative spine in intervertebral disc pathology. Musculoskelet Surg 2017; 101: 75-84.
8. Arrigoni F, Gregori LM, Zugaro L, Barile A, Masciocchi C. MRgFUS in the treatment of MSK lesions: A review based on the experience of the university of L'aquila, Italy. Transl Cancer Res 2014; 3: 442-48.
9. Reginelli A, Zappia M, Barile A, Brunese L. Strategies of imaging after orthopedic surgery. Musculoskelet Surg 2017; 101: 1.
10. Cicala D, Briganti F, Casale L, et al. Atraumatic vertebral compression fractures: Differential diagnosis between benign osteoporotic and malignant fractures by MRI. Musculoskelet Surg 2013; 97: S169-S79.
11. Barile A, Arrigoni F, Bruno F, et al. Present role and future perspectives of interventional radiology in the treatment of painful bone lesions. Future Oncol 2018; 14: 2945-55.

12. Arrigoni F, Bruno F, Zugaro L, et al. Developments in the management of bone metastases with interventional radiology. Acta Biomed 2018; 89: 166-74.
13. Zappia M, Capasso R, Berritto D, et al. Anterior cruciate ligament reconstruction: MR imaging findings. Musculoskelet Surg 2017; 101: 23-35.
14. Masciocchi C, Zugaro L, Arrigoni F, et al. Radiofrequency ablation versus magnetic resonance guided focused ultrasound surgery for minimally invasive treatment of osteoid osteoma: a propensity score matching study. Eur Radiol 2016; 26: 2472-81.
15. Barile A, Regis G, Masi R, et al. Musculoskeletal tumours: Preliminary experience with perfusion MRI. Radiol Med 2007; 112: 550-61.
16. Barile A, Arrigoni F, Zugaro L, et al. Minimally invasive treatments of painful bone lesions: state of the art. Med Oncol 2017; 34: 53.
17. Barile A, Arrigoni F, Bruno F, et al. Computed Tomography and MR Imaging in Rheumatoid Arthritis. Radiol Clin North Am 2017; 55: 997-1007.
18. Aliprandi A, Di Pietto F, Minafra P, Zappia M, Pozza S, Sconfienza LM. Femoro-acetabular impingement: What the general radiologist should know. Radiol Med 2014; 119: 103-12.
19. Cuomo G, Zappia M, Iudici M, Abignano G, Rotondo A, Valentini G. The origin of tendon friction rubs in patients with systemic sclerosis: a sonographic explanation. Arthritis Rheum 2012; 64: 1291-93.
20. Zappia M, Castagna A, Barile A, Chianca V, Brunese L, Pouliart N. Imaging of the coracoglenoid ligament: a third ligament in the rotator interval of the shoulder. Skeletal Radiol 2017; 46: 1101-11.
21. Di Pietto F, Chianca V, de Ritis R, et al. Postoperative imaging in arthroscopic hip surgery. Musculoskelet Surg 2017; 101: 43-49.
22. Perrotta FM, Astorri D, Zappia M, Reginelli A, Brunese L, Lubrano E. An ultrasonographic study of enthesis in early psoriatic arthritis patients naive to traditional and biologic DMARDs treatment. Rheumatol Int 2016; 36: 1579-83.
23. Barile A, La Marra A, Arrigoni F, et al. Anaesthetics, steroids and platelet-rich plasma (PRP) in ultrasound-guided musculoskeletal procedures. Br J Radiol 2016; 89: 20150355.
24. di Giacomo V, Trinci M, van der Byl G, Catania VD, Calisti A, Miele V. Ultrasound in newborns and children suffering from non-traumatic acute abdominal pain: imaging with clinical and surgical correlation. J Ultrasound 2015; 18: 385-93.
25. Farin PU, Jaroma H. Sonographic findings of rotator cuff calcifications. J Ultrasound Med 1995; 14: 7-14.
26. Tagliafico A, Russo G, Boccalini S, et al. Ultrasound-guided interventional procedures around the shoulder. Radiol Med 2014; 119: 318-26.
27. Gartner J, Heyer A. [Calcific tendinitis of the shoulder]. Orthopade 1995; 24: 284-302.
28. Zoccali C, Rossi B, Zoccali G, et al. A new technique for biopsy of soft tissue neoplasms: a preliminary experience using MRI to evaluate bleeding. Minerva Med 2015; 106: 117-20.
29. Masciocchi C, Conti L, D'Orazio F, Conchiglia A, Lanni G, Barile A, Errors in Musculoskeletal MRI, in: Romano L., Pinto A. (Eds.), Errors in Radiology, Springer Milan, Milano, 2012, pp. 209-17.
30. Limbucci N, Rossi F, Salvati F, Pistoia LM, Barile A, Masciocchi C. Bilateral suprascapular nerve entrapment by glenoid labral cysts associated with rotator cuff damage and posterior instability in an amateur weightlifter. J Sports Med Phys Fitness 2010; 50: 64-7.
31. Barile A, Bruno F, Mariani S, et al. What can be seen after rotator cuff repair: a brief review of diagnostic imaging findings. Musculoskelet Surg 2017; 101: 3-14.
32. de Witte PB, Selten JW, Navas A, et al. Calcific tendinitis of the rotator cuff: a randomized controlled trial of ultrasound-guided needling and lavage versus subacromial corticosteroids. Am J Sports Med 2013; 41: 1665-73.
33. Serafini G, Sconfienza LM, Lacelli F, Silvestri E, Aliprandi A, Sardanelli F. Rotator cuff calcific tendonitis: short-term and 10-year outcomes after two-needle us-guided percutaneous treatment--nonrandomized controlled trial. Radiology 2009; 252: 157-64.
34. Sconfienza LM, Serafini G, Sardanelli F. Treatment of calcific tendinitis of the rotator cuff by ultrasound-guided single-needle lavage technique. AJR Am J Roentgenol 2011; 197: W366; author reply 67.
35. Sconfienza LM, Bandirali M, Serafini G, et al. Rotator cuff calcific tendinitis: does warm saline solution improve the short-term outcome of double-needle US-guided treatment? Radiology 2012; 262: 560-6.
36. Oudelaar BW, Schepers-Bok R, Ooms EM, Huis In 't Veld R, Vochteloo AJ. Needle aspiration of calcific deposits (NACD) for calcific tendinitis is safe and effective: Six months follow-up of clinical results and complications in a series of 431 patients. Eur J Radiol 2016; 85: 689-94.
37. Tedeschi E, Caranci F, Giordano F, Angelini V, Cocozza S, Brunetti A. Gadolinium retention in the body: what we know and what we can do. Radiol Med 2017; 122: 589-600.
38. Briganti F, Leone G, Marseglia M, Cicala D, Caranci F, Maiuri F. P64 Flow Modulation Device in the treatment of intracranial aneurysms: Initial experience and technical aspects. J Neurointerv Surg 2016; 8: 173-80.
39. Arrigoni F, Barile A, Zugaro L, et al. Intra-articular benign bone lesions treated with Magnetic Resonance-guided Focused Ultrasound (MRgFUS): imaging follow-up and clinical results. Med Oncol 2017; 34: 55.
40. Cirillo M, Caranci F, Tortora F, et al. Structural neuroimaging in dementia. J Alzheimers Dis 2012; 29: 16-19.
41. Schicchi N, Valeri G, Moroncini G, et al. Myocardial perfusion defects in scleroderma detected by contrast-enhanced cardiovascular magnetic resonance. Radiol Med 2014; 119: 885-94.
42. Tarantini G, Favaretto E, Napodano M, et al. Design and methodologies of the postconditioning during coronary an-

gioplasty in acute myocardial infarction (POST-AMI) trial. Cardiology 2010; 116: 110-16.
43. Salvolini L, Urbinati C, Valeri G, Ferrara C, Giovagnoni A. Contrast-enhanced MR cholangiography (MRCP) with GD-EOB-DTPA in evaluating biliary complications after surgery. Radiol Med 2012; 117: 354-68.
44. Bertolini L, Vaglio A, Bignardi L, et al (2011). Subclinical interstitial lung abnormalities in stable renal allograft recipients in the era of modern immunosuppression. Transplantation Proceedings, vol. 43, p. 2617-2623, ISSN: 0041-1345, doi: 10.1016/j.transproceed.2011.06.033.
45. Palma BD, Guasco D, Pedrazzoni M, et al. Osteolytic lesions, cytogenetic features and bone marrow levels of cytokines and chemokines in multiple myeloma patients: Role of chemokine (C-C motif) ligand20. Leukemia. 2016 Feb;30(2):409-16. doi: 10.1038/leu.2015.259. Epub 2015 Sep 30.
46. Bozzetti C, Nizzoli R, Tiseo M, et al. ALK and ROS1 rearrangements tested by fluorescence in situ hybridization in cytological smears from advanced non-small cell lung cancer patients. Diagnostic Cytopathology, vol. 43, p. 941-946, ISSN: 8755-1039, doi: 10.1002/dc.23318.
47. De Filippo M, Gira F, Corradi D, Sverzellati N, Zompatori M, Rossi C. (2011). Benefits of 3D technique in guiding percutaneous retroperitoneal biopsies. RAD. MED, vol. 116(3), p. 407-416, ISSN: 0033-8362, doi: 10.1007/s11547-010-0604-2
48. De Filippo M, Onniboni M, Rusca M, et al. (2008). Advantages of multidetector row CT with multiplanar reformation in guiding percutaneous lung biopsies. RAD. MED, vol. 113, p. 945-953, ISSN: 0033-8362, doi: 10.1007/s11547-008-0325-y

Received: 26 March 2019
Accepted: 4 April 2019
Correspondence:
Bevilacqua Andrea
Department of Medicine and Surgery,
Unit of Radiologic Science, University of Parma,
Maggiore Hospital, Via Gramsci 14 - Parma, Italy
E-mail: andrea.bevilacqua2@studenti.unipr.it